Scuola Internazionale Superiore di Studi Avanzati

Doctoral Thesis

Probing the Possible TeV Scale See-saw Origin of Neutrino Masses with Charged Lepton Flavour Violation Processes and Neutrino Mass Spectroscopy Using Atoms

---

Author:
Dinh Nguyen Dinh

Supervisor:
Prof. S. T. Petcov

A thesis submitted in fulfilment of the requirements
for the degree of Doctor of Philosophy

in

Elementary Particle Physics

Trieste - September 2013

SCUOLA INTERNAZIONALE SUPERIORE DI STUDI AVANZATI

Abstract

Elementary Particle Physics

Doctor of Philosophy

Probing the Possible TeV Scale See-saw Origin of Neutrino Masses with Charged Lepton Flavour Violation Processes and Neutrino Mass Spectroscopy Using Atoms

by Dinh Nguyen Dinh

In the first part of this thesis, we perform a detailed analysis of lepton flavour violation (LFV) within minimal see-saw type extensions of the Standard Model (SM), which give a viable mechanism of neutrino mass generation and provide new particle content at the electroweak scale. We focus, mainly, on predictions and constraints set on each scenario from muon and tau decays ($\mu \to e\gamma$, $\mu \to 3e$, $\tau \to (\mu, e)\gamma$ and $\tau \to 3\mu$) and $\mu - e$ conversion in the nuclei. In particular, we show that in some regions of the parameters space of type I and type II see-saw models, the Dirac and Majorana phases of the neutrino mixing matrix, the ordering and hierarchy of the light neutrino mass spectrum as well as the value of the reactor mixing angle θ_{13} may considerably affect the size of the LFV observables. Besides, the possibilities to observe the LFV processes in the present and future experiments are also considered. The analytic results of the LFV rates might help to discriminate between the three types of neutrino mass generation models considered.

In the second part of the thesis, we study a process of collective de-excitation of atoms in a metastable level into emission mode of a single photon plus a neutrino pair, called radiative emission of neutrino pair (RENP). This process is sensitive to the absolute neutrino mass scale, to the neutrino mass hierarchy and to the nature (Dirac or Majorana) of massive neutrinos. We investigate how the indicated neutrino mass and mixing observables can be determined from the measurement of the corresponding continuous photon spectrum on the example of a transition between specific levels of the Yb atom. The possibility of determining the nature of massive neutrinos and, if neutrinos are Majorana fermions, of obtaining information about the Majorana phases in the neutrino mixing matrix, is analyzed in the cases of normal hierarchical, inverted hierarchical and

quasi-degenerate types of neutrino mass spectrum. We find, in particular, that the sensitivity to the nature of massive neutrinos depends critically on the atomic level energy difference relevant in the RENP.

The content of this thesis is based on the following works:

I, D. N. Dinh, A. Ibarra, E. Molinaro and S. T. Petcov,
The $\mu \to e$ Conversion in Nuclei, $\mu \to e + \gamma$, $\mu \to 3e$ Decays and TeV Scale See-Saw Scenarios of Neutrino Mass Generation,
JHEP **1208** (2012) 125, Erratum-ibid. 1309 (2013) 023 [arXiv:hep-ph/1205.4671v4].

II, D. N. Dinh and S. T. Petcov,
Lepton Flavor Violating τ Decays in TeV Scale Type I See-saw and Higgs Triplet Models,
JHEP **09** (2013) 086 [arXiv:hep-ph/1308.4311].

III, D. N. Dinh, S. T. Petcov, N. Sasao, M. Tanaka and M. Yoshimura,
Observables in Neutrino Mass Spectroscopy Using Atoms,
Phys. Lett. B **719** (2013) 154 [arXiv:hep-ph/1209.4808].

Other papers of the same author, which are not discussed in the thesis:

I, D. N. Dinh and S. T. Petcov,
Sterile Neutrino Determination Using Radiative Emission of Neutrino Pair,
Work in progress.

II, D. N. Dinh, N. A. Ky, N. T. H. Van and P. Q. Van,
Model of neutrino effective masses,
Phys. Rev. D **74** (2006) 077701.

Acknowledgements

First of all, I would like to express my deep sense of gratitude to Prof. Serguey Petcov for his invaluable help and guidance during my time in the School. I am highly indebted to him for constantly encouraging and giving me opportune advices whenever I have problems in the projects or life. The lessons and experiences I have learned from him will always accompany and help me in my career as a physicist.

I would like to thank Prof. Alejandro Ibarra and Dr. Emiliano Molinaro; also Prof. M. Yoshimura and his Coworkers for their cooperation works; especially Dr. E. Molinaro for the helpful discussion on the technique of one-loop calculation in the type II see-saw scenario.

I also would like to thank the Professors, who have given excellent lectures in the elementary particle physics Ph.D program in SISSA. These lectures do not only give us the basic background on the major, but they also provide us with the current trends of interest in high energy physics.

Family is the most peaceful place and always provides me support and encouragement. I want to thank my wife for her sacrifices and patience to take care of the family while I was away for the Ph.D project.

I have benefited a lot from high quality working conditions in SISSA and a friendly environment created by its officials and students. I want to give my thanks to the friends in the sector of elementary particle physics, especially the friends in my academic year for their discussions and helps.

Finally, I would like to thank SISSA and Vietnam Government for their financial support in the form of scholarships for this Ph.D work.

SISSA, Trieste, Italy — Dinh Nguyen Dinh

September 2013

Contents

Chapter 1

Introduction

It is well established at present that the flavor neutrino oscillations observed in the experiments with solar, atmospheric, reactor and accelerator neutrinos (see [1] and the references quoted therein) are caused by the existence of nontrivial neutrino mixing in the weak charged current interaction Lagrangian:

$$\mathcal{L}_{\rm CC} = -\frac{g}{\sqrt{2}} \sum_{\ell=e,\mu,\tau} \overline{\ell_L}(x)\,\gamma_\alpha \nu_{\ell L}(x)\,W^{\alpha\dagger}(x) + h.c.\,, \quad \nu_{\ell \rm L}(x) = \sum_{j=1}^{n} U_{\ell j}\nu_{j\rm L}(x), \qquad (1.1)$$

where $\nu_{\ell L}(x)$ are the flavour neutrino fields, $\nu_{j\rm L}(x)$ is the left-handed (LH) component of the field of the neutrino ν_j having a mass m_j, and U is a unitary matrix - the Pontecorvo-Maki-Nakagawa-Sakata (PMNS) neutrino mixing matrix [2–4], $U \equiv U_{PMNS}$. The data imply that among the neutrinos with definite mass at least three, say ν_1, ν_2 and ν_3, have masses $m_{1,2,3} \lesssim 1$ eV, i.e., are much lighter than the charged leptons and quarks.

The mixing of the three light neutrinos is described to a good approximation by 3×3 unitary PMNS matrix. In the widely used standard parametrization [1], $U_{\rm PMNS}$ is expressed in terms of the solar, atmospheric and reactor neutrino mixing angles θ_{12}, θ_{23} and θ_{13}, respectively, and one Dirac - δ, and two Majorana [5] - α_{21} and α_{31}, CP violation (CPV) phases:

$$U_{\rm PMNS} = \tilde{U} P\,, \quad P = {\rm diag}(1, e^{i\frac{\alpha_{21}}{2}}, e^{i\frac{\alpha_{31}}{2}})\,, \qquad (1.2)$$

where $\tilde{U}$ is a CKM-like matrix containing the Dirac CPV phase δ,

$$\tilde{U} = \begin{pmatrix} c_{12}c_{13} & s_{12}c_{13} & s_{13}e^{-i\delta} \\ -s_{12}c_{23} - c_{12}s_{23}s_{13}e^{i\delta} & c_{12}c_{23} - s_{12}s_{23}s_{13}e^{i\delta} & s_{23}c_{13} \\ s_{12}s_{23} - c_{12}c_{23}s_{13}e^{i\delta} & -c_{12}s_{23} - s_{12}c_{23}s_{13}e^{i\delta} & c_{23}c_{13} \end{pmatrix}. \qquad (1.3)$$

In eq. (1.3) we have used the standard notations $c_{ij} = \cos\theta_{ij}$, $s_{ij} = \sin\theta_{ij}$, the angles $\theta_{ij} = [0, \pi/2]$, $\delta = [0, 2\pi]$ and, in general, $0 \leq \alpha_{j1}/2 \leq 2\pi$, $j = 2, 3$ [6]. If CP invariance holds, we have $\delta = 0, \pi$, and [7–9] $\alpha_{21(31)} = k^{(\prime)}\,\pi$, $k^{(\prime)} = 0, 1, 2, 3, 4$.

In the recent years, the neutrino oscillation parameters were gradually measured with increasing precisions. The Super-Kamiokande collaboration established that the atmospheric neutrino mass squared splitting is $|\Delta m^2_A| \sim \mathcal{O}(10^{-3}\ \mathrm{eV}^2)$ and that the corresponding mixing angle is large, possibly maximal $\theta_{23} \cong \pi/4$ [10]. The data from SNO, Super-Kamiokande and KamLAND experiments [11–13] allowed to establish the large mixing angle solution as a unique solution of the long standing solar neutrino problem, with a solar neutrino mass squared splitting $\Delta m^2_\odot \sim \mathcal{O}(10^{-5}\ \mathrm{eV}^2)$ and mixing angle $\theta_{12} \cong \arcsin(\sqrt{0.3})$. A series of subsequent experiments, using reactor and accelerator neutrinos, have pinned down the atmospheric and solar neutrino oscillation parameters with a few to several percent accuracy.

Furthermore, in June of 2011 the T2K collaboration reported [14] evidence at 2.5σ for a non-zero value of the angle θ_{13}. Subsequently the MINOS [15] and Double Chooz [16] collaborations also reported evidence for $\theta_{13} \neq 0$, although with a smaller statistical significance. Global analyzes of the neutrino oscillation data, including the data from the T2K and MINOS experiments, performed in [17, 18] showed that actually $\sin\theta_{13} \neq 0$ at $\geq 3\sigma$. The first data of the Daya Bay reactor antineutrino experiment on θ_{13} [19] and the RENO experiment [20] reports are also consistent with the none vanishing of $\sin^2 2\theta_{13}$ with rather high precisions at 5.2σ and 4.9σ, respectively.

The current best fit values of these parameters, obtained in [21] from fitting the global neutrino oscillation data, read:

$$\Delta m^2_{21} = 7.54 \times 10^{-5}\ \mathrm{eV}^2\,, |\Delta m^2_{31(32)}| = 2.47\ (2.46) \times 10^{-3}\ \mathrm{eV}^2\,, \tag{1.4}$$

$$\sin^2\theta_{12} = 0.307\,,\ \ \sin^2\theta_{13} = 0.0241\ (0.0244)\,,\ \ \sin^2\theta_{23} = 0.386\ (0.392)\,, \tag{1.5}$$

where the values (values in brackets) correspond to $\Delta m^2_{31(32)} > 0$ ($\Delta m^2_{31(32)} < 0$), i.e., to neutrino mass spectrum with normal ordering (NO), $m_1 < m_2 < m_3$ (inverted ordering (IO), $m_3 < m_1 < m_2$) [1] (see, e.g., [1]). We will use these values in our numerical analyzes. Similar results have been obtained in the analyzes of the global neutrino oscillation data in [22].

[1] As is well known, depending on the value of the lightest neutrino mass, the spectrum can also be normal hierarchical (NH), $m_1 \ll m_2 < m_3$; inverted hierarchical (IH): $m_3 \ll m_1 < m_2$; or quasi-degenerate (QD): $m_1 \cong m_2 \cong m_3$, $m^2_j \gg |\Delta m^2_{31(32)}|$. The QD spectrum corresponds to $m_j \gtrsim 0.10$ eV, $j = 1, 2, 3$.

Despite the precise measurements of the parameters responsible for the oscillations of neutrinos, there are still many fundamental questions regarding directly or indirectly the neutrinos that need to be answered.

Firstly, from neutrino oscillation experiments, we know quite well the neutrino mass squared differences and mixing angles. However other properties, such as the absolute neutrino mass scale or the hierarchy of the neutrino mass spectrum, are still unknown. At present, information about the neutrino mass scale is obtained in the beta β-decays experiments. The Mainz-Troitsk experiment, after analyzing data of beta β-decays of trititum atoms, has set an upper bound of 2.2 eV for the electron antineutrino mass. With the upcoming experiments experiments KATRIN [23], it is planned to search for a mass bigger than 0.2 eV. Data from cosmological observations were used to set much tighter upper bounds on the sum of the light neutrino masses [24, 25]. For example, the Planck collaboration reported in March of 2013 an upper limit on that sum of the three light neutrino masses of 0.23 eV [25].

Besides probing neutrino mass scale and their mass hierarchy, we still need to understand the nature of neutrinos - whether they are Dirac or Majorana particles - and measure the value of the CPV Dirac phase, or of both Dirac and Majorana phases, if neutrinos are Majorana particles. The hierarchy of neutrino mass spectrum and the CPV Dirac phase can be determined in the long base-line neutrino oscillation experiments (see, e.g. [26, 27]). The only known feasible experiments which can reveal the Majorana nature of massive neutrinos are the searches for the process of neutrinoless double beta $(\beta\beta)_{0\nu}$-decay: $(A, Z) \to (A, Z+2) + e^- + e^-$ [28, 29]. It is impossible to make progress in our understanding of the origin of neutrino masses and mixing without determining the nature - Dirac or Majorana - of massive neutrinos. There are a large number of the neutrinoless double beta $(\beta\beta)_{0\nu}$-decay experiments of a new generation which take data or are under preparation at present: GERDA, EXO, KAMPLAND-ZEN, COURE, SNO+, MAJORANA, etc. These experiments will be sensitive to values of the neutrinoless double beta $(\beta\beta)_{0\nu}$-decay effective Majorana mass (see, e.g, [30–36]) $|\langle m \rangle_{ee}| \sim (0.01 - 0.05)$ eV.

Secondly, in spite of the compelling evidence for nonconservation of the leptonic flavour in neutrino oscillations, reflected in the neutrino mixing present in eq. (1.1), all searches for lepton flavour violation (LFV) in the charged lepton sector have produced negative results so far. The most stringent upper limits follow from the experimental searches for the LFV muon decays $\mu^+ \to e^+\gamma$ and $\mu^+ \to e^+e^-e^+$,

$$\mathrm{BR}(\mu^+ \to e^+\gamma) < 5.7 \times 10^{-13} \quad [37]\,, \tag{1.6}$$

$$\mathrm{BR}(\mu^+ \to e^+e^-e^+) < 1.0 \times 10^{-12} \quad [38]\,, \tag{1.7}$$

and from the non-observation of conversion of muons into electrons in Titanium,

$$\mathrm{CR}(\mu^- + \mathrm{Ti} \to e^- + \mathrm{Ti}) \; < \; 4.3 \times 10^{-12} \quad [39]\,. \tag{1.8}$$

Besides, there are stringent constraints on the tau-muon and tau-electron flavour violation as well from the non-observation of LFV tau decays [40]:

$$\mathrm{BR}(\tau \to \mu\gamma) < 4.4 \times 10^{-8}\,, \tag{1.9}$$

$$\mathrm{BR}(\tau \to e\gamma) < 3.3 \times 10^{-8}\,, \tag{1.10}$$

$$\mathrm{BR}(\tau \to 3\mu) < 2.1 \times 10^{-8}\,. \tag{1.11}$$

The role of the experiments searching for lepton flavour violation to test and constrain low scale see-saw models will be significantly strengthened in the next years. Searches for $\mu - e$ conversion at the planned COMET experiment at KEK [41] and Mu2e experiment at Fermilab [42] aim to reach sensitivity to $\mathrm{CR}(\mu\,\mathrm{Al} \to \mathrm{e}\,\mathrm{Al}) \approx 10^{-16}$, while, in the longer run, the PRISM/PRIME experiment in KEK [43] and the project-X experiment in Fermilab [44] are being designed to probe values of the $\mu - e$ conversion rate on Ti, which are by 2 orders of magnitude smaller, $\mathrm{CR}(\mu\,\mathrm{Ti} \to \mathrm{e}\,\mathrm{Ti}) \approx 10^{-18}$ [43]. There are also plans to perform a new search for the $\mu^+ \to e^+e^-e^+$ decay [45], which will probe values of the corresponding branching ratio down to $\mathrm{BR}(\mu^+ \to e^+e^-e^+) \approx 10^{-15}$, i.e., by 3 orders of magnitude smaller than the best current upper limit, eq. (1.7). Furthermore, searches for tau lepton flavour violation at superB factories aim to reach a sensitivity to $\mathrm{BR}(\tau \to (\mu, e)\gamma) \approx 10^{-9}$, while a next generation experiment on the $\tau \to 3\mu$ decay is expected to reach sensitivity to $\mathrm{BR}(\tau \to 3\mu) = 10^{-10}$ [46].

It is also important to note that the recently measured value of θ_{13} in eq. (1.5) will have far reaching implications for the program of research in neutrino physics. A relatively large value of $\sin\theta_{13} \sim 0.15$ opens up the possibilities, in particular, i) for searching for CP violation effects in neutrino oscillations experiments with high intensity accelerator neutrino beams (like T2K, NOνA, etc.); ii) for determining the sign of Δm^2_{32}, and thus the type of neutrino mass spectrum, which can be with normal or inverted ordering (see, e.g. [1]), in the long baseline neutrino oscillation experiments at accelerators (NOνA, etc.), in the experiments studying the oscillations of atmospheric neutrinos (see, e.g. [47–50]), as well as in experiments with reactor antineutrinos [51–53]. It has important implications for the neutrinoless double beta $(\beta\beta)_{0\nu}$-decay phenomenology in the case of neutrino mass spectrum with normal ordering (NO) [54]. A value of $\sin\theta_{13} \gtrsim 0.09$ is a necessary condition for a successful "flavoured" leptogenesis when the CP violation

required for the generation of the matter-antimatter asymmetry of the Universe is provided entirely by the Dirac CP violating phase in the neutrino mixing matrix [55, 56]. [2] As was already discussed to some extent in the literature and we will see further, in certain specific cases a value of $\sin\theta_{13} \sim 0.15$ can have important implications also for the phenomenology of the lepton flavour violation (LFV) processes involving the charged leptons in theories incorporating one of the possible TeV scale see-saw mechanisms of neutrino mass generation.

Concerning the issue of LFV in the charged lepton sector, in a minimal extension of the Standard Model with massive neutrinos [58, 59], in which the total lepton charge L is conserved ($L = L_e + L_\mu + L_\tau$ L_ℓ, $\ell = e, \mu, \tau$, being the individual lepton charges) and the neutrinos with definite mass are Dirac particles, the rates of the LFV violating processes involving the charged leptons are extremely strongly suppressed, $\mathrm{BR}(\mu \to e + \gamma) \sim 10^{-55}$. This branching ratio, of course, satisfies the current experimental upper limit quoted in eq. (1.6), however, the model [58, 59] does not give any insight of why the neutrino masses are so much smaller than the masses of the charged leptons and quarks. The enormous disparity between the magnitude of the neutrino masses and the masses of the charged fermions suggests that the neutrino masses are related to the existence of new mass scale Λ in physics, i.e., to new physics beyond the Standard Model (SM). A natural explanation of the indicated disparity is provided by the see-saw models of neutrino mass generation. In these models the scale Λ is set by the scale of masses of the new degrees of freedom present in the models. In the case of the type I and III see-saw scenarios, these are the masses of the heavy (right-handed (RH)) Majorana neutrinos. In the Higgs Triplet Model (HTM), which is often called also "type II see-saw model", the scale Λ is related to the masses of the new physical neutral, singly and doubly charged Higgs particles.

The scale Λ at which the new physics, associated with the existence of neutrino masses and mixing, manifests itself can, in principle, have an arbitrary large value, up to the GUT scale of 2×10^{16} GeV and even beyond, up to the Planck scale. An interesting possibility, which can also be theoretically and phenomenologically well motivated (see, e.g., [60–62]), is to have the new physics at the TeV scale, i.e., $\Lambda \sim (100 - 1000)$ GeV. In the TeV scale class of see-saw models the flavour structure of the couplings of the new particles to the charged leptons is basically determined by the requirement of reproducing the data on the neutrino oscillation parameters [60–63]. As a consequence, the rates of the LFV processes in the charged lepton sector can be calculated in terms of a few parameters. These parameters are constrained by different sets of data such as, e.g., data on neutrino oscillations, from EW precision tests and on the LFV violating

[2] If indeed $\sin\theta_{13} \cong 0.15$ and the neutrino mass spectrum is with inverted ordering (IO), further important implications for "flavoured" leptogenesis are possible [57].

processes $\ell \to \ell' + \gamma$, $\ell \to 3\ell'$, $\mu^- - e^-$ conversion in nuclei, etc. Nevertheless, the predicted rates of the LFV charged lepton decays $\ell \to \ell' + \gamma$, $\ell \to 3\ell'$ and of the $\mu^- - e^-$ conversion are within the reach of the future experiments searching for lepton flavour violation even when the parameters of the model do not allow production of the new particles with observable rates at the LHC [62].

As parts of the present thesis, we investigate the LFV processes of lepton decays, such as $\ell \to \ell' + \gamma$ ($\ell = \mu$ and $\ell' = e$, or $\ell = \tau$ and $\ell' = \mu, e$), $\mu \to 3e$ and $\tau \to 3\mu$, and $\mu \to e$ conversion in certain nuclei. These LFV processes are considered in the frameworks of the TeV scale type I see-saw, Higgs Triplet and type III see-saw models of neutrino mass generation. We derive predictions for the rates of the indicated LFV processes in the models of interest and analyze the possibilities to observe them in present and planned future experiments. Moreover, results of analyzing the behaviors of the LFV rates in each type of see-saw scheme could be used to determine the real scenario of neutrino mass generation in the nature.

Turning to the issues of the still unknown neutrino properties - the absolute neutrino mass scale, the type of spectrum the neutrino masses obey, the nature of massive neutrinos - all of them might be determined, in principle, by using a phenomenon, called radiative emission of neutrino pair (RENP), which is assumed to occur in atoms or molecules [64–66]. Atoms have a definite advantage over conventional target of nuclei: their available energies are much closer to neutrino masses. The new atomic process of RENP has a rich variety of neutrino phenomenology, since there are six independent thresholds for each target choice, having a strength proportional to different combinations of neutrino masses and mixing parameters. In the numerical results presented further we will show the sensitivity of the RENP related photon spectral shape to various observables; the absolute neutrino mass scale, the type of neutrino mass spectrum, the nature of massive of neutrinos and the Majorana CPV phases in the case of massive Majorana neutrinos.

The present thesis is organized as follows. In Chapter 2, we review the main features of the three types of the see-saw mechanisms and introduce the formulae of FLV rates of the interested processes for each type of light neutrino mass generation scheme. Then we discuss for each scenario the predictions and experimental constraints on the relevant parameter spaces arising from muon FLV processes in Chapter 3 and tau LFV processes in Chapter 4, respectively. In Chapter 5, after an introduction of the RENP spectral rate formula, its physical potential of measuring the absolute neutrino mass scale, determining the type of neutrino mass spectrum (or hierarchy) and the nature (Dirac or Majorana) of massive neutrino will be discussed in detail. Besides, there is a conclusion at the end of every chapter; and an overall conclusion is in Chapter 6.

Chapter 2

See-saw Type Models and Rates of LFV Processes

2.1 See-saw Type I and LFV Rates

2.1.1 See-saw Type I at TeV Scale

In the standard type I see-saw scenario [67–70], the Standard Model (SM) is expanded by adding k heavy right-handed (RH) neutrino fields ν_{aR}, $a = 1, ..., k$, $k \geq 2$, which are singlets with respect to the SM gauge symmetry group. The neutrino mass term in the considered model is written as:

$$\mathcal{L}_\nu = -\overline{\nu_{\ell L}}(M_D)_{\ell a}\nu_{aR} - \frac{1}{2}\overline{\nu^C_{aL}}(M_N)_{ab}\nu_{bR} \; + \; h.c., \tag{2.1}$$

where $\nu^C_{aL} \equiv C\overline{\nu_{aR}}^T$, C is the charge conjugation matrix, M_N is the RH neutrino mass matrix, which is $k \times k$ symmetric matrix, and M_D is the Dirac mass matrix. Then, the full mass matrix of neutrinos has following form

$$M = \begin{pmatrix} \mathbf{0} & M_D \\ M_D^T & M_N \end{pmatrix}. \tag{2.2}$$

This matrix, whose elements are complex in general, can be block-diagonalized by a $(3+k) \times (3+k)$ unitary matrix Ω [71]

$$\Omega^T \begin{pmatrix} \mathbf{0} & M_D \\ M_D^T & M_N \end{pmatrix} \Omega = \begin{pmatrix} U^* \hat{m} U^\dagger & \mathbf{0} \\ \mathbf{0}^T & V^* \hat{M} V^\dagger \end{pmatrix}, \tag{2.3}$$

where $\hat{m} \equiv diag(m_1, m_2, m_3)$ is a diagonal form of the light neutrino mass matrix, while $\hat{M} \equiv diag(M_1, M_2, ..., M_k)$ is the diagonal matrix of the heavy neutrinos. One should keep in mind that the matrix $\mathbf{0}$ in the two sides of the above equation have different dimensions. The null matrix in the left-hand side is a 3×3 matrix, while the matrix in the right-hand side is of $3 \times k$ dimensions.

The diagonalization matrix Ω can be expressed in terms of the exponential of a $3 \times k$ complex matrix R:

$$\Omega = exp \begin{pmatrix} \mathbf{0} & R \\ -R^\dagger & \mathbf{0} \end{pmatrix} = \begin{pmatrix} 1 - \frac{1}{2} R R^\dagger & R \\ -R^\dagger & 1 - \frac{1}{2} R^\dagger R \end{pmatrix} + \mathcal{O}(R^3). \tag{2.4}$$

The above equation is obtained by assuming that R is small. As one will see below that the assumption is relevant when deriving the well-known Pontecorvo, Maki, Nakgawa, Sakata (PMNS) neutrino mixing matrix:

$$U_{PMNS} = U_\ell^\dagger (1 + \eta) U, \tag{2.5}$$

where

$$\eta = -\frac{1}{2} R R^\dagger = -\frac{1}{2} (RV)(RV)^\dagger = \eta^\dagger, \tag{2.6}$$

U and U_ℓ diagonalize the LH neutrino mass matrix and the charged lepton mass matrix, respectively. As being easy to be seen, the matrix η characterises the deviations from unitarity of the PMNS matrix. The elements of $U_{\rm PMNS}$ are determined in experiments studying the oscillations of the flavour neutrinos and antineutrinos, ν_ℓ and $\bar{\nu}_\ell$, $\ell = e, \mu, \tau$, at relatively low energies. In these experiments, the initial states of the flavour neutrinos produced in some weak process, are coherent superpositions of the states of the light massive Majorana neutrino χ_i only. The states of the heavy Majorana neutrino N_j are not present in the superpositions representing the initial flavour neutrino states and this leads to deviations from unitarity of the PMNS matrix.

In the framework of this thesis, we work in the basis in which the charged lepton mass matrix is diagonal, then U_ℓ is set as unity. The charged and neutral current weak interactions involving the light Majorana neutrinos χ_i have the form:

$$\mathcal{L}^\nu_{CC} = -\frac{g}{\sqrt{2}} \bar{\ell} \gamma_\alpha \nu_{\ell L} W^\alpha + \text{h.c.} = -\frac{g}{\sqrt{2}} \bar{\ell} \gamma_\alpha ((1 + \eta) U)_{\ell i} \chi_{iL} W^\alpha + \text{h.c.}, \tag{2.7}$$

$$\mathcal{L}^\nu_{NC} = -\frac{g}{2 c_w} \overline{\nu_{\ell L}} \gamma_\alpha \nu_{\ell L} Z^\alpha = -\frac{g}{2 c_w} \overline{\chi_{iL}} \gamma_\alpha \left(U^\dagger (1 + \eta + \eta^\dagger) U \right)_{ij} \chi_{jL} Z^\alpha. \tag{2.8}$$

Moreover, the matrix η can be expressed in terms of a matrix RV whose elements $(RV)_{\ell k}$ determine the strength of the charged current (CC) and neutral current (NC) weak interaction couplings of the heavy Majorana neutrinos N_k to the $W^\pm$-boson and

the charged lepton ℓ, and to the Z^0 boson and the left-handed (LH) flavour neutrino $\nu_{\ell L}$, $\ell = e, \mu, \tau$:

$$\mathcal{L}^N_{CC} = -\frac{g}{2\sqrt{2}}\,\bar{\ell}\,\gamma_\alpha\,(RV)_{\ell k}(1-\gamma_5)\,N_k\,W^\alpha \;+\; \text{h.c.}\,, \tag{2.9}$$

$$\mathcal{L}^N_{NC} = -\frac{g}{4c_w}\,\overline{\nu_{\ell L}}\,\gamma_\alpha\,(RV)_{\ell k}\,(1-\gamma_5)\,N_k\,Z^\alpha \;+\; \text{h.c.}\,. \tag{2.10}$$

As the consequences of the unobservable signal from the heavy Majorana neutrinos and low energy data by the present experiments, (RV) (or η) should be constrained.

Let us continue by considering the constraints on (RV) from the experimental data of neutrino oscillations and absolute scale of neutrino masses. Expanding two sides of eq. (2.3) then using expression in eq. (2.4) and keeping only the leading order in R, one gets:

$$M_D - R^* M_N \simeq \mathbf{0}\,, \tag{2.11}$$

$$-M_D R^\dagger - R^* M_D^T + R^* M_N R^\dagger \simeq m_\nu = U^* \hat{m} U^\dagger\,, \tag{2.12}$$

$$M_N + R^T M_D + M_D^T R - V^* \hat{M} V^\dagger \simeq \mathbf{0}\,. \tag{2.13}$$

Extracting M_D from eq. (2.11) then insert it into (2.12) and (2.13):

$$m_\nu = U^* \hat{m} U^\dagger = -R^* M_N R^\dagger \simeq -(RV)^* \hat{M} (RV)^\dagger\,, \tag{2.14}$$

$$V^* \hat{M} V^\dagger \simeq M_N + R^T R^* M_N + M_N R^\dagger R\,. \tag{2.15}$$

Using the current upper limits on the absolute scale of neutrino masses and the data obtained in neutrino oscillation experiments, it is relevant to give an approximation $|(m_\nu)_{\ell'\ell}| \lesssim 1\text{eV},\ \ell, \ell' = e, \nu, \tau$, which leads to:

$$|\sum_k (RV)^*_{\ell' k}\, M_k\, (RV)^\dagger_{k\ell}| \lesssim 1\ \text{eV}\,,\ \ell', \ell = e, \mu, \tau\,. \tag{2.16}$$

This inequality can be satisfied in several cases, for example $|(RV)_{\ell k}| \ll 1$ for all ℓ and k. However, this scenario is not interesting and thus will not be considered in the thesis, since it can not render any observable effect at low energy, or possibility to probe the heavy RH neutrinos at the LHC. In this work, we take care a circumstance of having two heavy RH neutrinos (called $N_1,\ N_2$) with opposite CP parities and possessing approximately same masses. The pair of the RH neutrinos forms a pseudo-Dirac, then the eq. (2.16) is naturally fulfilled with sizable $|RV|$, provided:

$$(RV)_{\ell 2} = \pm i (RV)_{\ell 1} \sqrt{\frac{M_1}{M_2}}\,. \tag{2.17}$$

In this class of type I see-saw models with two heavy Majorana neutrinos we are considering (see, e.g., [72–80]), one of the three light (Majorana) neutrinos is massless and hence the neutrino mass spectrum is hierarchical. Two possible types of hierarchical spectrum are allowed by the current neutrino data (see, e.g., [1]): *i*) normal hierarchical (NH), $m_1 = 0$, $m_2 = \sqrt{\Delta m^2_{\odot}}$ and $m_3 = \sqrt{\Delta m^2_{\rm A}}$, where $\Delta m^2_{\odot} \equiv m_2^2 - m_1^2 > 0$ and $\Delta m^2_{\rm A} \equiv m_3^2 - m_1^2$; *ii*) inverted hierarchical (IH), $m_3 = 0$, $m_2 = \sqrt{|\Delta m^2_{\rm A}|}$ and $m_1 = \sqrt{|\Delta m^2_{\rm A}| - \Delta m^2_{\odot}} \cong \sqrt{|\Delta m^2_{\rm A}|}$, where $\Delta m^2_{\odot} \equiv m_2^2 - m_1^2 > 0$ and $\Delta m^2_{\rm A} = m_3^2 - m_2^2 < 0$. In both cases, we have: $\Delta m^2_{\odot}/|\Delta m^2_{\rm A}| \cong 0.03 \ll 1$.

We assume that the heavy RH neutrinos $N_{1,2}$ have masses in the range (100 - 1000) GeV, which makes possible, in principle, to be produced at LHC. To have large enough the CC and NC couplings such that RH neutrino signals could be observed at LHC in this considering type I seesaw scenario, the two RH Majorana neutrinos must be almost degenerate in mass. Suppose $M_2 > M_1 > 0$, M_2 can be expressed in form $M_2 = (1+z)M_1$, $z > 0$. Using the experimental limit on the neutrinoless double beta decay $(\beta\beta)_{0\mu}$, we can set an upper limit $z \lesssim 10^{-3}$ (10^{-2}) for $M_1 \sim 10^2$ (10^3) GeV.

Upper bounds on the couplings of RH neutrinos with SM particles can be also obtained from the low energy electroweak precision data on lepton number conserving processes like $\pi \to \ell\overline{\nu}_{\ell}$, $Z \to \nu\overline{\nu}$ and other tree-level processes involving light neutrinos in the final state [81–83]. These bounds read:

$$|(RV)_{e1}|^2 \lesssim 2 \times 10^{-3}\,, \tag{2.18}$$

$$|(RV)_{\mu 1}|^2 \lesssim 0.8 \times 10^{-3}\,, \tag{2.19}$$

$$|(RV)_{\tau 1}|^2 \lesssim 2.6 \times 10^{-3}\,. \tag{2.20}$$

Let us go further by expressing the RH neutrino mixing matrix participating into the CC and NC weak interactions in terms of low energy neutrino oscillation parameters, the light and heavy neutrino masses. We start by taking eq. (2.12) in [62]:

$$RV = -iU_{PMNS}\sqrt{\hat{m}}O^*\sqrt{\hat{M}^{-1}}\,, \tag{2.21}$$

where O is a complex orthogonal matrix. In the scheme with two heavy RH Majorana neutrinos and NH mass spectrum of the light neutrinos, O-matrix can be written in

form:

$$O = \frac{e^{i\hat{\theta}}}{2}\begin{pmatrix} 0 & 0 \\ 1 & \mp i \\ i & \pm 1 \end{pmatrix} + \frac{e^{-i\hat{\theta}}}{2}\begin{pmatrix} 0 & 0 \\ 1 & \pm i \\ -i & \pm 1 \end{pmatrix} = O_+ + O_-, \quad (NH) \tag{2.22}$$

$$O = \frac{e^{i\hat{\theta}}}{2}\begin{pmatrix} 1 & \mp i \\ i & \pm 1 \\ 0 & 0 \end{pmatrix} + \frac{e^{-i\hat{\theta}}}{2}\begin{pmatrix} 1 & \pm i \\ -i & \pm 1 \\ 0 & 0 \end{pmatrix}, \quad (IH) \tag{2.23}$$

where $\hat{\theta} = \omega - i\xi$.

Without loosing the generality, taking $\xi > 0$, to have sizable couplings between the heavy Majorana neutrinos and the charged leptons or gauge bosons, we need large enough ξ. In the limit of large ξ, in the case of NH neutrino mass spectrum, it is relevant to use the approximation:

$$O \approx O_+ = \frac{e^{i\omega}e^{\xi}}{2}\begin{pmatrix} 0 & 0 \\ 1 & \mp i \\ i & \pm 1 \end{pmatrix}. \tag{2.24}$$

Using (2.21) and (2.24), we can express the matrix RV as:

$$RV \approx -\frac{e^{-i\omega}e^{\xi}}{2}\sqrt{\frac{m_3}{|M_1|}}\begin{pmatrix} (U_{e3} + i\sqrt{m_2/m_3}U_{e2}) & \pm i(U_{e3} + i\sqrt{m_2/m_3}U_{e2})/\sqrt{1+z} \\ (U_{\mu 3} + i\sqrt{m_2/m_3}U_{\mu 2}) & \pm i(U_{\mu 3} + i\sqrt{m_2/m_3}U_{\nu 2})/\sqrt{1+z} \\ (U_{\tau 3} + i\sqrt{m_2/m_3}U_{\tau 2}) & \pm i(U_{\tau 3} + i\sqrt{m_2/m_3}U_{\tau 2})/\sqrt{1+z} \end{pmatrix}. \tag{2.25}$$

A similar formula could be obtained for the case of IH neutrino mass spectrum by replacing $m_{2,3} \to m_{1,2}$ and $U_{\ell 2,\ell 3} \to U_{\ell 1,\ell 2}$ ($\ell = e, \mu, \tau$). So that, for both types of neutrino mass spectrum, one has the relation:

$$(RV)_{\ell 2} = \pm i(RV)_{\ell 1}/\sqrt{1+z} \quad \ell = e, \mu, \tau\,, \tag{2.26}$$

which is consistent with eq. (2.21). The above equation holds only for $M_1 M_2 > 0$; when M_1 and M_2 have different signs, it becomes $(RV)_{\ell 2} = \mp(RV)_{\ell 1}/\sqrt{1+z}$.

Finally, using the relation

$$y^2 v^2 \equiv max\{eig(M_D M_D^\dagger)\} = max\{eig(\sqrt{\hat{m}}O\hat{M}O^\dagger\sqrt{\hat{m}})\} = \frac{1}{4}e^{2\xi}M_1(m_2+m_3)(2+z)\,, \tag{2.27}$$

in which y is the largest eigenvalue of Yukawa coupling matrix, $v = 174$ GeV, the CC and NC weak interaction couplings with participation of the heavy Majorana neutrinos

can be expressed as:

$$|(RV)_{\ell 1}|^2 = \frac{1}{2}\frac{y^2 v^2}{M_1^2}\frac{m_3}{m_2+m_3}\left|U_{\ell 3} + i\sqrt{m_2/m_3}U_{\ell 2}\right|^2, \quad \text{NH}, \tag{2.28}$$

$$|(RV)_{\ell 1}|^2 = \frac{1}{2}\frac{y^2 v^2}{M_1^2}\frac{m_2}{m_1+m_2}\left|U_{\ell 2} + i\sqrt{m_1/m_2}U_{\ell 1}\right|^2, \quad \text{IH}. \tag{2.29}$$

The numerical results present further will be obtained employing the standard parametrization for the unitary matrix U:

$$U = V(\theta_{12}, \theta_{23}, \theta_{13}, \delta)\, Q(\alpha_{21}, \alpha_{31})\,. \tag{2.30}$$

Here (see, e.g., [1])

$$V = \begin{pmatrix} 1 & 0 & 0 \\ 0 & c_{23} & s_{23} \\ 0 & -s_{23} & c_{23} \end{pmatrix} \begin{pmatrix} c_{13} & 0 & s_{13}e^{-i\delta} \\ 0 & 1 & 0 \\ -s_{13}e^{i\delta} & 0 & c_{13} \end{pmatrix} \begin{pmatrix} c_{12} & s_{12} & 0 \\ -s_{12} & c_{12} & 0 \\ 0 & 0 & 1 \end{pmatrix}, \tag{2.31}$$

where we have used the standard notations $c_{ij} \equiv \cos\theta_{ij}$, $s_{ij} \equiv \sin\theta_{ij}$, δ is the Dirac CP violation (CPV) phase and the matrix Q contains the two Majorana CPV phases [1] [5],

$$Q = \mathrm{diag}(1, e^{i\alpha_{21}/2}, e^{i\alpha_{31}/2})\,. \tag{2.32}$$

We recall that $U_{\rm PMNS} = (1+\eta)U$. Thus, up to corrections which depend on the elements of the matrix η whose absolute values, however, do not exceed approximately 5×10^{-3} [81], the values of the angles θ_{12}, θ_{23} and θ_{13} coincide with the values of the solar neutrino, atmospheric neutrino and the 1-3 (or "reactor") mixing angles, determined in the 3-neutrino mixing analyzes of the neutrino oscillation data.

Given the neutrino masses and mixing angles, the TeV scale type I see-saw scenario we are considering is characterized by four parameters [62]: the mass (scale) M_1, the Yukawa coupling y, the parameter z of the splitting between the masses of the two heavy Majorana neutrinos and a phase ω. The mass M_1 and the Yukawa coupling y can be determined, in principle, from the measured rates of two lepton flavor violating (LFV) processes, the $\mu \to e\gamma$ decay and the $\mu - e$ conversion in nuclei, for instance. The mass splitting parameter z and the phase ω, together with M_1 and y, enter, e.g., into the expression for the rate of $(\beta\beta)_{0\nu}$-decay predicted by the model. The latter was discussed in detail in [62].

[1] In the case of the type II see-saw mechanism, to be discussed in Section 2.2, we have $\eta = 0$ and thus the neutrino mixing matrix coincides with U: $U_{\rm PMNS} = U$. We will employ the parametrization (2.30) - (2.32) for U also in that case.

2.1.2 Calculation of LFV Rates

For more convenient in further discussion, in this section, we are going to summary or derive the rates of FLV processes of interest, such as $\mu \to e$ conversion, $\ell \to \ell' + \gamma$ and $\ell \to 3\ell'$, in the scenario of the type I see-saw model. In the type I see-saw, the above FLV processes can not happen in the tree-level, but in one-loop diagrams, whose form factors are calculated in the App. A.

Ignoring the subdominant contribution of the term proportional to $m_{l'}$ (supposes $m_l \gg m_{l'}$), eq. (A.32) can be rewritten in form:

$$-e\,\Gamma^{(\gamma)}_{\alpha}(\bar{l}l'\gamma) = \frac{g^2.e}{32\pi^2 M_w^2}\left[F_\gamma^{ll'}(q^2\gamma_\alpha - \hat{q}q_\alpha)P_L - im_l\, G_\gamma^{ll'}\sigma_{\alpha\beta}q^\beta P_R\right], \tag{2.33}$$

where

$$F_\gamma^{ll'} = \sum_{i=1}^{3+k} U_{li}U^*_{l'i}F_\gamma(\lambda_i)\,, \quad G_\gamma^{ll'} = \sum_{i=1}^{3+k} U_{li}U^*_{l'i}G_\gamma(\lambda_i)\,.^{2} \tag{2.34}$$

Here, $F_\gamma(\lambda_i)$ and $G_\gamma(\lambda_i)$ are defined in eqs. (A.27) and (A.27). The effective Lagrangian derived from (2.33) reads:

$$\mathcal{L}^{(\gamma)}_{eff} = \frac{g^2.e}{32\pi^2 M_w^2}\left[(eQ_\psi)F_\gamma^{ll'}(\bar{\psi}\gamma_\alpha\psi)(\bar{l}'\gamma^\alpha P_L l) + \frac{G_\gamma^{ll'}}{2}m_l\left(\bar{l}'\sigma_{\alpha\beta}P_R l\right)F^{\alpha\beta}\right], \tag{2.35}$$

where Q_ψ is electric charge of ψ, which is quark (for $\mu \to e$ conversion) or lepton (for $l \to 3l'$ decay).

Similarly, from eqs. (A.57), (A.64) and (A.71), we have effective Lagrangians from box and Z boson exchange diagrams:

$$\mathcal{L}^{(z)}_{eff} = \frac{g^4}{32\pi^2 M_w^2}F_z^{ll'}\left(\bar{\psi}\gamma_\alpha(I^3_\psi P_L - Q_\psi \sin^2\theta_W)\psi\right)(\bar{l}'\gamma^\alpha P_L l)\,, \tag{2.36}$$

$$\mathcal{L}^{(Box)}_{eff} = \frac{g^4}{64\pi^2 M_w^2}F_{Box}^{ll'\psi\psi}\left(\bar{\psi}\gamma_\alpha P_L\psi\right)(\bar{l}'\gamma^\alpha P_L l)\,. \tag{2.37}$$

Here, I^3_ψ is the weak isospin of the field ψ, while $F_z^{ll'}$ and $F_{Box}^{ll'\psi\psi}$ are expressed as:

$$F_z^{ll'} = \sum_{i,j=1}^{3+k} U_{li}U^*_{l'j}\left(\delta_{ij}F_z(\lambda_i) + C_{ij}G_z(\lambda_i,\lambda_j)\right), \tag{2.38}$$

[2] In this Subsection and the appendix A, U is understood as the full neutrino mixing matrix in the see-saw type I, which is of $(3+k)\times(3+k)$ dimensions.

$$F_{Box}^{ll'\psi\psi} = \sum_{i=1}^{3+k}\sum_{j} U_{li}U_{l'i}^{*}V_{\psi\chi_j}V_{\psi\chi_j}^{*}F_{Box}(\lambda_i,\lambda_j) \quad \text{for } \mathrm{Q}_\psi > 0\,, \tag{2.39}$$

$$F_{Box}^{ll'\psi\psi} = \sum_{i=1}^{3+k}\sum_{j} U_{li}U_{l'i}^{*}V_{\psi\chi_j}V_{\psi\chi_j}^{*}F_{XBox}(\lambda_i,\lambda_j) \quad \text{for } \mathrm{Q}_\psi < 0\,. \tag{2.40}$$

It is useful to note that $V_{\psi\chi_j}$ is quark or neutrino mixing matrix according to whether ψ is quark or lepton. If ψ is u quark, χ_j are (d,s,b) quarks; while, in the case where ψ is d quark or one of the charged leptons $(e^-,\ \mu^-,\ \tau^-)$, χ_j are (u,c,t) quarks or neutrinos (both the heavy and light neutrinos), respectively.

Using eq. (2.35), the ratio of the decay rates $\Gamma(l\to l'\gamma)$ and $\Gamma(l\to\nu_l l'\overline{\nu}_{l'})$, can be written as [59, 62, 84, 85]:

$$\frac{\Gamma(l\to l'\gamma)}{\Gamma(l\to\nu_l l'\overline{\nu}_{l'})} = \frac{3\alpha_{\rm em}}{2\pi}|G_\gamma^{ll'}|^2 = \frac{3\alpha_{\rm em}}{32\pi}|T_{(ll')}|^2\,, \tag{2.41}$$

where

$$T_{(ll')} \approx \sum_{i=4}^{3+k}(U)_{l'i}^{*}(U)_{li}\ [G(x_i)-G(0)]\ , \tag{2.42}$$

$$G(x) = \frac{10-43x+78x^2-49x^3+4x^4+18x^3\ln x}{3(x-1)^4}\,, \tag{2.43}$$

and $x_i = m_i^2/M_w^2$.

We have also obtained the $l\to 3l'$ decay rate by adapting the result of the calculation of the $\mu\to 3e$ decay rate performed in [86] in a scheme with heavy RH neutrinos and type I seesaw mechanism of neutrino mass generation. After applying the form factors introduced above and neglecting the corrections $\sim m_{l'}/m_l$, the decay branching ratio is expressed as:

$$\mathrm{BR}(l\to 3l') = \frac{\alpha_{em}^2}{64\pi^2\sin^4\theta_W}\,|C_{l3l'}|^2\times\mathrm{BR}(l\to l'\bar{\nu}_{l'}\nu_l)\,, \tag{2.44}$$

$$\begin{aligned}|C_{l3l'}|^2 &= 2\left|\frac{1}{2}F_{Box}^{ll'l'l'}+F_z^{ll'}-2\sin^2\theta_W(F_z^{ll'}-F_\gamma^{ll'})\right|^2+4\sin^4\theta_W\left|F_z^{ll'}-F_\gamma^{ll'}\right|^2\\ &+16\sin^2\theta_W\mathrm{Re}\left[(F_z^{ll'}+\frac{1}{2}F_{Box}^{ll'l'})G_\gamma^{ll'*}\right]-48\sin^4\theta_W\mathrm{Re}\left[(F_z^{ll'}-F_\gamma^{ll'})G_\gamma^{ll'*}\right]\\ &+32\sin^4\theta_W|G_\gamma^{ll'}|^2\left(\log\frac{m_l^2}{m_{l'}^2}-\frac{11}{4}\right)\,,\end{aligned} \tag{2.45}$$

where $G_\gamma^{ll'}$, $F_\gamma^{ll'}$, $F_{Box}^{ll'l'l'}$ and $F_z^{ll'}$ have been defined above.

In writing the expression for $\mathrm{BR}(l\to 3l')$ in eq. (2.44), we have used for the decay rate $\Gamma(l\to l'\bar{\nu}_{l'}\nu_l) = G_F^2 m_l^5/(192\pi^3)$.

Finally, we are going to calculate $\mu - e$ conversion rate using the effective Lagrangian in (2.35), (2.36), (2.37) and the general formula reported in [87]. Since the quark axial vector current $\bar{q}\gamma_\alpha\gamma_5 q$ does not contribute to the $\mu - e$ conversion, the effective Lagrangian $\mathcal{L}_{eff}^{(\mu-e)}$ reads:

$$\mathcal{L}_{eff}^{(\mu-e)} = \frac{g^2.e}{32\pi^2 M_W^2}\frac{G_\gamma^{\mu e}}{2} m_\mu \left(\bar{e}\sigma_{\alpha\beta}P_R\mu\right) F^{\alpha\beta} + \frac{g^4}{32\pi^2 M_W^2}\widetilde{F}_q^{\mu e}\left(\bar{q}\gamma_\alpha q\right)\left(\bar{e}\gamma^\alpha P_L\mu\right), \quad (2.46)$$

where

$$\widetilde{F}_q^{\mu e} = Q_q \sin^2\theta_W (F_\gamma^{\mu e} - F_z^{\mu e}) + \frac{1}{4}(2I_3 F_z^{\mu e} + F_{Box}^{\mu eqq}). \quad (2.47)$$

Using the result in [87], the conversion rate is easy to be obtained

$$\Gamma_{conv} = 2G_F^2 \left| \frac{e.D}{32\pi^2} G_\gamma^{\mu e} + \frac{g^2}{4\pi^2}\left\{(2\widetilde{F}_u^{\mu e} + \widetilde{F}_d^{\mu e})V^{(p)} + (\widetilde{F}_u^{\mu e} + 2\widetilde{F}_d^{\mu e})V^{(n)}\right\}\right|^2. \quad (2.48)$$

Here, the parameters D, $V^{(p)}$ and $V^{(n)}$, with $V^{(p)}/Z = V^{(n)}/N$, represent overlap integrals of the muon and electron wave functions and are related to the effective dipole and vector type operators in the interaction Lagrangian, respectively (see, *e.g.* [87]).

In the case of a light nucleus, *i.e.* for $Z \lesssim 30$, one has with a good approximation $D \simeq 8\sqrt{4\pi\alpha_{\rm em}}\, V^{(p)}$, with the vector type overlap integral of the proton, $V^{(p)}$, given by [87]:

$$V^{(p)} \simeq \frac{1}{4\pi} m_\mu^{5/2}\, \alpha_{\rm em}^{3/2}\, Z_{eff}^2\, Z^{1/2}\, F(-m_\mu^2). \quad (2.49)$$

Using the formulae quoted above, we have the final expression for the conversion rate

$$\begin{aligned}\Gamma_{conv} &= \frac{G_F^2 m_\mu^5 \alpha_W^2 \alpha^3}{8\pi^4}\frac{Z_{eff}^4}{Z}F^2(q^2)\left|ZG_\gamma^{\mu e}\sin^2\theta_W + Z(2\widetilde{F}_u^{\mu e} + \widetilde{F}_d^{\mu e}) + N(\widetilde{F}_u^{\mu e} + 2\widetilde{F}_d^{\mu e})\right|^2 \\ &= \frac{G_F^2 m_\mu^5 \alpha_W^2 \alpha^3}{8\pi^4}\frac{Z_{eff}^4}{Z}F^2(q^2)\left|Z(2F_u^{\mu e} + F_d^{\mu e}) + N(F_u^{\mu e} + 2F_d^{\mu e})\right|^2, \end{aligned} \quad (2.50)$$

in which

$$F_q^{\mu e} = Q_q \sin^2\theta_W (F_\gamma^{\mu e} - F_z^{\mu e} + G_\gamma^{\mu e}) + \frac{1}{4}(2I_3 F_z^{\mu e} + F_{Box}^{\mu eqq}). \quad (2.51)$$

In eqs. (2.49) and (2.50), Z is the proton number of the nucleus $\mathcal{N}$, θ_W is the weak mixing angle, $\sin^2\theta_W = 0.23$, $F(q^2)$ is the nuclear form factor as a function of transferred momentum q, and Z_{eff} is an effective atomic charge.

2.2 See-saw Type II (Higgs Triplet Model) and LFV Rates

2.2.1 See-saw Type II (Higgs Triplet Model) at TeV Scale

We will introduce briefly in this section the type II see-saw [88–90] extension of the SM for the generation of the light neutrino masses. In its minimal formulation it includes one additional $SU(2)_L$ triplet Higgs field Δ, which has weak hypercharge $Y_W = 2$:

$$\Delta \;=\; \begin{pmatrix} \Delta^+/\sqrt{2} & \Delta^{++} \\ \Delta^0 & -\Delta^+/\sqrt{2} \end{pmatrix} . \tag{2.52}$$

The Lagrangian of the type II see-saw scenario, which is sometimes called also the "Higgs Triplet Model" (HTM), reads [3]:

$$\mathcal{L}^{\rm II}_{\rm seesaw} = -M_\Delta^2\,{\rm Tr}\left(\Delta^\dagger\Delta\right) - \left(h_{ll'}\,\overline{\psi^C}_{lL}\,i\tau_2\,\Delta\,\psi_{l'L} \;+\; \mu_\Delta\,H^T\,i\tau_2\,\Delta^\dagger\,H \;+\; {\rm h.c.}\right) , \tag{2.53}$$

where $(\psi_{lL})^T \equiv (\nu_{lL}^T \quad l_L^T)$, $\overline{\psi^C}_{lL} \equiv (-\,\nu_{lL}^T C^{-1} \quad -\,l_L^T C^{-1})$, and H are, respectively, the SM lepton and Higgs doublets, C being the charge conjugation matrix, and μ_Δ is a real parameter characterising the soft explicit breaking of the total lepton charge conservation. We are interested in the low energy see-saw scenario, where the new physics scale M_Δ associated with the mass of Δ takes values 100 GeV $\lesssim M_\Delta \lesssim$ 1 TeV, which, in principle, can be probed by LHC [93–96].

The flavour structure of the Yukawa coupling matrix h and the size of the lepton charge soft breaking parameter μ_Δ are related to the light neutrino mass matrix m_ν, which is generated when the neutral component of Δ develops a "small" vev $v_\Delta \propto \mu_\Delta$. Indeed, setting $\Delta^0 = v_\Delta$ and $H^T = (0 \quad v)^T$ with $v \simeq 174$ GeV, from Lagrangian (2.53) one obtains:

$$(m_\nu)_{ll'} \equiv m_{ll'} \;\simeq\; 2\,h_{ll'}\,v_\Delta\ . \tag{2.54}$$

The matrix of Yukawa couplings $h_{ll'}$ is directly related to the PMNS neutrino mixing matrix $U_{\rm PMNS} \equiv U$, which is unitary in this case:

$$h_{ll'} \;\equiv\; \frac{1}{2v_\Delta}\left(U^*\,{\rm diag}(m_1, m_2, m_3)\,U^\dagger\right)_{ll'} . \tag{2.55}$$

An upper limit on v_Δ can be obtained from considering its effect on the parameter $\rho = M_W^2/M_Z^2\cos^2\theta_W$. In the SM, $\rho = 1$ at tree-level, while in the HTM one has

$$\rho \equiv 1 + \delta\rho = \frac{1+2x^2}{1+4x^2}\,, \quad x \equiv v_\Delta/v. \tag{2.56}$$

[3] We do not give here, for simplicity, all the quadratic and quartic terms present in the scalar potential (see, *e.g.*, [91, 92]).

The measurement $\rho \approx 1$ leads to the bound $v_\Delta/v \lesssim 0.03$, or $v_\Delta < 5$ GeV (see, e.g., [97]).

As we will see, the amplitudes of the LFV processes $\mu \to e\gamma$, $\mu \to 3e$ and $\mu + \mathcal{N} \to e + \mathcal{N}$ in the model under discussion are proportional, to leading order, to a product of 2 elements of the Yukawa coupling matrix h. This implies that in order for the rates of the indicated LFV processes to be close to the existing upper limits and within the sensitivity of the ongoing MEG and the planned future experiments for $M_\Delta \sim (100-1000)$ GeV, the Higgs triplet vacuum expectation value v_Δ must be relatively small, roughly $v_\Delta \sim (1-100)$ eV. In the case of $M_\Delta \sim v = 174$ GeV we have $v_\Delta \cong \mu_\Delta$, while if $M_\Delta^2 >> v^2$, then $v_\Delta \cong \mu_\Delta v^2/(2M_\Delta^2)$ (see, e.g., [91, 92, 97]) with $v^2/(2M_\Delta^2) \cong 0.015$ for $M_\Delta = 1000$ GeV. Thus, in both cases a relatively small value of v_Δ implies that μ_Δ has also to be small. A nonzero but relatively small value of μ_Δ can be generated, e.g., at higher orders in perturbation theory [98] or in the context of theories with extra dimensions (see, e.g., [99]).

The physical singly-charged Higgs scalar field practically coincides with the triplet scalar field Δ^+, the admixture of the doublet charged scalar field being suppressed by the factor v_Δ/v. The singly- and doubly- charged Higgs scalars Δ^+ and Δ^{++} have, in general, different masses [98, 100–102]: $m_{\Delta^+} \neq m_{\Delta^{++}}$. Both situations $m_{\Delta^+} > m_{\Delta^{++}}$ and $m_{\Delta^+} < m_{\Delta^{++}}$ are possible. In some cases, for simplicity, we will present numerical results for $m_{\Delta^+} \cong m_{\Delta^{++}} \equiv M_\Delta$, but one must keep in mind that m_{Δ^+} and $m_{\Delta^{++}}$ can have different values.

2.2.2 Calculation of LFV Rates

In the mass eigenstate basis, the effective charged lepton flavour changing operators arise at one-loop order from the exchange of the singly- and doubly-charged physical Higgs scalar fields, whose form factors are detail calculated in App. B. The effective low energy LFV Lagrangian corresponding to eqs. (B.74) and (B.75) can be written in forms:

$$\begin{aligned} \mathcal{L}^{eff} &= -4\,\frac{e\,G_F}{\sqrt{2}}\,\Big(m_l\,A_R\,\overline{l'}\,\sigma^{\alpha\beta}\,P_R\,l\,F_{\beta\alpha} + \text{h.c.}\Big) \\ &\quad -\frac{e^2\,G_F}{\sqrt{2}}\,\left(A_L(q^2)\,\overline{l'}\,\gamma^\alpha\,P_L\,l\sum_{Q=u,d} q_Q\,\overline{Q}\,\gamma_\alpha\,Q + \text{h.c.}\right), \end{aligned} \tag{2.57}$$

where e is the proton charge, and $q_u = 2/3$ and $q_d = -1/3$ are the electric charges of the up and down quarks (in units of the proton charge). The form factors $A_{R,L}$ have

expressions:

$$A_R = -\frac{1}{\sqrt{2}\,G_F}\frac{(h^\dagger h)_{l'l}}{48\pi^2}\left(\frac{1}{8\,m^2_{\Delta^+}}+\frac{1}{m^2_{\Delta^{++}}}\right), \tag{2.58}$$

$$A_L(q^2) = -\frac{1}{\sqrt{2}\,G_F}\frac{h^*_{kl'}h_{kl}}{6\pi^2}\left(\frac{1}{12\,m^2_{\Delta^+}}+\frac{1}{m^2_{\Delta^{++}}}\,f\left(\frac{-q^2}{m^2_{\Delta^{++}}},\frac{m^2_k}{m^2_{\Delta^{++}}}\right)\right). \tag{2.59}$$

Here, $(m_l,\ m_k)$ are the masses of the charged lepton $(l,\ k)$, $(l,\ k) = e,\mu,\tau$ and q is the momentum carried by the photon.

In the limit where the transition is dominated by the exchange of a virtual doubly charged scalar Δ^{++}, these expressions reduce to those obtained in [102–105]; to the best of our knowledge the expression of $A_L(q^2)$ for the general case is a new result. The term with the form factor A_R in eq. (2.57) generates the $\mu \to e\gamma$ decay amplitude. It corresponds to the contribution of the one loop diagrams with virtual neutrino and Δ^+ [106] and with virtual charged lepton and Δ^{++} [104, 105] (see also [28]). The second term involving the form factor A_L, together with A_R, generates the $\mu - e$ conversion amplitude. The loop function $f(r, s_l)$ is well known [102, 103]:

$$f(r,s_l) = \frac{4s_l}{r} + \log(s_l) + \left(1-\frac{2s_l}{r}\right)\sqrt{1+\frac{4s_l}{r}}\,\log\frac{\sqrt{r}+\sqrt{r+4s_l}}{\sqrt{r}-\sqrt{r+4s_l}}, \tag{2.60}$$

where $r = m^2_\mu/M^2_\Delta$ and $s_l = m^2_l/M^2_\Delta$.

Notice that in the limit in which the charged lepton masses m_l are much smaller than the doubly-charged scalar mass $m_{\Delta^{++}}$, one has $f(r, s_l) \simeq \log(r) = \log(m^2_\mu/m^2_{\Delta^{++}})$. For $m_{\Delta^{++}} = (100 - 1000)$ GeV, this is an excellent approximation for $f(r, s_e)$, but cannot be used for $f(r, s_\mu)$ and $f(r, s_\tau)$. The ratios $f(r, s_e)/f(r, s_\mu)$ and $f(r, s_e)/f(r, s_\tau)$ change relatively little when $m_{\Delta^{++}}$ increases from 100 GeV to 1000 GeV, and at $m_{\Delta^{++}} =$ 100 (1000) GeV take the values: $f(r, s_e)/f(r, s_\mu) \cong 1.2$ (1.1) and $f(r, s_e)/f(r, s_\tau) \cong$ 2.1 (1.7). More generally, $f(r, s_l)$, $l = e, \mu, \tau$, are monotonically (slowly) decreasing functions of $m_{\Delta^{++}}$ [4]: for $m_{\Delta^{++}} = 100$ (1000) GeV we have, e.g., $f(r, s_e) \cong -13.7$ (-18.3).

In the Higgs triplet model considered, the $l \to l' + \gamma$ decay amplitude receives at leading order contributions from one loop diagrams with exchange of virtual singly and doubly-charged Higgs scalars. A detailed calculation of these contributions leads to the result [91, 92, 106, 107]:

$$\begin{aligned}\mathrm{BR}(l\to l'\gamma) &\cong 384\,\pi^2\,(4\pi\,\alpha_{\rm em})\,|A_R|^2 \times \mathrm{BR}(l\to \nu_l\, l'\,\overline{\nu}_{l'}) \\ &= \frac{\alpha_{\rm em}}{192\,\pi}\frac{\left|(h^\dagger h)_{ll'}\right|^2}{G_F^2}\left(\frac{1}{m^2_{\Delta^+}}+\frac{8}{m^2_{\Delta^{++}}}\right)^2 \mathrm{BR}(l\to \nu_l\, l'\,\overline{\nu}_{l'}),\end{aligned} \tag{2.61}$$

[4] Note that we have $f(r, s_l) < 0$, $l = e, \mu, \tau$.

where $l = \mu$ and $l' = e$, or $l = \tau$ and $l' = \mu, e$.

Similarly, the leading contribution in the $l \to 3l'$ decay amplitude in the TeV scale HTM is due to a tree level diagram with exchange of the virtual doubly-charged Higgs scalar Δ^{++}. The corresponding $l \to 3l'$ decay branching ratio is given by [104, 105] (see also, e.g., [28, 92]):

$$\mathrm{BR}(l \to 3l') = \frac{\left|h^*_{l'l'} h_{ll'}\right|^2}{G_F^2\, m^4_{\Delta^{++}}}\, \mathrm{BR}(l \to l' \bar{\nu}_{l'} \nu_l) \;=\; \frac{1}{G_F^2\, m^4_{\Delta^{++}}}\, \frac{\left|m^*_{l'l'} m_{ll'}\right|^2}{16 v_\Delta^4} \mathrm{BR}(l \to l' \bar{\nu}_{l'} \nu_l)\,. \tag{2.62}$$

We consider next the $\mu - e$ conversion in a generic nucleus $\mathcal{N}$ using the effective Lagrangian introduced in eq. (2.57). In the same way has done in Sector 2.1.2, we parametrize the corresponding conversion rate following the effective field theory approach developed in [87]. Taking into account the interaction Lagrangian (2.57), we get in the type II see-saw scenario

$$\mathrm{CR}(\mu\mathcal{N} \to e\mathcal{N}) \;\cong\; (4\pi\alpha_{\mathrm{em}})^2\, \frac{2\, G_F^2}{\Gamma_{\mathrm{capt}}} \left| A_R\, \frac{D}{\sqrt{4\pi\, \alpha_{\mathrm{em}}}} \;+\; (2\, q_u + q_d)\, A_L\, V^{(p)} \right|^2 . \tag{2.63}$$

Using the properties $D \cong 8e\; V^{(p)}$, $V^{(p)}/Z = V^{(n)}/N = m_\mu^{5/2} \alpha^{3/2} Z_{eff}^2 Z^{-1/2} F(q^2)/4\pi$, eqs. (2.58), (2.59) and (2.49), the conversion rate (2.63) reads

$$\begin{aligned} \mathrm{CR}(\mu\mathcal{N} \to e\mathcal{N}) \;\cong\; & \frac{\alpha_{\mathrm{em}}^5}{36\,\pi^4}\, \frac{m_\mu^5}{\Gamma_{\mathrm{capt}}}\, Z_{eff}^4\, Z\, F^2(-m_\mu^2) \left| \left(h^\dagger h\right)_{e\mu} \left[\frac{5}{24\, m^2_{\Delta^+}} + \frac{1}{m^2_{\Delta^{++}}} \right] \right. \\ & \left. +\; \frac{1}{m^2_{\Delta^{++}}} \sum_{l=e,\mu,\tau} h^\dagger_{el}\, f(r, s_l)\, h_{l\mu} \right|^2 , \end{aligned} \tag{2.64}$$

where Γ_{capt} is the experimentally known total muon capture rate.

2.3 See-saw Type III Model

Now, we turn to the study of the type III see-saw [108, 109] extensions of the SM. In the scenarios under discussion, the SM particle content is enlarged by adding $SU(2)_L$-triplets of fermions, $\boldsymbol{F}_{jR} \equiv \left(F^1_{jR}, F^2_{jR}, F^3_{jR}\right)$, $j \geq 2$, possessing zero weak hypercharge and a mass M_k at the electroweak scale: $M_k \approx (100 - 1000)$ GeV. The corresponding interaction and mass terms in the see-saw Lagrangian read:

$$\mathcal{L}^{\mathrm{III}}_{\mathrm{seesaw}} \;=\; -\lambda_{\ell j}\, \overline{\psi}_{\ell L}\, \boldsymbol{\tau}\, \widetilde{H} \cdot \boldsymbol{F}_{jR} \;-\; \frac{1}{2}\, (M_R)_{ij}\, \overline{\boldsymbol{F}^C_{iL}} \cdot \boldsymbol{F}_{jR} \;+\; \mathrm{h.c.}\,, \tag{2.65}$$

where $\boldsymbol{\tau} \equiv (\tau^1, \tau^2, \tau^3)$, τ^a being the usual $SU(2)_L$ generators in the fundamental representation.

It is convenient in the following discussion to work with the charge eigenstates $F^{\pm}_{jR} \equiv (F^1_{jR} \mp i F^2_{jR})$ and $F^0_{jR} \equiv F^3_{jR}$. Then, the physical states in the above Lagrangian correspond to electrically charged Dirac and neutral Majorana fermions, which are denoted as E_j and N_j, respectively: [5]

$$E_j \equiv F^-_{jR} + F^{+C}_{jL} \qquad N_j \equiv F^{0C}_{jL} + F^0_{jR} \,. \tag{2.66}$$

In the basis in which the charged lepton mass matrix is diagonal, the CC and NC weak interaction Lagrangian of the light Majorana neutrino mass eigenstates χ_j read:

$$\mathcal{L}^{\nu}_{CC} = -\frac{g}{\sqrt{2}}\,\bar{\ell}\,\gamma_\alpha\,((1-\eta)U)_{\ell i}\,\chi_{iL}\,W^\alpha + \text{h.c.}\,, \tag{2.67}$$

$$\mathcal{L}^{\nu}_{NC} = -\frac{g}{2c_w}\,\overline{\chi_{iL}}\,\gamma_\alpha\,\left(U^\dagger(1+2\,\eta)U\right)_{ij}\,\chi_{jL}\,Z^\alpha \,. \tag{2.68}$$

Similarly to the type I see-saw scenario discussed earlier, the heavy Majorana mass eigenstates N_k might acquire a sizable coupling to the weak gauge bosons through the mixing with the light Majorana neutrinos:

$$\mathcal{L}^{N}_{CC} = \frac{g}{2\sqrt{2}}\,\bar{\ell}\,\gamma_\alpha\,(RV)_{\ell k}(1-\gamma_5)\,N_k\,W^\alpha + \text{h.c.}\,, \tag{2.69}$$

$$\mathcal{L}^{N}_{NC} = -\frac{g}{4c_w}\,\overline{\nu}_\ell\,\gamma_\alpha\,(RV)_{\ell j}(1-\gamma_5)\,N_j\,Z^\alpha + \text{h.c.}\,. \tag{2.70}$$

In the expressions given above, the non-unitary part of the neutrino mixing matrix, *i.e.* the matrix η, and the matrix R are defined as in the type I see-saw scenario discussed in Section 2.1 (see eq. (2.6)), while V in this case diagonalizes the symmetric mass matrix M_R in eq. (2.65): $M_R \cong V^* \text{diag}(M_1, M_2, \ldots) V^\dagger$.

The neutrino Yukawa couplings $\lambda_{\ell j}$ can be partially constrained by low-energy neutrino oscillation data and electroweak precision observable (see, *e.g.* [110, 111]). Notice that, unlike the type I see-saw extension of the Standard Model, now we have flavour changing neutral currents (FCNCs) in the charged lepton sector. The latter are described by the interaction Lagrangian:

$$\mathcal{L}^{\ell}_{NC} = \frac{g}{2c_w}\,\left(\bar{\ell}_L\,\gamma_\alpha\,(\mathbf{1}-4\,\eta)_{\ell\ell'}\,\ell'_L - 2\,s^2_w\,\bar{\ell}\,\gamma_\alpha\,\ell\right)\,Z^\alpha \,. \tag{2.71}$$

Finally, [6] the interactions of the new heavy charged leptons, E_j, with the weak gauge bosons at leading order in the mixing angle between the heavy and the light mass

[5] In the following we will denote as E_j and N_j the mass eigenstates obtained from the diagonalization of the full charged and neutral lepton mass matrices.

[6] Flavour changing couplings between the charged leptons and the SM Higgs boson H arise as well in the TeV-scale type III see-saw scenarios [111] which enter at one-loop in the lepton flavour violating processes (see next subsection).

eigenstates read:

$$\mathcal{L}^{E}_{CC} = -g\,\overline{E}_j\,\gamma_\alpha\,N_j\,W^\alpha + g\,\overline{E}_j\,\gamma_\alpha\,(RV)_{\ell j}\,\nu^{C}_{\ell R}\,W^\alpha + \text{h.c.}\,, \tag{2.72}$$

$$\mathcal{L}^{E}_{NC} = g\,c_w\,\overline{E}_j\,\gamma_\alpha\,E_j\,Z^\alpha - \frac{g}{2\sqrt{2}c_w}\left(\overline{\ell}\,\gamma_\alpha\,(RV)_{\ell j}(1-\gamma_5)\,E_j\,Z^\alpha + \text{h.c.}\right). \tag{2.73}$$

To obtain eqns. from 2.67 to 2.73, we have used the results reported in [111] and taken into account the equalities:

$$\epsilon \equiv (RV)(RV)^\dagger = -2\eta\,, \tag{2.74}$$

$$(RV) \equiv \frac{v}{\sqrt{2}} Y^\dagger_\Sigma M^{-1}_\Sigma, \tag{2.75}$$

which are easy to be seen by comparing our expression for the matrix used to diagonalize the neutrino mass matrix and those in [111]. Here, ϵ and $Y^\dagger_\Sigma M^{-1}_\Sigma v/\sqrt{2}$ are two notations appearing in [111].

2.4 Chapter Conclusion

In this chapter, we have introduced LFV processes in the class of models, whose effective Majorana mass term for the light left-handed active neutrinos is generated after electroweak symmetry breaking due to the decoupling of additional "heavy" scalar and/or fermion representations. We have analyzed in full generality the phenomenology of the three different and well-known (see-saw) mechanisms of neutrino mass generation, in their minimal formulation: *i*) type I see-saw models, in which the new particle content consist of at least 2 RH neutrinos, which are not charged under the SM gauge group; *ii*) type III see-saw models, where the RH neutrinos are taken in the adjoint representation of $SU(2)_L$ with zero hypercharge; *iii*) type II see-saw (or Higgs triplet) models, where the scalar sector of the theory is extended with the addition of at least one scalar triplet of $SU(2)_L$ coupled to charged leptons.

In the models considered, the scale of new physics associated with the existence of nonzero neutrino masses and neutrino mixing is assumed to be in the range of $\sim (100 - 1000)$ GeV. In the type I and III see-saw scenarios, this scale is determined by the masses of the heavy Majorana neutrinos, while in the Higgs Triplet model it corresponds to the masses of the new singly charged, doubly charged and neutral physical Higgs particles. In the type I and III see-saw classes of models of interest, the flavour structure of the couplings of the new particles - the heavy Majorana neutrinos N_j - to the charged leptons and $W^\pm$-boson and to the flavour neutrino fields and the Z^0-boson, $(RV)_{lj}$, $l = e, \mu, \tau$, are basically determined by the requirement of reproducing the data on the neutrino oscillation parameters (see, e.g., [62]). In the Higgs Triplet model the Yukawa couplings

of the new scalar particles to the charged leptons and neutrinos are proportional to the Majorana mass matrix of the LH active flavour neutrinos.

As a consequence, the rates of the LFV processes in the charged lepton sector can be calculated in the considered models in terms of a few unknown parameters. These parameters are constrained by different sets of data such as, e.g., data on neutrino oscillations, from EW precision tests, on the LFV processes $\mu \to e + \gamma$, $\mu \to 3e$, etc. In the TeV scale type I and III see-saw scenarios considered, all the constraints can be satisfied for sizeable values of the couplings $|(RV)_{lj}|$ with two heavy Majorana neutrinos $N_{1,2}$, in which the latter have close masses forming a pseudo-Dirac state, $M_2 = M_1(1+z)$, $M_{1,2}, z > 0$, $z \ll 1$. In those schemes the lightest neutrino mass $m_0 = 0$ and the neutrino mass spectrum is either normal hierarchical (NH) or inverted hierarchical (IH).

Chapter 3

LFV μ Processes in TeV Scale See-saw Type models

The content of this chapter is based on the results obtained in [107]. We have used the most updated data of the neutrino oscillation parameters at the given time, which are reported in [17, 19, 20]. The value of $\sin^2 2\theta_{13}$ was measured with a rather high precision and was found to be different from zero at 5.2σ [19]:

$$\sin^2 2\theta_{13} = 0.092 \pm 0.016 \pm 0.005\,, \quad 0.04 \leq \sin^2 2\theta_{13} \leq 0.14\,,\ 3\sigma\,. \tag{3.1}$$

The results of the analysis [17], in which $\Delta m^2_{21} \equiv \Delta m^2_{\odot}$ and $|\Delta m^2_{31}| \equiv |\Delta m^2_{\rm A}|$ were determined as well, are shown in Table 3.1. The best fit values of neutrino parameters, summarized in the Table 3.1, in fact, are different very little from the current best fit values (see, e.g., [21], eqs. (1.4) and (1.5)), therefore the results of analyzing LFV rates of the processes interested with new and old neutrino oscillation data are not very different.

TABLE 3.1: The best-fit values and 3σ allowed ranges of the 3-neutrino oscillation parameters, derived from a global fit of the current neutrino oscillation data, including the T2K and MINOS (but not the Daya Bay) results (from [17]). The Daya Bay data [19] on $\sin^2\theta_{13}$ is given in the last line. The values (values in brackets) of $\sin^2\theta_{12}$ are obtained using the "old" [112] ("new" [113]) reactor $\bar{\nu}_e$ fluxes in the analysis.

Parameter	best-fit ($\pm 1\sigma$)	3σ
$\Delta m^2_{\odot}$ [10^{-5} eV^2]	$7.58^{+0.22}_{-0.26}$	6.99 - 8.18
$\lvert\Delta m^2_{A}\rvert$ [10^{-3} eV^2]	$2.35^{+0.12}_{-0.09}$	2.06 - 2.67
$\sin^2\theta_{12}$	$0.306^{+0.018}_{-0.015}$	0.259(0.265) - 0.359(0.364)
$\sin^2\theta_{23}$	$0.42^{+0.08}_{-0.03}$	0.34 - 0.64
$\sin^2\theta_{13}$ [17]	$0.021(0.025)\ ^{+0.007}_{-0.007}$	0.001(0.005) - 0.044(0.050)
$\sin^2\theta_{13}$ [19]	0.0236 ± 0.0042	0.010 - 0.036

3.1 TeV Scale Type I See-Saw Model

3.1.1 The $\mu \to e\gamma$ Decay

In this subsection we update briefly the discussion of the limits on the parameters of the TeV scale type I see-saw model, derived in [62] using the experimental upper bound on the $\mu \to e\gamma$ decay rate obtained in 1999 in the MEGA experiment [114]. After the publication of [62], the MEG collaboration reported a new more stringent upper bound on the $\mu \to e\gamma$ decay rate [37] given in eq. (1.6). Such an update is also necessary in view of the relatively large nonzero value of the reactor angle θ_{13} measured in the Daya Bay and RENO experiments [19, 20]. As was discussed in [62], in particular, the rate of the $\mu \to e\gamma$ decay in the type I see-saw scheme considered can be strongly suppressed for certain values of θ_{13}.

Following eq. (4.3), the $\mu \to e\gamma$ decay branching ratio in the scenario under discussion is given by [58, 59, 85]:

$$\mathrm{BR}(\mu \to e\gamma) = \frac{\Gamma(\mu \to e\gamma)}{\Gamma(\mu \to e + \nu_\mu + \overline{\nu}_e)} \quad = \quad \frac{3\alpha_{\mathrm{em}}}{32\pi} \left|T_{(\mu e)}\right|^2 , \tag{3.2}$$

where α_{em} is the fine structure constant and [62]

$$\left|T_{(\mu e)}\right| \;\cong\; \frac{2+z}{1+z} \left|(RV)^*_{\mu 1}\,(RV)_{e1}\right| \left|G(x) - G(0)\right| . \tag{3.3}$$

In deriving the expression for the matrix element $T_{(\mu e)}$, eq. (3.3), we have used eq. (4.2) and assumed that the difference between M_1 and M_2 is negligibly small and used $M_1 \cong M_2$. It is easy to verify that $G(x)$ (see, eq. (2.43)) is a monotonic function which takes values in the interval $[4/3, 10/3]$, with $G(x) \cong \frac{10}{3} - x$ for $x \ll 1$.

Using the expressions of $|(RV)_{\mu 1}|^2$ and $|(RV)_{e1}|^2$ in terms of neutrino parameters, eqs. (2.28) and (2.29), we obtain the $\mu \to e\gamma$ decay branching ratio for the NH and IH spectra:

$$\begin{aligned} &\textbf{NH}: \;\; \mathrm{BR}(\mu \to e\gamma) \cong \\ &\frac{3\alpha_{\mathrm{em}}}{32\pi} \left(\frac{y^2 v^2}{M_1^2} \frac{m_3}{m_2 + m_3}\right)^2 \left|U_{\mu 3} + i\sqrt{\frac{m_2}{m_3}} U_{\mu 2}\right|^2 \left|U_{e3} + i\sqrt{\frac{m_2}{m_3}} U_{e2}\right|^2 \left[G(X) - G(0)\right]^2 , \end{aligned} \tag{3.4}$$

$$\begin{aligned} &\textbf{IH}: \;\; \mathrm{BR}(\mu \to e\gamma) \cong \\ &\frac{3\alpha_{\mathrm{em}}}{32\pi} \left(\frac{y^2 v^2}{M_1^2} \frac{1}{2}\right)^2 \left|U_{\mu 2} + iU_{\mu 1}\right|^2 \left|U_{e2} + iU_{e1}\right|^2 \left[G(X) - G(0)\right]^2 . \end{aligned} \tag{3.5}$$

The data on the process $\mu \to e\gamma$ set very stringent constraints on the TeV scale type I see-saw mechanism. The upper bound on $\mathrm{BR}(\mu \to e\gamma)$ was obtained in the MEG experiment at PSI [37] and is given in eq. (1.6). It is an improvement by a factor of 21 of the upper limit of the MEGA experiment, published in 1999 [114]. The projected sensitivity of the MEG experiment is $\mathrm{BR}(\mu \to e\gamma) \sim 10^{-13}$ [37, 115]. For $M_1 = 100$ GeV ($M_1 = 1$ TeV) and $z \ll 1$ we get the following upper limit on the product $|(RV)^*_{\mu 1}(RV)_{e1}|$ of the heavy Majorana neutrino couplings to the muon (electron) and the $W^\pm$ boson and to the Z^0 boson from the the upper limit eq. (1.6):

$$\left|(RV)^*_{\mu 1}\,(RV)_{e1}\right| < 0.39 \times 10^{-4}\,(0.15 \times 10^{-4})\,, \tag{3.6}$$

where we have used eqs. (3.2) and (3.3). This can be recast as an upper bound on the neutrino Yukawa coupling y. Taking, *e.g.*, the best fit values of the solar and atmospheric oscillation parameters given in Table 3.1, we get:

$$y \lesssim 0.024\ (0.15)\ \text{ for NH with } M_1 = 100\,\text{GeV}\,(1000\,\text{GeV}) \text{ and } \sin\theta_{13} = 0.1\,, \tag{3.7}$$

$$y \lesssim 0.018\ (0.11)\ \text{ for IH with } M_1 = 100\,\text{GeV}\,(1000\,\text{GeV}) \text{ and } \sin\theta_{13} = 0.1\,. \tag{3.8}$$

The constraints which follow from the current MEG upper bound on $\mathrm{BR}(\mu \to e\gamma)$ will not be valid in the case of a cancellation between the different terms in one of the factors $|U_{\ell 3} + i\sqrt{m_2/m_3}U_{\ell 2}|^2$ and $|U_{\ell 2} + iU_{\ell 1}|^2$, $\ell = e, \mu$, in the expressions (3.4) and (3.5) for $\mathrm{BR}(\mu \to e\gamma)$. Employing the standard parametrisation of U, eqs. (2.30) - (2.32), one can show that in the case of NH spectrum we can have $|U_{e3} + i\sqrt{m_2/m_3}U_{e2}| = 0$ if [62] (see also [63]) $\sin(\delta + (\alpha_{21} - \alpha_{31})/2) = 1$ and $\tan\theta_{13} = (\Delta m^2_\odot/\Delta m^2_{\rm A}\,)^{1/4}\sin\theta_{12}$. Using the 3σ allowed ranges of $\Delta m^2_\odot$, $\Delta m^2_{\rm A}$ and $\sin^2\theta_{12}$ given in Table 3.1, we find that the second condition can be satisfied provided $\sin^2\theta_{13} \gtrsim 0.04$, which lies outside the 3σ range of allowed values of $\sin^2\theta_{13}$ found in the Daya Bay experiment [19] (see eq. (3.1)).

In the case of IH spectrum, the factor $|U_{e2} + iU_{e1}|^2$ can be rather small for $\sin(\alpha_{21}/2) = -1$: $|U_{e2} + iU_{e1}|^2 = c^2_{13}(1 - \sin 2\theta_{12}) \cong 0.0765$, where we have used the best fit values of $\sin^2\theta_{12} = 0.306$ and $\sin^2\theta_{13} = 0.0236$. It is also possible to have a strong suppression of the factor $|U_{\mu 2} + iU_{\mu 1}|^2$ [62]. Indeed, using the standard parametrisation of the matrix U, it is not difficult to show that for fixed values of the angles θ_{12}, θ_{23} and of the phases α_{21} and δ, $|U_{\mu 2} + iU_{\mu 1}|^2$ has a minimum for

$$\sin\theta_{13} \;=\; \frac{c_{23}}{s_{23}}\,\frac{\cos 2\theta_{12}\cos\delta\sin\frac{\alpha_{21}}{2} - \cos\frac{\alpha_{21}}{2}\sin\delta}{1 + 2c_{12}\,s_{12}\,\sin\frac{\alpha_{21}}{2}}\,. \tag{3.9}$$

At the minimum we get:

$$\min\left(|U_{\mu 2}+iU_{\mu 1}|^2\right) \;=\; c_{23}^2\,\frac{\left(\cos\delta\cos\frac{\alpha_{21}}{2}+\cos 2\theta_{12}\sin\delta\sin\frac{\alpha_{21}}{2}\right)^2}{1+2c_{12}\,s_{12}\,\sin\frac{\alpha_{21}}{2}}\,. \tag{3.10}$$

Notice that, from the equation above, the $\mu\to e\gamma$ branching ratio is highly suppressed if the Dirac and Majorana phases take CP conserving values, mainly: $\delta\simeq 0$ and $\alpha_{21}\simeq\pi$. In this case, from eq. (3.9) we get the lower bound $\sin\theta_{13}\gtrsim 0.13$, which is in agreement with the Daya Bay measurement reported in Tab. 3.1. On the other hand, assuming CPV phases, we still may have $\min(|U_{\mu 2}+iU_{\mu 1}|^2)=0$, provided θ_{12} and the Dirac and Majorana phases δ and α_{21} satisfy the following conditions: $\cos\delta\cos(\alpha_{21}/2)+\cos 2\theta_{12}\sin\delta\sin(\alpha_{21}/2)=0$ and $\mathrm{sgn}(\cos\delta\cos\frac{\alpha_{21}}{2})=-\mathrm{sgn}(\sin\delta\sin\frac{\alpha_{21}}{2})$. Taking $\cos\delta>0$ ($\cos\delta<0$) and using $\tan\delta=-\tan(\alpha_{21}/2)/\cos 2\theta_{12}$ in eq. (3.9), we get the relation between s_{13}, δ and $\cos 2\theta_{12}$, for which $\min(|U_{\mu 2}+iU_{\mu 1}|^2)=0$:

$$\sin\theta_{13} \;=\; \frac{c_{23}}{s_{23}}\,\frac{\sqrt{1+\tan^2\delta}\,\cos 2\theta_{12}}{\sqrt{1+\cos^2 2\theta_{12}\,\tan^2\delta}+2c_{12}\,s_{12}\,\mathrm{sgn}(\cos\delta)}\,. \tag{3.11}$$

Using the 3σ intervals of allowed values of $\sin^2\theta_{12}$ and $\sin^2\theta_{23}$ (found with the "new" reactor $\bar\nu_e$ fluxes, see Table 3.1) and allowing δ to vary in the interval $[0,2\pi]$, we find that the values of $\sin\theta_{13}$ obtained using eq. (3.11) lie in the interval $\sin\theta_{13}\gtrsim 0.11$. As it follows from eq. (3.1), we have at 3σ: $0.10\lesssim\sin\theta_{13}\lesssim 0.19$. The values of $0.11\lesssim\sin\theta_{13}\lesssim 0.19$ correspond to $0\leq\delta\lesssim 0.7$. These conclusions are illustrated in Fig. 3.1. For $\sin\theta_{13}$ and δ lying in the indicated intervals we can have $|U_{\mu 2}+iU_{\mu 1}|^2=0$ and thus a strong suppression of the $\mu\to e\gamma$ decay rate. As we will see in subsections 3.1.2 and 3.1.3, in the model we are considering, the predicted $\mu-e$ conversion rate in a given nucleus and $\mu\to 3e$ decay rate are also proportional to $|(RV)^*_{\mu 1}(RV)_{e1}|^2$, as like the $\mu\to e\gamma$ decay rate. This implies that in the case of the TeV scale type I see-saw mechanism and IH light neutrino mass spectrum, if, e.g., $\mathrm{BR}(\mu\to e\gamma)$ is strongly suppressed due to $|U_{\mu 2}+iU_{\mu 1}|^2\cong 0$, the $\mu-e$ conversion and the $\mu\to 3e$ decay rates will also be strongly suppressed [1]. The suppression under discussion cannot hold if, for instance, it is experimentally established that δ is definitely bigger than 1.0. That would be the case if the existing indications [17] that $\cos\delta<0$ receive unambiguous confirmation.

[1] Let us note that in the case of IH spectrum we are discussing actually one has $|(RV)_{\mu 1}|^2\propto|U_{\mu 2}+i\sqrt{m_1/m_2}U_{\mu 1}|^2$ (see eq. (2.29)), with $m_2=\sqrt{|\Delta m^2_{\rm A}|}$ and $m_1=\sqrt{|\Delta m^2_{\rm A}|-\Delta m^2_\odot}\cong\sqrt{|\Delta m^2_{\rm A}|}(1-0.5\Delta m^2_\odot/|\Delta m^2_{\rm A}|)$. Therefore when $|U_{\mu 2}+iU_{\mu 1}|=0$ we still have $|U_{\mu 2}+i\sqrt{m_1/m_2}U_{\mu 1}|^2\neq 0$. However, in this case $|U_{\mu 2}+i\sqrt{m_1/m_2}U_{\mu 1}|^2\cong(\Delta m^2_\odot/(4|\Delta m^2_{\rm A}|))^2|U_{\mu 1}|^2\lesssim 1.7\times 10^{-5}$, where we have used $\delta=0$ (which maximises $|U_{\mu 1}|^2$) and the best fit values of the other neutrino oscillation parameters. Thus, our conclusions about the suppression of $\mathrm{BR}(\mu\to e\gamma)$, the $\mu-e$ conversion and the $\mu\to 3e$ decay rates are still valid.

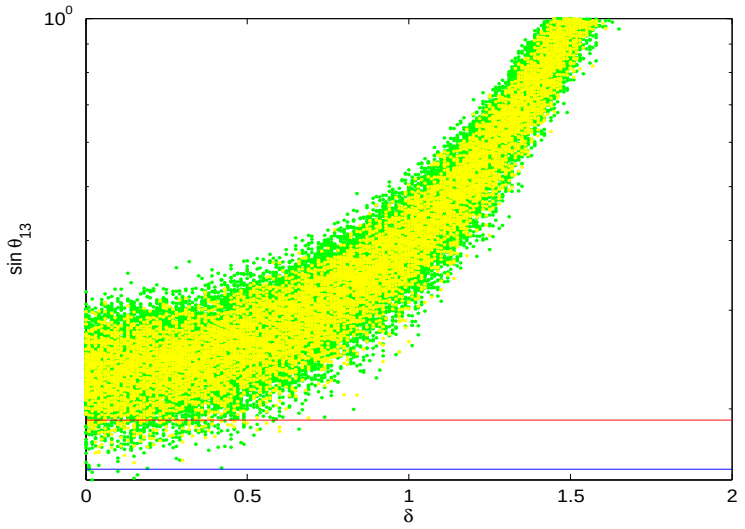

FIGURE 3.1: Values of $\sin\theta_{13}$, as a function of the phase δ in the case of IH light neutrino mass spectrum, which yield a suppressed rate of the process $\mu \to e\gamma$. The values are obtained using eq. (3.11), the 2σ (3σ) intervals of allowed values of $\sin^2\theta_{12}$ and $\sin^2\theta_{23}$, yellow (green) points (found with the "new" reactor $\bar{\nu}_e$ fluxes, see Table 3.1) and allowing δ to vary in the interval $[0,2\pi]$. The red and blue horizontal lines correspond to the 3σ upper limit $\sin\theta_{13} = 0.191$ and the best fit value $\sin\theta_{13} = 0.156$.

The limits on the parameters $|(RV)_{\mu 1}|$ and $|(RV)_{e1}|$, implied by the electroweak precision data, eqs. (2.18) - (2.20), and the upper bound on $\mathrm{BR}(\mu \to e\gamma)$, eq. (1.6), are illustrated in Fig. 3.2. The results shown are obtained for the best fit values of $\sin\theta_{13} = 0.156$ and of the other neutrino oscillation parameters given in Table 3.1.

3.1.2 The $\mu - e$ Conversion in Nuclei

We will discuss next the predictions of the TeV scale type I see-saw extension of the SM for the rate of the $\mu - e$ conversion in nuclei, as well as the experimental constraints that can be imposed on this see-saw scenario by the current and prospective $\mu - e$ conversion data. In the type I see-saw scenario of interest, the $\mu - e$ conversion ratio in a nucleus $\mathcal{N}$ is straightforward from eq. (2.50), then we arrive at the expression [2]:

$$\mathrm{CR}(\mu\mathcal{N} \to e\mathcal{N}) \equiv \frac{\Gamma(\mu\mathcal{N} \to e\mathcal{N})}{\Gamma_{\mathrm{capt}}} = \frac{\alpha_{\mathrm{em}}^5}{2\,\pi^4 \sin^4\theta_W}\,\frac{Z_{eff}^4}{Z}\,\left|F(-m_\mu^2)\right|^2\,\frac{G_F^2 m_\mu^5}{\Gamma_{\mathrm{capt}}} \times \left|(RV)^*_{\mu 1}(RV)_{e1}\right|^2\,|\mathcal{C}_{\mu e}|^2\ , \tag{3.12}$$

[2] In the earlier version of the article [107] we have used the expression for $|\mathcal{C}_{\mu e}|$ found in [116] (in the notations of ref. [117]) in a model with an active heavy Majorana neutrino. It was pointed out in [118], however, that the result for $|\mathcal{C}_{\mu e}|$ of [116] is not directly applicable to the case of TeV scale type I see-saw model we are considering. The authors of [118] performed a detailed calculation of $|\mathcal{C}_{\mu e}|$ in the model of interest and obtained a new expression for $|\mathcal{C}_{\mu e}|$. We have performed an independent calculation of the factor $|\mathcal{C}_{\mu e}|$ in the model under discussion. Our result for $|\mathcal{C}_{\mu e}|$ coincides with that derived in [118].

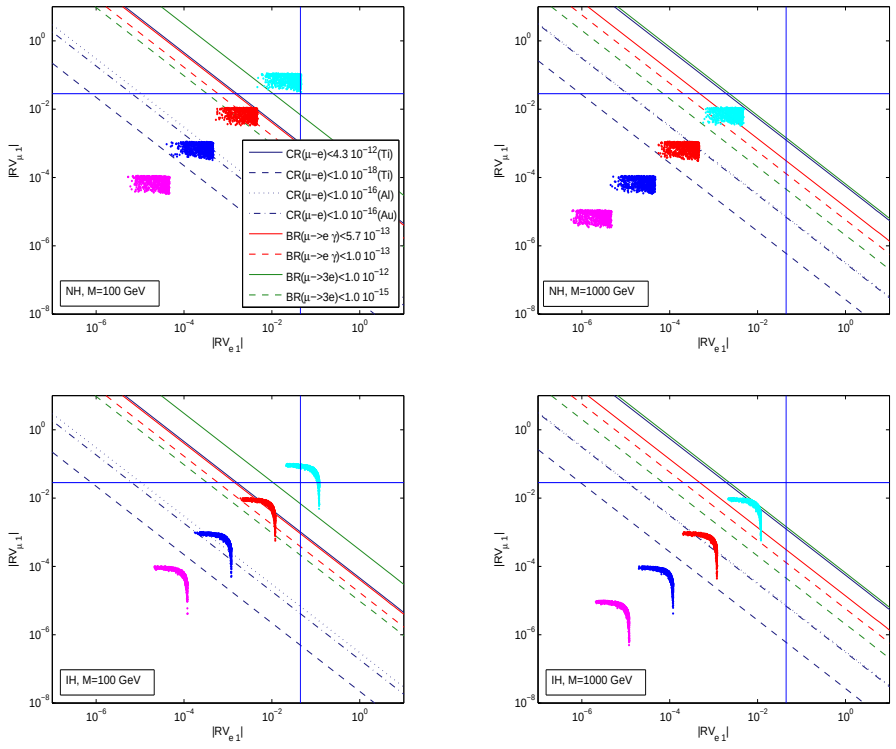

FIGURE 3.2: Correlation between $|(RV)_{e1}|$ and $|(RV)_{\mu 1}|$ in the case of NH (upper panels) and IH (lower panels) light neutrino mass spectrum, for $M_1 = 100\,(1000)$ GeV and, *i*) $y = 0.0001$ (magenta points), *ii*) $y = 0.001$ (blue points), *iii*) $y = 0.01$ (red points) and *iv*) $y = 0.1$ (cyan points), while neutrino oscillation parameters are varying in the 3σ allowed ranges. The constraints from several LFV processes discussed in the text are shown.

where $\Gamma_{\rm capt}$ is the total muon capture rate, the loop integral factor

$$\mathcal{C}_{\mu e} \cong Z\left[2F_u^{(\mu e)}(x) + F_d^{(\mu e)}(x)\right] + N\left[F_u^{(\mu e)}(x) + 2F_d^{(\mu e)}(x)\right], \tag{3.13}$$

$$F_q^{(\mu e)}(x) = Q_q \sin^2\theta_W \left[F_\gamma(x) - F_z^{(\mu e)}(x) + G_\gamma(x)\right] + \frac{1}{4}\left[2I_3 F_z^{(\mu e)}(x) + F_B^{(\mu eqq)}(x)\right], \tag{3.14}$$

$$F_z^{(\mu e)}(x) = F_z(x) + 2G_z(0,x), \quad F_{Box}^{(\mu euu)}(x) = F_{Box}(x,0) - F_{Box}(0,0), \tag{3.15}$$

$$F_{Box}^{(\mu edd)}(x) = F_{XBox}(x,0) - F_{XBox}(0,0), \tag{3.16}$$

and $x = M_1^2/M_w^2$.

In the following we will present the results for three nuclei which were used in the past, and are of interest for possible future $\mu - e$ conversion experiments: $^{48}_{22}$Ti, $^{27}_{13}$Al and $^{197}_{79}$Au. For these nuclei, one has, respectively: i) $Z_{eff} = 17.6;\ 11.62\ ;\ 33.64$, ii) $F(q^2 = -m_\mu^2) \approx 0.54;\ 0.64;\ 0.20$, and iii) $\Gamma_{\rm capt} = 2.59;\ 0.69;\ 13.07 \times 10^6\,{\rm sec}^{-1}$ [43].

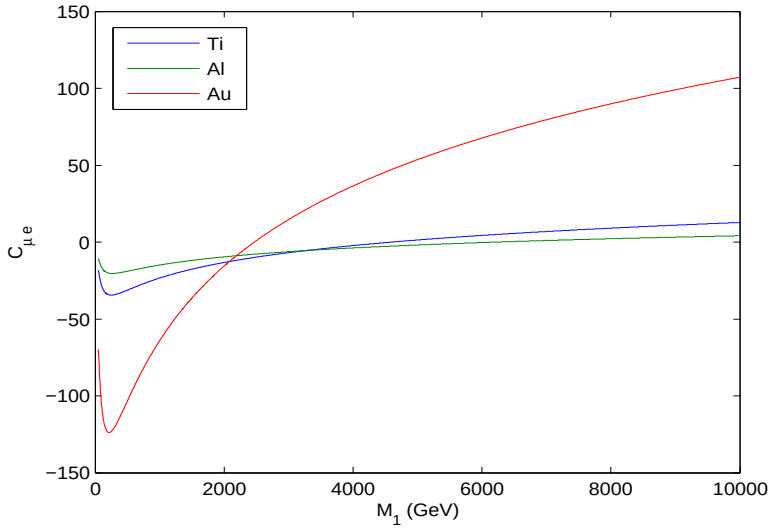

FIGURE 3.3: The $\mu - e$ conversion loop integration factor $C_{\mu e}$ versus the see-saw mass scale M_1, for three different nuclei: *i*) $^{48}_{22}$Ti (blue line), *ii*) $^{27}_{13}$Al, (green line), and *iii*) $^{197}_{79}$Au (red line).

The dependence of the loop integration factor $\mathcal{C}_{\mu e}$ on the see-saw mass scale M_1 for the three nuclei of interest is shown in Fig. 3.3. The first feature to notice is that $|\mathcal{C}_{\mu e}|$ for $^{48}_{22}$Ti, $^{27}_{13}$Al and $^{197}_{79}$Au has maxima $|\mathcal{C}_{\mu e}| = 34.4;\ 20.4;\ 124$ at $M_1 = 250;\ 267;\ 214$ GeV, respectively. At $M_1 = 250$ GeV, $|\mathcal{C}_{\mu e}|$ for $^{27}_{13}$Al and $^{197}_{79}$Au takes the values $|\mathcal{C}_{\mu e}(\mathrm{Al})| \cong 20.4$ and $|\mathcal{C}_{\mu e}(\mathrm{Au})| \cong 123.1$; at $M_1 = 267$ GeV, we have $|\mathcal{C}_{\mu e}(\mathrm{Ti})| \cong 34.4$ and $|\mathcal{C}_{\mu e}(\mathrm{Au})| \cong 122.4$; and finally, at $M_1 = 214$ GeV, we find $|\mathcal{C}_{\mu e}(\mathrm{Ti})| \cong 34.3$ and $|\mathcal{C}_{\mu e}(\mathrm{Al})| \cong 20.2$. These maxima of $|\mathcal{C}_{\mu e}|$ give the biggest enhancement factors for the conversion rate when $M_1 \leq 1000$ GeV. Beside the maxima, $|\mathcal{C}_{\mu e}|$ goes through zero at $M_1 = 4595;\ 6215;\ 2470$ GeV for $^{48}_{22}$Ti, $^{27}_{13}$Al and $^{197}_{79}$Au, respectively, as was noticed also in [118].

Qualitatively, the dependence of the factor $|\mathcal{C}_{\mu e}|$ defined in eq. (3.15) on M_1 exhibits the same features as the factor $|\mathcal{C}_{\mu e}|$ derived in [116], namely [107], at goes through zero at a certain value of $M_1 = M_1^0(\mathcal{N})$ which depends on the nucleus $\mathcal{N}$ and is a monotonically increasing function of M_1 in the interval [50 GeV, 10^4 GeV] when M_1 decreases (increases) starting from the value $M_1 = M_1^0(\mathcal{N})$. The values of $M_1^0(\mathcal{N})$ at which $|\mathcal{C}_{\mu e}|$ given in (3.15)) and that obtained in [116] are zero differ roughly by a factor of 10 to 20, depending on the nucleus $\mathcal{N}$.

For M_1 lying inside the interested interval (100 - 1000) GeV, the loop integration factor $|\mathcal{C}_{\mu e}|$ takes rather large values for each of the three nuclei. As our calculations show, $|\mathcal{C}_{\mu e}|$ is not smaller than 23.4 for the Ti and 14.9 for the Al, while for the Au nucleus it exceeds 64.1. Since the $\mu - e$ conversion rate is enhanced by the factor $|\mathcal{C}_{\mu e}|^2$, it is

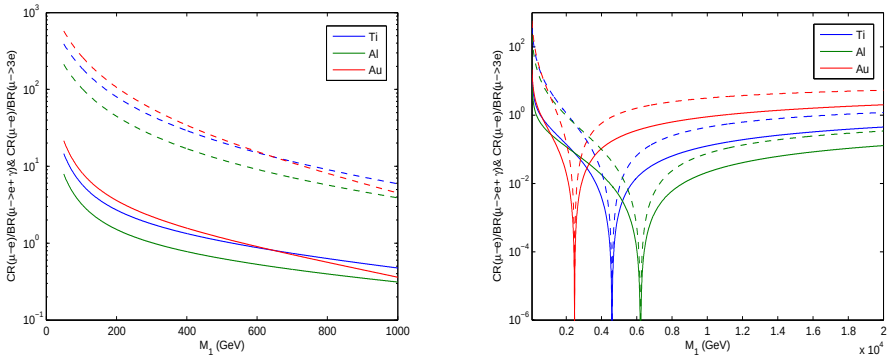

FIGURE 3.4: The ratio of the $\mu - e$ relative conversion rate and the branching ratio of the i) $\mu \to e\gamma$ decay (solid lines), ii) $\mu \to 3e$ decay (dashed lines), versus the type I see-saw mass scale M_1, for three different nuclei: $^{48}_{22}$Ti (blue lines), $^{27}_{13}$Al (green lines) and $^{197}_{79}$Au (red lines).

very sensitive to the product $|(RV)^*_{\mu 1}(RV)_{e1}|$ of CC couplings of the heavy Majorana neutrinos to the electron and muon for the values of M_1 in the interval of interest.

The best experimental upper bound on the conversion rate is [39]: $\mathrm{CR}(\mu\,\mathrm{Ti} \to e\,\mathrm{Ti}) \lesssim 4.3 \times 10^{-12}$. This bound implies a constraint on $|(RV)^*_{\mu 1}(RV)_{e1}|$, which is shown in Fig. 3.2 for $M_1 = 100;\ 1000$ GeV. It is quite remarkable that, as Fig. 3.2 shows, the constraint on the product of couplings $|(RV)^*_{\mu 1}(RV)_{e1}|$ implied by the best experimental upper limit on $\mathrm{CR}(\mu\,\mathrm{Ti} \to e\,\mathrm{Ti})$ and $\mathrm{BR}(\mu \to e\gamma)$ are almost the same for $M_1 = 100$ GeV although the experimental upper limits for $\mathrm{BR}(\mu \to e\gamma)$ is about 4 time more stringent than those for $\mathrm{BR}(\mu \to e\gamma)$ and the expression for $\mathrm{CR}(\mu\,\mathrm{Ti} \to e\,\mathrm{Ti})$ has an additional factor of $\alpha = 1/137$ with respect to the expression for $\mathrm{BR}(\mu \to e\gamma)$. For $M_1 = 1000$ GeV, the constraint from $\mathrm{BR}(\mu \to e\gamma)$ is more stringent.

Future experimental searches for $\mu - e$ conversion in $^{48}_{22}$Ti can reach the sensitivity of $\mathrm{CR}(\mu\,\mathrm{Ti} \to e\,\mathrm{Ti}) \approx 10^{-18}$ [43]. Therefore, for values of M_1 outside the narrow intervals quoted above for which the loop integration factor $|\mathcal{C}_{\mu e}|$ is strongly suppressed, an upper bound on the $\mu - e$ conversion ratio of $\mathcal{O}(10^{-18})$ can be translated into the following stringent constraint on the heavy Majorana neutrino CC couplings to the muon and electron:

$$\left|(RV)^*_{\mu 1}(RV)_{e1}\right| \lesssim 2.17 \times 10^{-8}\ (2.63 \times 10^{-8}) \quad \text{for} \quad M_1 \approx 100\ (1000)\ \ \mathrm{GeV}\,. \tag{3.17}$$

As being noticed earlier, the two parameters of the type I see-saw model considered, the mass scale M_1 and the Yukawa coupling y, can be determined, in principle, from data on $\mathrm{BR}(\mu \to e\gamma)$ (or $\mathrm{BR}(\mu \to 3e)$) and $\mathrm{CR}(\mu\,\mathrm{Ti} \to e\,\mathrm{Ti})$ if the two processes will be observed. Actually, the ratio of the rates of $\mu - e$ conversion in any given nucleus $\mathcal{N}$, $\mathrm{CR}(\mu\mathcal{N} \to e\mathcal{N})$ and of the $\mu \to e\gamma$ decay depends only on the mass (scale) M_1 and

can be used, in principle, to determine the latter. In the case of $\mu - e$ conversion on titanium, for instance, we find:

$$R\left(\frac{\mu - e}{\mu \to e\gamma}\right) \equiv \frac{\mathrm{CR}(\mu\,\mathrm{Ti} \to e\,\mathrm{Ti})}{\mathrm{BR}(\mu \to e\gamma)} \approx 5.95\ (0.48) \quad \text{for} \quad M_1 \approx 100\ (1000)\ \ \mathrm{GeV}\,. \tag{3.18}$$

The correlation between $\mathrm{CR}(\mu\mathcal{N} \to e\mathcal{N})$ and $\mathrm{BR}(\mu \to e\gamma)$ in the model considered is illustrated in Fig. 3.4. The type I see-saw mass scale M_1 would be uniquely determined if $\mu - e$ conversion is observed in two different nuclei or if, e.g., the $\mu \to e\gamma$ decay or $\mu - e$ conversion in a given nucleus is observed and it is experimentally established that $R(\frac{\mu-e}{\mu\to e\gamma}) \lesssim 10^{-3}$. In the latter case M_1 could be determined with a relatively high precision. Furthermore, as Fig. 3.4 indicates, if the RH neutrino mass M_1 lies in the interval $(50 - 1000)$ GeV, M_1 would be uniquely determined provided $R(\frac{\mu-e}{\mu\to e\gamma})$ is measured with a sufficiently high precision.

We also note that the correlation between $\mathrm{CR}(\mu\mathcal{N} \to e\mathcal{N})$ and $\mathrm{BR}(\mu \to e\gamma)$ in the type I see-saw model considered is qualitatively and quantitatively very different from the correlation in models where the $\mu - e$ conversion is dominated by the photon penguin diagram, e.g., the supersymmetric high-scale see-saw model which predicts approximately [119] $\mathrm{CR}(\mu\,\mathrm{Ti} \to e\,\mathrm{Ti}) \approx 5 \times 10^{-3}\,\mathrm{BR}(\mu \to e\gamma)$.

3.1.3 The $\mu \to 3e$ Decay

The $l \to 3l'$ decay branching ratio has been introduced in Subsection 2.1.2 in a type I see-saw mechanism of neutrino mass generation with arbitrary fixed number of heavy RH neutrinos. After adapting the result for $\mu \to 3e$ decay in the scenario considered with two approximately equal mass heavy neutrinos N_1 and N_2, we find in the model of interest to the leading order in the small parameters $|(RV)_{l1}|$:

$$\mathrm{BR}(\mu \to 3e) = \frac{\alpha_{em}^2}{16\pi^2 \sin^4\theta_W} \left|(RV)^*_{\mu 1}(RV)_{e1}\right|^2 |C_{\mu 3e}(x)|^2\,, \tag{3.19}$$

$$\begin{aligned} |C_{\mu 3e}(x)|^2 = {} & 2\left|\frac{1}{2}F_B^{\mu 3e} + F_z^{\mu 3e} - 2\sin^2\theta_W(F_z^{\mu 3e} - F_\gamma)\right|^2 + 4\sin^4\theta_W \left|F_z^{\mu 3e} - F_\gamma\right|^2 \\ & + 16\sin^2\theta_W \left[(F_z^{\mu 3e} + \frac{1}{2}F_B^{\mu 3e})G_\gamma\right] - 48\sin^4\theta_W \left[(F_z^{\mu 3e} - F_\gamma^{\mu 3e})G_\gamma\right] \\ & + 32\sin^4\theta_W |G_\gamma|^2 \left(\log\frac{m_\mu^2}{m_e^2} - \frac{11}{4}\right)\,, \end{aligned} \tag{3.20}$$

where $F_\gamma(x)$, $G_\gamma(x)$, $F_z(x)$, $G_z(x,y)$, $F_{XBox}(x,y)$ can be found in (A.27), (A.28), (A.54), (A.56), (A.72), and

$$F_z^{\mu 3e}(x) = F_z(x) + 2G_z(0,x), \quad F_B^{\mu 3e}(x) = -2(F_{XBox}(0,x) - F_{XBox}(0,0)). \tag{3.21}$$

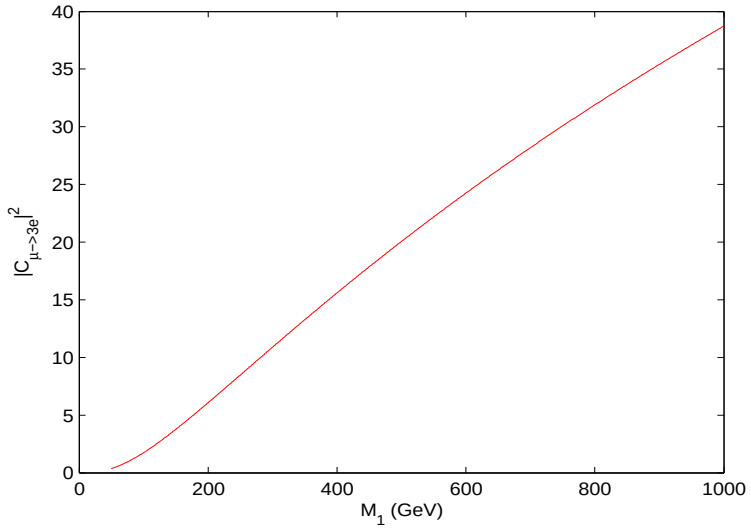

FIGURE 3.5: The $\mu \to 3e$ decay rate factor $|C_{\mu 3e}|^2$ as a function of the see-saw mass scale M_1.

The dependence of the $\mu \to 3e$ decay rate factor $|C_{\mu 3e}|^2$ on the type I see-saw mass scale M_1 is shown in Fig. 3.5. At $M_1 = 100$ (1000) GeV we have: $|C_{\mu 3e}|^2 \cong 1.75$ (38.73), i.e., $|C_{\mu 3e}|^2$ increases by a factor of 22 when M_1 changes from 100 GeV to 1000 GeV. Using the quoted values of $|C_{\mu 3e}|^2$ we get the following constraint from the current limit on BR($\mu \to 3e$), eq. (1.7):

$$\left|(RV)^*_{\mu 1}(RV)_{e1}\right| \lesssim 3.01 \times 10^{-4}\ (6.39 \times 10^{-5}) \quad \text{for} \quad M_1 = 100\ (1000)\ \text{GeV}\,. \tag{3.22}$$

Thus, for $M_1 = 100$ (1000) GeV the constraint on $|(RV)^*_{\mu 1}(RV)_{e1}|$ obtained using the current experimental upper limit on BR($\mu \to 3e$) is by a factor of 7.7 (4.3) less stringent than that obtained from the current upper limit on BR($\mu \to e\gamma$) (see eq. (3.6)), respectively. In conclusion, for $M_1 = 100$ GeV, the upper limit on $|(RV)^*_{\mu 1}(RV)_{e1}|$ from the current experimental bound on the $\mu - e$ conversion and $\mu \to e\gamma$ decay, are similar qualitative; while for $M_1 = 1000$ GeV, the most stringent constraint is from $\mu \to e\gamma$ current upper bound. This is clearly seen in Fig. 3.2. It follows also from Fig. 3.2 that an experiment sensitive to a $\mu - e$ conversion rate CR($\mu\,\mathrm{Al} \to e\,\mathrm{Al}$) $\approx 10^{-16}$, will probe smaller values of the product of couplings $|(RV)^*_{\mu 1}(RV)_{e1}|$ than an experiment sensitive to BR($\mu \to 3e$) $= 10^{-15}$.

In Fig. 3.4 we show the correlation between CR($\mu\mathcal{N} \to e\mathcal{N}$) and BR($\mu \to 3e$) in the TeV scale see-saw model considered. As it follows from Fig. 3.4, the observation of the $\mu \to 3e$ decay or of the $\mu - e$ conversion in a given nucleus, combined with data on the ratio CR($\mu\mathcal{N} \to e\mathcal{N}$)/BR($\mu \to 3e$) would lead either to a unique determination of the type I see-saw scale M_1, or to two values, or else to a relatively narrow interval of values,

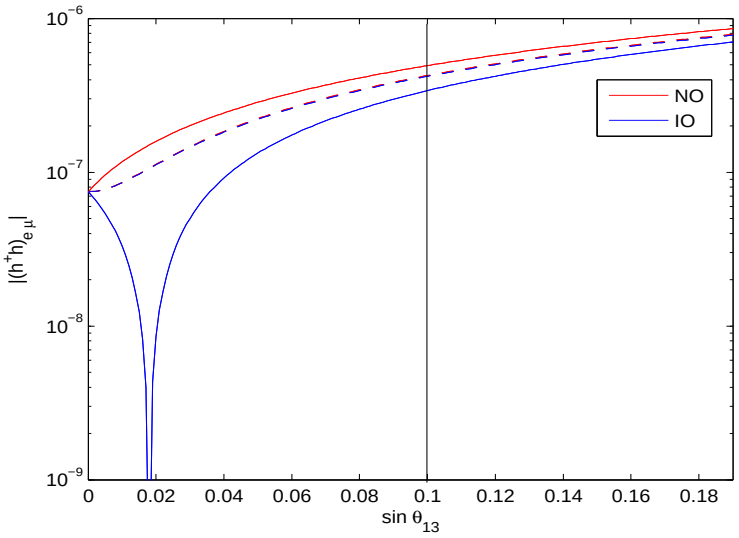

FIGURE 3.6: The dependence of $|(h^\dagger h)_{e\mu}|$ on $\sin\theta_{13}$ for $v_\Delta = 9.5$ eV and $\delta = 0$ (solid lines) and $\delta = \pi/2$ (dashed line). The other neutrino oscillation parameters are set to their best fit values given in Table 3.1. The vertical line corresponds to the current 3σ allowed minimal value of $\sin\theta_{13}$ (see eq. (3.1)).

of M_1 compatible with the data. One can get the same type of information on the scale M_1 from data on the ratio $\mathrm{BR}(\mu \to 3e)/\mathrm{BR}(\mu \to e\gamma)$, provided at least one of the two decays $\mu \to e\gamma$ and $\mu \to 3e$ is observed.

It should be added finally that for $M_1 \gtrsim 100$ GeV we have: $\mathrm{BR}(\mu \to 3e)/\mathrm{BR}(\mu \to e\gamma) \gtrsim 0.031$. Thus, if it is experimentally established that $\mathrm{BR}(\mu \to 3e)/\mathrm{BR}(\mu \to e\gamma)$ is definitely smaller than the quoted lower bound, the model considered with $M_1 \gtrsim 100$ GeV will be ruled out. Such a result would be consistent also just with a see-saw scale $M_1 < 100$ GeV.

3.2 TeV Scale Type II See-Saw Model

3.2.1 The $\mu \to e\gamma$ Decay

The $\mu \to e\gamma$ decay branching ratio in the case under discussion is taken from (2.61):

$$\mathrm{BR}(\mu \to e\gamma) \;\cong\; \frac{\alpha_{\mathrm{em}}}{192\,\pi}\,\frac{\left|\left(h^\dagger h\right)_{e\mu}\right|^2}{G_F^2}\left(\frac{1}{m^2_{\Delta^+}} + \frac{8}{m^2_{\Delta^{++}}}\right)^2 . \tag{3.23}$$

For $m_{\Delta^+} \cong m_{\Delta^{++}} \equiv M_\Delta$, the upper limit on BR($\mu \to e\gamma$) reported by the MEG experiment, eq. (1.6), implies the following upper bound on $|(h^\dagger h)_{e\mu}|$:

$$\left|\left(h^\dagger h\right)_{e\mu}\right| \;<\; 2.8 \times 10^{-6} \left(\frac{M_\Delta}{100\,\text{GeV}}\right)^2 . \tag{3.24}$$

One can use this upper bound, in particular, to obtain a lower bound on the vacuum expectation value of Δ^0, v_Δ [3]. Indeed, from eq. (2.55) it is not difficult to get:

$$\left|\left(h^\dagger h\right)_{e\mu}\right| = \frac{1}{4v_\Delta^2}\left|U_{e2}\,U_{2\mu}^\dagger\,\Delta m^2_{21} + U_{e3}\,U_{3\mu}^\dagger\,\Delta m^2_{31}\right| , \tag{3.25}$$

where we have used the unitarity of U. The above expression for $|(h^\dagger h)_{e\mu}|$ is exact. It follows from eq. (3.25) that the prediction for $|(h^\dagger h)_{e\mu}|$, and thus for BR($\mu \to e\gamma$), depends, in general, on the Dirac CPV phase δ of the standard parametrisation of the PMNS matrix U (see eq. (2.30)). For the best fit values of $\sin^2\theta_{13} = 0.0236$ and of the other neutrino oscillation parameters listed in Table 3.1, the term $\propto \Delta m^2_{21}$ in eq. (3.25) is approximately a factor of 10 smaller than the term $\propto \Delta m^2_{31}$. In this case, BR($\mu \to e\gamma$) exhibits a relatively weak dependence on the type of the neutrino mass spectrum and on the Dirac phase δ. Neglecting the term $\propto \Delta m^2_{21}$, we obtain from (3.24) and (3.25):

$$v_\Delta > 2.98 \times 10^2 \left|s_{13}\,s_{23}\,\Delta m^2_{31}\right|^{\frac{1}{2}} \left(\frac{100\,\text{GeV}}{M_\Delta}\right) \cong 4.30\,\text{eV} \left(\frac{100\,\text{GeV}}{M_\Delta}\right) . \tag{3.26}$$

For the 3σ allowed ranges of values of $\sin^2 2\theta_{13}$ given in eq. (3.1) and of the other neutrino oscillation parameters quoted in Table 3.1, the absolute lower bound on v_Δ corresponds approximately to $v_\Delta > 2.1$ eV $(100\,\text{GeV})/M_\Delta$ and is reached in the case of $\Delta m^2_{31} > 0$ ($\Delta m^2_{31} < 0$) for $\delta = \pi$ (0).

We note further that if $\delta \cong \pi/2$ ($3\pi/2$), the term $\propto \Delta m^2_{21}$ in the expression for $|(h^\dagger h)_{e\mu}|$ (and thus for BR($\mu \to e\gamma$)) always plays a subdominant role as long as the other neutrino oscillation parameters lie in their currently allowed 3σ ranges. Therefore in this case the dependence of BR($\mu \to e\gamma$) on the type of neutrino mass spectrum is negligible. The specific features of the predictions for $|(h^\dagger h)_{e\mu}|$ discussed above are illustrated in Fig. 3.6.

Exploiting the fact that $v_\Delta^2|(h^\dagger h)_{e\mu}|$ is known with a rather good precision, we can write:

$$\text{BR}(\mu \to e\gamma) \cong 2.7 \times 10^{-10} \left(\frac{1\,\text{eV}}{v_\Delta}\right)^4 \left(\frac{100\,\text{GeV}}{M_\Delta}\right)^4 , \tag{3.27}$$

where we have used eq. (3.23) and the best fit values of the neutrino oscillation parameters. It follows from eq. (3.27) that for the values of v_Δ and M_Δ (or m_{Δ^+} and/or $m_{\Delta^{++}}$)

[3] This was noticed also in [120].

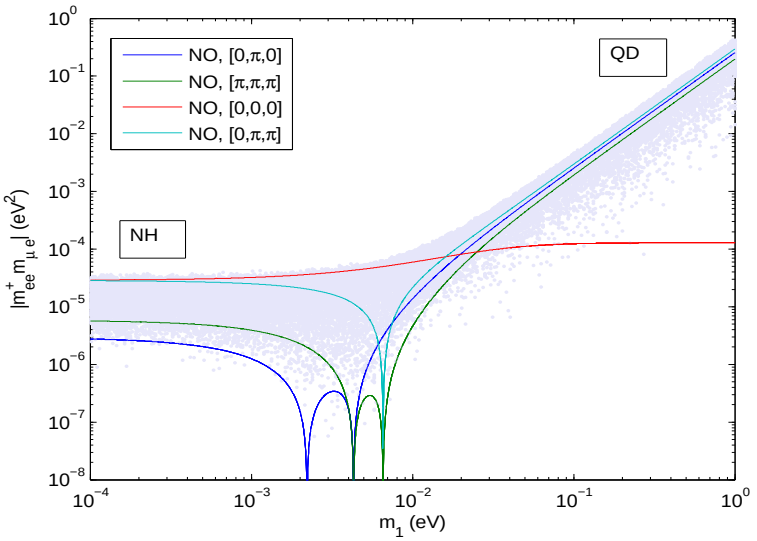

FIGURE 3.7: The dependence of $|m^*_{ee}m_{\mu e}|$ on the lightest neutrino mass m_1 in the case of neutrino mass spectrum with normal ordering ($\Delta m^2_{\rm A} > 0$), for four sets of values of the Dirac and the two Majorana CPV phases, $[\delta, \alpha_{21}, \alpha_{31}]$. The depicted curves correspond to the best fit values of $\sin\theta_{13}$ (eq. (3.1)) and of the other neutrino oscillation parameters given in Table 3.1. The scattered points are obtained by varying the neutrino oscillation parameters within their corresponding 3σ intervals and giving random values to the CPV Dirac and Majorana phases.

of interest, BR($\mu \to e\gamma$) can have a value within the projected sensitivity of the ongoing MEG experiment.

3.2.2 The $\mu \to 3e$ Decay

Let us start this subsection by writing down the $\mu \to 3e$ decay branching ratio in the scenario of Tev scale type II seesaw from the general case, which was expressed in eq. (2.62)

$$\text{BR}(\mu \to 3e) = \frac{1}{G_F^2}\frac{|(h^\dagger)_{ee}(h)_{\mu e}|^2}{m^4_{\Delta^{++}}} = \frac{1}{G_F^2\, m^4_{\Delta^{++}}}\frac{|m^*_{ee}\, m_{\mu e}|^2}{16\, v^4_\Delta}\,, \tag{3.28}$$

where we have used eq. (2.54). From the present limit BR($\mu \to 3e$) $< 10^{-12}$, one can obtain the following constraint on $|(h^\dagger)_{ee}(h)_{\mu e}|$:

$$|(h^\dagger)_{ee}(h)_{\mu e}| < 1.2 \times 10^{-7} \left(\frac{m_{\Delta^{++}}}{100\,\text{GeV}}\right)^2 . \tag{3.29}$$

In the model under discussion, BR($\mu \to 3e$) depends on the factor $|m^*_{ee}m_{\mu e}|$, which involves the product of two elements of the neutrino Majorana mass matrix, on the neutrino mass spectrum and on the Majorana and Dirac CPV phases in the PMNS matrix U. For the values of m_{Δ^+} and $m_{\Delta^{++}}$ in the range of $\sim (100 - 1000)$ GeV and of $v_\Delta \ll 1$ MeV of interest, m_{ee} practically coincides with the effective Majorana mass in

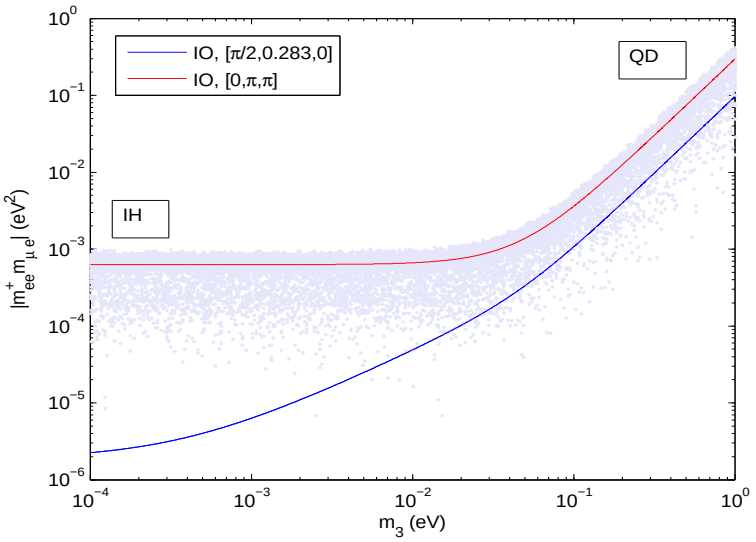

FIGURE 3.8: The same as in Fig. 3.7 in the case of a light neutrino mass spectrum with inverted ordering ($\Delta m^2_{\rm A} < 0$) (see text for details).

neutrinoless double beta ($(\beta\beta)_{0\nu}$-) decay (see, e.g., [28, 121–124]), $\langle m \rangle$:

$$|m_{ee}| = \left| \sum_{j=1}^{3} m_j U^2_{ej} \right| \cong |\langle m \rangle| \,. \tag{3.30}$$

Depending on the type of neutrino mass spectrum, the value of the lightest neutrino mass and on the values of the CPV Majorana and Dirac phases in the PMNS matrix, $|m_{ee}|$ can take any value between 0 and m_0, where $m_0 = m_1 \cong m_2 \cong m_3$ is the value of the neutrino masses in the case of quasi-degenerate (QD) spectrum, $m_0 \gtrsim 0.1$ eV (see, e.g., [121–123]). It follows from the searches for the $(\beta\beta)_{0\nu}$-decay that $|m_{ee}| \lesssim m_0 \lesssim 1$ eV, while the cosmological constraints on the sum of the neutrino masses imply $m_0 \lesssim 0.3$ eV (see, e.g., [1]). As is well known, the $(\beta\beta)_{0\nu}$-decay is claimed to have been observed in [125, 126], with the reported half-life corresponding to [126] $|m_{ee}| = 0.32 \pm 0.03$ eV. This claim will be tested in a new generation of $(\beta\beta)_{0\nu}$-decay experiments which either are already taking data or are in preparation at present (see, e.g., [1, 29]).

In the case of NH light neutrino mass spectrum with $m_1 \ll 10^{-4}$ eV, $|m_{ee}|$ lies in the interval 3.6×10^{-4} eV $\lesssim |m_{ee}| \lesssim 5.2 \times 10^{-3}$ eV. This interval was obtained by taking into account the 3σ allowed ranges of values of $\sin^2\theta_{13}$ (eq. (3.1)), $\sin^2\theta_{12}$, $\sin^2\theta_{23}$ and $\Delta m^2_{\odot}$ and $\Delta m^2_{\rm A}$. For the best fit values of the latter we get [4]: 1.45×10^{-3} eV $\lesssim |m_{ee}| \lesssim 3.75 \times 10^{-3}$ eV. The minimal and the maximal values correspond to the combination of the CPV phases $(\alpha_{21} - \alpha_{31} + 2\delta) = \pi$ and 0, respectively. However, for $m_1 \gtrsim 10^{-4}$ eV,

[4] The numerical values quoted further in this subsection are obtained for the indicated best fit values of the neutrino oscillation parameters, unless otherwise stated.

one can have $|m_{ee}| = 0$ for specific values of m_1 if the CPV phases α_{21} and $\alpha_{31} - 2\delta$ possess the CP conserving values $\alpha_{21} = \pi$ and $(\alpha_{31} - 2\delta) = 0, \pi$ (see, e.g., [54]): for the $[\pi, 0]$ combination this occurs at $m_1 \cong 2.3 \times 10^{-3}$ eV, while in the case of the $[\pi, \pi]$ one we have $|m_{ee}| = 0$ at $m_1 \cong 6.5 \times 10^{-3}$ eV. If the light neutrino mass spectrum is with inverted ordering ($\Delta m^2_{\rm A} \equiv \Delta m^2_{32} < 0$, $m_3 < m_1 < m_2$) or of inverted hierarchical (IH) type ($m_3 \ll m_1 < m_2$), we have [127] $|m_{ee}| \gtrsim \sqrt{|\Delta m^2_{\rm A}| + m_3^2}\cos 2\theta_{12} \gtrsim 1.27 \times 10^{-2}$ eV, while in the case of QD spectrum, $|m_{ee}| \gtrsim m_0 \cos 2\theta_{12} \gtrsim 2.8 \times 10^{-2}$ eV, where we used the 3σ minimal allowed values of $|\Delta m^2_{\rm A}|$ and $\cos 2\theta_{12}$.

We consider next briefly the dependence of the neutrino mass matrix element $|m_{\mu e}|$ on the type of the neutrino mass spectrum and on the CPV Majorana and Dirac phases. In the case of NH spectrum with $m_1 = 0$, the maximal value of $|m_{\mu e}|$ is obtained for $\alpha_{31} - \alpha_{21} = \delta$, $\delta = \pi$, and reads: $\max(|m_{\mu e}|) \cong 8.1 \times 10^{-3}$ eV. We get $|m_{\mu e}| = 0$ for $\alpha_{21} = \pi$, $\delta = 0$ (π) and $\alpha_{31} = 0$ (π). As can be shown, for each of these two sets of values of the CPV phases, the zeros take place at essentially the same value of $m_1 \cong 4.3 \times 10^{-3}$ eV (Fig. 3.7). If the neutrino mass spectrum is of the IH type with negligible $m_3 \cong 0$, the maximal value of $|m_{\mu e}|$ corresponds to $\delta = 0$ and $\alpha_{21} = \pi$ and is given by $\max(|m_{\mu e}|) \cong \sqrt{|\Delta m^2_{\rm A}|}\, c_{13}(c_{23}\sin 2\theta_{12} + s_{23}s_{13}\cos 2\theta_{12})$. The element $|m_{\mu e}|$ is strongly suppressed, i.e., we have $|m_{\mu e}| \ll \max(|m_{\mu e}|)$, for $\delta \cong \pi/2$ and a value of the Majorana phase α_{21} which is determined by the equation:

$$c_{23}\, c_{12}\, s_{12}\, \sin\alpha_{21} \cong \left(c_{12}^2 + s_{12}^2 \cos\alpha_{21}\right)\, s_{23}\, s_{13}\,. \tag{3.31}$$

For the best fit values of the neutrino mixing angles this equation is satisfied for $\alpha_{21} \cong 0.283$.

The properties of $|m_{ee}|$ and $|m_{\mu e}|$ described above allow us to understand most of the specific features of the dependence of the quantity $|m^*_{ee}m_{\mu e}|$ of interest on the the neutrino mass spectrum and the leptonic CPV phases. For NH spectrum and negligible $m_1 \cong 0$, the maximum of the latter is obtained for $\alpha_{31} - \alpha_{21} = \delta = 0$ and is given by:

$$\max(|m^*_{ee}m_{\mu e}|) = \left|\left(m_2\, s_{12}^2\, c_{13}^2 + m_3\, s_{13}^2\right)\, c_{13}\, (m_2\, s_{12}(c_{12}\, c_{23} - s_{12}\, s_{23}\, s_{13}) + m_3\, s_{23}\, s_{13})\right|\,, \tag{3.32}$$

with $m_2 = \sqrt{\Delta m^2_{\odot}}$ and $m_3 = \sqrt{\Delta m^2_{\rm A}}$. Using the best fit values of the neutrino oscillation parameters we get $\max(|m^*_{ee}m_{\mu e}|) \cong 2.9 \times 10^{-5}$ eV^2 (see Fig. 3.7). This implies $\mathrm{BR}(\mu \to 3e) \lesssim 6 \times 10^{-9}(1\ \mathrm{eV}/v_\Delta)^4(100\ \mathrm{GeV}/m_{\Delta^{++}})^4$. In the case of NH spectrum and non-negligible m_1 we have $|m^*_{ee}m_{\mu e}| = 0$ for the values of the CPV phases and m_1 discussed above, for which either $|m_{ee}| = 0$ or $|m_{\mu e}| = 0$. The scattered points in Fig. 3.7 correspond to the possible values the quantity $|m^*_{ee}m_{\mu e}|$ can assume when varying

the neutrino oscillation parameters within their corresponding 3σ intervals and giving random values to the CPV Dirac and Majorana phases from the interval [0,2π].

The maximum of $|m_{ee}m_{\mu e}|$ for the IH spectrum with a negligible m_3 is reached for $\delta = 0$ and $\alpha_{21} = \pi$, and reads:

$$\max(|m^*_{ee}m_{\mu e}|) \cong \left|\Delta m^2_{\rm A}\right| \, c^3_{13} \left(\frac{1}{2}\, c_{23} \, \sin 4\theta_{12} + s_{23}\, s_{13} \, \cos^2 2\theta_{12}\right) . \tag{3.33}$$

Numerically this gives $\max(|m_{ee}m_{\mu e}|) \cong 6.1 \times 10^{-4}$ eV^2 (Fig. 3.8). For BR($\mu \to 3e$) we thus obtain: BR($\mu \to 3e$) $\lesssim 2.4 \times 10^{-6}(1 \text{ eV}/v_\Delta)^4(100 \text{ GeV}/m_{\Delta^{++}})^4$. One can have $|m_{ee}m_{\mu e}| \ll \max(|m_{ee}m_{\mu e}|)$ in the case of IH spectrum with $m_3 = 0$ for, e.g., $\delta \cong \pi/2$ and $\alpha_{21} \cong 0.283$, for which $|m_{\mu e}|$ has a minimum. For the indicated values of the phases we find: $|m_{ee}m_{\mu e}| \cong 1.2 \times 10^{-6}$ eV^2 (see Fig. 3.8). Similarly to the case of a neutrino mass spectrum with normal ordering discussed above, we show in Fig. 3.8 the range of values the LFV term $|m_{ee}m_{\mu e}|$ can assume (scattered points).

Finally, in the case of QD spectrum, $|m_{ee}m_{\mu e}|$ will be relatively strongly suppressed with respect to its possible maximal value for this spectrum (i.e., we will have $|m_{ee}m_{\mu e}| \ll \max(|m^*_{ee}m_{\mu e}|)$) if, e.g., the Majorana and Dirac phases are zero, thus conserving the CP symmetry: $\alpha_{21} = \alpha_{31} = \delta = 0$. Then one has: $|m_{ee}m_{\mu e}| \cong |\Delta m^2_{\rm A}| s_{13}s_{23}c_{13}/2 \cong 1.2 \times 10^{-4}$ eV^2. Note that this value is still larger than the maximal value of $|m_{ee}m_{\mu e}|$ for the NH neutrino mass spectrum with a negligible m_1 (see Fig. 3.7). The maximum of $|m_{ee}m_{\mu e}|$ takes place for another set of CP conserving values of the Majorana and Dirac phases: $\alpha_{21} = \alpha_{31} = \pi$ and $\delta = 0$. At the maximum we have:

$$\max(|m^*_{ee}m_{\mu e}|) \cong m_0^2 \, \left(c^3_{13} \, \cos 2\theta_{12} - s^2_{13}\right) \, c_{13} \, \left(c_{23} \, \sin 2\theta_{12} + 2\, c^2_{12} s_{23}\, s_{13}\right) \, , \;\; m_0 \gtrsim 0.1 \text{ eV} \, . \tag{3.34}$$

For the best fit values of the neutrino mixing angles we get $\max(|m^*_{ee}m_{\mu e}|) \cong 0.3\, m_0^2$. For $m_0 \lesssim 0.3$ eV this implies $\max(|m^*_{ee}m_{\mu e}|) \lesssim 2.7 \times 10^{-2}$ eV^2, leading to an upper bound on BR($\mu \to 3e$), which is by a factor approximately of 4.1×10^3 larger than in the case of IH spectrum.

The features of $|m_{ee}m_{\mu e}|$ discussed above are illustrated in Figs. 3.7 and 3.8.

It should be clear from the preceding discussion that in the case of the type II see-saw model considered, the value of the quantity $|(h^\dagger)_{ee}(h)_{\mu e}|^2 \propto |m^*_{ee}m_{\mu e}|^2$, and thus the prediction for BR($\mu \to 3e$), depends very strongly on the type of neutrino mass spectrum. For a given spectrum, it exhibits also a very strong dependence on the values of the Majorana and Dirac CPV phases α_{21}, α_{31} and δ, as well as on the value of the lightest neutrino mass, $\min(m_j)$. As a consequence, the prediction for BR($\mu \to 3e$) for given v_Δ and $m_{\Delta^{++}}$ can vary by a few to several orders of magnitude when one varies the

values of $\min(m_j)$ and of the CPV phases. Nevertheless, for all possible types of neutrino mass spectrum - NH, IH, QD, etc., there are relatively large regions of the parameter space of the model where $\mathrm{BR}(\mu \to 3e)$ has a value within the sensitivity of the planned experimental searches for the $\mu \to 3e$ decay [45]. The region of interest for the NH spectrum is considerably smaller than those for the IH and QD spectra. In the case NO spectrum ($\Delta m^2_{\mathrm{A}} > 0$), $\mathrm{BR}(\mu \to 3e)$ can be strongly suppressed for certain values of the lightest neutrino mass m_1 from the interval $\sim (2 \times 10^{-3} - 10^{-2})$ eV (Fig. 3.7). For the IO spectrum ($\Delta m^2_{\mathrm{A}} < 0$), a similar suppression can take place for $m_3 \ll 10^{-2}$ eV (Fig. 3.8). In the cases when $|m^*_{ee} m_{\mu e}|^2$ is very strongly suppressed, the one-loop corrections to the $\mu \to 3e$ decay amplitude should be taken into account since they might give a larger contribution than that of the tree level diagram we are considering. The analysis of this case, however, is beyond the scope of the present investigation.

3.2.3 The $\mu - e$ Conversion in Nuclei

Using the formula (2.64) and assuming that $m_{\Delta^+} \cong m_{\Delta^{++}} \equiv M_\Delta$, the conversion rate can be written as

$$\mathrm{CR}(\mu\mathcal{N} \to e\mathcal{N}) \;\cong\; \frac{\alpha^5_{\mathrm{em}}}{36\,\pi^4}\,\frac{m^5_\mu}{\Gamma_{\mathrm{capt}}}\,Z^4_{eff}\,Z\,F^2(-m^2_\mu)\,\left|C^{(II)}_{\mu e}\right|^2 , \tag{3.35}$$

where

$$C^{(II)}_{\mu e} \equiv \frac{1}{4v^2_\Delta}\left[\frac{29}{24}\left(m^\dagger\, m\right)_{e\mu} + \sum_{l=e,\mu,\tau} m^\dagger_{el}\, f(r, s_l)\, m_{l\mu}\right] , \tag{3.36}$$

$r = m^2_\mu/M^2_\Delta$, $s_l = m^2_l/M^2_\Delta$ and we have used eq. (2.54).

The upper limit on the $\mu - e$ conversion rate in Ti, eq. (1.8), leads to the following upper limit on $|C^{(II)}_{\mu e}|$:

$$|C^{(II)}_{\mu e}| < 1.24 \times 10^{-4}\,\left(\frac{M_\Delta}{100\,\mathrm{GeV}}\right)^2 . \tag{3.37}$$

In obtaining it we have used the values of Γ_{capt}, Z_{eff}, Z and $F(-m^2_\mu)$ for Ti given in subsection 3.1.2. An experiment sensitive to $\mathrm{CR}(\mu\,\mathrm{Ti} \to e\,\mathrm{Ti}) \approx 10^{-18}$ [43] will be able to probe values of $|C^{(II)}_{\mu e}| \gtrsim 5.8 \times 10^{-8}\ (M_\Delta/(100\,\mathrm{GeV}))^2$.

The $\mu - e$ conversion rate in a given nucleus depends through the quantity $C^{(II)}_{\mu e}$, on the type of neutrino mass spectrum and the Majorana and Dirac CPV phases in the PMNS matrix. Using the best fit values of the the neutrino oscillation parameters and performing a scan over the values of the CPV phases and the lightest neutrino mass, which in the cases of NO ($\Delta m^2_{\mathrm{A}} > 0$) and IO ($\Delta m^2_{\mathrm{A}} < 0$) spectra was varied in the intervals $(10^{-4} - 1)$ eV and $(10^{-5} - 1)$ eV, respectively, we have identified the possible ranges of values of $4v^2_\Delta |C^{(II)}_{\mu e}|$. The latter are shown in Figs. (3.9) and (3.10).

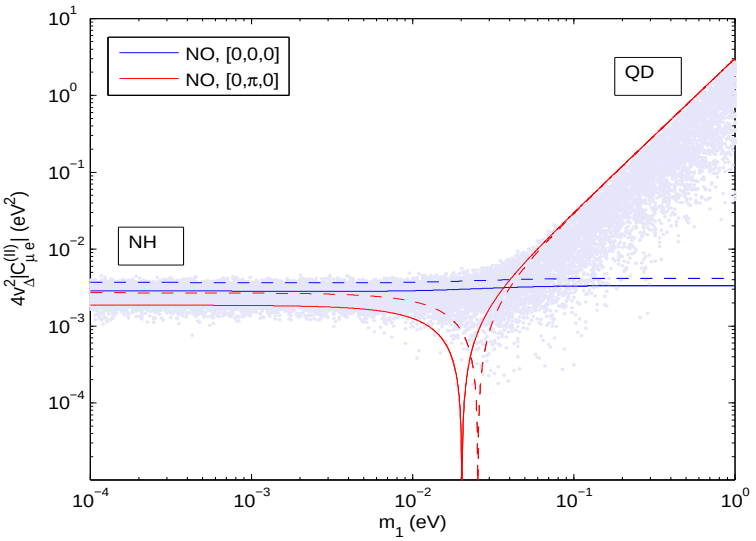

FIGURE 3.9: The dependence of $4v_\Delta^2|C_{\mu e}^{(II)}|$ (given in eV^2) on the lightest neutrino mass m_1 in the case of neutrino mass spectrum with normal ordering ($\Delta m^2_{\rm A} > 0$), for two sets of values of the Dirac and the two Majorana CPV phases, $[\delta, \alpha_{21}, \alpha_{31}]$ and $M_\Delta = 200$ (1000) GeV, plain (dashed) curves. The figure is obtained for the best fit values of $\sin\theta_{13}$ (eq. (3.1)) and of the other neutrino oscillation parameters given in Table 3.1 (see text for details).

For $M_\Delta = 200$ (1000) GeV and NH spectrum with negligible m_1 ($m_1 \ll 10^{-3}$ eV), the maximal value of $4v_\Delta^2|C_{\mu e}^{(II)}|$ occurs for $[\delta, \alpha_{21}, \alpha_{31}] = [0, 0, 0]$ and at the maximum we have $4v_\Delta^2|C_{\mu e}^{(II)}| \cong 2.9\ (3.8) \times 10^{-3}$ eV^2. For values of the CPV phases $[\delta, \alpha_{21}, \alpha_{31}] = [0, \pi, 0]$ and $M_\Delta = 200$ GeV, $4v_\Delta^2|C_{\mu e}^{(II)}|$ goes through zero at $m_1 \cong 2 \times 10^{-2}$ eV (Fig. 3.9). In the case of a larger charged scalar mass, *i.e.* $M_\Delta = 1000$ GeV, such cancellation occurs at a different value of the lightest neutrino mass, mainly $m_1 = 0.025$ eV.

The maximum of $4v_\Delta^2|C_{\mu e}^{(II)}|$ in the case of IH spectrum with negligible m_3, occurs for maximal CPV phases: $[\delta, \alpha_{21}, \alpha_{31}] = [\pi/2, 3\pi/2, 0]$. At the maximum in this case one has $4v_\Delta^2|C_{\mu e}^{(II)}| \cong 6\ (7) \times 10^{-3}$ eV^2 for $M_\Delta = 200$ (1000) GeV. As Fig. 3.10 shows, for other sets of values of the CPV phases, $4v_\Delta^2|C_{\mu e}^{(II)}|$ can be much smaller. Taking again CP conserving phases, *e.g.* $[\pi, \pi, 0]$, one can get a strong suppression of the branching ratio for $m_3 = 7.2\ (15) \times 10^{-3}$ eV and $M_\Delta = 200$ (1000) GeV. Allowing $\sin\theta_{13}$ to take values other than the best fit one, we find that $4v_\Delta^2|C_{\mu e}^{(II)}|$ can even go through zero at, e.g., $[\delta, \alpha_{21}, \alpha_{31}] = [\pi, \pi, \pi/2]$ for $\sin\theta_{13} \cong 0.137$, which lies within the 2σ allowed region. In Fig. 3.10 we report other examples in which the CPV phases in the PMNS matrix take different sets of CP violating values and the quantity $4v_\Delta^2|C_{\mu e}^{(II)}|$ (and the conversion rate) can vary by several orders of magnitude for specific values of the lightest neutrino mass m_3 and the see-saw mass scale M_Δ.

If the neutrino mass spectrum is quasi-degenerate, $m_{1,2,3} \cong m_0 \gtrsim 0.1$ eV, we have for

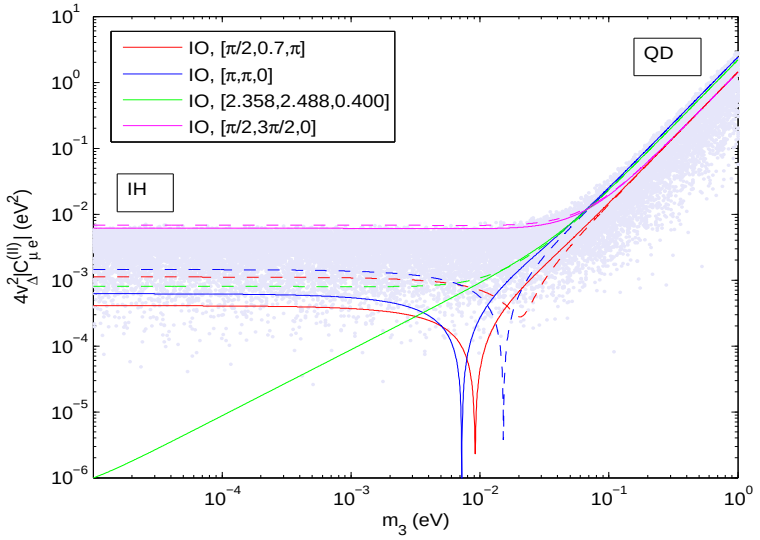

FIGURE 3.10: The same as in Fig. 3.9 in the case of a light neutrino mass spectrum with inverted ordering.

$m_0 \lesssim 0.3$ eV: 2.8×10^{-3} eV$^2 \lesssim 4v_\Delta^2|C_{\mu e}^{(II)}| \lesssim 0.4$ eV^2. The minimal value corresponds to $\Delta m^2_{\rm A} > 0$ (NO spectrum) and $[\delta, \alpha_{21}, \alpha_{31}] = [\pi, 0, 0]$; for *e.g.* $[\delta, \alpha_{21}, \alpha_{31}] = [0, 0, 0]$ and $M_\Delta = 200$ GeV we get in the QD region $4v_\Delta^2|C_{\mu e}^{(II)}| \cong 3.3 \times 10^{-3}$ eV^2 (Fig. 3.9).

Finally, the scattered points in Figs. 3.9 and 3.10 are obtained by varying all the neutrino oscillation parameters within the corresponding 3σ intervals and allowing for arbitrary values of the Dirac and Majorana phases in the interval [0,2π].

We remark that the previous estimates, as well as Figs 3.9 and 3.10, were realized under the assumption that the singly- and doubly-charged scalars have masses of the same order, *i.e.* $m_{\Delta^+} \cong m_{\Delta^{++}} \equiv M_\Delta$. The case in which the dominant contribution to the conversion amplitude is provided by the exchange of Δ^{++}, *i.e.* for $m_{\Delta^+} \gg m_{\Delta^{++}} \gtrsim 100$ GeV, shows similar features: the upper limits of the conversion ratio in the cases of NO and IO spectra are unchanged and a strong suppression can occur for specific values of the CPV phases and min(m_j). Taking, instead, the opposite limit $m_{\Delta^{++}} \gg m_{\Delta^+}$, with $m_{\Delta^+} = (100-1000)$ GeV, the dominant contribution to the $\mu-e$ conversion amplitude is given by the exchange of the singly-charged scalar, therefore we have: $|C_{\mu e}^{(II)}| \propto |(h^\dagger h)_{e\mu}|$. As it was pointed out in subsection 3.2.1, $|(h^\dagger h)_{e\mu}|$ shows a relative weak dependance on the type of neutrino mass spectrum and on the CPV phases in the PMNS matrix. Moreover, no suppression of the conversion amplitude occurs if $\sin\theta_{13}$ is taken within the current 3σ experimental bound (see Fig. 3.6). In this case, from the best experimental upper bound on the conversion rate in Ti, CR(μ Ti $\to e$ Ti) $< 4.3 \times 10^{-12}$, we get the constraint:

$$|(h^\dagger h)_{e\mu}| \;<\; 6 \times 10^{-4} \left(\frac{m_{\Delta^+}}{100\,\text{GeV}}\right)^2 , \tag{3.38}$$

which provides a weaker bound with respect to that obtained from the $\mu \to e\gamma$ decay (see eq. (3.24)). A $\mu - e$ conversion experiment sensitive to *i.e.* $\mathrm{CR}(\mu\,\mathrm{Ti} \to e\,\mathrm{Ti}) \approx 10^{-18}$, can probe values of $|(h^\dagger h)_{e\mu}|$ which are by a factor 2×10^3 smaller and could set the limit:

$$|(h^\dagger h)_{e\mu}| \;<\; 3 \times 10^{-7} \left(\frac{m_{\Delta^+}}{100\,\mathrm{GeV}}\right)^2 . \tag{3.39}$$

3.3 TeV Scale Type III See-Saw Model

In this section, we are going to study briefly the $\mu \to e\gamma$, $\mu \to 3e$ decays and the $\mu \to e$ conversion in the scenario of type III see-saw model, which has been introduced in section 2.3.

3.3.1 The $\mu \to e\gamma$ Decay

Charged lepton radiative decays receive additional contributions with respect to the scenario with singlet RH neutrinos, due to the presence of new lepton flavour violating interactions in the low energy effective Lagrangian (see eqs. (2.71) and (2.73)). Following the computation reported in [111], we have for the $\mu \to e\gamma$ decay branching ratio in the present scenario:

$$\mathrm{BR}(\mu \to e\gamma) \;=\; \frac{3\alpha_{\mathrm{em}}}{32\pi}\,|T|^2\,, \tag{3.40}$$

where the amplitude T is given by

$$T \;\cong\; -2\left(\frac{13}{3} + \mathcal{C}\right)\eta_{\mu e} \;+\; \sum_k (RV)_{ek}(RV)^*_{\mu k}\,\left[\,A(x_k) + B(y_k) + C(z_k)\,\right]\,, \tag{3.41}$$

with $x_k = (M_k/M_W)^2$, $y_k = (M_k/M_Z)^2$, $z_k = (M_k/M_H)^2$ and $\mathcal{C} \simeq -6.56$. The loop functions $A(x_k)$, $B(y_k)$ and $C(z_k)$ read [111]:

$$A(x) \;=\; \frac{-30 \,+\, 153\,x \,-\, 198\,x^2 \,+\, 75\,x^3 \,+\, 18\,(4 - 3\,x)\,x^2\,\log x}{3(x-1)^4}\,, \tag{3.42}$$

$$B(y) \;=\; \frac{33 \,-\, 18\,y \,-\, 45\,y^2 \,+\, 30\,y^3 \,+\, 18\,(4 - 3\,y)\,y\,\log y}{3(y-1)^4}\,, \tag{3.43}$$

$$C(z) \;=\; \frac{-7 \,+\, 12\,z \,+\, 3\,z^2 \,-\, 8\,z^3 \,+\, 6\,(3\,z - 2)\,z\,\log z}{3(z-1)^4}\,. \tag{3.44}$$

In the simple scenario of degenerate fermion triplets with an overall mass scale $\overline{M}$ we obtain taking $M_H = 125$ GeV:

$$T/\eta_{\mu e} \;\cong\; 11.6\;(5.2)\,, \quad \text{for} \quad \overline{M} = 100\;(1000)\;\mathrm{GeV}\,. \tag{3.45}$$

$\mathcal{N}$	$D\ m_\mu^{-5/2}$	$V^{(p)}\ m_\mu^{-5/2}$	$V^{(n)}\ m_\mu^{-5/2}$	$\Gamma_{\rm capt}\ (10^6\,{\rm s}^{-1})$
$^{48}_{22}$Ti	0.0864	0.0396	0.0468	2.590
$^{27}_{13}$Al	0.0362	0.0161	0.0173	0.7054
$^{197}_{79}$Au	0.189	0.0974	0.146	13.07

TABLE 3.2: Nuclear parameters related to $\mu - e$ conversion in $^{48}_{22}$Ti, $^{27}_{13}$Al and $^{197}_{79}$Au. The numerical values of the overlap integrals D, $V^{(p)}$ and $V^{(n)}$ are taken from [87].

For $\overline{M} = 100\ (1000)$ GeV, the current best upper limit on the $\mu \to e\gamma$ decay branching ratio obtained in the MEG experiment, eq. (1.6), implies the bound:

$$|\eta_{\mu e}| \ < \ 4.4\ (9.7) \times 10^{-6}\,, \quad \text{for} \quad \overline{M} = 100\ (1000)\ \text{GeV}\,. \tag{3.46}$$

If no positive signal will be observed by the MEG experiment, that is if it results that $\text{BR}(\mu \to e\gamma) < 10^{-13}$, the following upper limit on the non-unitarity lepton flavour violating coupling $|\eta_{\mu e}|$ can be set:

$$|\eta_{\mu e}| \ < \ 2\ (4) \times 10^{-6}\,, \quad \text{for} \quad \overline{M} = 100\ (1000)\ \text{GeV}\,. \tag{3.47}$$

3.3.2 The $\mu \to 3\,e$ and $\mu - e$ Conversion in Nuclei

The effective $\mu - e - Z$ effective coupling in the Lagrangian (2.71) provides the dominant contribution (at tree-level) to the $\mu \to 3e$ decay rate and the $\mu - e$ conversion rate in a nucleus. In the case of the first process we have (see, *e.g.*, [110]):

$$\text{BR}(\mu \to 3e) \ \simeq \ 16\,|\eta_{\mu e}|^2 \left(3\sin^4\theta_W \ - \ 2\sin^2\theta_W \ + \ \frac{1}{2}\right)\,. \tag{3.48}$$

Taking into account the experimental upper limit reported in (1.7), we get the following upper limit on the $\mu - e$ effective coupling:

$$|\eta_{\mu e}| \ < \ 5.6 \times 10^{-7}\,. \tag{3.49}$$

which is a stronger constraint with respect to the one derived from the non-observation of the $\mu \to e\gamma$ decay (see eqs. (3.47) and (3.46)), mediated (at one-loop) by an effective dipole operator.

More stringent constraints on the effective $\mu - e - Z$ coupling can be obtained using the data from the $\mu - e$ conversion experiments. Indeed, according to the general parametrisation given in [87] (see also [111, 128]), we have for the $\mu - e$ conversion ratio in a

nucleus $\mathcal{N}$ with N neutrons and Z protons:

$$\mathrm{CR}(\mu\mathcal{N}\to e\mathcal{N}) \;\cong\; \frac{2\,G_F^2}{\Gamma_{\rm capt}}\,|\mathcal{C}_{\mu e}|^2\,\Big|(2\,g_{LV(u)}+g_{LV(d)})\,V^{(p)}+(g_{LV(u)}+2\,g_{LV(d)})\,V^{(n)}\Big|^2\,, \tag{3.50}$$

where in this case

$$\mathcal{C}_{\mu e} \;\equiv\; 4\,\eta_{\mu e}\,, \tag{3.51}$$

$$V^{(n)} \;\simeq\; \frac{N}{Z}\,V^{(p)}\,,\quad g_{LV(u)} \;=\; 1-\frac{8}{3}s_w^2 \quad\text{and}\quad g_{LV(d)} \;=\; -1+\frac{4}{3}\,s_w^2\,. \tag{3.52}$$

The parameters $D\,m_\mu^{-5/2}$, $V^{(p)}\,m_\mu^{-5/2}$ and $\Gamma_{\rm capt}$ for $^{48}_{22}$Ti, $^{27}_{13}$Al and $^{197}_{79}$Au are given in Table 3.2.

An upper bound on $|\eta_{\mu e}|$ can be derived from the present experimental upper limit on the $\mu-e$ conversion rate in the nucleus of $^{48}_{22}$Ti, $\mathrm{CR}(\mu\,\mathrm{Ti}\to e\,\mathrm{Ti})\lesssim 4.3\times10^{-12}$. From eqs. (3.50)-(3.52) we get:

$$|\eta_{\mu e}| \;\lesssim\; 2.6\times10^{-7}\,. \tag{3.53}$$

If in the $\mu-e$ conversion experiments with $^{48}_{22}$Ti the prospective sensitivity to $\mathrm{CR}(\mu\,\mathrm{Ti}\to e\,\mathrm{Ti})\sim10^{-18}$ will be reached, these experiments will be able to probe values of $|\eta_{\mu e}|$ as small as $|\eta_{\mu e}|\sim1.3\times10^{-10}$.

3.4 Chapter Conclusion

In this chapter, we have performed a detailed analysis of charged lepton flavour violating (LFV) processes – $\mu\to e\gamma$, $\mu\to 3e$ and $\mu-e$ conversion in nuclei – in the context of see-saw type extensions of the Standard Model, in which the scale of new physics Λ is taken in the TeV range, $\Lambda\sim(100-1000)$ GeV. We summarize below the phenomenological implications of a possible observation of the LFV processes given above for each kind of (TeV scale) see-saw extensions of the SM.

Type I see-saw results. In this case, the $\mu\to e\gamma$ and $\mu\to 3e$ decay branching ratios $\mathrm{BR}(\mu\to e\gamma)$ and $\mathrm{BR}(\mu\to 3e)$, and the $\mu-e$ conversion rate in a nucleus $\mathcal{N}$, $\mathrm{CR}(\mu\mathcal{N}\to e\mathcal{N})$, $\mathcal{N}=$ Al, Ti, Au, can have values close to the existing upper limits and within the sensitivity of the ongoing MEG experiment searching for the $\mu\to e\gamma$ decay and the future planned $\mu-e$ conversion and $\mu\to 3e$ decay experiments [41–45]. The relevant LFV observable in the minimal scenario, with the addition of only two RH

neutrinos to the SM particle content, is provided by the quantity $|(RV)^*_{\mu 1}(RV)_{e1}|$, where $(RV)_{\ell j}$ $(j = 1, 2)$ denote the couplings of the fermion singlets to the SM charged leptons (see eqs. (2.28) and (2.29)). If MEG experiment reaches the projected sensitivity and no positive signal will be observed implying that $\mathrm{BR}(\mu \to e\gamma) < 10^{-13}$, there still will be a relatively large interval of values of $|(RV)^*_{\mu 1}(RV)_{e1}|$, as Fig. 3.2 shows, for which the $\mu - e$ conversion and $\mu \to 3e$ decay are predicted to have observable rates in the planned next generation of experiments.

It follows from the analysis performed by us that as a consequence of an accidental cancellation between the contributions due to the different one-loop diagrams in the $\mu - e$ conversion amplitude, the rate of $\mu - e$ conversion in Al and Ti or in Au can be strongly suppressed for certain values of the see-saw scale M_1. As we have seen, this suppression can be efficient either for the conversion in Al and Ti or for the conversion in Au, but not for all the three nuclei, the reason being that the values of M_1 for which it happens in Al and Ti differ significantly from those for which it occurs in Au. In both the cases of Al or Ti and Au, the suppression can be effective only for values of M_1 lying in very narrow intervals (see Figs. 3.3 and 3.4).

In the case of IH light neutrino mass spectrum, all the three LFV observables, $\mathrm{BR}(\mu \to e\gamma)$, $\mathrm{BR}(\mu \to 3e)$ and $\mathrm{CR}(\mu\mathcal{N} \to e\mathcal{N})$, can be strongly suppressed due to the fact that the LFV factor $|(RV)_{\mu 1}|^2 \propto |U_{\mu 2} + i\sqrt{m_1/m_2}U_{\mu 1}|^2 \cong |U_{\mu 2} + iU_{\mu 1}|^2$, in the expressions of the three rates can be exceedingly small. This requires a special relation between the Dirac and the Majorana CPV phases δ and α_{21}, as well as between the neutrino mixing angle θ_{13} and the phase δ (see eq. (3.11)). For the values of $\sin\theta_{13}$ from the current 3σ allowed interval, eq. (3.1), one can have $|U_{\mu 2} + iU_{\mu 1}|^2 \cong 0$ provided $0 \leq \delta \lesssim 0.7$. *A priori* it is not clear why the relations between δ and α_{21}, and between δ and θ_{13}, leading to $|U_{\mu 2} + iU_{\mu 1}|^2 = 0$, should take place (although, in general, it might be a consequence of the existence of an approximate symmetry). The suppression under discussion cannot hold if, for instance, it is experimentally established that δ is definitely bigger than 1.0. That would be the case if the existing indications [17] that $\cos\delta < 0$ receive unambiguous confirmation.

We note finally that for $M_1 \gtrsim 100$ GeV we have: $\mathrm{BR}(\mu \to 3e)/\mathrm{BR}(\mu \to e\gamma) \gtrsim 0.031$. Thus, if it is experimentally established that $\mathrm{BR}(\mu \to 3e)/\mathrm{BR}(\mu \to e\gamma)$ is definetely smaller than the quoted lower bound, the model considered with $M_1 \gtrsim 100$ GeV will be ruled out. Such a result would be consistent also just with a see-saw scale $M_1 < 100$ GeV.

Type II see-saw results. It follows from the results obtained in Section 3.2 that the predictions for the $\mu \to e\gamma$ and $\mu \to 3e$ decay branching ratios, as well as the $\mu - e$

conversion rate in a nucleus $\mathcal{N}$, in the TeV scale type II see-saw scenario considered exhibit, in general, different dependence on the masses of the singly- and doubly-charged Higgs particles Δ^+ and Δ^{++}, which mediate (to leading order) the three processes. For $m_{\Delta^+} \cong m_{\Delta^{++}} \cong M_\Delta$, all the three rates are proportional to M_Δ^{-4}, i.e., they diminish as the 4th power of the see-saw scale when the latter increases.

The matrix of Yukawa couplings $h_{\ell\ell'}$ which are responsible for the LFV processes of interest, is directly related to the neutrino Majorana mass matrix and thus to the PMNS neutrino mixing matrix U. As a consequence, BR($\mu \to e\gamma$), BR($\mu \to 3e$) and CR($\mu\mathcal{N} \to e\mathcal{N}$) depend, in general, on the neutrino mass and mixing parameters, including the CPV phases in U.

To be more specific, BR($\mu \to e\gamma$) does not depend on the Majorana CPV phases and on $\min(m_j)$, and its dependence on the Dirac CPV phase and on the type of neutrino mass spectrum is insignificant. In contrast, both BR($\mu \to 3e$) and CR($\mu\mathcal{N} \to e\mathcal{N}$) exhibit very strong dependence on the type of neutrino mass spectrum and on the values of the Majorana and Dirac CPV phases. As a consequence, the predictions for BR($\mu \to 3e$) and CR($\mu\mathcal{N} \to e\mathcal{N}$) for given M_Δ can vary by several orders of magnitude not only when the spectrum changes from NH (IH) to QD as a function of the lightest neutrino mass, but also when one varies only the values of the CPV phases keeping the type of the neutrino mass spectrum fixed. All the three observables under discussion can have values within the sensitivity of the currently running MEG experiment on the $\mu \to e\gamma$ decay and the planned future experiments on the $\mu \to 3e$ decay and $\mu - e$ conversion. However, for a given see-saw scale in the range of $\sim (100 - 1000)$ GeV, the planned experiments on $\mu - e$ conversion in Al or Ti will provide the most sensitive probe of the LFV Yukawa couplings of the TeV scale type II see-saw model.

Type III see-saw results. Unlike the type I see-saw extension of the SM discussed in Section 3.1, in this scenario we have several − possibly sizable − lepton flavour violating interactions in the low energy effective Lagrangian, due to the higher $SU(2)_L$ representation of the new fermion fields. In particular, FCNCs arise at tree-level from the non-unitarity of the PMNS matrix (see eq. (2.71)). Thus, the effective $\mu - e - Z$ coupling in (2.71) makes it possible an enhancement of at least two orders of magnitude of the rates of $\mu \to e\gamma$, $\mu \to 3e$ and $\mu - e$ conversion with respect to the ones predicted in the type I see-saw scenario, with RH neutrinos taken in the TeV range. Consequently, all the predicted LFV observables may be probed in the related present and future experiments. As in the previous scenarios, the strongest constraint on the flavour structure of this class of models is by far provided by the expected very high

sensitivity reach of $\mu - e$ conversion experiments.

In conclusion, the oncoming combination of data on neutrino oscillations, collider searches and lepton number/flavour violating processes represent an important opportunity to reveal in the next future the fundamental mechanism at the basis of the generation of neutrino masses as well as the underlying physics beyond the standard theory.

Chapter 4

LFV τ Processes in TeV Scale See-saw Type models

4.1 TeV Scale Type I See-Saw Model

4.1.1 The $\tau \to \mu\gamma$ and $\tau \to e\gamma$ Decays

That have been introduced in the Subsection 2.1.2, for convenience, we write down here the ratio $\Gamma(l_\alpha \to l_\beta\gamma)/\Gamma(l_\alpha \to \nu_\alpha l_\beta \overline{\nu}_\beta)$ after adapting the result for the see-saw type I scheme with two heavy neutrinos possessing approximately equal masses:

$$\frac{\Gamma(l_\alpha \to l_\beta\gamma)}{\Gamma(l_\alpha \to \nu_\alpha l_\beta \overline{\nu}_\beta)} = \frac{3\alpha_{\rm em}}{32\pi}|T|^2\,, \tag{4.1}$$

where

$$T \approx 2|(RV)^*_{\beta 1}(RV)_{\alpha 1}|\,|G(x) - G(0)|\,, \tag{4.2}$$

and $G(x)$ was defined in eq. (2.43). The $l_\alpha \to l_\beta\gamma$ decay branching ratio is given by:

$$\mathrm{BR}(l_\alpha \to l_\beta\gamma) = \frac{\Gamma(l_\alpha \to l_\beta\gamma)}{\Gamma(l_\alpha \to \nu_\alpha l_\beta \overline{\nu}_\beta)}\mathrm{Br}(l_\alpha \to \nu_\alpha l_\beta \overline{\nu}_\beta), \tag{4.3}$$

with $\mathrm{BR}(\mu \to \nu_\mu\, e\, \overline{\nu}_e) \approx 1$, $\mathrm{BR}(\tau \to \nu_\tau\, \mu\, \overline{\nu}_\mu) = 0.1739$, and $\mathrm{BR}(\tau \to \nu_\tau\, e\, \overline{\nu}_e) = 0.1782$ [1].

The predictions of the model under discussion for $\mathrm{BR}(\mu \to e\gamma)$ and the constraints on the product of couplings $|(RV)^*_{e1}(RV)_{\mu 1}|$, as well as on the Yukawa coupling y, following from the experimental upper limit on $\mathrm{BR}(\mu \to e\gamma)$, were discussed in detail in [62, 107].

Here we concentrate on the phenomenology of the $\tau \to \mu\gamma$ and $\tau \to e\gamma$ decays. Using the current upper limits on BR($\tau \to \mu\gamma$) and Br($\tau \to e\gamma$) quoted in eqs. (1.9) and (1.10), we obtain the following upper bounds:

$$\tau \to \mu\gamma : \quad |(RV)^*_{\mu 1}(RV)_{\tau 1}| \leq 2.7 \times 10^{-2}\ (0.9 \times 10^{-2}) \quad M_1 = 100\ (1000)\,\text{GeV}\,, \tag{4.4}$$

$$\tau \to e\gamma : \quad |(RV)^*_{e 1}(RV)_{\tau 1}| \leq 2.3 \times 10^{-2}\ (0.8 \times 10^{-2}) \quad M_1 = 100\ (1000)\,\text{GeV}. \tag{4.5}$$

These constraints are weaker than those implied by the limits quoted in eqs. (2.18) - (2.20). The planned experiments at the SuperB factory, which are expected to probe values of BR($\tau \to (\mu, e)\gamma$) $\geq 10^{-9}$, will be sensitive to

$$\tau \to (\mu, e)\gamma : \qquad |(RV)^*_{(\mu,e)1}(RV)_{\tau 1}| \geq 4.0 \times 10^{-3}\ (1.4 \times 10^{-3}) \quad \text{for} \quad M_1 = 100\ (1000)\,\text{GeV}\,. \tag{4.6}$$

The minimal values quoted above are of the same order as the upper limits following from the constraints (2.18) - (2.20).

The τ decay branching ratios of interest depend on the neutrino mixing parameters via the quantity $|(RV)^*_{l1}(RV)_{\tau 1}|$, $l = e, \mu$. In the case of NH neutrino mass spectrum, $|(RV)_{l1}| \propto |U_{l3} + i\sqrt{m_2/m_3}\,U_{l2}|$ is different from zero for any values of the neutrino mixing parameters from their 3σ experimentally determined allowed ranges and for any $l = e$, μ, τ. This implies that there cannot be further suppression of the $\tau \to (\mu, e)\gamma$ decay rates due to a cancellation between the terms in the expressions for $|(RV)_{l1}|$.

In contrast, depending on the values of the Dirac and Majorana CPV phases δ and α_{21} of the PMNS matrix, we can have strong suppression of the couplings $|(RV)_{l1}|$, $l = e, \mu$, which enter into the expressions for BR($\tau \to (\mu, e)\gamma$) if the neutrino mass spectrum is of the IH type [62, 107]. Indeed, in this case we have $|(RV)_{l1}| \propto |U_{l3} + i\,U_{l2}|$, $l = e, \mu, \tau$. For $\alpha_{21} = -\pi$, $|U_{e3} + i\,U_{e2}|$ can be rather small: $|U_{e2} + iU_{e1}|^2 = c^2_{13}(1 - \sin 2\theta_{12}) \cong 0.0765$, where we have used the best fit values of $\sin^2\theta_{12} = 0.307$ and $\sin^2\theta_{13} = 0.0236$. As was shown in Section 3.1, we can have $|U_{\mu 2} + iU_{\mu 1}|^2 = 0$ for specific values of δ lying the interval $0 \leq \delta \lesssim 0.7$. In this case the value of the phases α_{21} is determined by the values of δ and θ_{12}.

We analyse next the possibility of having strongly suppressed coupling $|(RV)_{\tau 1}|^2$, i.e., to have $|(RV)_{\tau 1}|^2 \propto |U_{\tau 2} + iU_{\tau 1}|^2 = 0$, in the case of IH spectrum. The suppression in question can take place if

$$\sin\theta_{13} = \frac{s_{12} - c_{12}\,\sin\frac{\alpha_{21}}{2}}{c_{12}\,\cos\delta + s_{12}\,\sin(\delta + \frac{\alpha_{21}}{2})}\,\tan\theta_{23}\,, \tag{4.7}$$

and if in addition the values of the phases δ and α_{21} are related via the equation:

$$c_{12}\, s_{23}\, \cos\frac{\alpha_{21}}{2} - c_{23}\, s_{13}\left[c_{12}\, \sin\delta - s_{12}\, \cos(\delta + \frac{\alpha_{21}}{2}\right] = 0\,. \tag{4.8}$$

One simple solution to eq. (4.8) obviously is $\delta = \alpha_{21} = \pi$. For these values of δ and α_{21}, eq. (4.7) becomes:

$$\sin\theta_{13} = \frac{c_{12} - s_{12}}{c_{12} + s_{12}}\, \tan\theta_{23}\,. \tag{4.9}$$

Using the the best fit values of $\sin^2\theta_{12}$ and $\sin^2\theta_{23}$ quoted in eq. (1.5), we get from eq. (4.9): $\sin\theta_{13} = 0.162$, which is very close to the best fit value of 0.155 (0.156) quoted in eq. (1.5). For $|U_{\tau 2} + iU_{\tau 1}|^2 \cong 0$, all LFV decays of the τ charged lepton, including $\tau^- \to \mu^- + \mu^+ + \mu^-$, $\tau^- \to \mu^- + e^+ + e^-$, etc., in the TeV scale type I seesaw model we are considering will be strongly suppressed.

4.1.2 The $\tau \to 3\mu$ Decay

We consider next the $\tau \to 3\mu$ decay in the same scenario of the previous subsection, the branching ratio is directly taken from eq. (2.44):

$$\mathrm{BR}(\tau \to 3\mu) = \frac{\alpha_{em}^2}{16\pi^2 \sin^4\theta_W} \left|(RV)^*_{\tau 1}(RV)_{\mu 1}\right|^2 \left|C_{\tau 3\mu}(x)\right|^2 \times \mathrm{BR}(\tau \to \mu\bar{\nu}_\mu\nu_\tau), \tag{4.10}$$

$$\begin{aligned} |C_{\tau 3\mu}(x)|^2 = {} & 2\left|\frac{1}{2}F_B^{\tau 3\mu} + F_z^{\tau 3\mu} - 2\sin^2\theta_W(F_z^{\tau 3\mu} - F_\gamma)\right|^2 + 4\sin^4\theta_W \left|F_z^{\tau 3\mu} - F_\gamma\right|^2 \\ & + 16\sin^2\theta_W\left[(F_z^{\tau 3\mu} + \frac{1}{2}F_B^{\tau 3\mu})G_\gamma\right] - 48\sin^4\theta_W\left[(F_z^{\tau 3\mu} - F_\gamma^{\tau 3\mu})G_\gamma\right] \\ & + 32\sin^4\theta_W|G_\gamma|^2\left(\log\frac{m_\tau^2}{m_\mu^2} - \frac{11}{4}\right)\,. \end{aligned} \tag{4.11}$$

Here

$$F_z^{\tau 3\mu}(x) = F_z(x) + 2G_z(0,x),\;\; F_B^{\tau 3\mu}(x) = -2(F_{XBox}(0,x) - F_{XBox}(0,0)). \tag{4.12}$$

The factor $|C_{\tau 3\mu}(x)|^2$ in the expression for $\mathrm{BR}(\tau \to 3\mu)$ is a monotonically increasing function of the heavy Majorana neutrino mass M_1. The dependence of $|C_{\tau 3\mu}(x)|^2$ on M_1 is shown in Fig. 1. At $M_1 = 100$ (1000) GeV, the function $|C_{\tau 3\mu}(x)|^2$ has values 1.53 (36.85).

The present experimental limit on $\mathrm{BR}(\tau \to 3\mu)$, eq. (1.11), leads to a weaker constraint than that following from the upper limits quoted in eqs. (2.19) and (2.20):

$$|(RV)^*_{\tau 1}(RV)_{\mu 1}| < 1.1 \times 10^{-1}\ (2.3 \times 10^{-2}) \text{ for } \mathrm{M}_1 = 100\ (1000)\ \mathrm{GeV}. \tag{4.13}$$

The next generation of experiments will be sensitive to $\mathrm{BR}(\tau \to 3\mu) \geq 10^{-10}$, and thus to:

$$|(RV)^*_{\tau 1}(RV)_{\mu 1}| \geq 7.7 \times 10^{-3}\ (1.6 \times 10^{-3}) \text{ for } \mathrm{M}_1 = 100\ (1000)\ \mathrm{GeV}\,. \tag{4.14}$$

As we see, in the case of $M_1 = 1000$ GeV, the minimal value of $|(RV)^*_{\tau 1}(RV)_{\mu 1}|$ to which the future planned experiments will be sensitive is of the order of the upper bound on $|(RV)^*_{\tau 1}(RV)_{\mu 1}|$ following from the limits (2.19) and (2.20).

Consider next the dependence of the decay rate on the CPV phases and the neutrino oscillation parameters. In the case of NH mass spectrum we have:

$$\mathrm{BR}(\tau \to 3\mu) \propto |(RV)^*_{\tau 1}(RV)_{\mu 1}|^2 \propto |U_{\tau 3} + i\sqrt{\frac{m_2}{m_3}}U_{\tau 2}|^2\, |U_{\mu 3} + i\sqrt{\frac{m_2}{m_3}}U_{\mu 2}|^2\,. \tag{4.15}$$

Using the best fit values of the neutrino mixing angles and mass squared differences, quoted in eqs. (1.4) and (1.5) and varying the Dirac and Majorana CPV phases in the interval of $[0, 2\pi]$, we find that $|U_{\mu 3} + i\sqrt{m_2/m_3}U_{\mu 2}||U_{\tau 3} + i\sqrt{m_2/m_3}U_{\tau 2}|$ takes values in the interval $(0.31 - 0.59)$. It follows from this result and the inequality (4.14) that the future experiments on the $\tau \to 3\mu$ decay will be sensitive to values of the Yukawa coupling $y \geq 0.10\ (0.46)$ for $M_1 = 100\ (1000)$ GeV. The minimal values in these lower limits are larger than the upper limits on y following from the current upper bound (1.6) on $\mathrm{BR}(\mu \to e + \gamma)$ [107].

A suppression of the $\tau \to 3\mu$ decay rate might occur in the case of IH mass due to possible cancellations between the terms in the factors $|(RV)_{\mu 1}|$ and $|(RV)_{\tau 1}|$, as was discussed in the previous subsection. Using again the best fit values of the neutrino oscillation parameters and varying the leptonic CPV phases in the interval $[0, 2\pi]$, we find $0.003 \leq |U_{\mu 2} + iU_{\mu 1}||U_{\tau 2} + iU_{\tau 1}| \leq 0.51$. Thus, in the case of IH spectrum, the future experiments with sensitivity to $\mathrm{BR}(\tau \to 3\mu) \geq 10^{-10}$ will probe values of $y \geq 0.14\ (0.64)$ for $M_1 = 100\ (1000)$ GeV. Again the minimal values in these lower limits are larger than the upper limits on y following from the current upper bound (1.6) on $\mathrm{BR}(\mu \to e + \gamma)$ [107].

For specific values of, e.g., the CPV phases of the neutrino mixing matrix one can obtain more stringent upper bounds than those already discussed on the branching ratios of the $\tau \to \mu + \gamma$, $\tau \to e + \gamma$ and $\tau \to 3\mu$ decays due to their relation to the $\mu \to e + \gamma$ decay branching ratio and the fact that the latter is severely constrained. Indeed, it follows

from eqs. (4.3), (2.43) and (4.10) that we have:

$$\frac{\mathrm{BR}(\tau \to e+\gamma)}{\mathrm{BR}(\mu \to e+\gamma)} = \frac{|(RV)_{\tau 1}|^2}{|(RV)_{\mu 1}|^2}\, BR(\tau \to e\bar{\nu}_e\nu_\tau)\,, \tag{4.16}$$

$$\frac{\mathrm{BR}(\tau \to \mu+\gamma)}{\mathrm{BR}(\mu \to e+\gamma)} = \frac{|(RV)_{\tau 1}|^2}{|(RV)_{e 1}|^2}\, BR(\tau \to \mu\bar{\nu}_\mu\nu_\tau)\,, \tag{4.17}$$

$$\frac{\mathrm{BR}(\tau \to 3\mu)}{\mathrm{BR}(\mu \to 3e)} = \frac{|(RV)_{\tau 1}|^2}{|(RV)_{e 1}|^2}\, BR(\tau \to \mu\bar{\nu}_\mu\nu_\tau) \;= \frac{\mathrm{BR}(\tau \to \mu+\gamma)}{\mathrm{BR}(\mu \to e+\gamma)}\,, \tag{4.18}$$

$$\frac{\mathrm{BR}(\tau \to 3\mu)}{\mathrm{BR}(\mu \to e+\gamma)} = \frac{\alpha_{em}}{6\pi \sin^4\theta_W}\, \frac{|C_{\tau 3\mu}(x)|^2}{|G(x)-G(0)|^2}\, \frac{|(RV)_{\tau 1}|^2}{|(RV)_{e 1}|^2}\, BR(\tau \to \mu\bar{\nu}_\mu\nu_\tau)\,. \tag{4.19}$$

The explicit expressions for $|(RV)_{l1}|^2$, eqs. (2.28) and (2.29), imply that the ratios of interest in eqs. (4.16) - (4.18) do not depend on the heavy Majorana neutrino mass M_1 and on the Yukawa coupling y and are determined by the values of the neutrino oscillation parameters and of the CPV phases in the neutrino mixing matrix. Using the best fit values quoted in eqs. (1.4) and (1.5) and varying the Dirac and Majorana phases in the interval $[0, 2\pi]$ we obtain in the case of NH neutrino mass spectrum:

$$0.37 \leq \frac{|(RV)_{\tau 1}|^2}{|(RV)_{\mu 1}|^2} \leq 9.06\,, \tag{4.20}$$

$$1.90 \leq \frac{|(RV)_{\tau 1}|^2}{|(RV)_{e 1}|^2} \leq 191.82\,, \tag{4.21}$$

In a similar way, we get in the case of IH neutrino mass spectrum:

$$4.84 \times 10^{-4} \leq \frac{|(RV)_{\tau 1}|^2}{|(RV)_{\mu 1}|^2} \leq 15.13\,, \tag{4.22}$$

$$3.25 \times 10^{-4} \leq \frac{|(RV)_{\tau 1}|^2}{|(RV)_{e 1}|^2} \leq 0.56\,. \tag{4.23}$$

Thus, in the case of the best fit values of the neutrino oscillation parameters we always have

$$\mathrm{BR}(\tau \to e+\gamma) \lesssim 2.67 \times \mathrm{BR}(\mu \to e+\gamma) < 1.52 \times 10^{-12}\,, \tag{4.24}$$

$$\mathrm{BR}(\tau \to \mu+\gamma) \lesssim 33.36 \times \mathrm{BR}(\mu \to e+\gamma) < 1.90 \times 10^{-11}\,, \tag{4.25}$$

where we have used the current upper bound on $\mathrm{BR}(\mu \to e+\gamma)$, eq. (1.6). The limits in eqs. (4.24) and (4.25) correspond respectively to the IH and NH spectra. These values are beyond the expected sensitivity reach of the planned future experiments.

Using the 2σ (3σ) allowed ranges of the neutrino oscillations parameters in the case of NH neutrino mass spectrum we obtain larger intervals of allowed values of the ratios of

interest:

$$NH: \quad 0.26\ (0.08) \leq \frac{|(RV)_{\tau 1}|^2}{|(RV)_{\mu 1}|^2} \leq 14.06\ (16.73)\,, \tag{4.26}$$

$$NH: \quad 1.39\ (0.53) \leq \frac{|(RV)_{\tau 1}|^2}{|(RV)_{e 1}|^2} \leq 497.74\ (980.32)\,. \tag{4.27}$$

The maximal value of $|(RV)_{\tau 1}|^2/|(RV)_{e1}|^2$ correspond to $\sin^2\theta_{12} = 0.275\ (0.259)$, $\sin^2\theta_{23} = 0.359\ (0.348)$, $\sin^2\theta_{13} = 0.0298\ (0.0312)$, $\delta = 0.203\ (0.234)$, $\alpha_{21} = 6.199\ (3.560)$ and $\alpha_{31} = 3.420\ (0.919)$. At these values of the neutrino mixing parameters we have $|(RV)_{\mu 1}|^2|(RV)_{e1}|^2 \cong 6.98 \times 10^{-4}\ (3.41 \times 10^{-4})\, y^4v^4/(16M_1^4)$, $|(RV)_{\tau 1}|^2|(RV)_{\mu 1}|^2 \cong 0.347\ (0.335)\, y^4v^4/(16M_1^4)$. Thus, the bound on $\mathrm{BR}(\mu \to e + \gamma)$, eq. (1.6), is satisfied for $M_1 = 100$ GeV if $y^4v^4/(16M_1^4) \lesssim 2.29\ (4.69) \times 10^{-6}$, and for $M_1 = 1000$ GeV provided $y^4v^4/(16M_1^4) \lesssim 2.68\ (5.48) \times 10^{-7}$. This implies that $|(RV)_{\tau 1}|^2|(RV)_{\mu 1}|^2 \lesssim 7.95\ (15.7) \times 10^{-7}$ if $M_1 = 100$ GeV, and $|(RV)_{\tau 1}|^2|(RV)_{\mu 1}|^2 \lesssim 9.30\ (18.4) \times 10^{-8}$ for $M_1 = 1000$ GeV. The bound for $M_1 = 1000$ GeV is a stronger constraint than that following from the limits (2.19) and (2.20).

Using the inequalities in eqs. (4.26) and (4.27) we obtain:

$$\mathrm{BR}(\tau \to e + \gamma) \lesssim 2.50\ (2.98) \times \mathrm{BR}(\mu \to e + \gamma) < 1.43\ (1.70) \times 10^{-12}\,, \tag{4.28}$$

$$\mathrm{BR}(\tau \to \mu + \gamma) \lesssim 86.56\ (170.48) \times \mathrm{BR}(\mu \to e + \gamma) < 4.93\ (9.72) \times 10^{-11}\,. \tag{4.29}$$

These are the maximal values of $\mathrm{BR}(\tau \to e + \gamma)$ and $\mathrm{BR}(\tau \to \mu + \gamma)$, allowed by the current upper bound on the $\mu \to e + \gamma$ decay rate in the TeV scale type I seesaw model considered and in the case of NH neutrino mass spectrum. If the $\tau \to e + \gamma$ and/or $\tau \to \mu + \gamma$ decays are observed to proceed with branching ratios which are larger than the bounds quoted above and it is established that the neutrino mass spectrum is of the NH type, the model under discussion will be strongly disfavored, if not ruled out.

Performing a similar analysis in the case of IH spectrum by employing the 2σ (3σ) allowed ranges of the neutrino oscillations parameters we get:

$$IH: \quad 0.0\ (0.0) \leq \frac{|(RV)_{\tau 1}|^2}{|(RV)_{\mu 1}|^2} < \infty\ (\infty)\,, \tag{4.30}$$

$$IH: \quad 0.0\ (0.0) \leq \frac{|(RV)_{\tau 1}|^2}{|(RV)_{e 1}|^2} \leq 0.64\ (0.83)\,. \tag{4.31}$$

The infinity in eq. (4.30) corresponds to $|(RV)_{\mu 1}| = 0$, $|(RV)_{\tau 1}| \neq 0$, i.e., to very strongly suppressed $\mathrm{BR}(\mu \to e + \gamma)$ and $\mathrm{BR}(\tau \to \mu + \gamma)$. One obtains $|(RV)_{\mu 1}| = 0$ for the following values of the neutrino mixing angles from the 2σ allowed intervals, and of the CPV phases: $\sin^2\theta_{12} = 0.340$, $\sin^2\theta_{23} = 0.547$, $\sin^2\theta_{13} = 0.0239$, $\delta = 6.185$, $\alpha_{21} = 3.077$ and $\alpha_{31} = 4.184$ (i.e., $\delta \cong 2\pi$, $\alpha_{21} \cong \pi$ and $\alpha_{31} \cong 1.3\pi$). For $|(RV)_{\mu 1}| = 0$, the branching

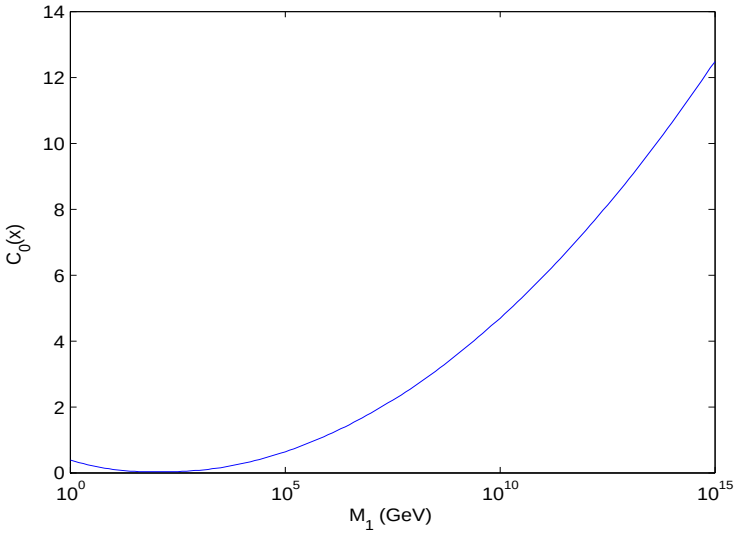

FIGURE 4.1: The dependence of $C_0(x)$ as a function of the see-saw mass scale M_1.

ratios BR($\tau \to e + \gamma$) and BR($\mu \to e + \gamma$) are "decoupled". Correspondingly, the upper bound on BR($\tau \to e + \gamma$) is determined in this case by the limits quoted in eqs. (2.18) and (2.20) and has already been discussed by us.

Using the same strategy and eq. (4.18), we obtain the constraint on BR($\tau \to 3\mu$) following from the upper bound on BR($\mu \to 3e$) at the best fit values, 2σ (3σ) allowed ranges of the neutrino oscillation parameters:

$$\text{BR}(\tau \to 3\mu) \lesssim 33.36 \times \text{BR}(\mu \to 3e) < 3.34 \times 10^{-11}\,, \tag{4.32}$$

$$\text{BR}(\tau \to 3\mu) \lesssim 86.56\ (170.48) \times \text{BR}(\mu \to 3e) < 8.66\ (17.0) \times 10^{-11}\,. \tag{4.33}$$

The relation between BR($\tau \to 3\mu$) and BR($\mu \to e\gamma$) is somewhat less straightforward, since it involves the M_1 dependent factor $C_0(x)$:

$$C_0(x) = \frac{\alpha_{em}}{6\pi \sin^4\theta_W} \frac{|C_{\tau 3\mu}(x)|^2}{|G(x) - G(0)|^2}. \tag{4.34}$$

For 50 GeV $\leq M_1 \leq$ 1000 GeV, $C_0(x)$ has its maximum of 0.0764 at $M_1 = 1000$ GeV. This leads to

$$\text{BR}(\tau \to 3\mu) \lesssim 2.55 \times \text{BR}(\mu \to e + \gamma) < 1.45 \times 10^{-12}\,, \tag{4.35}$$

$$\text{BR}(\tau \to 3\mu) \lesssim 6.61\ (13.02) \times \text{BR}(\mu \to e + \gamma) < 3.77\ (7.42) \times 10^{-12}\,. \tag{4.36}$$

Thus, for M_1 having a value in the interval [50, 1000] GeV, the branching ratio BR($\tau \to 3\mu$) is predicted to be beyond the sensitivity reach of $\sim 10^{-10}$ of the planned next generation experiment. The observation of the $\tau \to 3\mu$ decay with a branching ratio

BR($\tau \to 3\mu$) which is definitely larger than the upper bounds quoted in eq. (4.36) would strongly disfavor (if not rule out) the TeV scale type I seesaw model under discussion with $M_1 \sim (50 - 1000)$ GeV.

It should be added that for $M_1 \geq 10^3$ GeV, the factor $C_0(x)$ is a monotonically (slowly) increasing function of M_1 (see Fig. 4.1). The upper bound on BR($\tau \to 3\mu$) following from the upper bound on BR($\mu \to e + \gamma$) and the 3σ ranges of the neutrino oscillation parameters, can be bigger than 10^{-10} if $C_0(x) \geq 1.8$, which requires $M_1 \geq 8.5 \times 10^6$ GeV. However, the rates of the processes of interest scale as $\propto (v/M_1)^4$ and at values of $M_1 \geq 8.5 \times 10^6$ GeV are too small to be observed in the currently planned experiments.

4.2 TeV Scale Type II See-Saw Model

4.2.1 The $\tau \to \mu\gamma$ and $\tau \to e\gamma$ Decays

In this part, we consider the $\tau \to (\mu,\ e) + \gamma$ decays in the type II see-saw scheme with equal masses $m_{\Delta^+} \approx m_{\Delta^{++}}$. For $m_{\Delta^+} \approx m_{\Delta^{++}} = M_\Delta$, the expression in eq. (2.61) can be cast in the form:

$$\text{BR}(\ell \to \ell' + \gamma) = \frac{27\alpha_{\rm em}}{64\,\pi} \frac{\left|(m^\dagger m)_{\ell\ell'}\right|^2}{16 v_\Delta^4\, G_F^2\, M_\Delta^4} \text{BR}(\ell \to \nu_\ell\, \ell'\, \overline{\nu}_{\ell'})\,, \tag{4.37}$$

where $\ell = \mu$ and $\ell' = e$, or $\ell = \tau$ and $\ell' = \mu, e$.

The factor $|(m^\dagger m)_{\ell\ell'}|$, as it is not difficult to show, is given by:

$$|\left(m^\dagger\, m\right)_{\ell\ell'}| = |U_{\ell 2} U^*_{\ell' 2} \Delta m^2_{21} + U_{\ell 3} U^*_{\ell' 3} \Delta m^2_{31}|\,, \tag{4.38}$$

where we have used eqs. (2.54) and (2.55) and the unitarity of the PMNS matrix. The expression in eq. (4.38) is exact. Obviously, $|(m^\dagger\, m)_{\ell\ell'}|$ does not depend on the Majorana phases present in the PMNS matrix U.

The branching ratios, BR($\ell \to \ell' + \gamma$), are inversely proportional to $(v_\Delta M_\Delta)^4$. From the the current upper bound on BR($\mu \to e + \gamma$), eq. (1.6), and the expression for $|(m^\dagger\, m)_{\mu e}|$ in terms of the neutrino oscillation parameters, one can obtain a lower limit on $v_\Delta M_\Delta$ [107]:

$$v_\Delta > 2.98 \times 10^2 \left|s_{13}\, s_{23}\, \Delta m^2_{31}\right|^{\frac{1}{2}} \left(\frac{100\,\text{GeV}}{M_\Delta}\right). \tag{4.39}$$

Using the the best fit values (3σ allowed ranges) of $\sin\theta_{13}$, $\sin\theta_{23}$ and Δm^2_{31}, obtained in the global analysis [21] we find:

$$v_\Delta\, M_\Delta > 4.60\ (3.77) \times 10^{-7}\ \text{GeV}^2\,.^{1} \tag{4.40}$$

As in the case of type I seesaw model, we can obtain an upper bounds on the branching ratios $\text{BR}(\tau \to \mu + \gamma)$ and $\text{BR}(\tau \to e + \gamma)$ of interest using their relation with $\text{BR}(\mu \to e + \gamma)$ and the current experimental upper bound on $\text{BR}(\mu \to e + \gamma)$. We have:

$$\frac{\text{BR}(\tau \to \mu(e) + \gamma)}{\text{BR}(\mu \to e + \gamma)} = \frac{\left|(m^+ m)_{\tau\mu(e)}\right|^2}{|(m^+ m)_{\mu e}|^2}\, \text{BR}(\tau \to \nu_\tau\, \mu(e)\, \bar{\nu}_{\mu(e)})\,. \tag{4.41}$$

Using again the expressions for $|(m^\dagger\, m)_{\ell\ell'}|$ in terms of neutrino oscillation parameters and the best fit values quoted in eqs. (1.4) and (1.5) we get in the case of NO (IO) neutrino mass spectrum:

$$4.41\ (4.47) \leq \frac{|(m^+ m)_{\tau\mu}|}{|(m^+ m)_{\mu e}|} \leq 5.57\ (5.64)\,, \quad \text{NO (IO)} \quad \text{b.f.} \tag{4.42}$$

$$1.05\ (1.03) \leq \frac{|(m^+ m)_{\tau e}|}{|(m^+ m)_{\mu e}|} \leq 1.53\ (1.51) \quad \text{NO (IO)} \quad \text{b.f.} \tag{4.43}$$

Employing the 3σ allowed ranges of the neutrino oscillation parameters derived in [21] we obtain:

$$0.87\ (0.57) \leq \frac{|(m^+ m)_{\tau e}|}{|(m^+ m)_{\mu e}|} \leq 1.79\ (1.78) \quad \text{NO (IO)} \quad 2\sigma\,; \tag{4.44}$$

$$3.07\ (3.04) \leq \frac{|(m^+ m)_{\tau\mu}|}{|(m^+ m)_{\mu e}|} \leq 7.72\ (7.85) \quad \text{NO (IO)} \quad 3\sigma\,; \tag{4.45}$$

$$0.55\ (0.52) \leq \frac{|(m^+ m)_{\tau e}|}{|(m^+ m)_{\mu e}|} \leq 1.95\ (1.95) \quad \text{NO (IO)} \quad 3\sigma\,. \tag{4.46}$$

From eqs. (1.6), (4.41), (4.45) and (4.46) it follows that

$$\text{BR}(\tau \to \mu + \gamma) < 5.9\ (6.1) \times 10^{-12}\,, \quad \text{BR}(\tau \to e + \gamma) < 3.9 \times 10^{-13}\,, \quad \text{NO (IO)}\,. \tag{4.47}$$

These values are significantly below the planned sensitivities of the future experiments on the $\tau \to \mu + \gamma$ and $\tau \to e + \gamma$ decays. The observation of the any of the two decays having a branching ratio definitely larger than that quoted in eq. (4.47) would rule out the TeV scale Higgs triplet model under discussion.

[1] It is little different from eq. (3.26) with the latest neutrino experimental data.

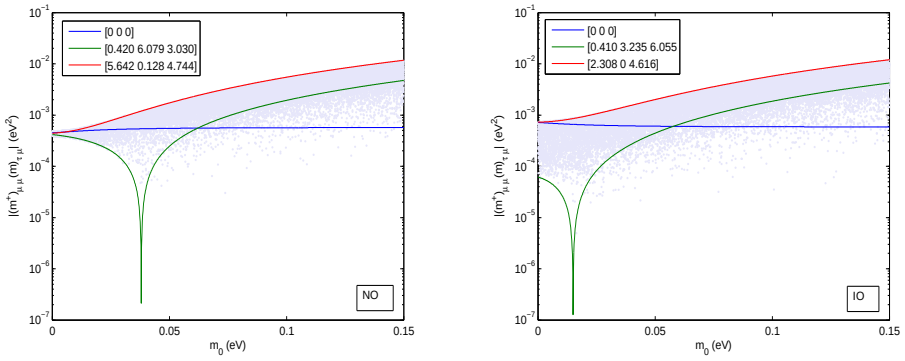

FIGURE 4.2: The dependence of $|m^*_{\mu\mu} m_{\tau\mu}|$ on the lightest neutrino mass m_0 in the cases of NO (left panel) and IO (right panel) neutrino mass spectra, for three sets of values of the Dirac and Majorana CPV phases, $[\delta, \alpha_{21}, \alpha_{31}]$. The neutrino oscillation parameters $\sin\theta_{12}$, $\sin\theta_{23}$, $\sin\theta_{13}$, Δm^2_{21} and Δm^2_{31} have been set to their best fit values, eqs. (1.4) and (1.5). The scattered points are obtained by varying Dirac and Majorana CPV phases randomly in the interval $[0, 2\pi]$.

4.2.2 The $\tau \to 3\mu$ Decay

The $\tau \to 3\mu$ decay occurring in the TeV scale HTM at tree level diagram with exchange of the virtual doubly-charged Higgs scalar Δ^{++}. The corresponding $\tau \to 3\mu$ decay branching ratio is taken from eq. (2.62):

$$\mathrm{BR}(\tau \to 3\mu) = \frac{\left|h^*_{\mu\mu} h_{\tau\mu}\right|^2}{G_F^2\, M_\Delta^4}\, \mathrm{BR}(\tau \to \mu \bar{\nu}_\mu \nu_\tau) \;=\; \frac{1}{G_F^2\, M_\Delta^4}\, \frac{\left|m^*_{\mu\mu} m_{\tau\mu}\right|^2}{16 v_\Delta^4} \mathrm{BR}(\tau \to \mu \bar{\nu}_\mu \nu_\tau)\,, \tag{4.48}$$

where $M_\Delta \equiv m_{\Delta^{++}}$ is the Δ^{++} mass and we have neglected corrections $\sim m_\mu/m_\tau \cong 0.06$.

Using the current upper bound on $\mathrm{BR}(\tau \to 3\mu)$, eq. (1.11), and eq. (4.48), we get the following constraint:

$$\left|h^*_{\mu\mu} h_{\tau\mu}\right| < 4.1 \times 10^{-5} \left(\frac{M_\Delta}{100\ \mathrm{GeV}}\right)^2 . \tag{4.49}$$

Further, the lower limit on the product of v_Δ and M_Δ, eq. (4.40), implies the following upper limit on $\mathrm{BR}(\tau \to 3\mu)$:

$$\mathrm{BR}(\tau \to 3\mu) < 1.88\ (4.17) \times 10^{-3}\, \frac{\left|m^*_{\mu\mu} m_{\tau\mu}\right|^2}{(1\,\mathrm{eV})^4} . \tag{4.50}$$

The factor $|m^*_{\mu\mu} m_{\tau\mu}|$, as can be shown using eqs. (2.54) and (2.55), depends not only on the neutrino oscillation parameters, but also on the type of the neutrino mass spectrum, the lightest neutrino mass $m_0 \equiv \min(m_j)$, $j = 1, 2, 3$ (i.e., on the absolute neutrino mass scale), and on the Majorana CPV phases α_{21} and α_{31}, present in the PMNS matrix. The dependence of $|m^*_{\mu\mu} m_{\tau\mu}|$ on m_0 for three sets of values of the CPV Dirac and Majorana

phases δ, α_{21} and α_{31} in the cases of NO and IO neutrino mass spectra is illustrated in Fig. 4.2. The neutrino oscillation parameters were set to their best fit values quoted in eqs. (1.4) and (1.5). As Fig. 4.2 indicates, both for the NO and IO spectra, the maximal allowed value of $|m^*_{\mu\mu} m_{\tau\mu}|$ is a monotonically increasing function of m_0.

The intervals of possible values of $|m^*_{\mu\mu} m_{\tau\mu}|$ in the cases of NO and IO neutrino mass spectra determine the ranges of allowed values of $\mathrm{BR}(\tau \to 3\mu)$ in the TeV scale HTM. Varying the three CPV phases independently in the interval $[0, 2\pi]$ and using the best fit, the 2σ and the 3σ allowed ranges of values of $\sin\theta_{12}$, $\sin\theta_{23}$, $\sin\theta_{13}$, Δm^2_{21} and Δm^2_{31} derived in [21], we get for $m_0 = 0;\ 0.01\ ; 0, 10$ eV:

- $m_0 = 0$ eV, NO (IO)

$$38.0\ (5.35) \times 10^{-5}\ \mathrm{eV}^2 \leq |(m^*)_{\mu\mu}(m)_{\tau\mu}| \leq 4.82\ (7.38) \times 10^{-4}\ \mathrm{eV}^2 \quad \text{b.f;} \quad (4.51)$$

$$2.77\ (0.00) \times 10^{-4}\ \mathrm{eV}^2 \leq |(m^*)_{\mu\mu}(m)_{\tau\mu}| \leq 5.89\ (8.11) \times 10^{-4}\ \mathrm{eV}^2 \quad 2\sigma; \quad (4.52)$$

$$2.33\ (0.00) \times 10^{-4}\ \mathrm{eV}^2 \leq |(m^*)_{\mu\mu}(m)_{\tau\mu}| \leq 8.35\ (8.45) \times 10^{-4}\ \mathrm{eV}^2 \quad 3\sigma. \quad (4.53)$$

- $m_0 = 0.01$ eV, NO (IO)

$$33.6\ (1.66) \times 10^{-5}\ \mathrm{eV}^2 \leq |(m^*)_{\mu\mu}(m)_{\tau\mu}| \leq 5.34\ (8.06) \times 10^{-4}\ \mathrm{eV}^2 \quad \text{b.f;} \quad (4.54)$$

$$2.24\ (0.00) \times 10^{-4}\ \mathrm{eV}^2 \leq |(m^*)_{\mu\mu}(m)_{\tau\mu}| \leq 6.41\ (8.99) \times 10^{-4}\ \mathrm{eV}^2 \quad 2\sigma; \quad (4.55)$$

$$1.76\ (0.00) \times 10^{-4}\ \mathrm{eV}^2 \leq |(m^*)_{\mu\mu}(m)_{\tau\mu}| \leq 8.96\ (9.41) \times 10^{-4}\ \mathrm{eV}^2 \quad 3\sigma. \quad (4.56)$$

- $m_0 = 0.1$ eV, NO (IO)

$$0.00\ (0.00)\ \mathrm{eV}^2 \leq |(m^*)_{\mu\mu}(m)_{\tau\mu}| \leq 5.48\ (5.76) \times 10^{-3}\ \mathrm{eV}^2 \quad \text{b.f;} \quad (4.57)$$

$$0.00\ (0.00)\ \mathrm{eV}^2 \leq |(m^*)_{\mu\mu}(m)_{\tau\mu}| \leq 5.57\ (5.85) \times 10^{-3}\ \mathrm{eV}^2 \quad 2\sigma; \quad (4.58)$$

$$0.00\ (0.00)\ \mathrm{eV}^2 \leq |(m^*)_{\mu\mu}(m)_{\tau\mu}| \leq 5.85\ (5.88) \times 10^{-3}\ \mathrm{eV}^2 \quad 3\sigma. \quad (4.59)$$

We would like to determine next whether $\mathrm{BR}(\tau \to 3\mu)$ predicted by the TeV scale HTM considered can be bigger than the sensitivity limit of $\sim 10^{-10}$ of the future planned experiment on $\tau \to 3\mu$ decay, given the stringent upper bounds on the $\mu \to e + \gamma$ and $\mu \to 3e$ decay branching ratios, eqs. (1.6) and (1.7). As we have seen, the current upper bound on $\mathrm{BR}(\mu \to \mathrm{e} + \gamma)$ leads to the lower limit eq. (4.40) of $v_\Delta M_\Delta$. We have to take into account also the important constraint on $\mathrm{BR}(\tau \to 3\mu)$ following from the current upper bound on $\mu \to 3e$ decay branching ratio $\mathrm{BR}(\mu \to 3\mathrm{e})$, eq. (1.7). In the

case of BR($\mu \to 3e$) we have BR($\mu \to 3e$) $\propto |m^*_{\mu e} m_{ee}|^2$. The quantity $|m^*_{\mu e} m_{ee}|$, and thus BR($\mu \to 3e$), depends on the same set of neutrino mass and mixing parameters as $|(m^*)_{\mu\mu}(m)_{\tau\mu}|$, and thus BR($\tau \to 3\mu$). We have performed a numerical analysis in order to determine the regions of values of the neutrino oscillation parameters and of the three CPV phases δ, α_{21} and α_{31}, in which the experimental upper bounds on BR($\mu \to e + \gamma$) and BR($\mu \to 3e$), eqs. (1.6) and (1.7), and the following requirement,

$$10^{-10} \leq \text{BR}(\tau \to 3\mu) \leq 10^{-8}\,, \tag{4.60}$$

are simultaneously satisfied. The analysis is performed for three values of $m_0 = 0$; 0.01 eV; 0.10 eV. The neutrino oscillation parameters $\sin\theta_{12}$, $\sin\theta_{23}$, $\sin\theta_{13}$, Δm^2_{21} and Δm^2_{31} were varied in their respective 3σ allowed ranges taken from [21]. The CPV phases δ, α_{21} and α_{31} were varied independently in the interval $[0, 2\pi]$. The results of this analysis are presented graphically in Fig. 4.3, in which we show the regions of values of the quantities $|m^*_{\mu\mu} m_{\tau\mu}|$ and $v_\Delta M_\Delta$ where the three conditions (1.6), (1.7) and (4.60) are simultaneously fulfilled in the cases of $m_0 = 0$; 0.01 eV; 0.10 eV for the NO and IO spectra. For $m_0 = 0$ and NO spectrum, the results depend weakly on the CPV phases; they are independent of the phase α_{31} if $m_0 = 0$ and the spectrum is of the IO type. The analysis performed by us shows that the maximal values BR($\tau \to 3\mu$) can have are the following:

$$\text{BR}(\tau \to 3\mu) \leq 1.02\ (1.68) \times 10^{-9}\,, \quad m_0 = 0 \text{ eV}, \quad \text{NO (IO)}\,, \tag{4.61}$$

$$\text{BR}(\tau \to 3\mu) \leq 1.24\ (2.05) \times 10^{-9}\,, \quad m_0 = 0.01 \text{ eV}, \quad \text{NO (IO)}\,, \tag{4.62}$$

$$\text{BR}(\tau \to 3\mu) \leq 8.64\ (9.11) \times 10^{-9}\,, \quad m_0 = 0.10 \text{ eV}, \quad \text{NO (IO)}\,. \tag{4.63}$$

Thus, for all the three values of m_0 considered, which span essentially the whole interval of possible values of m_0, the maximal allowed values of BR($\tau \to 3\mu$) is by a factor of ~ 10 to ~ 90 bigger than the projected sensitivity limit of 10^{-10} of the future experiment on the $\tau \to 3\mu$ decay. The regions on the $|m^*_{\mu\mu} m_{\tau\mu}| - v_\Delta M_\Delta$ plane, where the three conditions of interest are satisfied, are sizeable. The maximal value of BR($\tau \to 3\mu$) for, e.g., $m_0 = 0.01$ eV and NO (IO) spectrum, quoted in eq. (4.62), is reached for $\sin^2\theta_{12} = 0.269$ (0.308), $\sin^2\theta_{23} = 0.527$ (0.438), $\sin^2\theta_{13} = 0.0268$ (0.0203), $\Delta m^2_{21} = 7.38\ (7.56) \times 10^{-5}$ eV^2, $\Delta m^2_{31} = 2.14\ (2.40) \times 10^{-3}$ eV^2 and $[\delta, \alpha_{21}, \alpha_{31}] = [2.300, 5.098, 3.437]$ ([1.577,0.161,3.436]).

As it follows from Fig. 4.2 and the results quoted in eqs. (4.51) - (4.59), for certain values of the absolute neutrino mass scale m_0 and the CPV phases, $|m^*_{\mu\mu} m_{\tau\mu}|$ can be strongly suppressed; we can have even $|m^*_{\mu\mu} m_{\tau\mu}| = 0$. For NO (IO) neutrino mass spectrum, such a strong suppression can happen for $m_0 \gtrsim 38$ meV ($m_0 \gtrsim 15$ meV). The strong suppression of $|m^*_{\mu\mu} m_{\tau\mu}|$ seen in Fig. 4.2 takes place in the case of NO (IO) spectrum at

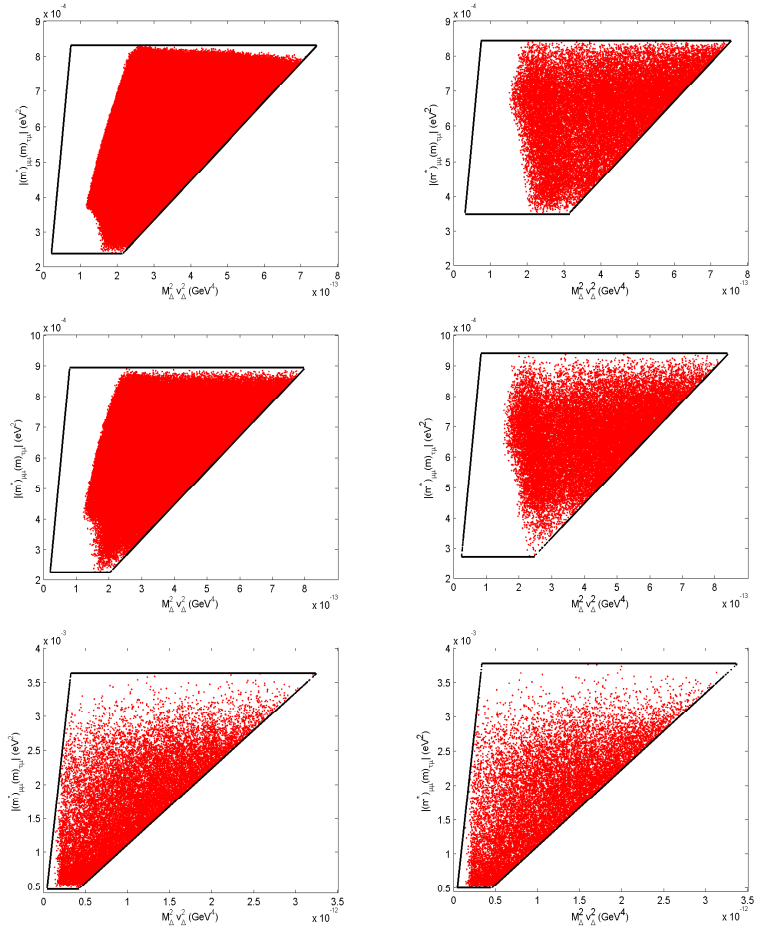

FIGURE 4.3: The regions in the $v_\Delta^2 M_\Delta^2 - |(m^*_{\mu\mu})(m_{\tau\mu})|$ plane where $10^{-10} \leq BR(\tau \to 3\mu) \leq 10^{-8}$ (the areas deliminated by the black lines) and the the upper limits $BR(\tau \to 3e) < 10^{-12}$ and $BR(\tau \to e\gamma) < 5.7 \times 10^{-13}$ are satisfied (the colored areas), for $m_0 = 0$ (upper panels), 0.01 eV (middle panels), 0.10 eV (lower panels) and NO (left panels) and IO (right panels) neutrino mass spectra. The figures are obtained by varying the neutrino oscillation parameters in their 3σ allowed ranges [21]; the CPV Dirac and Majorana phases were varied in the interval $[0, 2\pi]$.

$m_0 = 38$ meV and $[\delta, \alpha_{21}, \alpha_{31}] = [0.420, 6.079, 3.030]$ ($m_0 = 15$ meV and $[\delta, \alpha_{21}, \alpha_{31}] = [0.410, 3.235, 6.055]$). For $m_0 = 0.10$ eV, for instance, we have $|m^*_{\mu\mu} m_{\tau\mu}| = 0$ in the case of NO mass spectrum at $\delta = 2.633$, $\alpha_{21} = 2.533$ and $\alpha_{31} = 5.349$, while for the IO spectrum $|m^*_{\mu\mu} m_{\tau\mu}|$ goes through zero for $\delta = 4.078$, $\alpha_{21} = 2.161$ and $\alpha_{31} = 5.212$. The above examples of the vanishing of $|m^*_{\mu\mu} m_{\tau\mu}|$ when $m_0 = 0.10$ eV are not unique, it can happen also at other specific sets of values of the Dirac and Majorana CPV phases.

If in the planned experiment on the $\tau \to 3\mu$ decay the limit $\mathrm{BR}(\tau \to 3\mu) < 10^{-10}$ will be obtained, this will imply the following upper limit on the product $|h^*_{\mu\mu} h_{\tau\mu}|$ of Yukawa couplings:

$$\left|h^*_{\mu\mu} h_{\tau\mu}\right| < 2.83 \times 10^{-6} \left(\frac{M_\Delta}{100\ \mathrm{GeV}}\right)^2 . \tag{4.64}$$

4.3 Chapter Conclusion

In the present chapter we have investigated in detail the $\tau \to (e,\mu)+\gamma$ and $\tau \to 3\mu$ decays in the TeV scale type I see-saw and Higgs Triplet models of neutrino mass generation. Future experiments at the SuperB factory are planned to have sensitivity to the branching rations of the these decays $\mathrm{BR}(\tau \to (\mathrm{e},\mu) + \gamma) \gtrsim 10^{-9}$ and $\mathrm{BR}(\tau \to 3\mu) \gtrsim 10^{-10}$, which is an improvement by one and two orders of magnitude with respect to that reached so far in the searches for the $\tau \to (e,\mu) + \gamma$ and $\tau \to 3\mu$ decays, respectively.

We find using the constraints on the couplings $(RV)_{lj}$, $j = 1, 2$, from the low energy electroweak precision data, eqs. (2.18) - (2.20), that the branching ratios of the decays $\tau \to (e,\mu) + \gamma$ and $\tau \to 3\mu$ predicted in the TeV scale type I see-saw model can at most be of the order of the sensitivity of the planned future experiments, $\mathrm{BR}(\tau \to (\mathrm{e},\mu) + \gamma) \lesssim 10^{-9}$ and $\mathrm{BR}(\tau \to 3\mu) \lesssim 10^{-10}$. Taking into account the stringent experimental upper bounds on the $\mu \to e + \gamma$ and $\mu \to 3e$ decay rates has the effect of constraining further the maximal values of $\mathrm{BR}(\tau \to (\mathrm{e},\mu) + \gamma)$ and $\mathrm{BR}(\tau \to 3\mu)$ compatible with the data. In the case of NH spectrum, for instance, we get using the 2σ (3σ) ranges of the neutrino oscillations parameters from [21] and varying the CPV Dirac and Majorana phases δ, α_{21} and α_{31} independently in the interval $[0, 2\pi]$: $\mathrm{BR}(\tau \to \mathrm{e} + \gamma) \lesssim 1.4\ (1.7) \times 10^{-12}$, $\mathrm{BR}(\tau \to \mu + \gamma) \lesssim 4.9\ (9.7) \times 10^{-11}$, and $\mathrm{BR}(\tau \to 3\mu) \lesssim 3.8\ (7.4) \times 10^{-12}$. For specific values of the neutrino mixing parameters in the case of the IH spectrum, the predicted rates of the $\mu \to e + \gamma$ and $\mu \to 3e$ decays are strongly suppressed and the experimental upper bounds on these rates are automatically satisfied. In this special case the $\tau \to \mu + \gamma$ and the $\tau \to 3\mu$ decay rates are also predicted to be strongly suppressed and significantly smaller than the planned sensitivity of the future experiments, while for the $\tau \to e + \gamma$ decay we have $\mathrm{BR}(\tau \to \mathrm{e} + \gamma) \lesssim 10^{-9}$. Clearly, if any of the three τ decays under discussion is observed in the planned experiments, the TeV scale type I see-saw model we have considered will be strongly disfavored if not ruled out.

The predicted rates of the $\mu \to e + \gamma$ and of the $\tau \to (e,\mu) + \gamma$ decays in the Higgs Triplet model are also correlated. Using the existing experimental upper bound on $\mathrm{BR}(\mu \to \mathrm{e} + \gamma)$ we find the following upper limits on the $\tau \to \mu + \gamma$ and $\tau \to e + \gamma$ decay branching ratios for the NO (IO) neutrino mass spectrum: $\mathrm{BR}(\tau \to \mu + \gamma) \lesssim 5.9\ (6.1) \times 10^{-12}$, $\mathrm{BR}(\tau \to \mathrm{e} + \gamma) \lesssim 3.9 \times 10^{-12}$. These values are significantly below the planned sensitivity of the future experiments on the $\tau \to \mu + \gamma$ and $\tau \to e + \gamma$ decays. The observation of the any of the two decays having a branching ratio definitely larger than that quoted above would rule out the TeV scale Higgs triplet model under discussion. In contrast, we find that in a sizeable region of the parameter space of the Higgs Triplet model, the $\tau \to 3\mu$ decay branching ratio $\mathrm{BR}(\tau \to 3\mu)$ can have a value in the interval

$(10^{-10} - 10^{-8})$ and the predicted values of BR($\mu \to \mathrm{e} + \gamma$) and BR($\mu \to 3\mathrm{e}$) satisfy the existing stringent experimental upper bounds. Thus, the observation of the $\tau \to 3\mu$ decay with BR($\tau \to 3\mu$) $\gtrsim 10^{-10}$ and the non-observation of the $\tau \to \mu + \gamma$ and $\tau \to e + \gamma$ decays in the planned experiments having a sensitivity to BR($\tau \to (\mathrm{e}, \mu) + \gamma$) $\geq 10^{-9}$, would constitute an evidence in favor of the Higgs Triplet model.

Finally, the planned searches for the $\tau \to \mu + \gamma$, $\tau \to e + \gamma$ and $\tau \to 3\mu$ decays with sensitivity to BR($\tau \to (\mathrm{e}, \mu) + \gamma$) $\gtrsim 10^{-9}$ and to BR($\tau \to 3\mu$) $\gtrsim 10^{-10}$ will provide additional important test of the TeV scale see-saw type I and Higgs Triplet models of neutrino mass generation.

Chapter 5

Neutrino Mass Spectroscopy Using Atoms

In the following, we are going to consider a process which is cooperative de-excitation of atoms in a metastable state. For the single atom the process is $|e\rangle \to |g\rangle + \gamma + (\nu_i + \nu_j)$, $i, j = 1, 2, 3$, where ν_i's are neutrino mass eigenstates. If ν_i are Dirac fermions, $(\nu_i + \nu_j)$ should be understood for $i = j$ as $(\nu_i + \bar{\nu}_i)$, and as either $(\nu_i + \bar{\nu}_j)$ or $(\nu_j + \bar{\nu}_i)$ when $i \neq j$, $\bar{\nu}_i$ being the antineutrino with mass m_i. If ν_i are Majorana particles, we have $\bar{\nu}_i \equiv \nu_i$ and $(\nu_i + \nu_j)$ are the Majorana neutrinos with masses m_i and m_j.

The proposed experimental method is to measure, under irradiation of two counter-propagating trigger lasers, the continuous photon (γ) energy spectrum below each of the six thresholds ω_{ij} corresponding to the production of the six different pairs of neutrinos, $\nu_1\nu_1$, $\nu_1\nu_2$,..., $\nu_3\nu_3$: $\omega < \omega_{ij}$, ω being the photon energy, and [64–66]

$$\omega_{ij} = \omega_{ji} = \frac{\epsilon_{eg}}{2} - \frac{(m_i + m_j)^2}{2\epsilon_{eg}}\,, \quad i, j = 1, 2, 3, \quad m_{1,2,3} \geq 0\,, \tag{5.1}$$

where ϵ_{eg} is the energy difference between the two relevant atomic levels.

The disadvantage of atomic targets is their smallness of rates which are very sensitive to available energy of order eV. This can be overcome by developing, with the aid of a trigger laser, macro-coherence of atomic polarization to which the relevant amplitude is proportional, as discussed in [129, 130]. A similar amplification observed experimentally in the case of a single photon emission, which is called "Super-radiance" predicted by Dicke in 1954. The macroscopic polarization supported by trigger field gives rise to enhanced rate $\propto n^2 V$, where n is the number density of excited atoms and V is the volume irradiated by the trigger laser. The proposed atomic process may be called radiative emission of neutrino pair, or RENP in short. The estimated rate roughly of

order mHz or a little less makes it feasible to plan realistic RENP experiments for a target number of order of the Avogadro number, within a small region of order $1 \sim 10^2$ cm^3, if the rate enhancement works as expected.

The macro-coherence of interest is developed by irradiation of two trigger lasers of frequencies ω_1, ω_1, satisfying $\omega_1 + \omega_2 = \epsilon_{eg}$. It is a complicated dynamical process. The asymptotic state of fields and target atoms in the latest stage of trigger irradiation is described by a static solution of the master evolution equation. In many cases there is a remnant state consisting of field condensates (of the solition type) accompanied with a large coherent medium polarisation. This asymptotic target state is stable against two photon emission, while RENP occurs from any point in the target. The Group at Okayama University is working on the experimental realisation of the macro-coherent RENP. We hope the efforts of the University of Okayama Group will be successful.

All of the observables - the absolute neutrino mass scale, the type of neutrino mass spectrum, the nature of massive neutrinos and the Majorana CPV phases in the case of Majorana neutrinos - can be determined in one experiment, each observable with a different degree of difficulty, once the RENP process is experimentally established. For atomic energy available in the RENP process of the order of a fraction of eV, the observables of interest can be ranked in the order of increasing difficulty of their determination as follows:
(1) The absolute neutrino mass scale, which can be fixed by, e.g., measuring the smallest photon energy threshold $\min(\omega_{ij})$ near which the RENP rate is maximal: $\min(\omega_{ij})$ corresponds to the production of a pair of the heaviest neutrinos ($\max(m_j) \gtrsim 50$ meV).
(2) The neutrino mass hierarchy, i.e., distinguishing between the normal hierarchical (NH), inverted hierarchical (IH) and quasi-degenerate (QD) spectra, or a spectrum with partial hierarchy (see, e.g., [1]).
(3) The nature (Dirac or Majorana) of massive neutrinos.
(4) The measurement on the Majorana CPV phases if the massive neutrinos are Majorana particles.

The last item is particularly challenging. The importance of getting information about the Majorana CPV violation phases in the proposed RENP experiment stems, in particular, from the possibility that these phases play a fundamental role in the generation of the baryon asymmetry of the Universe [55, 56]. The only other experiments which, in principle, might provide information about the Majorana CPV phases are the neutrinoless double beta $(\beta\beta)_{0\nu}$-decay experiments.

5.1 Photon Energy Spectrum in RENP

The considered process occurs in the 3rd order (counting the four Fermi weak interaction as the 2nd order) of electroweak theory as a combined weak and QED process, as depicted in Fig. 5.1. Its effective amplitude has the form of

$$\langle g|\vec{d}|p\rangle \cdot \vec{E}\frac{G_F \sum_{ij} a_{ij}\nu_j^\dagger \vec{\sigma}\nu_i}{\epsilon_{pg}-\omega} \cdot \langle p|\vec{S}_e|e\rangle\,, \tag{5.2}$$

$$a_{ij} = U_{ei}^* U_{ej} - \frac{1}{2}\delta_{ij}\,, \tag{5.3}$$

where U_{ei}, $i = 1, 2, 3$, are the elements of the first row of the neutrino mixing matrix U_{PMNS}, expressed as:

$$U_{e1} = c_{12}\,c_{13}\,,\ U_{e2} = s_{12}\,c_{13}\,e^{i\alpha}\,,\ U_{e3} = s_{13}\,e^{i(\beta-\delta)}\,. \tag{5.4}$$

Here we have used the standard notation $c_{ij} = \cos\theta_{ij}$, $s_{ij} = \sin\theta_{ij}$ with $0 \le \theta_{ij} \le \pi/2$, $0 \le \delta \le 2\pi$ and, in the case of interest for our analysis [1], $0 \le \alpha, \beta \le \pi$, (see, however, [6]). If CP invariance holds, we have $\delta = 0, \pi$, and [7–9] $\alpha, \beta = 0, \pi/2, \pi$.

The atomic part of the probability amplitude involves three states $|e\rangle, |g\rangle, |p\rangle$, where the two states $|e\rangle, |p\rangle$, responsible for the neutrino pair emission, are connected by a magnetic dipole type operator, the electron spin $\vec{S}_e$. The $|g\rangle - |p\rangle$ transition involves a stronger electric dipole operator $\vec{d}$. From the point of selecting candidate atoms, E1×M1 type transition must be chosen between the initial and the final states ($|e\rangle$ and $|g\rangle$). The field $\vec{E}$ in eq. (5.2) is the one stored in the target by the counter-propagating fields.

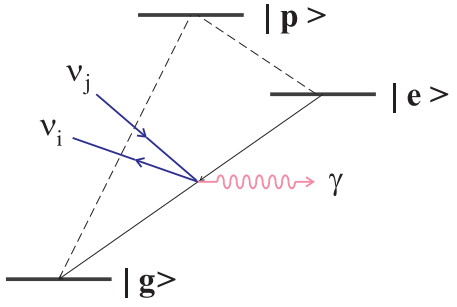

FIGURE 5.1: Λ−type atomic level for RENP $|e\rangle \to |g\rangle + \gamma + \nu_i\nu_j$ with ν_i a neutrino mass eigenstate. Dipole forbidden transition $|e\rangle \to |g\rangle + \gamma + \gamma$ may also occur via weak E1× M1 couplings to $|p\rangle$.

[1] Note that the two Majorana phases α_{21} and α_{31} defined in [1] are twice the phases α and β: $\alpha_{21} = 2\alpha$, $\alpha_{31} = 2\beta$.

When the target becomes macro-coherent by irradiation of trigger laser, RENP process conserves both the momentum and the energy which are shared by a photon and two emitted neutrinos. The atomic recoil can be neglected to a good approximation. Since neutrinos are practically impossible to measure, one sums over neutrino momenta and helicities, and derives the single photon spectrum as a function of photon energy ω. We think of experiments that do not apply magnetic field and neglect effects of atomic spin orientation. The neutrino helicity (denoted by $h_r\,, r = 1, 2$) summation in the squared neutrino current $j^k = a_{ij}\nu_i^\dagger \sigma_k \nu_j$ gives bilinear terms of neutrino momenta (see [64] and the discussion after eq. (5.19)):

$$K^S_{kn} \equiv \sum_{h_1,h_2} j^k (j^n)^\dagger = |a_{ij}|^2 \left[\left(1 - \delta_M \frac{m_i m_j}{E_i E_j} \left(1 - 2\frac{(\mathrm{Im}(a_{ij}))^2}{|a_{ij}|^2} \right) \right) \delta_{kn} + \frac{1}{E_i E_j} \left(p_i^k p_j^n + p_j^k p_i^n - \delta_{kn} \vec{p}_i \cdot \vec{p}_j \right) \right] . \tag{5.5}$$

The case $\delta_M = 1$ applies to Majorana neutrinos, $\delta_M = 0$ corresponds to Dirac neutrinos. The term $\propto m_i m_j (1 - 2(\mathrm{Im}(a_{ij}))^2/|a_{ij}|^2)$ is similar to, and has the same physical origin as, the term $\propto M_i M_j$ in the production cross section of two different Majorana neutralinos χ_i and χ_j with masses M_i and M_j in the process of $e^- + e^+ \to \chi_i + \chi_j$ [131]. The term $\propto M_i M_j$ of interest determines, in particular, the threshold behavior of the indicated cross section.

The subsequent neutrino momentum integration (with $E_i = \sqrt{\vec{p}_i^{\,2} + m_i^2}$ being the neutrino energy)

$$\int \frac{d^3p_1 d^3p_2}{(2\pi)^2} \delta^3(\vec{k} + \vec{p}_1 + \vec{p}_2) \delta(\epsilon_{eg} - \omega - E_1 - E_2) K^S_{ij} \equiv \frac{1}{2\pi} \int d\mathcal{P}_\nu K^S_{ij}\,, \tag{5.6}$$

can be written as a second rank tensor of photon momentum, $k_i k_j G^{(1)} + \delta_{ij} \vec{k}^2 G^{(2)}$ from rotational covariance. Two coefficient functions $G^{(i)}$ are readily evaluated by taking the trace $\sum_{i=j}$ and a product with $k_i k_j$ and using the energy-momentum conservation. But their explicit forms are not necessary in subsequent computation.

We now consider sum over magnetic quantum numbers of E1×M1 amplitude squared:

$$R = \int d\mathcal{P}_\nu \frac{\sum_{M_e}}{2J_e + 1} \sum_{M_g} |\sum_{M_p} \langle g M_g | \vec{d} \cdot \vec{E} | p M_p \rangle \cdot \langle p M_p | \vec{S}_e \cdot \vec{j}_\nu | e M_e \rangle|^2 . \tag{5.7}$$

The field $\vec{E}$ is assumed to be oriented along the trigger axis taken parallel to 3−axis. Since there is no correlation of neutrino pair emission to the trigger axis, one may use the isotropy of space and replace $(\vec{S}_e \cdot \vec{k})_{ni} (\vec{S}_e \cdot \vec{k})_{in'}$ by $(\vec{S}_e)_{ni} \cdot (\vec{S}_e)_{in'} \vec{k}^2/3$. Using the

isotropy, we define the atomic spin factor $C_{ep}(\mathrm{X})$ of X atom by

$$\frac{\sum_{M_e}}{2J_e+1}\langle pM_p|\vec{S}_e|eM_e\rangle\cdot\langle eM_e|\vec{S}_e|pM_p'\rangle=\delta_{M_pM_p'}C_{ep}(\mathrm{X})\,. \tag{5.8}$$

This means that only the trace part of eq. (5.5), $4K_{ii}^S/3$, is relevant for the neutrino phase space integration.

The result is summarized by separating the interference term relevant to the case of Majorana neutrinos ν_i:

$$\Gamma_{\gamma 2\nu}(\omega)=\Gamma_0 I(\omega)\eta_\omega(t)\,,\qquad \Gamma_0=\frac{3n^2VG_F^2\gamma_{pg}\epsilon_{eg}n}{2\epsilon_{pg}^3}(2J_p+1)C_{ep}\,, \tag{5.9}$$

$$I(\omega)=\frac{1}{(\epsilon_{pg}-\omega)^2}\sum_{ij}(B_{ij}I_{ij}^D(\omega)+\delta_M B_{ij}^M I_{ij}^M(\omega))\,, \tag{5.10}$$

$$B_{ij}^M=\frac{\Re(a_{ij}^2)}{|a_{ij}|^2}=\left(1-2\,\frac{(\mathrm{Im}(a_{ij}))^2}{|a_{ij}|^2}\right),\quad B_{ij}=|a_{ij}|^2=|U_{ei}^*U_{ej}-\frac{1}{2}\delta_{ij}|^2\,, \tag{5.11}$$

$$\begin{aligned} I_{ij}^D(\omega) &= \frac{1}{\omega}\int_0^\infty\int_0^\infty dE_1dE_2\delta(E_1+E_2+\omega-\epsilon_{eg})\theta\left(C_{ij}(E_1,E_2)\right.\\ &\times \left.\left[E_1E_2+\frac{1}{6}\left(E_1^2+E_2^2-m_i^2m_j^2-\omega^2\right)\right]\right., \end{aligned} \tag{5.12}$$

$$I_{ij}^M(\omega) = -\frac{m_im_j}{\omega}\int_0^\infty\int_0^\infty dE_1dE_2\delta(E_1+E_2+\omega-\epsilon_{eg})\theta\left(C_{ij}(E_1,E_2)\right)\,, \tag{5.13}$$

$$C_{ij}(E_1,E_2) = -(E_1^2+E_2^2-m_i^2-m_j^2-\omega^2)+4(E_1^2-m_i^2)(E_2^2-m_j^2). \tag{5.14}$$

Here, Γ_0 is a constant characterizing the experimental target with volume V and number density n.

It is important to note that $C_{ij}(E_1,E_2)$ has origin from the momentum conservation. Integration with respect to E_1, E_2 over the space limited by $C_{ij}(E_1,E_2)$ leads to a threshold on photon energy for each pair of neutrinos, below which the given neutrino pair is possible to be produced:

$$\omega_{ij}=\omega_{ji}=\frac{\epsilon_{eg}}{2}-\frac{(m_i+m_j)^2}{2\epsilon_{eg}}\,,\quad i,j=1,2,3,\quad m_{1,2,3}\geq 0\,. \tag{5.15}$$

If one can organize an experiment to measure one of the thresholds, the absolute neutrino mass scale will be determined.

After carrying out the integration and rewriting the result, we have final expression for $I(\omega)$:

$$I(\omega) = \frac{1}{(\epsilon_{pg}-\omega)^2}\sum_{ij}|a_{ij}|^2\,\Delta_{ij}(\omega)\left(I_{ij}(\omega)-\delta_M m_i\,m_j\,B_{ij}^M\right), \tag{5.16}$$

$$\Delta_{ij}(\omega) = \frac{1}{\epsilon_{eg}(\epsilon_{eg}-2\omega)}\left\{\left(\epsilon_{eg}(\epsilon_{eg}-2\omega)-(m_i+m_j)^2\right)\right. \\ \left.\times\left(\epsilon_{eg}(\epsilon_{eg}-2\omega)-(m_i-m_j)^2\right)\right\}^{1/2}, \tag{5.17}$$

$$I_{ij}(\omega) = \left(\frac{1}{3}\epsilon_{eg}(\epsilon_{eg}-2\omega)+\frac{1}{6}\omega^2-\frac{1}{18}\omega^2\Delta_{ij}^2(\omega)-\frac{1}{6}(m_i^2+m_j^2)\right. \\ \left.-\frac{1}{6}\frac{(\epsilon_{eg}-\omega)^2}{\epsilon_{eg}^2(\epsilon_{eg}-2\omega)^2}(m_i^2-m_j^2)^2\right). \tag{5.18}$$

The term $\propto \delta_M\, m_i m_j$ appears only for the Majorana case. We shall define and discuss the dynamical dimensionless factor $\eta_\omega(t)$ further below. The limit of massless neutrinos gives the spectral form,

$$I(\omega; m_i=0) = \frac{\omega^2-6\epsilon_{eg}\omega+3\epsilon_{eg}^2}{12(\epsilon_{pg}-\omega)^2}, \tag{5.19}$$

where the prefactor of $\sum_{ij}|a_{ij}|^2 = 3/4$ is calculated using the unitarity of the neutrino mixing matrix. On the other hand, near the threshold these functions have the behavior $\propto \sqrt{\omega_{ij}-\omega}$.

We will explain next the origin of the interference term for Majorana neutrinos. The two-component Majorana neutrino field can be decomposed in terms of plane wave modes as

$$\psi^M(\vec{x},t) = \sum_{i,\vec{p}}\left(u(\vec{p})e^{-iE_it+i\vec{p}\cdot\vec{x}}b_i(\vec{p})+u^c(\vec{p})e^{iE_it-i\vec{p}\cdot\vec{x}}b_i^\dagger(\vec{p})\right), \tag{5.20}$$

where the annihilation $b_i(\vec{p})$ and creation $b_i^\dagger(\vec{p})$ operators appears as a conjugate pair of the same type of operator b in the expansion (the index i gives the $i-$th neutrino of mass m_i, and the helicity summation is suppressed for simplicity). The concrete form of the 2-component conjugate wave function $u^c \propto i\sigma_2 u^*$ is given in [64]. A similar expansion can be written in terms of four component field if one takes into account the chiral projection $(1-\gamma_5)/2$ in the interaction. The Dirac case is different involving different type of operators $b_i(\vec{p})$ and $d_i^\dagger(\vec{p})$:

$$\psi^D(\vec{x},t) = \sum_{i,\vec{p}}\left(u(\vec{p})e^{-iE_it+i\vec{p}\cdot\vec{x}}b_i(\vec{p})+v(\vec{p})e^{iE_it-i\vec{p}\cdot\vec{x}}d_i^\dagger(\vec{p})\right). \tag{5.21}$$

Neutrino pair emission amplitude of modes $i\vec{p}_1, j\vec{p}_2$ contains two terms in the case of Majorana particle:

$$b_i^\dagger b_j^\dagger \left(a_{ij}u^*(\vec{p}_1)u^c(\vec{p}_2) - a_{ji}u^*(\vec{p}_2)u^c(\vec{p}_1)\right) , \tag{5.22}$$

and its rate involves

$$\begin{aligned}&\frac{1}{2}\left|a_{ij}u^*(\vec{p}_1)u^c(\vec{p}_2) - a_{ji}u^*(\vec{p}_2)u^c(\vec{p}_1)\right|^2 \\ &\quad = \frac{1}{2}|a_{ij}|^2\left(|\psi(1,2)|^2 + |\psi(2,1)|^2\right) - \Re(a_{ij}^2)\left(\psi(1,2)\psi(2,1)^*\right) ,\end{aligned} \tag{5.23}$$

where the relation $a_{ji} = a_{ij}^*$ is used and $\psi(1,2) = u^*(\vec{p}_1)u^c(\vec{p}_2)$. The result of the helicity sum $\sum(\psi(1,2)\psi(2,1)^*)$ is in [64], which then gives the interference term $\propto B_{ij}^M$ in the formula (5.11).

We see from eqs. (5.9) and (5.16) that the overall decay rate is determined by the energy independent Γ_0, while the spectral information is in the dimensionless function $I(\omega)$. The rate Γ_0 given here is obtained by replacing the field amplitude E of eq. (5.2) squared by $\epsilon_{eg}n$, which is the atomic energy density stored in the upper level $|e\rangle$.

The dynamical factor $\eta_\omega(t)$ is defined by a space integral of a product of macroscopic polarization squared times field strength, both in dimensionless units,

$$\eta_\omega(t) = \frac{1}{\alpha_m L}\int_{-\alpha_m L/2}^{\alpha_m L/2} d\xi \frac{r_1(\xi\,,\alpha_m t)^2 + r_2(\xi\,,\alpha_m t)^2}{4}|e(\xi\,,\alpha_m t)|^2 . \tag{5.24}$$

Here $r_1 \pm i r_2$ is the medium polarization normalized to the target number density.

The dimensionless field strength $|e(\xi,\tau)|^2 = |E(\xi = \alpha_m x, \tau = \alpha_m t)|^2/(\epsilon_{eg}n)$ is to be calculated using the evolution equation for field plus medium polarization in [130], where $\xi = \alpha_m x$ ($\alpha_m = \epsilon_{eg}\mu_{ge}n/2$ with μ_{ge} the off-diagonal coefficient of AC Stark shifts [65, 66]) is the atomic site position in dimensionless unit along the trigger laser direction ($-L/2 < x < L/2$ with L the target length), and $\tau = \alpha_m t$ is the dimensionless time. The characteristic unit of length and time are $\alpha_m^{-1} \sim (1\text{cm})(n/10^{21}\text{cm}^{-3})^{-1}$ and $(40\text{ps})(n/10^{21}\text{cm}^{-3})^{-1}$ for Yb discussed below. We expect that $\eta_\omega(t)$ in the formula given above is roughly of order unity or less.[2] We shall have more comments on this at the end of this section.

Note that what we calculate here is not the differential spectrum at each frequency, instead it is the spectral rate of number of events per unit time at each photon energy. Experiments for the same target atom are repeated at different frequencies $\omega_1 \leq \omega_{11}$

[2] There is a weak dependence of the dynamical factor $\eta_\omega(t)$ on the photon energy ω, since the field e in eq. (5.24), a solution of the evolution equation, is obtained for the initial boundary condition of frequency ω dependent trigger laser irradiation.

in the NO case (or $\omega_1 \leq \omega_{33}$ in the IO case) since it is irradiated by two trigger lasers of different frequencies of ω_i (constrained by $\omega_1 + \omega_2 = \epsilon_{eg}$) from counter-propagating directions.

As a standard reference target we take Yb atom and the following de-excitation path,

$$\text{Yb}; \quad |e\rangle = (6s6p)\,^3P_0\,, \quad |g\rangle = (6s^2)\,^1S_0\,, \quad |p\rangle = (6s6p)\,^3P_1\,. \tag{5.25}$$

The relevant atomic parameters are as follows [132]:

$$\epsilon_{eg} = 2.14349 \text{ eV}\,, \quad \epsilon_{pg} = 2.23072 \text{ eV}\,, \quad \gamma_{pg} = 1.1 \text{ MHz}\,. \tag{5.26}$$

The notation based on LS coupling is used for Yb electronic configuration, but this approximation must be treated with care, since there might be a sizable mixing based on jj coupling scheme. The relevant atomic spin factor C_{ep}(Yb) is estimated, using the spin Casimir operator within an irreducible representation of LS coupling. Namely,

$$\langle {}^3P_0|\vec{S}_e|{}^3P_1, M\rangle \cdot \langle {}^3P_1, M|\vec{S}_e|{}^3P_0\rangle = \frac{1}{3}\sum_M \langle {}^3P_0|\vec{S}_e|{}^3P_1, M\rangle \cdot \langle {}^3P_1, M|\vec{S}_e|{}^3P_0\rangle = \frac{2}{3}\,, \tag{5.27}$$

since $\vec{S}_e \cdot \vec{S}_e = 2$ for the spin triplet. This gives C_{ep}(Yb)= 2/3 for the intermediate path chosen.

We also considered another path, taking the intermediate state of Yb, $^1P_1$ with $\epsilon_{pg} =$ 3.10806 eV , $\gamma_{pg} = 0.176$ GHz. Using a theoretical estimate of A-coefficient 4.6×10^{-2} Hz for $^1P_1 \to {}^3P_1$ transition given in NIST [132] and taking the estimated Lande g-factor [133], 3/2 for the $^3P_1$ case, we calculate the mixed fraction of jj coupling scheme in LS forbidden amplitude squared $|\langle {}^1P_1|\vec{S}_e|{}^3P_1\rangle|^2$, to give $C_{ep} \sim 1 \times 10^{-4}$.

Summarizing, the overall rate factor Γ_0 is given by

$$\Gamma_0 = \frac{3n^2 V G_F^2 \gamma_{pg} \epsilon_{eg} n}{2\epsilon_{pg}^3}(2J_p + 1)C_{ep} \sim 0.37 \text{ mHz}\left(\frac{n}{10^{21} \text{ cm}^{-3}}\right)^3 \frac{V}{10^2 \text{ cm}^3}\,, \tag{5.28}$$

where the number is valid for the Yb first excited state of $J = 0$. If one chooses the other intermediate path, $^1P_1$, the rate Γ_0 is estimated to be of order, 1×10^{-3} mHz, a value much smaller than that of the $^3P_1$ path. The denominator factor $1/(\epsilon_{pg} - \omega)^2$ is slightly larger for the $^3P_1$ path, too. We consider the intermediate $^3P_1$ path alone in the following.

The high degree of sensitivity to the target number density n seems to suggest that solid environment is the best choice. But de-coherence in solids is fast, usually sub-picoseconds, and one has to verify how efficient coherence development is achieved in

the chosen target.

Finally, we discuss a stationary value of time independent $\eta_\omega(t)$ (5.24) some time after trigger irradiation. The stationary value may arise when many soliton pairs of absorber-emitter [130] are created, since the target in this stage is expected not to emit photons of PSR origin (due to the macro-coherent $|e\rangle \to |g\rangle + \gamma\gamma$), or emits very little only at target ends, picking up an exponentially small leakage tail. This is due to the stability of solitons against two photon emission. Thus the PSR background is essentially negligible. According to [134], the $\eta_\omega(t)$ integral (5.24) is time dependent in general. Its stationary standard reference value may be obtained by taking the field from a single created soliton. This quantity depends on target parameters such as α_m and relaxation times. Moreover, a complication arises, since many solitons may be created within the target, and the number of created solitons should be multiplied in the rate. This is a dynamical question that has to be addressed separately. In the following sections we compute spectral rates, assuming $\eta_\omega(t) = 1$.

5.2 Sensitivity of the Spectral Rate to Neutrino Mass Observables and the Nature of Massive Neutrinos

We will discuss in what follows the potential of an RENP experiment to get information about the absolute neutrino mass scale, the type of the neutrino mass spectrum and the nature of massive neutrinos. We begin by recalling that the existing data do not allow one to determine the sign of $\Delta m^2_{\rm A} = \Delta m^2_{31(2)}$ and in the case of 3-neutrino mixing, the two possible signs of $\Delta m^2_{31(2)}$ corresponding to two types of neutrino mass spectrum. In the standard convention [1] the two spectra read:
i) spectrum with normal ordering (NO): $m_1 < m_2 < m_3$, $\Delta m^2_{\rm A} = \Delta m^2_{31} > 0$, $\Delta m^2_{21} > 0$, $m_{2(3)} = (m^2_1 + \Delta m^2_{21(31)})^{\frac{1}{2}}$; *ii) spectrum with inverted ordering (IO)*: $m_3 < m_1 < m_2$, $\Delta m^2_{\rm A} = \Delta m^2_{32} < 0$, $\Delta m^2_{21} > 0$, $m_2 = (m^2_3 + \Delta m^2_{23})^{\frac{1}{2}}$, $m_1 = (m^2_3 + \Delta m^2_{23} - \Delta m^2_{21})^{\frac{1}{2}}$. Depending on the values of the smallest neutrino mass, $\min(m_j) \equiv m_0$, the neutrino mass spectrum can also be normal hierarchical (NH), inverted hierarchical (IH) and quasi-degenerate (QD):

$$\text{NH}: \quad m_1 \ll m_2 < m_3\,,\ m_2 \cong (\Delta m^2_{21})^{\frac{1}{2}} \cong 0.009\ \text{eV}\,,\ m_3 \cong (\Delta m^2_{31})^{\frac{1}{2}} \cong 0.05\ \text{eV}\,, \tag{5.29}$$

$$\text{IH}: \quad m_3 \ll m_1 < m_2\,,\ m_{1,2} \cong |\Delta m^2_{32}|^{\frac{1}{2}} \cong 0.05\ \text{eV}\,, \tag{5.30}$$

$$\text{QD}: \quad m_1 \cong m_2 \cong m_3 \cong m\,,\ m^2_j \gg |\Delta m^2_{31(32)}|\,,\ m \gtrsim 0.10\ \text{eV}\,. \tag{5.31}$$

All three types of spectrum are compatible with the existing constraints on the absolute scale of neutrino masses m_j.

5.2.1 General Features of the Spectral Rate

The first thing to notice is that the rate of emission of a given pair of neutrinos $(\nu_i + \nu_j)$ is suppressed, in particular, by the factor $|a_{ij}|^2$, independently of the nature of massive neutrinos. The expressions for the six different factors $|a_{ij}|^2$ in terms of the sines and cosines of the mixing angles θ_{12} and θ_{13}, as well as their values corresponding to the best fit values of $\sin^2\theta_{12}$ and $\sin^2\theta_{13}$ quoted in eq. (1.5), are given in Table 5.1. It follows from Table 5.1 that the least suppressed by the factor $|a_{ij}|^2$ is the emission of the pairs $(\nu_3+\nu_3)$ and $(\nu_1+\nu_2)$, while the most suppressed is the emission of $(\nu_2+\nu_3)$. The values of $|a_{ij}|^2$ given in Table 5.1 suggest that in order to be able to identify the emission of each of the six pairs of neutrinos, the photon spectrum, i.e., the RENP spectral rate, should be measured with a relative precision not worse than approximately 5×10^{-3}.

As it follows from eqs. (5.16) and (5.11), the rate of emission of a pair of Majorana neutrinos with masses m_i and m_j differs from the rate of emission of a pair of Dirac neutrinos with the same masses by the interference term $\propto m_i m_j B^M_{ij}$. For $i = j$ we have $B^M_{ij} = 1$, the interference term is negative and tends to suppress the neutrino emission rate. In the case of $i \neq j$, the factor B^M_{ij}, and thus the rate of emission of a pair of different Majorana neutrinos, depends on specific combinations of the Majorana and Dirac CPV phases of the neutrino mixing matrix: from eqs. (5.11) and (5.4) we get

$$B^M_{12} = \cos 2\alpha\,, \quad B^M_{13} = \cos 2(\beta - \delta)\,, \quad B^M_{23} = \cos 2(\alpha - \beta + \delta)\,. \tag{5.32}$$

In contrast, the rate of emission of a pair of Dirac neutrinos does not depend on the CPV phases of the PMNS matrix. In the case of CP invariance we have $\alpha, \beta = 0, \pi/2, \pi$, $\delta = 0, \pi$, and, correspondingly, $B^M_{ij} = -1$ or $+1$, $i \neq j$. For $B^M_{ij} = +1$, the interference term tends to suppress the neutrino emission rate, while for $B^M_{ij} = -1$ it tends to increase it. If some of the three relevant (combinations of) CPV phases, say α, has a CP violating value, we would have $-1 < B^M_{12} < 1$; if all three are CP violating, the inequality will be valid for each of the three factors B^M_{ij}: $-1 < B^M_{ij} < 1$, $i \neq j$. Note, however, that the rates of emission of $(\nu_1 + \nu_3)$ and of $(\nu_2 + \nu_3)$ are suppressed by

TABLE 5.1: The quantity $|a_{ij}|^2 = |U^*_{ei}U_{ej} - \frac{1}{2}\delta_{ij}|^2$

$\lvert a_{11}\rvert^2 = \lvert c^2_{12}c^2_{13} - \frac{1}{2}\rvert^2$	$\lvert a_{12}\rvert^2 = c^2_{12}s^2_{12}c^4_{13}$	$\lvert a_{13}\rvert^2 = c^2_{12}s^2_{13}c^2_{13}$
0.0311	0.2027	0.0162
$\lvert a_{22}\rvert^2 = \lvert s^2_{12}c^2_{13} - \frac{1}{2}\rvert^2$	$\lvert a_{23}\rvert^2 = s^2_{12}s^2_{13}c^2_{13}$	$\lvert a_{33}\rvert^2 = \lvert s^2_{13} - \frac{1}{2}\rvert^2$
0.0405	0.0072	0.2266

$|a_{13}|^2 = 0.016$ and $|a_{23}|^2 = 0.007$, respectively. Thus, studying the rate of emission of $(\nu_1 + \nu_2)$ seems the most favorable approach to get information about the Majorana phase α, provided the corresponding interference term $\propto m_1 m_2 B_{12}^M$ is not suppressed by the smallness of the factor $m_1 m_2$. The mass m_1 can be very small or even zero in the case of NH neutrino mass spectrum, while for the IH spectrum we have $m_1 m_2 \gtrsim |\Delta m^2_{32}| \cong 2.5 \times 10^{-3}$ eV^2. We note that all three of the CPV phases in eq. (5.32) enter into the expression for the $(\beta\beta)_{0\nu}-$ decay effective Majorana mass as their linear combination (see, e.g., [28, 121, 135–137]):

$$|\sum_i m_i U_{ei}^2|^2 = m_3^2 s_{13}^4 + m_2^2 s_{12}^4 c_{13}^4 + m_1^2 c_{12}^4 c_{13}^4 + 2 m_1 m_2 s_{12}^2 c_{12}^2 c_{13}^4 \cos(2\alpha) + 2 m_1 m_3 s_{13}^2 c_{12}^2 c_{13}^2 \cos 2(\beta - \delta) + 2 m_2 m_3 s_{13}^2 s_{12}^2 c_{13}^2 \cos 2(\alpha - \beta + \delta)\,. \quad (5.33)$$

In the case of $m_1 < m_2 < m_3$ (NO spectrum), the ordering of the threshold energies at $\omega_{ij} = \omega_{ji}$ is the following: $\omega_{11} > \omega_{12} > \omega_{22} > \omega_{13} > \omega_{23} > \omega_{33}$. For NH spectrum with negligible m_1 which can be set to zero, the factors $(m_i + m_j)^2 \equiv \kappa_{ij}$ in the expression (5.15) for the threshold energy ω_{ij} are given by: $\kappa_{11} = 0$, $\kappa_{12} = \Delta m^2_{21}$, $\kappa_{22} = 4\Delta m^2_{21}$, $\kappa_{13} = \Delta m^2_{31}$, $\kappa_{23} = (\sqrt{\Delta m^2_{31}} + \sqrt{\Delta m^2_{21}})^2$, $\kappa_{33} = 4\Delta m^2_{31}$. It follows from eq. (5.15) and the expressions for κ_{ij} that ω_{11}, ω_{12} and ω_{22} are very close, ω_{13} and ω_{23} are somewhat more separated and the separation is the largest between ω_{22} and ω_{13}, and ω_{23} and ω_{33}:

$$\text{NH}: \quad \omega_{11} - \omega_{12} = \frac{1}{3}(\omega_{12} - \omega_{22}) = \frac{1}{2\epsilon_{eg}} \Delta m^2_{21} \cong 1.759\ (8.794) \times 10^{-5}\ \text{eV}\,, \quad (5.34)$$

$$\text{NH}: \quad \omega_{13} - \omega_{23} = \frac{1}{2\epsilon_{eg}} (2\sqrt{\Delta m^2_{21}}\sqrt{\Delta m^2_{31}} + \Delta m^2_{21}) \cong 0.219\ (1.095) \times 10^{-3}\ \text{eV}\,, \quad (5.35)$$

$$\text{NH}: \quad \omega_{22} - \omega_{13} = \frac{1}{2\epsilon_{eg}} (\Delta m^2_{31} - 4\Delta m^2_{21}) \cong 0.506\ (2.529) \times 10^{-3}\ \text{eV}\,, \quad (5.36)$$

$$\text{NH}: \quad \omega_{23} - \omega_{33} = \frac{1}{2\epsilon_{eg}} (3\Delta m^2_{31} - 2\sqrt{\Delta m^2_{21}}\sqrt{\Delta m^2_{31}} - \Delta m^2_{21}) \cong 1.510\ (7.548) \times 10^{-3}\ \text{eV}\,, \quad (5.37)$$

where the numerical values correspond to Δm^2_{21} given in eq. (1.4) and $\epsilon_{eg} = 2.14349$ (numbers in parenthesis corresponding to the 1/5 of Yb value, namely 0.42870) eV. We get similar results in what concerns the separation between the different thresholds in the

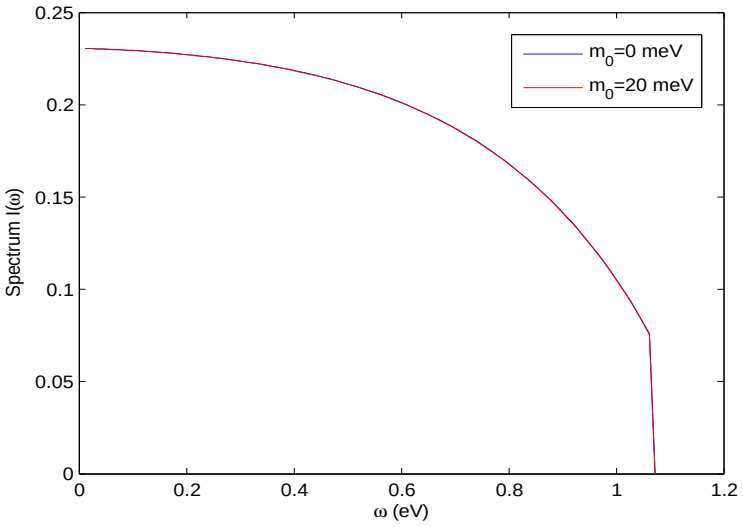

FIGURE 5.2: Global feature of photon energy spectrum $I(\omega)$ for the ${}^3P_0 \to {}^1S_0$ transitions in Yb. The lines corresponding to $m_0 = 20$ meV (red line) and to massless neutrinos, $m_i = 0$ (blue line), are practically indistinguishable in this figure (see text for details).

case of QD spectrum and $\Delta m^2_{31} > 0$:

$$\text{QD}: \quad \omega_{11} - \omega_{12} \cong \omega_{12} - \omega_{22} \cong \omega_{13} - \omega_{23} \cong \frac{1}{\epsilon_{eg}} \Delta m^2_{21}$$
$$\cong 3.518\ (17.588) \times 10^{-5}\ \text{eV}\,, \tag{5.38}$$
$$\text{QD}: \quad \omega_{22} - \omega_{13} \cong \omega_{23} - \omega_{33} - \frac{1}{\epsilon_{eg}} \Delta m^2_{21} = \frac{1}{\epsilon_{eg}} (\Delta m^2_{31} - 2\Delta m^2_{21})$$
$$\cong 1.082\ (5.410) \times 10^{-3}\ \text{eV}\,. \tag{5.39}$$

For spectrum with inverted ordering, $m_3 < m_1 < m_2$, the ordering of the threshold energies is different: $\omega_{33} > \omega_{13} > \omega_{23} > \omega_{11} > \omega_{12} > \omega_{22}$. In the case of IH spectrum with negligible $m_3 = 0$, we have: $\kappa_{33} = 0$, $\kappa_{13} = \Delta m^2_{23} - \Delta m^2_{21}$, $\kappa_{23} = \Delta m^2_{23}$, $\kappa_{11} = 4(\Delta m^2_{23} - \Delta m^2_{21})$, $\kappa_{12} = (\sqrt{\Delta m^2_{23}} + \sqrt{\Delta m^2_{23} - \Delta m^2_{21}})^2$, $\kappa_{22} = 4\Delta m^2_{23}$. Now not only ω_{11}, ω_{12} and ω_{22}, but also ω_{13} and ω_{23}, are very close, the corresponding differences being all $\sim \Delta m^2_{21}/\epsilon_{eg}$. The separation between the thresholds ω_{33} and ω_{13}, and between ω_{23} and ω_{11}, are considerably larger, being $\sim \Delta m^2_{23}/\epsilon_{eg}$. These results remain valid also in the case of QD spectrum and $\Delta m^2_{32} < 0$.

It follows from the preceding discussion that in order to observe and determine all six threshold energies ω_{ij}, the photon energy ω should be measured with a precision not worse than approximately 10^{-5} eV. This precision is possible in our RENP experiments since the energy resolution in the spectrum is determined by accuracy of the trigger laser frequency, which is much better than 10^{-5} eV.

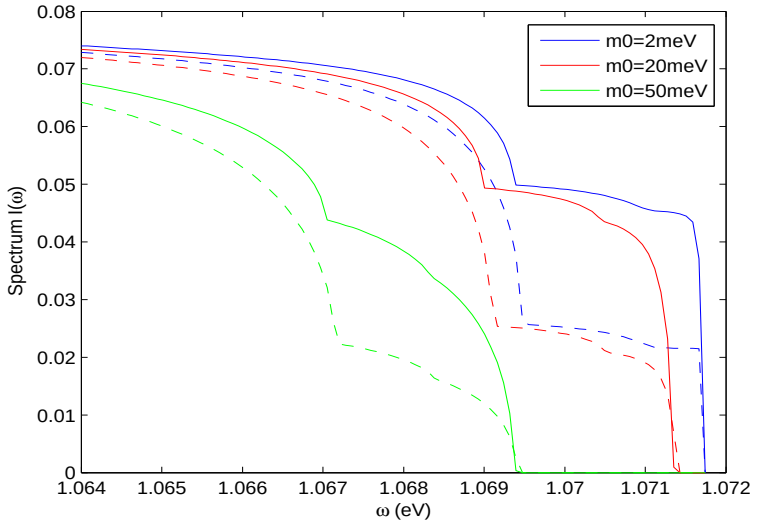

FIGURE 5.3: Photon energy spectrum from Yb $^3P_0 \to {}^1S_0$ transitions in the threshold region in the cases of NH spectrum (solid lines) and IH spectrum (dashed lines) and for 3 different sets of Dirac neutrinos masses corresponding to $m_0 = 2$ meV (blue lines), 20 meV (red lines) and 50 meV (green lines).

5.2.2 Neutrino Observables

We will concentrate in what follows on the analysis of the dimensionless spectral function $I(\omega)$ which contains all the neutrino physics information of interest.

In Fig. 5.2 we show the global features of the photon energy spectrum for the Yb $^3P_0 \to {}^1S_0$ transition in the case of massive Dirac neutrinos and NH and IH spectra. For the lightest neutrino mass $m_0 \leq 20$ meV, all spectra (including those corresponding to massive Majorana neutrinos which are not plotted) look degenerate owing to the horizontal and vertical axes scales used to draw the figure.

The Absolute Neutrino Mass Scale. Much richer physics information is contained in the spectrum near the thresholds ω_{ij}. Figure 5.3 shows the Dirac neutrino spectra for three different sets of values of the neutrino masses (corresponding to the smallest mass $m_0 = 2,\ 20,\ 50$ meV) and for both the NO ($\Delta m^2_{31(32)} > 0$) and IO ($\Delta m^2_{31(32)} < 0$) neutrino mass spectra. One sees that the locations of the thresholds corresponding to the three values of m_0 (and that can be seen in the figure) differ substantially. This feature can be used to determine the absolute neutrino mass scale, including the smallest mass, as evident in differences of spectrum shapes for different masses of m_0, 2, 20, 50 meV in Fig. 5.3. In particular, the smallest mass can be determined by locating the highest threshold (ω_{11} for NO and ω_{33} for IO). Also the location of the most prominent kink, which comes from the heavier neutrino pair emission thresholds (ω_{33} in the NO

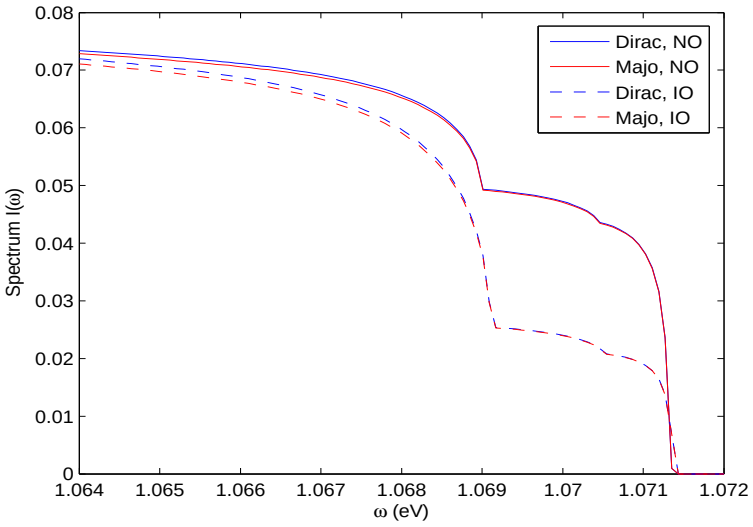

FIGURE 5.4: Spectra from Yb $^3P_0 \to {}^1S_0$ transitions in the cases of Dirac neutrinos (blue lines) and Majorana neutrinos (red lines) with masses corresponding to $m_0 = 20$ meV, for NH spectrum (solid lines) and IH spectrum (dashed lines).

case and ω_{12} in the IO case), can independently be used to extract the smallest neutrino mass value, and thus to check consistency of two experimental methods.

If the spectrum is of the NO type, the measurement of the position of the kink will determine the value of ω_{33} and therefore of m_3. For the IO spectrum, the threshold ω_{12} is very close to the thresholds ω_{22} and ω_{11}. The rates of emission of the pairs $(\nu_2+\nu_2)$ and $(\nu_1+\nu_1)$, however, are smaller approximately by the factors 10.0 and 12.7, respectively, than the rate of emission of $(\nu_1+\nu_2)$. Thus, the kink due to the $(\nu_1+\nu_2)$ emission will be the easiest to observe. The position of the kink will allow to determine $(m_1+m_2)^2$ and thus the absolute neutrino mass scale. If the kink due to the emission of $(\nu_2+\nu_2)$ or $(\nu_1+\nu_1)$ will also be observed, it can be used for the individual m_1, m_2 determination as well.

The Neutrino Mass Spectrum (or Hierarchy). Once the absolute neutrino mass scale is determined, the distinction between the NH (NO) and IH (IO) spectra can be made by measuring the ratio of rates below and above the thresholds ω_{33} and ω_{12} (or ω_{11}), respectively. We note that both of these measurements can be done without knowing the absolute counting rates. For $m_0 \lesssim 20$ meV and NH (IH) spectrum, the ratio of the rates at ω just above the ω_{33} (ω_{11}) threshold and sufficiently far below the

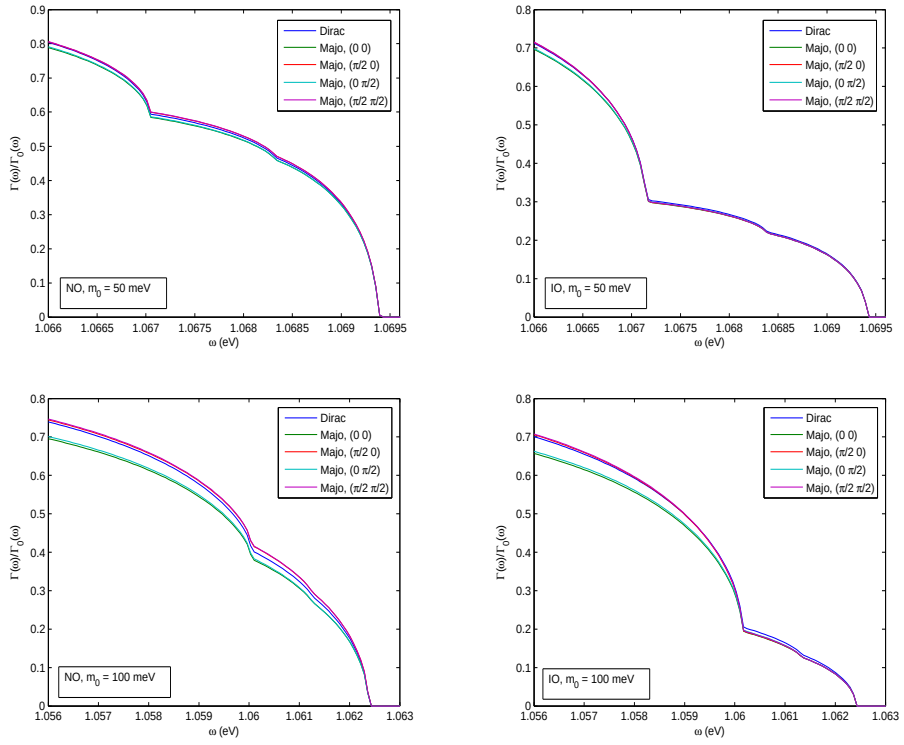

FIGURE 5.5: The ratio $R(\Gamma) \equiv \Gamma_{\gamma 2\nu}(\omega)/\Gamma_{\gamma 2\nu}(\omega; m_i = 0)$ in the case of emission of Dirac and Majorana massive neutrinos having NO (left panels) or IO (right panels) mass spectrum corresponding to $m_0 = 50; 100$ meV, for $\epsilon_{eg} = 2.14$ eV and four values of the CPV phases $(\alpha, \beta - \delta)$ in the Majorana case.

indicated thresholds, $\tilde{R}$, is given by:

$$\text{NH}: \qquad \tilde{R}(\omega_{33}; NH) \cong \frac{\sum_{i,j} |a_{ij}|^2 - |a_{33}|^2}{\sum_{i,j} |a_{ij}|^2} \cong 0.70\,, \tag{5.40}$$

$$\text{IH}: \qquad \tilde{R}(\omega_{11}; IH) \cong \frac{|a_{33}|^2 + 2\,(|a_{13}|^2 + (|a_{23}|^2)}{\sum_{i,j} |a_{ij}|^2} \cong 0.36\,. \tag{5.41}$$

In obtaining the result (5.41) in the IH case we have assumed that ω_{22} and ω_{12} are not resolved, but the kink due to the ω_{11} threshold could be observed. The latter does not corresponds to the features shown in Fig. 5.3 (and in the subsequent figures of the paper), where the kink due to the ω_{11} threshold is too small to be seen and only the kink due to the ω_{12} threshold is prominent.

The Nature of Massive Neutrinos. The Majorana vs Dirac neutrino distinction is much more challenging experimentally, if not impossible, with the Yb atom. This is illustrated in Fig. 5.4, where the Dirac and Majorana spectra are almost degenerate for both the NH and IH cases. The figure is obtained for $m_0 = 20$ meV and the CPV phases

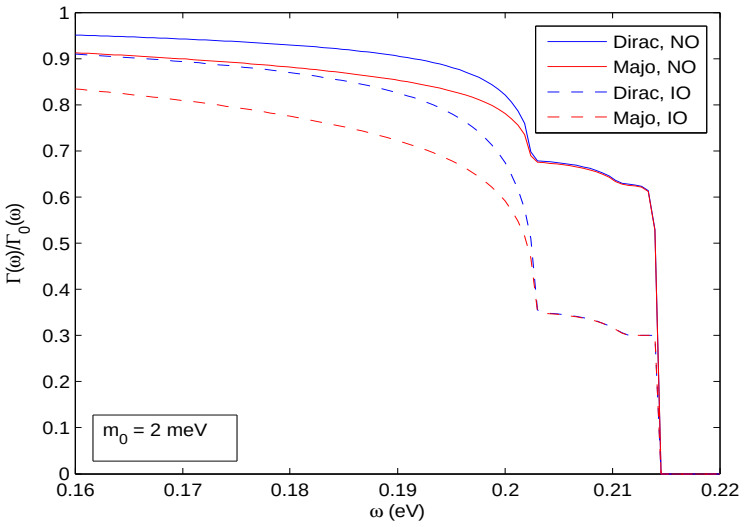

FIGURE 5.6: Majorana vs Dirac neutrino comparison of $R(\Gamma)$ in the case of hypothetic atom X with energy difference $\epsilon_{eg} = \epsilon_{eg}(\mathrm{Yb})/5$ for $m_0 = 2$ meV and NH (solid lines) and IH (dashed lines) spectra. The red and blue lines correspond respectively to Majorana and Dirac massive neutrinos.

set to zero, $(\alpha, \beta - \delta) = (0, 0)$, but the conclusion is valid for other choices of the values of the phases as well.

The difference between the emission of pairs of Dirac and Majorana neutrinos can be noticeable in the case of QD spectrum with $m_0 \sim 100$ meV and for values of the phases $\alpha \cong 0$, as is illustrated in Fig. 5.5, where we show the ratio $R(\Gamma) \equiv \Gamma_{\gamma 2\nu}(\omega)/\Gamma_{\gamma 2\nu}(\omega; m_i = 0) = I(\omega)/I(\omega; m_i = 0)$ as a function of ω. As Fig. 5.5 indicates, the relative difference between the Dirac and Majorana spectra can reach approximately 6% at values of ω sufficiently far below the threshold energies ω_{ij}. For $m_0 = 50$ meV, this difference cannot exceed 2% (Fig. 5.5).

A lower atomic energy scale $\epsilon_{eg} > 100$ meV, which is closer in value to the largest neutrino mass, would provide more favorable conditions for determination of the nature of massive neutrinos and possibly for getting information about at least some (if not all) of the CPV phases. In view of this we now consider a hypothetical atom X scaled down in energy by 1/5 from the real Yb, thus $\epsilon_{eg} \sim 0.4$ eV. There may or may not be good candidate atoms/molecules experimentally accessible, having level energy difference of order of the indicated value. Figure 5.6 shows comparison between the ratios $R(\Gamma)$ from X $^3P_0 \to ^1 S_0$ for Majorana and Dirac neutrinos with $m_0 = 2$ meV, for both the NH and IH cases. As seen in Fig. 5.6, the Majorana vs Dirac difference is bigger than 5% (10%) above the heaviest pair threshold in the NH (IH) case. The difference becomes bigger for larger values of the smallest neutrino mass m_0, making the measurement easier.

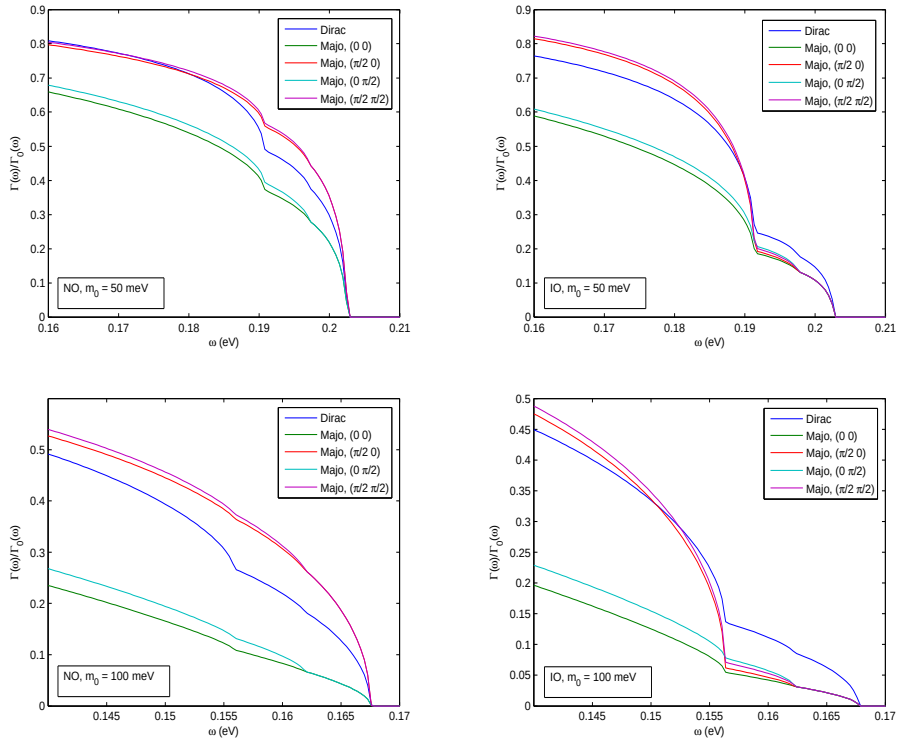

FIGURE 5.7: The same as in Fig. 5.5 but for $\epsilon_{eg} = 0.43$ eV.

This is illustrated in Fig. 5.7, where we show again the ratio $R(\Gamma) = I(\omega)/I(\omega; m_i = 0)$ as a function of ω in the case of Dirac and Majorana pair neutrino emission for $m_0 = 50$; 100 meV and NO and IO spectra. In the Majorana neutrino case, the ratio $R(\Gamma)$ is plotted for the four combinations of CP conserving values of the phases $(\alpha, \beta - \delta) = (0, 0); (0, \pi/2); (\pi/2, 0); (\pi/2, \pi/2)$. There is a significant difference between the Majorana neutrino emission rates corresponding to $(\alpha, \beta - \delta) = (0, 0)$ and $(\pi/2, \pi/2)$. The difference between the emission rates of Dirac and Majorana neutrinos is largest for $(\alpha, \beta - \delta) = (0, 0)$. For $m_0 = 50$ (100) meV and $(\alpha, \beta - \delta) = (0, 0)$. for instance, the rate of emission of Dirac neutrinos at ω sufficiently smaller than ω_{33} in the NO case and ω_{22} in the IO one, can be larger than the rate of Majorana neutrino emission by $\sim 20\%$ (70%). The Dirac and Majorana neutrino emission spectral rates never coincide.

In Figs. 5.8 and 5.9 we show the dependence of the ratios $R(\Gamma)$ on the CPV phases α and $\beta - \delta$ for $m_0 = 2$ meV. Generally speaking, the CPV phase measurement is challenging, requiring a high statistics data acquisition. A possible exception is the case of α and IH spectrum, as shown in Fig. 5.9, where the difference between the ratios $R(\Gamma)$ for $\alpha = 0$ and $\alpha = \pi/2$ can reach 10%. For the NH spectrum, the analogous difference is at most a few percent; observing this case requires large statistics in actual measurements.

It follows from these results that one of the most critical atomic physics parameters for

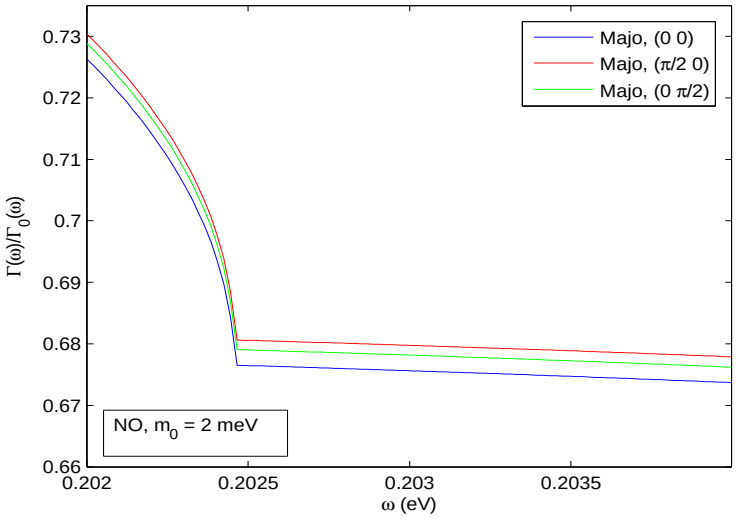

FIGURE 5.8: The dependence of $R(\Gamma)$ on the CPV phases α and $(\beta-\delta)$ in the case of NH spectrum with $m_0 = 2$ meV and for the transitions corresponding to Fig. 5.6. The blue, red, and green solid lines are obtained for $(\alpha, \beta-\delta) = (0,0), (\pi/2, 0)$ and $(0, \pi/2)$, respectively.

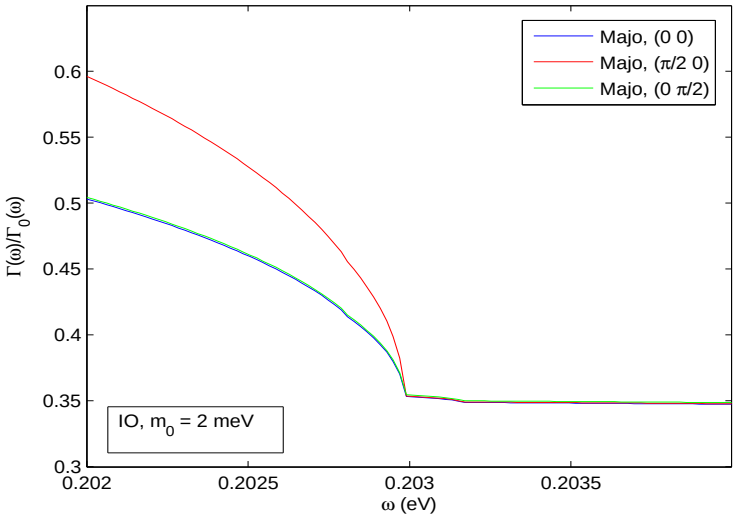

FIGURE 5.9: The same as in Fig. 5.8 for IH spectrum. The blue, red, and lines correspond to $(\alpha, \beta-\delta) = (0,0), (\pi/2, 0)$ and $(0, \pi/2)$, respectively.

the potential of an RENP experiment to provide information on the largest number of fundamental neutrino physics observables of interest is the value of the energy difference ϵ_{eg}. Values $\epsilon_{eg} \leq 0.4$ eV are favorable for determining the nature of massive neutrinos, and, if neutrinos are Majorana particles, for getting information about at least some of the leptonic CPV phases, which are the most difficult neutrino related observables to probe experimentally.

5.3 Chapter Conclusion

As the content of this chapter, we have investigated the sensitivity to undetermined neutrino parameters and properties (the absolute mass scale, the type of neutrino mass spectrum, the nature - Dirac or Majorana, of massive neutrinos and the CP violating phases) of the observables in macro-coherent RENP experiments.

The specific case of a potential RENP experiment measuring the photon spectrum originating from $^3P_0 \to {}^1S_0$ transitions in Yb atoms was considered. The relevant atomic level energy difference is $\epsilon_{eg} = 2.14349$ eV. Our results show that once the RENP events are unambiguously identified experimentally, the least challenging would be the measurement of the largest neutrino mass (or the absolute neutrino mass scale). The next in the order of increasing difficulty is the determination of the neutrino mass spectrum or hierarchy (NH, IH, QD). The Majorana vs Dirac distinction and the measurement of the CPV phases are considerably more challenging, requiring high statistics data from atoms (or molecules) with lower energy difference $\epsilon_{eg} \lesssim 0.5$ eV. Although the measurements of the indicated fundamental parameters of neutrino physics might be demanding, a single RENP experiment might provide a systematic strategy to determine almost all of these parameters, and thus can contribute to the progress in understanding the origin of neutrino masses and of the physics beyond the Standard Model possibly associated with their existence.

The present work points to the best atom/molecule candidate with level energy difference of less than O(0.5 eV) for the indicator ϵ_{eg}. Besides the desirable richness of detectable observables, good candidates for realistic RENP experiments have to be searched also from the point of least complexity of target preparation.

Chapter 6

Conclusion

In the present thesis, we have investigated the LFV processes in the charged lepton sector in the three scenarios of light neutrino mass generation, see-saw type I, see-saw type II (or Higgs Triplet Model) and see-saw type III, at the TeV scale. We also discussed the sensitivity of the radiative emission of neutrino pair experiment for determining the still unknown neutrino properties, such as their nature - Dirac or Majonana, absolute mass scale, hierarchy of the mass spectrum. The results are summarized as below.

In Chapter 2, the three well-known types of see-saw models have been introduced with assumption that the masses of the additional particles (heavy Majorana neutrinos for see-saw type I and III, or physical Higgs particles in case of Higgs triplet model) are at the TeV scale. We have considered type I and type III scenarios, whose two heavy Majorana neutrinos with similar masses forming a pseudo-Dirac state, such that it could have sizeable enough couplings $|(RV)_{li}|$, which might provide observable effects at low energy scale, after being constrained by the experimental data of neutrino oscillations and EW precision tests. Then, in the same Chapter, the rates of the LFV processes $\ell \to \ell' + \gamma$, $\ell \to 3\ell'$ ($\ell = \mu$ and $\ell' = e$, or $\ell = \tau$ and $\ell' = \mu, e$) and $\mu \to e$ conversion, are calculated in the type I and type II see-saw models, while the $\mu \to e + \gamma$, $\mu \to 3e$ decays and the $\mu \to e$ conversion rates in the type III see-saw scheme were discussed later in Chapter 3.

In Chapter 3 and Chapter 4, we have analyzed in detail the dependence of the LFV rates on the light neutrino masses and the CPV phases using the current data on the neutrino oscillation parameters. We also set constraints on the couplings $|(RV)_{\ell i}|$ of the heavy Majorana neutrinos to the charged leptons $l^{\mp}$ and $W^{\pm}$ and to $\nu_{\ell L}$ and Z^0 using the current experimental upper bounds on the LFV $\ell \to \ell' + \gamma$, $\ell \to 3\ell'$ decay and $\mu \to e$ conversion rates.

In the type I see-saw, our results show that the muon LFV decays ($\mu \to e + \gamma$, $\mu \to 3e$) and $\mu \to e$ conversion have observable rates within the sensitivities of the next generation of the LFV experiments. In contrast, the LFV rates of the processes involving the τ lepton, $\tau \to (\mu, e) + \gamma$, $\tau \to 3\mu$, are predicted to be lower than the detectable limits of the planned experiments. Thus, any detected signal of the LFV τ decays in the next generation of experiments will rule out the TeV scale type I see-saw model. It is also important to note that, in the case of IH spectrum, the decay rates of $\ell \to \ell' + \gamma$, $\ell \to 3\ell'$ ($\ell = \mu$ and $\ell' = e$, or $\ell = \tau$ and $\ell' = \mu, e$), with the exception of $\tau \to e\gamma$, might be strongly suppressed at some specific values of the CPV phases and lightest neutrino mass. Furthermore, the $\mu \to e$ conversion rate in the nuclei considered (Al, Ti, Au) could also pass through zero at a certain value of the heavy Majorana neutrino mass M_1 of a few TeV.

In the case of the Higgs triplet model, one has to keep in mind that all considered LFV rates are proportional to M_Δ^{-4}, M_Δ being the mass of the physical singly charged and doubly charged Higgs particles. Thus, the values of the LFV rates are strongly suppressed when M_Δ increases beyond the TeV scale. Therefore, if the physical scale of neutrino mass generation is too high, this will rule out any possibility to observe LFV signal in the μ and τ decays as well as in the searches for $\mu \to e$ conversion. The rates, in general, are also functions of the mixing angles, neutrino masses and both Dirac and Majorana CPV phases. However, in the special case of the charged lepton LFV decays with emission of a real photon ($\mu \to e\gamma$, $\tau \to \mu\gamma$ and $\tau \to e\gamma$), the rates do not depend on the lightest neutrino mass nor on the Majorana CPV phases. Detailed analysis shows that rates of $\mu \to e + \gamma$, $\mu \to 3e$, $\tau \to 3\mu$ decays and $\mu \to e$ conversion have values within the sensitivities of the next generation experiments. Furthermore, we have also considered the possibility of the branching ratio $\mathrm{Br}(\tau \to 3\mu)$ in the range of $10^{-10} \leq \mathrm{Br}(\tau \to 3\mu) \leq 10^{-8}$, which is the interval between the present experimental upper bound and the limit of next generation experimental sensitivity. Finally, using the correlation between $\mathrm{Br}(\mu \to e + \gamma)$, $\mathrm{Br}(\mu \to 3e)$ and $\mathrm{Br}(\tau \to (\mu, e) + \gamma)$ in the see-saw type II scenario, it is proved that $\mathrm{Br}(\tau \to \mu + \gamma) \leq 5.9\ (6.1) \times 10^{-12}$ NO (IO) and $\mathrm{Br}(\tau \to e + \gamma) \leq 3.9 \times 10^{-12}$, respectively.

With the FCNCs arising at tree-level in the type III see-saw model, the effective $\mu - e - Z$ coupling will provide large magnitudes of the rates of considered LFV processes. Thus, either the LFV processes of $\mu \to e + \gamma$, $\mu \to 3e$, and $\mu \to e$ conversion would be observed in the future experiments or the couplings $|(RV)_{\ell i}|$ will be severely constrained.

It follows from the results obtained on the LFV processes in the three well-known types of see-saw models of neutrino mass generation that it will be relatively easy to discriminate the type III and the type I and type II see-saw models. To discriminate between the

type I and type II see-saw is trickier. In principle, one might use the independence of the branching ratios $\mathrm{Br}(\ell \to \ell'\gamma)$ on the lightest neutrino mass and the CPV phase in the Higgs triplet model to distinguish it from the type I see-saw. However the values of the CPV phases and neutrino mass scale are still unknown at present. Our results also show that the channel of $\tau \to 3\mu$ decay is the only process that could be used, in principle, to discriminate between them.

As the last topic discussed in the thesis, in Chapter 5, we have introduced and carried out numerical analysis the phenomenon of radiative emission of neutrino pair in atoms. The process is sensitive to the absolute neutrino mass scale, the type of neutrino mass spectrum, the nature - Dirac or Majorana - of massive neutrinos, and the CPV Majorana phases in the neutrino mixing matrix. These are basically all of the unknown neutrino properties. The neutrino masses and the mass spectrum are determined by measuring the threshold energy of the photon which accompanies each emitted pair of neutrinos. In order to get information about the nature of massive neutrinos, and if neutrinos are Majorana particles - about the Majorana CPV phases - requires a high precision measurements of the emission rate from atoms with energy differences of $\epsilon_{eg} \leq 0.5$ eV.

Appendix A

See-saw Type I Form Factor

In this appendix, we are going to calculate the form factors of the diagrams which have contributions to the LFV processes such as $\mu \to e\gamma$, $\mu \to 3e$ decays and $\mu - e$ conversion etc., in the scheme of see-saw type I model. For convenience, we use the same Feynman rule conventions and notations reported in [138]. As the first step, we write down here the definitions of the functions and notations that will be used in the further calculation [138]:

$$D_3(x,y) = (1-y)m_i^2 + y\left[M_w^2 - q^2x(1-x)\right] - y(1-y)\overline{p}^2\,, \tag{A.1}$$

$$D_{3F}(x,y) = (1-y)M_w^2 + y\left\{\overline{m}^2 - q^2x(1-x)\right\} - y(1-y)\overline{p}^2\,, \tag{A.2}$$

$$D_{2a} = M_w^2(1-x) + m_i^2x - p_1^2x(1-x)\,, \tag{A.3}$$

$$D_{2b} = M_w^2(1-x) + m_i^2x - p_2^2x(1-x)\,, \tag{A.4}$$

$$\overline{p} = (1-x)p_1 + xp_2\,, \quad q = p_1 - p_2\,, \quad \overline{m}^2 = (1-x)m_i^2 + m_j^2x\,, \tag{A.5}$$

$$S_l = \frac{m_l^2}{M_w^2} \quad l = e,\mu,\tau\,, \quad \lambda_i = \frac{m_i^2}{M_w^2} \quad i = 1,2,...,3+k\,, \tag{A.6}$$

where m_i is mass of the Majorana neutrino n_i or quark q_i; p_i $(i = 1,..,4)$ stand for momentums of the incoming and outgoing particles; while k is number of the heavy neutrinos participating in the model.

The ultraviolet divergent part is expressed as

$$C_{UV} = \frac{1}{\varepsilon} - \gamma + \log 4\pi\,. \tag{A.7}$$

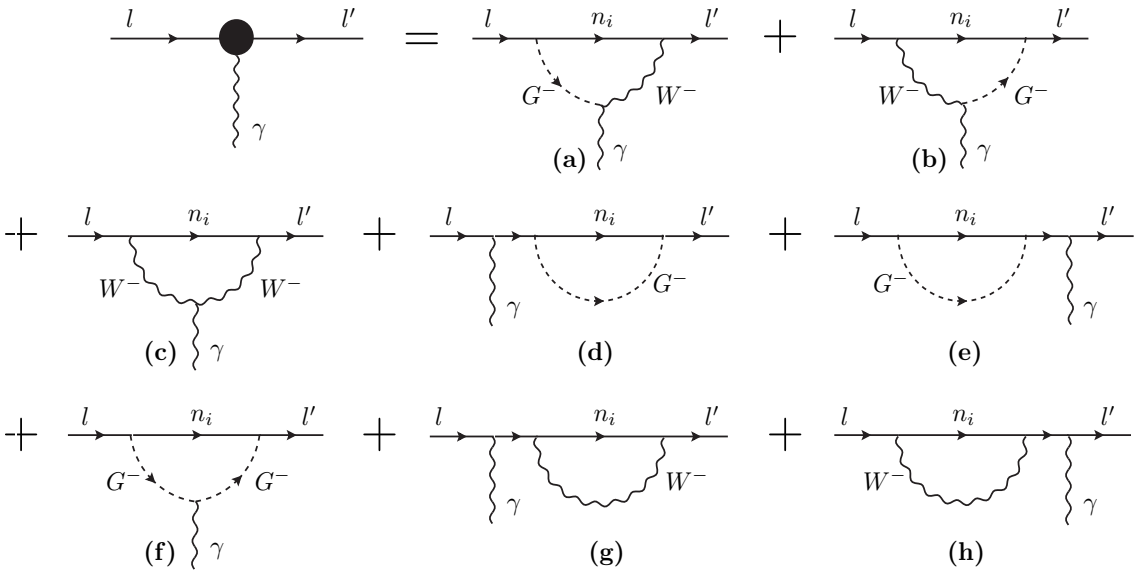

FIGURE A.1: Feynman diagrams contribute to the effective vertex $\bar{l}l'\gamma$ ($l \neq l'$).

We also define new notations:

$$Int\left(f(x)\right) = \int_0^1 dx\ f(x)\,, \tag{A.8}$$

$$Int\left(f(x,y)\right) = \int_0^1 dx \int_0^1 dy\ f(x,y)\,, \tag{A.9}$$

$$Int\left(f(x,y,z)\right) = \int_0^1 dx \int_0^1 dy \int_0^1 dz\ f(x,y,z)\,. \tag{A.10}$$

$$\tag{A.11}$$

A.1 Calculation of the Gamma Exchange Diagrams

The diagrams which contribute to the effective vertex $\bar{l}l'\gamma$ ($l \neq l'$) are shown in the Fig. A.1. Using the results reported in the appendix B of [138] and defining the effective coupling $\bar{l}l'\gamma$ in the following

$$-\,e\ \Gamma^{\gamma}_{\alpha} = -e\ \sum_{r=a}^{h} \Gamma^{(r)}_{\alpha} = \sum_{r=a}^{h} \text{Diag.}^{(\text{r})}\,, \tag{A.12}$$

one obtains:

$$\Gamma^{(a)}_{\alpha} = -\frac{g^2}{32\pi^2} U_{li} U^*_{l'i} \left[-m_i^2 P_R \gamma_\alpha \int_0^1 \frac{y\ dx\ dy}{D_3(x,y)} + m_\alpha P_R \gamma_\alpha \int_0^1 \frac{dx\ dy}{D_3(x,y)} y^2 \overline{\not{p}} \right]\,, \tag{A.13}$$

$$\Gamma^{(b)}_{\alpha} = \frac{g^2}{32\pi^2} U_{li} U^*_{l'i} \left[m_i^2 P_R \gamma_\alpha \int_0^1 \frac{y\ dx\ dy}{D_3(x,y)} - m_\beta P_L \int_0^1 \frac{dx\ dy}{D_3(x,y)} y^2 \overline{\not{p}} \gamma_\alpha \right]\,, \tag{A.14}$$

$$\begin{aligned}\Gamma_\alpha^{(c)} &= -\frac{g^2}{32\pi^2}U_{li}U_{l'i}^*\left[-\gamma_\alpha P_L\left\{3C_{UV}-2-6\int_0^1 dx\ dy\ y\log\left[D_3(x,y)\right]\right\}\right.\\ &+ P_R\int_0^1\frac{y^2\ dx\ dy}{D_3(x,y)}\left\{(\not p_2-2\not p_1+y\overline{\not p})\overline{\not p}\gamma_\alpha-2(p_1+p_2-2y\overline{p})_\alpha\overline{\not p}\right.\\ &+ \left.\left.\gamma_a\overline{\not p}(\not p_1-2\not p_2+y\overline{\not p})\right\}\right]\,, \end{aligned} \tag{A.15}$$

$$\Gamma_\alpha^{(d)} = -\frac{g^2}{32\pi^2}U_{li}U_{l'i}^*\not p_2 P_L\left[C_{UV}-1-2\int_0^1 dx(1-x)\log\left[D_{2b}(x)\right]\right]\frac{\not p_2+m_\alpha}{m_\beta^2-m_\alpha^2}\gamma_\alpha\,, \tag{A.16}$$

$$\Gamma_\alpha^{(e)} = -\frac{g^2}{32\pi^2}U_{li}U_{l'i}^*\gamma_\alpha\frac{\not p_1+m_\beta}{m_\alpha^2-m_\beta^2}\not p_1 P_L\left[C_{UV}-1-2\int_0^1 dx(1-x)\log\left[D_{2a}(x)\right]\right]\,, \tag{A.17}$$

$$\begin{aligned}\Gamma_\alpha^{(f)} &= -\frac{g^2}{64\pi^2M_w^2}U_{li}U_{l'i}^*\left[m_i^2\left\{(m_\alpha+m_\beta)+\gamma_5(m_\alpha-m_\beta)\right\}\int_0^1\frac{dx\ dy\ y}{D_3(x,y)}\right.\\ &\times (p_1+p_2-2y\overline{p})_\alpha-\frac{1}{2}\left\{(m_\alpha m_\beta+m_i^2)-\gamma_5(m_\alpha m_\beta-m_i^2)\right\}\gamma_\alpha\\ &\times \left\{C_{UV}-2\int_0^1 dx\ dy\ y\log\left[D_3(x,y)\right]\right\}-\left\{(m_\alpha m_\beta+m_i^2)-\gamma_5(m_\alpha m_\beta-m_i^2)\right\}\\ &\times \left.\int_0^1\frac{dx\ dy\ y^2}{D_3(x,y)}(p_1+p_2-2y\overline{p})_\alpha\overline{\not p}\right]\,. \end{aligned} \tag{A.18}$$

$$\begin{aligned}\Gamma_\alpha^{(g)} &= \frac{g^2}{64\pi^2M_w^2}U_{li}U_{l'i}^*\left[m_i^2\left\{(m_\alpha+m_\beta)+\gamma_5(m_\alpha-m_\beta)\right\}\left\{C_{UV}-\int_0^1 dx\log\left[D_{2b}(x)\right]\right\}\right.\\ &- \left.\frac{\not p_2}{2}\left\{(m_\alpha m_\beta+m_i^2)+\gamma_5(m_\alpha m_\beta-m_i^2)\right\}\left\{C_{UV}-2\int_0^1 dx(1-x)\log\left[D_{2b}(x)\right]\right\}\right]\\ &\times \frac{\not p_2+m_\alpha}{m_\beta^2-m_\alpha^2}\gamma_\alpha\,, \end{aligned} \tag{A.19}$$

$$\begin{aligned}\Gamma_\alpha^{(h)} &= \frac{g^2}{64\pi^2M_w^2}U_{li}U_{l'i}^*\ \gamma_\alpha\frac{\not p_1+m_\beta}{m_\alpha^2-m_\beta^2}\left[m_i^2\left\{(m_\alpha+m_\beta)+\gamma_5(m_\alpha-m_\beta)\right\}\{C_{UV}-\right.\\ &- \left.\int_0^1 dx\log\left[D_{2a}(x)\right]\right\}-\frac{\not p_1}{2}\left\{(m_\alpha m_\beta+m_i^2)+\gamma_5(m_\alpha m_\beta-m_i^2)\right\}\{C_{UV}-\\ &- \left.2\int_0^1 dx(1-x)\log\left[D_{2a}(x)\right]\right\}\right]\,, \end{aligned} \tag{A.20}$$

From the above results, one can see that the divergences appear in $\Gamma_\alpha^{(i)}$ for $i=c,...,f$. The divergences in diagrams (c), (d) and (e) vanish explicitly because of the unitarity of the neutrino mixing matrix $\sum_i^{3+k}U_{\alpha i}U_{\beta i}^*=0$ $(\alpha\neq\beta)$, while the divergences in $\Gamma_\alpha^{(f)}$, $\Gamma_\alpha^{(g)}$, and $\Gamma_\alpha^{(h)}$ cancel each other. After ignoring the divergences and simplifying the

result, we have:

$$\begin{aligned}
\Gamma_\alpha^{(a)} &= \frac{g^2}{32\pi^2}U_{li}U_{l'i}^*\left[A_1^{(1)}Int\left(\frac{y}{D_3(x,y)}\right)+B_1^{(1)}Int\left(\frac{y^2x}{D_3(x,y)}\right)\right.\\
&+ \left. B_2^{(1)}Int\left(\frac{y^2}{D_3(x,y)}\right)\right],\\
&A_1^{(1)}=M_w^2\lambda_i\gamma_\alpha P_L,\quad B_1^{(1)}=M_w^2S_\alpha\gamma_\alpha P_L-2\not{p}_1p_{2\alpha}P_L+\not{p}_2\gamma_\alpha\not{p}_1P_L,\\
&B_2^{(1)}=-M_w^2S_\alpha\gamma_\alpha P_L. \qquad (A.21)
\end{aligned}$$

$$\begin{aligned}
\Gamma_\alpha^{(b)} &= \frac{g^2}{32\pi^2}U_{li}U_{l'i}^*\left[A_1^{(2)}Int\left(\frac{y}{D_3(x,y)}\right)+B_1^{(2)}Int\left(\frac{y^2x}{D_3(x,y)}\right)\right.\\
&+ \left. B_2^{(2)}Int\left(\frac{y^2}{D_3(x,y)}\right)\right],\\
&A_1^{(1)}=M_w^2\lambda_i\gamma_\alpha P_L,\quad B_1^{(1)}=-M_w^2S_\beta\gamma_\alpha P_L+2\not{p}_2p_{1\alpha}P_L-\not{p}_2\gamma_\alpha\not{p}_1P_L,\\
&B_2^{(2)}=\not{p}_2\gamma_\alpha\not{p}_1P_L-2\not{p}_2p_{1\alpha}P_L. \qquad (A.22)
\end{aligned}$$

$$\begin{aligned}
\Gamma_\alpha^{(c)} &= \frac{g^2}{32\pi^2}U_{li}U_{l'i}^*\left[A_1^{(5)}Int\left(\frac{y^3x^2}{D_3(x,y)}\right)+A_2^{(5)}Int\left(\frac{y^3x}{D_3(x,y)}\right)+A_3^{(5)}Int\left(\frac{y^3}{D_3(x,y)}\right)\right.\\
&+ \left. B_1^{(5)}Int\left(\frac{y^2x}{D_3(x,y)}\right)+B_2^{(5)}Int\left(\frac{y^2}{D_3(x,y)}\right)+C_1^{(5)}Int\left(y\log D_3(x,y)\right)\right],\\
&A_1^{(5)}=2M_w^2r\gamma_\alpha P_L-4\not{p}_1p_{1\alpha}P_L+4\not{p}_2p_{1\alpha}P_L+4\not{p}_1p_{2\alpha}P_L-4\not{p}_2p_{2\alpha}P_L\ ,\\
&A_2^{(5)}=8\not{p}_1p_{1\alpha}P_L-4\not{p}_2p_{1\alpha}P_L-4\not{p}_1p_{2\alpha}P_L+2M_w^2(S_\alpha-S_\beta-r)\gamma_aP_L\ ,\\
&A_3^{(5)}=-4\not{p}_1p_{1\alpha}P_L-2M_w^2S_\alpha\gamma_\alpha P_L\ ,\quad B_1^{(5)}=-2\not{p}_1p_{1\alpha}P_L+2\not{p}_2p_{2\alpha}P_L\\
&-M_w^2(S_\alpha-S_\beta)\gamma_\alpha P_L\ ,\quad B_2^{(5)}=2\not{p}_1p_{1\alpha}P_L-2\not{p}_1p_{2\alpha}P_L-2\not{p}_2p_{1\alpha}P_L\\
&+3\not{p}_2\gamma_\alpha\not{p}_1P_L+M_w^2(3S_\alpha+2S_\beta+2r)\gamma_\alpha P_L\ ,\quad C_1^{(5)}=-6\gamma_\alpha P_L\ . \qquad (A.23)
\end{aligned}$$

$$\begin{aligned}
\Gamma_\alpha^{(d)}+\Gamma_\alpha^{(e)} &= \frac{g^2}{16\pi^2}U_{li}U_{l'i}^*\left[A^{(34)}\left\{Int\left[(1-x)\log D_{2a}(x)\right]-Int\left[(1-x)\log D_{2b}(x)\right]\right\}\right.\\
&+ \left. B^{(34)}\left\{S_\alpha Int\left[(1-x)\log D_{2a}(x)\right]-S_\beta Int\left[(1-x)\log D_{2b}(x)\right]\right\}\right]\ ,\\
&A^{(34)}=\frac{1}{S_\alpha-S_\beta}\frac{\not{p}_2\gamma_\alpha\not{p}_1P_L}{M_w^2}\ ,\quad B^{(34)}=\frac{1}{S_\alpha-S_\beta}\gamma_\alpha P_L\ . \qquad (A.24)
\end{aligned}$$

$$
\begin{aligned}
\Gamma_\alpha^{(f)} &= \frac{g^2}{32\pi^2} U_{li} U_{l'i}^* \left[-\lambda_i \left\{ A_1^{(8)} Int\left(\frac{y^2 x}{D_3(x,y)}\right) + A_2^{(8)} Int\left(\frac{y^2}{D_3(x,y)}\right) \right.\right. \\
&+ \left.\left. A_3^{(8)} Int\left(\frac{y}{D_3(x,y)}\right) \right\} + \lambda_i \left\{ B_1^{(8)} Int\left(\frac{y^3 x^2}{D_3(x,y)}\right) + B_2^{(8)} Int\left(\frac{y^3 x}{D_3(x,y)}\right) \right. \\
&+ \left. B_3^{(8)} Int\left(\frac{y^3}{D_3(x,y)}\right) + C_1^{(8)} Int\left(\frac{y^2 x}{D_3(x,y)}\right) + C_2^{(8)} Int\left(\frac{y^2 x}{D_3(x,y)}\right) \right\} \\
&+ \left. D_1^{(8)} Int\left[y \log D_3(x,y)\right] \right] ,
\end{aligned}
$$

$$
\begin{aligned}
&A_1^{(8)} = 2\not{p}_1 p_{1\alpha} P_L + 2\not{p}_2 p_{1\alpha} P_L - 2\not{p}_1 p_{2\alpha} P_L - 2\not{p}_2 p_{2\alpha} P_L , \quad A_2^{(8)} = -2\not{p}_1 p_{1\alpha} P_L \\
&-2\not{p}_2 p_{1\alpha} P_L , \quad A_3^{(8)} = \not{p}_1 p_{1\alpha} P_L + \not{p}_2 p_{1\alpha} P_L + \not{p}_1 p_{2\alpha} P_L + \not{p}_2 p_{2\alpha} P_L , \\
&B_1^{(8)} = -2\not{p}_1 p_{1\alpha} P_L + 2\not{p}_2 p_{1\alpha} P_L + 2\not{p}_1 p_{2\alpha} P_L - 2\not{p}_2 p_{2\alpha} P_L , \\
&B_2^{(8)} = 4\not{p}_1 p_{1\alpha} P_L - 2\not{p}_2 p_{1\alpha} P_L - 2\not{p}_1 p_{2\alpha} P_L , \quad B_3^{(8)} = -2\not{p}_1 p_{1\alpha} P_L , \\
&C_1^{(8)} = -\not{p}_1 p_{1\alpha} P_L + \not{p}_2 p_{1\alpha} P_L - \not{p}_1 p_{2\alpha} P_L + \not{p}_2 p_{2\alpha} P_L , \quad C_2^{(8)} = \not{p}_1 p_{1\alpha} P_L \\
&+\not{p}_1 p_{2\alpha} P_L , \quad D_1^{(8)} = -\lambda_i \gamma_\alpha P_L - \frac{\not{p}_2 \gamma_\alpha \not{p}_1 P_L}{M_w^2} . \qquad \text{(A.25)}
\end{aligned}
$$

$$
\begin{aligned}
\Gamma_\alpha^{(g)} + \Gamma_\alpha^{(h)} &= \frac{g^2}{32\pi^2} U_{li} U_{l'i}^* \left[A^{(67)} \left\{ Int\left[\log D_{2a}(x)\right] - Int\left[\log D_{2b}(x)\right] \right\} \right. \\
&+ B_1^{(67)} \left\{ Int\left[(1-x)\log D_{2a}(x)\right] - Int\left[(1-x)\log D_{2b}(x)\right] \right\} \\
&+ \left. B_2^{(67)} \left\{ S_\alpha Int\left[(1-x)\log D_{2a}(x)\right] - S_\beta Int\left[(1-x)\log D_{2b}(x)\right] \right\} \right] ,
\end{aligned}
$$

$$
\begin{aligned}
&A^{(67)} = -\frac{\lambda_i}{S_\alpha - S_\beta} \left[(S_\alpha + S_\beta)\gamma_\alpha P_L + \frac{2\not{p}_2 \gamma_\alpha \not{p}_1 P_L}{M_w^2} \right] , \\
&B_1^{(67)} = \frac{1}{S_\alpha - S_\beta} \left[S_\alpha S_\beta \gamma_\alpha P_L + \lambda_i \frac{\not{p}_2 \gamma_\alpha \not{p}_1 P_L}{M_w^2} \right] , \\
&B_2^{(67)} = \frac{1}{S_\alpha - S_\beta} \left[\frac{\not{p}_2 \gamma_\alpha \not{p}_1 P_L}{M_w^2} + \lambda_i \gamma_\alpha P_L \right] . \qquad \text{(A.26)}
\end{aligned}
$$

Carrying on the integrations and keeping only the leading order terms, $\Gamma_\alpha^\gamma(\lambda)$ is arrived at the form:

$$
\begin{aligned}
\Gamma_\alpha^\gamma(\lambda) &= \sum_{r=a}^{h} \Gamma_\alpha^{(i)}(\lambda) = \frac{g^2}{32\pi^2} U_{li} U_{l'i}^* P_R \left[F_\gamma(\lambda_i) \left\{ -\frac{q^2}{M_w^2}\gamma_\alpha + \frac{(\not{p}_1 - \not{p}_2)(p_1 - p_2)_\alpha}{M_w^2} \right\} \right. \\
&+ G_\gamma(\lambda_i) \left\{ \frac{\not{p}_1 (p_1 + p_2)_\alpha}{M_w^2} - S_\alpha \gamma_\alpha - \frac{\not{p}_2 \gamma_\alpha \not{p}_1}{M_w^2} \right\} + G_\gamma(\lambda_i) \left\{ \frac{\not{p}_2 (p_1 + p_2)_\alpha}{M_w^2} \right. \\
&- \left. \left. S_\beta \gamma_\alpha - \frac{\not{p}_2 \gamma_\alpha \not{p}_1}{M_w^2} \right\} \right] ,
\end{aligned}
$$

$$
F_\gamma(x) = \frac{x(7x^2 - x - 12)}{12(1-x)^3} - \frac{x^2(12 - 10x + x^2)}{6(1-x)^4} \log x , \qquad \text{(A.27)}
$$

$$
G_\gamma(x) = -\frac{x(2x^2 + 5x - 1)}{4(1-x)^3} - \frac{3x^3}{2(1-x)^4} \log x . \qquad \text{(A.28)}
$$

Finally, using the property of the Dirac equation

$$\overline{u}(p_2)\left[\not{p}_1(p_1+p_2)_\alpha - m_\mu^2\gamma_\alpha - \not{p}_2\gamma_\alpha\not{p}_1\right]u(p_1) = m_\mu\overline{u}(p_2)i\sigma_{\alpha\beta}q^\beta u(p_1)\ , \tag{A.29}$$

$$\overline{u}(p_2)\left[\not{p}_2(p_1+p_2)_\alpha - m_e^2\gamma_\alpha - \not{p}_2\gamma_\alpha\not{p}_1\right]u(p_1) = m_e\overline{u}(p_2)i\sigma_{\alpha\beta}q^\beta u(p_1)\ , \tag{A.30}$$

we can rewrite the effective coupling in the gauge covariant form

$$\begin{aligned} -e\ \overline{u}(p_2)\Gamma^\gamma_\alpha(\lambda)u(p_1) &= \frac{g^2 e}{32\pi^2 M_w^2}U_{li}U^*_{l'i}\overline{u}(p_2)\left[F_\gamma(\lambda)\left(q^2\gamma_\alpha - \not{q}q_\alpha\right)P_L\right. \\ &- \left. i\sigma_{\alpha\beta}q^\beta G_\gamma(\lambda)\left(m_e P_L + m_\mu P_R\right)\right]u(p_1)\ , \end{aligned} \tag{A.31}$$

$$\begin{aligned} -e\ \Gamma^\gamma_\alpha(\lambda) &= \frac{g^2 e}{32\pi^2 M_w^2}U_{li}U^*_{l'i}\left[F_\gamma(\lambda)\left(q^2\gamma_\alpha - \not{q}q_\alpha\right)P_L\right. \\ &- \left. i\sigma_{\alpha\beta}q^\beta G_\gamma(\lambda)\left(m_e P_L + m_\mu P_R\right)\right]\ . \end{aligned} \tag{A.32}$$

A.2 Calculation of the Z Boson Exchange Diagrams

In the type I see-saw scenario, the diagrams, which give one-loop correction to the effective vertex $\bar{l}l'Z$ $(l \neq l')$ are listed in the Fig. A.2. In this case, let us define the effective vertex as

$$\frac{g}{4\cos\theta_w}\ \Gamma^z_\alpha = \frac{g}{4\cos\theta_w}\ \sum_{r=a}^{k}\Gamma^{(r)}_\alpha = \sum_{r=a}^{k}\text{Diag.}^{(\text{r})}\ . \tag{A.33}$$

Using the same trick like the previous case, we obtain the contributions of the diagrams quoted in Fig. A.2:

$$\Gamma^{(a)}_\alpha = \frac{g^2}{8\pi^2}U_{li}U^*_{l'i}\sin^2\theta_w\left[m_i^2 P_R\gamma_\alpha\int_0^1\frac{y\ dx\ dy}{D_3(x,y)} - m_\alpha P_R\gamma_\alpha\int_0^1\frac{dx\ dy}{D_3(x,y)}y^2\overline{\not{p}}\right]\ , \tag{A.34}$$

$$\Gamma^{(b)}_\alpha = \frac{g^2}{8\pi^2}U_{li}U^*_{l'i}\sin^2\theta_w\left[m_i^2 P_R\gamma_\alpha\int_0^1\frac{y\ dx\ dy}{D_3(x,y)} - m_\beta P_L\int_0^1\frac{dx\ dy}{D_3(x,y)}y^2\overline{\not{p}}\gamma_\alpha\right]\ , \tag{A.35}$$

$$\begin{aligned} \Gamma^{(c)}_\alpha &= \frac{g^2}{8\pi^2}U_{li}U^*_{l'i}\cos^2\theta_w\left[-\gamma_\alpha P_L\left\{3C_{UV} - 2 - 6\int_0^1 dx\ dy\ y\log\left[D_3(x,y)\right]\right\}\right. \\ &+ P_R\int_0^1\frac{y^2\ dx\ dy}{D_3(x,y)}\left\{(\not{p}_2 - 2\not{p}_1 + y\overline{\not{p}})\overline{\not{p}}\gamma_\alpha - 2(p_1+p_2-2y\overline{p})_\alpha\overline{\not{p}} + \right. \\ &+ \left.\left.\gamma_\alpha\overline{\not{p}}(\not{p}_1 - 2\not{p}_2 + y\overline{\not{p}})\right\}\right]\ , \end{aligned} \tag{A.36}$$

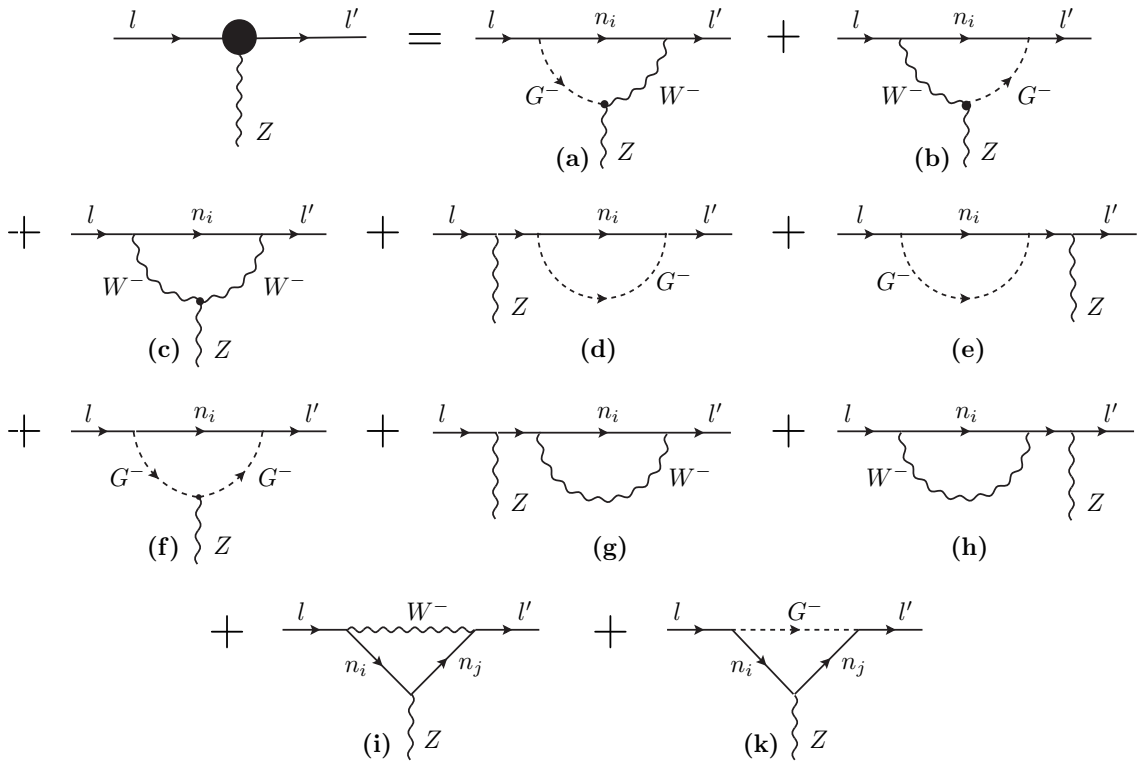

FIGURE A.2: Feynman diagrams contribute to the effective vertex $\bar{l}l'Z$ ($l \neq l'$).

$$\begin{aligned}\Gamma_\alpha^{(d)} &= \frac{g^2}{32\pi^2} U_{li} U_{l'i}^* \not{p}_2 P_L \left[C_{UV} - 1 - 2\int_0^1 dx(1-x)\log\left[D_{2b}(x)\right] \right] \frac{\not{p}_2 + m_\alpha}{m_\beta^2 - m_\alpha^2} \\ &\times \gamma_\alpha \left(2P_L - 4\sin^2\theta_w\right) , \end{aligned} \tag{A.37}$$

$$\begin{aligned}\Gamma_\alpha^{(e)} &= \frac{g^2}{32\pi^2} U_{li} U_{l'i}^* \gamma_\alpha \left(2P_L - 4\sin^2\theta_w\right) \frac{\not{p}_1 + m_\beta}{m_\alpha^2 - m_\beta^2} \not{p}_1 P_L \\ &\times \left[C_{UV} - 1 - 2\int_0^1 dx(1-x)\log\left[D_{2a}(x)\right] \right] , \end{aligned} \tag{A.38}$$

$$\begin{aligned}\Gamma_\alpha^{(f)} &= \frac{g^2}{32\pi^2 M_w^2} U_{li} U_{l'i}^* \left(1 - 2\sin^2\theta_w\right) \left[m_i^2 \left\{ (m_\alpha + m_\beta) + \gamma_5 (m_\alpha - m_\beta) \right\} \right. \\ &\times \int_0^1 \frac{dx\ dy\ y}{D_3(x,y)} (p_1 + p_2 - 2y\overline{p})_\alpha - \left\{ (m_\alpha m_\beta + m_i^2) - \gamma_5 (m_\alpha m_\beta - m_i^2) \right\} \\ &\times \int_0^1 \frac{dx\ dy\ y^2}{D_3(x,y)} (p_1 + p_2 - 2y\overline{p})_\alpha \overline{\not{p}} - \frac{1}{2} \left\{ (m_\alpha m_\beta + m_i^2) - \gamma_5 (m_\alpha m_\beta - m_i^2) \right\} \gamma_\alpha \\ &\times \left. \left\{ C_{UV} - 2\int_0^1 dx\ dy\ y \log\left[D_3(x,y)\right] \right\} \right] , \end{aligned} \tag{A.39}$$

$$\Gamma_\alpha^{(g)} = -\frac{g^2}{64\pi^2 M_w^2} U_{li} U_{l'i}^* \Big[m_i^2 \{(m_\alpha + m_\beta) + \gamma_5 (m_\alpha - m_\beta)\} \{C_{UV} - \int_0^1 dx \log [D_{2b}(x)] \Big\} - \frac{\not p_2}{2} \{(m_\alpha m_\beta + m_i^2) + \gamma_5 (m_\alpha m_\beta - m_i^2)\} \{C_{UV} - 2 \int_0^1 dx (1-x) \log [D_{2b}(x)] \Big\} \Big] \frac{\not p_2 + m_\alpha}{m_\beta^2 - m_\alpha^2} \gamma_\alpha \left(2P_L - 4 \sin^2 \theta_w\right) , \quad \text{(A.40)}$$

$$\Gamma_\alpha^{(h)} = -\frac{g^2}{64\pi^2 M_w^2} U_{li} U_{l'i}^* \, \gamma_\alpha \left(2P_L - 4 \sin^2 \theta_w\right) \frac{\not p_1 + m_\beta}{m_\alpha^2 - m_\beta^2} \Big[m_i^2 \{(m_\alpha + m_\beta) + \gamma_5 (m_\alpha - m_\beta)\} \times \Big\{ C_{UV} - \int_0^1 dx \log [D_{2a}(x)] \Big\} - \frac{\not p_1}{2} \{(m_\alpha m_\beta + m_i^2) + \gamma_5 (m_\alpha m_\beta - m_i^2)\} \times \Big\{ C_{UV} - 2 \int_0^1 dx (1-x) \log [D_{2a}(x)] \Big\} \Big] , \quad \text{(A.41)}$$

$$\Gamma_\alpha^{(i)} = \frac{g^2}{8\pi^2 M_w^2} U_{li} C_{ij} U_{l'j}^* \Big[P_R \int_0^1 \frac{dx \; dy \; y}{D_{3F}(x,y)} (\not p_1 - y \not{\bar p}) \gamma_\alpha (\not p_2 - y \not{\bar p}) + \frac{1}{2} \gamma_\alpha P_L \times \Big\{ C_{UV} - 2 - 2 \int_0^1 dx \; dy \; y \log D_{3F}(x,y) \Big\} \Big] , \quad \text{(A.42)}$$

$$\Gamma_\alpha^{(k)} = -\frac{g^2}{16\pi^2 M_w^2} U_{li} C_{ij} U_{l'j}^* \Big[-m_i^2 m_j^2 \gamma_\alpha P_L \int_0^1 \frac{dx \; dy \; y}{D_{3F}(x,y)} + m_\beta m_i^2 P_L \times \int_0^1 \frac{dx \; dy \; y}{D_{3F}(x,y)} (\not p_2 - y \not{\bar p}) \gamma_\alpha + m_\alpha m_j^2 \gamma_\alpha P_L \int_0^1 \frac{dx \; dy \; y}{D_{3F}(x,y)} (\not p_1 - y \not{\bar p}) - m_\alpha m_\beta P_L \int_0^1 \frac{dx \; dy \; y}{D_{3F}(x,y)} \, (\not p_2 - y \not{\bar p}) \gamma_\alpha (\not p_1 - y \not{\bar p}) - \frac{m_\alpha m_\beta \gamma_\alpha P_R}{2} \times \Big\{ C_{UV} - 1 - 2 \int_0^1 dx \; dy \; y \log D_{3F}(x,y) \Big\} \Big] , \quad \text{(A.43)}$$

where $C_{ij} = \sum_\alpha^{e,\mu,\tau} U_{\alpha i}^* U_{\alpha j}$.

In the case considered, the unitarity of the mixing matrix will eliminate the divergences in the (e), (i) and (k) diagrams, the divergences remained also vanishes since:

$$\Gamma_\alpha^{(d)}(C_{UV}) + \Gamma_\alpha^{(e)}(C_{UV}) = 0 , \quad \text{(A.44)}$$

$$\Gamma_\alpha^{(f)}(C_{UV}) + \Gamma_\alpha^{(g)}(C_{UV}) + \Gamma_\alpha^{(h)}(C_{UV}) = 0 . \quad \text{(A.45)}$$

One can simplify the above results by keeping only the leading order terms that contribute to the effective vertex:

$$\Gamma_\alpha^{(a,b)} = \frac{g^2}{8\pi^2} U_{li} U_{l'i}^* \sin^2 \theta_w \; M_w^2 \lambda_i \; Int \left(\frac{y^2}{D_3(x,y)} \right) \; \gamma_\alpha P_L , \quad \text{(A.46)}$$

$$\Gamma_\alpha^{(c)} = \frac{g^2}{8\pi^2} U_{li} U_{l'i}^* \cos^2\theta_w \; Int\left[y \log D_3(x,y)\right] \; 6\gamma_\alpha P_L \,, \tag{A.47}$$

$$\begin{aligned} \Gamma_\alpha^{(d)} + \Gamma_\alpha^{(e)} &= -\frac{g^2}{8\pi^2} U_{li} U_{l'i}^* \; \frac{1-2\sin^2\theta_w}{S_\alpha - S_\beta} \left\{ S_\alpha Int\left[(1-x)\log D_{2a}(x)\right] \right. \\ &- \left. S_\beta Int\left[(1-x)\log D_{2b}(x)\right] \right\} \gamma_\alpha P_L \,, \end{aligned} \tag{A.48}$$

$$\Gamma_\alpha^{(f)} = \frac{g^2}{16\pi^2} U_{li} U_{l'i}^* \; \lambda_i (1-2\sin^2\theta_w) \; Int\left[y \log D_3(x,y)\right] \; \gamma_\alpha P_L \,, \tag{A.49}$$

$$\begin{aligned} \Gamma_\alpha^{(g)} + \Gamma_\alpha^{(h)} &= -\frac{g^2}{16\pi^2} U_{li} U_{l'i}^* \; \frac{\lambda_i (1-2\sin^2\theta_w)}{S_\alpha - S_\beta} \left\{ S_\alpha Int\left[\log D_{2a}(x)\right] \right. \\ &- \left. S_\beta Int\left[\log D_{2b}(x)\right] \right\} \gamma_\alpha P_L \,, \end{aligned} \tag{A.50}$$

$$\Gamma_\alpha^{(i)} = -\frac{g^2}{8\pi^2} U_{li} C_{ij} U_{l'j}^* \; Int\left[y \log D_{3F}(x,y)\right] \; \gamma_\alpha P_L \,, \tag{A.51}$$

$$\Gamma_\alpha^{(k)} = \frac{g^2}{16\pi^2} U_{li} C_{ij} U_{l'j}^* \; \lambda_i \lambda_j M_w^2 \; Int\left[\frac{y}{D_{3F}(x,y)}\right] \; \gamma_\alpha P_L \,, \tag{A.52}$$

Performing the integrations with respect to x and y, the results read:

$$\sum_{r=a}^{h} \Gamma_\alpha^{(r)} = -\frac{g^2}{8\pi^2} U_{li} U_{l'i}^* \; F_z(\lambda_i) \; \gamma_\alpha P_L \,, \tag{A.53}$$

$$F_z(x) = -\frac{5x}{2(1-x)} - \frac{5x^2}{2(1-x)^2} \log x \,, \tag{A.54}$$

$$\Gamma_\alpha^{(i)} + \Gamma_\alpha^{(k)} = -\frac{g^2}{8\pi^2} U_{li} C_{ij} U_{l'j}^* \; G_z(\lambda_i, \lambda_j) \; \gamma_\alpha P_L \,, \tag{A.55}$$

$$G_z(x,y) = -\frac{1}{2(x-y)} \left[\frac{x^2(1-y)}{(1-x)} \log x - \frac{y^2(1-x)}{(1-y)} \log y \right] . \tag{A.56}$$

Then, we have the final expression for the effective vertex $\bar{l} l' Z$ $(l \neq l')$

$$\frac{g}{4\cos\theta_w} \; \Gamma_\alpha^z = -\frac{g^3}{32\pi^2 \cos\theta_w} U_{li} U_{l'j}^* \; \left[\delta_{ij} F_z(\lambda_i) + C_{ij} \; G_z(\lambda_i, \lambda_j)\right] \; \gamma_\alpha P_L \,. \tag{A.57}$$

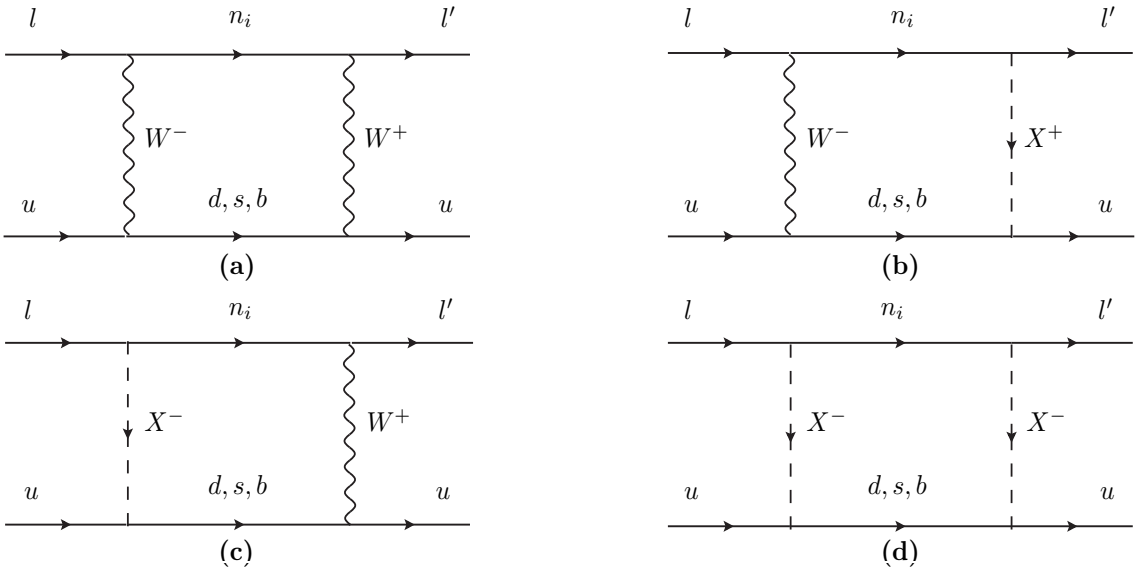

FIGURE A.3: u-type box diagrams.

A.3 Calculation of the Box Diagrams

There are two groups of box diagrams, which give contribution to the $\mu - e$ conversion rate. They are u-type box diagrams (Fig. A.3) or d-type box diagrams (Fig. A.4). The virtual quarks participating in the u-type graphs are d, s and b, while the quarks taking part in the d-type ones are u, c and t. It is important to note that result of the calculation of the d-type diagrams can also be applied to the box diagrams, whose origins are d-type box diagrams with d quark replaced by negative leptons (e^-, μ^-, τ^-) and virtual (u, c, t) quarks by neutrinos.

We introduce next a common function $D_4(x, y, z)$, which will be used in further calculation

$$D_4(x, y, z) = (1 - z)M_w^2 + z\left\{(1 - y)m_i^2 + ym_j^2\right\} + \dots , \tag{A.58}$$

where the dots stand for the ignored terms in the function which give subdominant contribution to the form factor.

A.3.1 u-Type Box Diagrams

Let us start to calculate the u-type box diagrams. Using the result in [138] and ignoring the subdominant terms, the contribution of the (a) diagram is expressed as:

$$\begin{aligned} \mathcal{M}^u_{(a)} &= \frac{g^4}{128\pi^2} U_{li} U^*_{l'i} V_{ud_j} V^*_{ud_j} \int_0^1 dx\ dy\ dz\ \frac{z(1-z)}{D_4(x,y,z)}\ [\overline{u}(p_4) P_R \gamma_\rho \gamma_\alpha \gamma_\sigma u(p_3)] \\ &\times\ [\overline{u}(p_2) P_R \gamma^\rho \gamma^\alpha \gamma^\sigma u(p_1)]\ . \end{aligned} \tag{A.59}$$

Using

$$[\overline{u}(p_4)P_R\gamma_\rho\gamma_\alpha\gamma_\sigma u(p_3)]\times[\overline{u}(p_2)P_R\gamma^\rho\gamma^\alpha\gamma^\sigma u(p_1)] = 16\ [\overline{u}(p_4)P_R\gamma_\alpha u(p_3)] \times [\overline{u}(p_2)P_R\gamma^\alpha u(p_1)]\ . \quad (A.60)$$

the above equation is simplified into the form

$$\mathcal{M}^u_{(a)} = \frac{g^4}{8\pi^2}U_{li}U^*_{l'i}V_{ud_j}V^*_{ud_j}\int_0^1 dx\ dy\ dz\ \frac{z(1-z)}{D_4(x,y,z)}\ [\overline{u}(p_4)P_R\gamma_\alpha u(p_3)] \times [\overline{u}(p_2)P_R\gamma^\alpha u(p_1)]\ . \quad (A.61)$$

Performing the same calculations for diagrams (b), (c) and (d), we obtain:

$$\mathcal{M}^u_{(b,\ c)} = \frac{g^4}{64\pi^2}U_{li}U^*_{l'i}V_{ud_j}V^*_{ud_j}\int_0^1 dx\ dy\ dz\ \frac{z(1-z)}{D_4^2(x,y,z)}\ m_i^2m_j^2\ [\overline{u}(p_4)P_R\gamma_\alpha u(p_3)] \times [\overline{u}(p_2)P_R\gamma^\alpha u(p_1)]\ , \quad (A.62)$$

$$\mathcal{M}^u_{(d)} = \frac{g^4}{128\pi^2}U_{li}U^*_{l'i}V_{ud_j}V^*_{ud_j}\int_0^1 dx\ dy\ dz\ \frac{z(1-z)}{D_4(x,y,z)}\ m_i^2m_j^2\ [\overline{u}(p_4)P_R\gamma_\alpha u(p_3)] \times [\overline{u}(p_2)P_R\gamma^\alpha u(p_1)]\ . \quad (A.63)$$

Summing up the contributions of the four graphs and carrying out the integrations with respect to x, y and z, the result is easy to be obtained:

$$\begin{aligned}\sum_{r=a}^{d}\mathcal{M}^u_{(r)} &= \frac{g^4}{64\pi^2M_w^2}U_{li}U^*_{l'i}V_{ud_j}V^*_{ud_j}\left[M_w^2\left(8+\frac{1}{2}\lambda_i\lambda_j\right)Int\left(\frac{z(1-z)}{D_4(x,y,z)}\right)\right.\\ &+ \left. 2M_w^4\lambda_i\lambda_j Int\left(\frac{z(1-z)}{D_4^2(x,y,z)}\right)\right]\ [\overline{u}(p_4)P_R\gamma_\alpha u(p_3)]\times[\overline{u}(p_2)P_R\gamma^\alpha u(p_1)]\\ &= \frac{g^4}{64\pi^2M_w^2}U_{li}U^*_{l'i}V_{ud_j}V^*_{ud_j}F_{XBox}(\lambda_i,\lambda_j)\ [\overline{u}(p_4)P_R\gamma_\alpha u(p_3)]\\ &\times [\overline{u}(p_2)P_R\gamma^\alpha u(p_1)]\ , \end{aligned} \quad (A.64)$$

where

$$\begin{aligned}F_{Box}(x,y) &= \frac{1}{x-y}\left\{(4+\frac{xy}{4})\left[\frac{1}{1-x}+\frac{x^2}{(1-x)^2}\log x-\frac{1}{1-y}-\frac{y^2}{(1-y)^2}\log y\right]\right.\\ &- \left. 2xy\left[\frac{1}{1-x}+\frac{x}{(1-x)^2}\log x-\frac{1}{1-y}-\frac{y}{(1-y)^2}\log y\right]\right\}. \end{aligned} \quad (A.65)$$

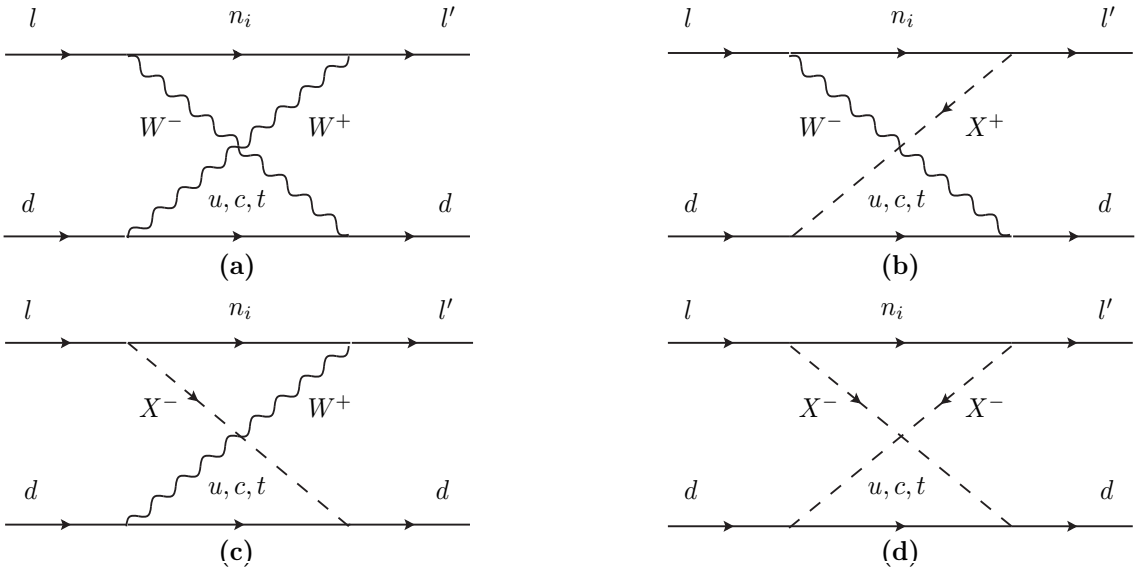

FIGURE A.4: d-type box diagrams.

A.3.2 d-Type Box Diagrams

The d-box diagrams are calculated similarly, the result of diagram (a) is:

$$\begin{aligned}\mathcal{M}^d_{(a)} &= -\frac{g^4}{128\pi^2}U_{li}U^*_{l'i}V_{du_j}V^*_{du_j}\int_0^1 dx\ dy\ dz\ \frac{z(1-z)}{D_4(x,y,z)}\ [\overline{u}(p_4)P_R\gamma_\rho\gamma_\alpha\gamma_\sigma u(p_3)] \\ &\times\ [\overline{u}(p_2)P_R\gamma^\sigma\gamma^\alpha\gamma^\rho u(p_1)]\ . \end{aligned} \tag{A.66}$$

Using

$$\begin{aligned}[\overline{u}(p_4)P_R\gamma_\rho\gamma_\alpha\gamma_\sigma u(p_3)]\times[\overline{u}(p_2)P_R\gamma^\sigma\gamma^\alpha\gamma^\rho u(p_1)] &= 4\,[\overline{u}(p_4)P_R\gamma_\alpha u(p_3)] \\ &\times\ [\overline{u}(p_2)P_R\gamma^\alpha u(p_1)]\ . \end{aligned} \tag{A.67}$$

we have

$$\begin{aligned}\mathcal{M}^d_{(a)} &= -\frac{g^4}{32\pi^2}U_{li}U^*_{l'i}V_{du_j}V^*_{du_j}\int_0^1 dx\ dy\ dz\ \frac{z(1-z)}{D_4(x,y,z)}\ [\overline{u}(p_4)P_R\gamma_\alpha u(p_3)] \\ &\times\ [\overline{u}(p_2)P_R\gamma^\alpha u(p_1)]\ . \end{aligned} \tag{A.68}$$

We also have expressions for diagrams (b), (c) and (d):

$$\begin{aligned}\mathcal{M}^d_{(b,\ c)} &= -\frac{g^4}{64\pi^2}U_{li}U^*_{l'i}V_{du_j}V^*_{du_j}\int_0^1 dx\ dy\ dz\ \frac{z(1-z)}{D_4^2(x,y,z)}\ m_i^2m_j^2\ [\overline{u}(p_4)P_R\gamma_\alpha u(p_3)] \\ &\times\ [\overline{u}(p_2)P_R\gamma^\alpha u(p_1)]\ , \end{aligned} \tag{A.69}$$

$$\begin{aligned}\mathcal{M}^d_{(d)} &= -\frac{g^4}{128\pi^2}U_{li}U^*_{l'i}V_{du_j}V^*_{du_j}\int_0^1 dx\ dy\ dz\ \frac{z(1-z)}{D_4(x,y,z)}\ m_i^2 m_j^2\ [\overline{u}(p_4)P_R\gamma_\alpha u(p_3)] \\ &\times\ [\overline{u}(p_2)P_R\gamma^\alpha u(p_1)]\ . \end{aligned} \tag{A.70}$$

Summing up the contributions obtained above, we arrive at the final expression of the the d-type diagram form factor:

$$\begin{aligned}\sum_{r=a}^{d}\mathcal{M}^d_{(r)} &= -\frac{g^4}{64\pi^2 M_w^2}U_{li}U^*_{l'i}V_{du_j}V^*_{du_j}\left[M_w^2\left(2+\frac{1}{2}\lambda_i\lambda_j\right)Int\left(\frac{z(1-z)}{D_4(x,y,z)}\right)\right. \\ &+ \left. 2M_w^4\lambda_i\lambda_j Int\left(\frac{z(1-z)}{D_4^2(x,y,z)}\right)\right]\ [\overline{u}(p_4)P_R\gamma_\alpha u(p_3)]\times[\overline{u}(p_2)P_R\gamma^\alpha u(p_1)] \\ &= \frac{g^4}{64\pi^2 M_w^2}U_{li}U^*_{l'i}V_{du_j}V^*_{du_j}F_{XBox}(\lambda_i,\lambda_j)\ [\overline{u}(p_4)P_R\gamma_\alpha u(p_3)] \\ &\times\ [\overline{u}(p_2)P_R\gamma^\alpha u(p_1)]\ , \end{aligned} \tag{A.71}$$

where

$$\begin{aligned}F_{XBox}(x,y) &= -\frac{1}{x-y}\left\{(1+\frac{xy}{4})\left[\frac{1}{1-x}+\frac{x^2}{(1-x)^2}\log x-\frac{1}{1-y}-\frac{y^2}{(1-y)^2}\log y\right]\right. \\ &- \left. 2xy\left[\frac{1}{1-x}+\frac{x}{(1-x)^2}\log x-\frac{1}{1-y}-\frac{y}{(1-y)^2}\log y\right]\right\}\ . \end{aligned} \tag{A.72}$$

Appendix B

See-saw Type II Form Factor

B.1 Lagrangian and Feynman Rules

We start this section by writing down here the interested part of the see-saw type II (Higgs triplet model) Lagrangian involving the interaction between leptons and heavy charged scalars:

$$\mathcal{L}_{\text{int}} = \frac{1}{2}(y_N)_{ij}\left[\overline{e}_i^c e_j \xi^{++} + \frac{1}{\sqrt{2}}\left(\overline{\nu}_i^c e_j + \overline{e}_i^c \nu_j\right)\xi^{+} + h.c\right], \tag{B.1}$$

here $(y_N)_{ij}$ is two times bigger than h_{ij}, which was introduced in eq. (2.53).

In the framework of this calculation, we use the following Feynman rules:

- Vertexes

- $\bar{l}_i\ \nu_k^c\ \xi^-$

$$\frac{i}{\sqrt{2}}(y_N)_{ik}\ P_L\,, \tag{B.2}$$

- $\bar{l}_i\ l_k^c\ \xi^{--}$

$$i(y_N)_{ik}\ P_L \tag{B.3}$$

- $\xi^*(p)\ \xi(p')\ A_\alpha$

$$iq_\xi\ e\ (p+p')_\alpha\,, \tag{B.4}$$

- $\bar{l}\ l\ A_\alpha$

$$iq_l\ e\ \gamma_\alpha\,. \tag{B.5}$$

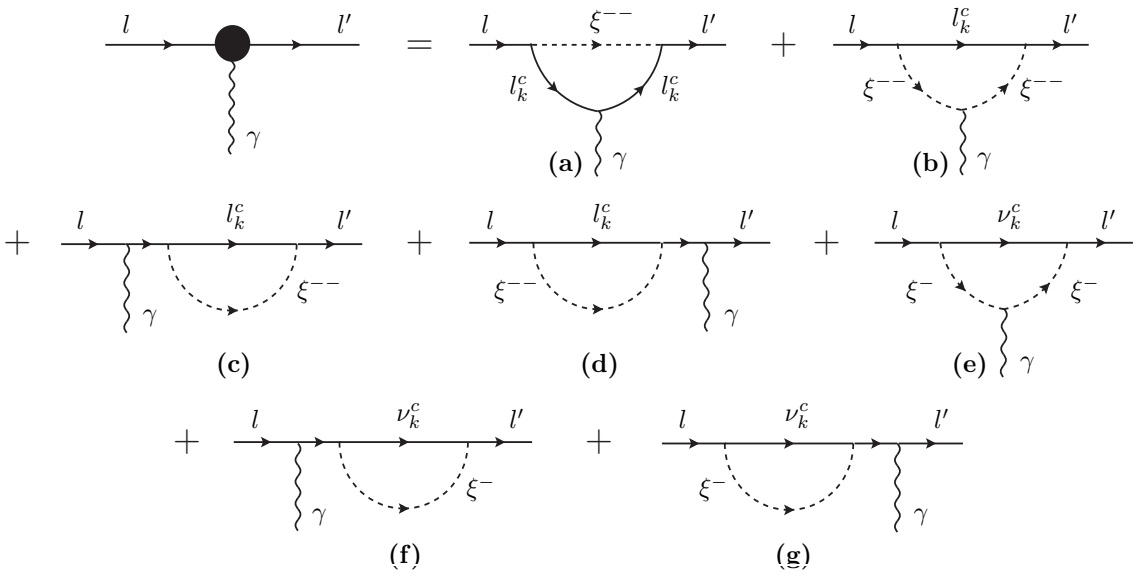

FIGURE B.1: One-loop diagrams contribute to seesaw type-II form factor.

- Propagators

- Fermion field

$$\frac{i}{\not{k} - m + i\epsilon}\,, \tag{B.6}$$

- Scalar field

$$\frac{i}{k^2 - m^2 + i\epsilon}\,. \tag{B.7}$$

Here q_ξ is the heavy scalar charge, and e is the electromagnetic coupling constant.

B.2 Calculation of the See-saw Type II Form Factor

At order of one-loop correction, the Feynman diagrams which contribute to the form factors are shown in the Fig. B.1.

From the Feynman rules listed above, the contribution of the graph (a) (see Fig. B.2) is easy to be written down:

$$\Lambda^{(a)}_\mu = i(y^*_N)_{ek}(y_N)_{\mu k}\mu^\varepsilon \int \frac{d^dk}{(2\pi)^d} \frac{P_R\left[(\not{p}_2 - \not{k}) + m_k\right]\gamma_\mu\left[(\not{p}_1 - \not{k}) + m_k\right]P_L}{\left[(p_2-k)^2 - m_k^2\right]\left[(p_1-k)^2 - m_k^2\right]\left(k^2 - M^2_{\xi^{--}}\right)}\,, \tag{B.8}$$

where, μ is an arbitrary mass dimensional parameter and $\varepsilon = 4 - d$.

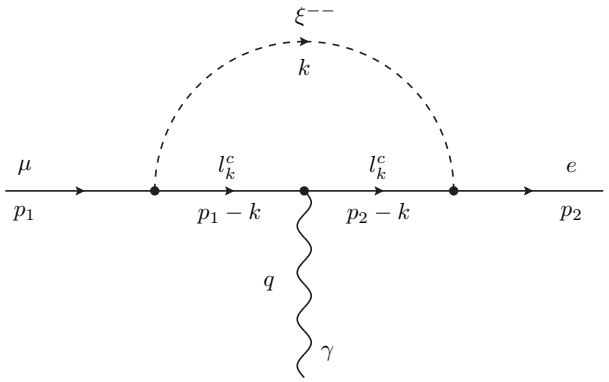

FIGURE B.2: Diagram (a)

Using Feynman parametrization

$$\frac{1}{a\ b\ c} = \int_0^1 dx \int_0^1 2y\ dy\ \frac{1}{\left[\{a(1-x)+bx\}\,y + c(1-y)\right]^3}\,, \tag{B.9}$$

for $a = (p_1 - k)^2 - m_k^2$, $b = (p_2 - k)^2 - m_k^2$ and $c = k^2 - M_{\xi^{--}}^2$, we rewrite eq. (B.8) in the form

$$\Lambda_\mu^{(a)} = i(y_N^*)_{ek}(y_N)_{\mu k}\ \mu^\varepsilon \int_0^1 dx \int_0^1 2y\ dy \int \frac{d^dk}{(2\pi)^d}\frac{NM}{(k^2-\Delta^2)^3}\,. \tag{B.10}$$

Here,

$$NM = P_R\left[\frac{2A_0(d-2)}{d}k^2 + A_1 - y(A_{21} + xA_{22}) + y^2(A_{31} + xA_{32} + x^2A_{33})\right]\,, \tag{B.11}$$

$$A_0 = -\frac{1}{2}\gamma_\mu\,,\quad A_1 = m_k^2\gamma_\mu + \not{p}_2\gamma_\mu\not{p}_1\,,\quad A_{21} = \not{p}_1\gamma_\mu\not{p}_1 + \not{p}_2\gamma_\mu\not{p}_2\,,$$
$$A_{22} = \not{p}_2\gamma_\mu\not{p}_1 - \not{p}_1\gamma_\mu\not{p}_1\,,\quad A_{31} = \not{p}_1\gamma_\mu\not{p}_1\,,\quad A_{32} = -2\not{p}_1\gamma_\mu\not{p}_1 + \not{p}_1\gamma_\mu\not{p}_2 + \not{p}_2\gamma_\mu\not{p}_1\,,$$
$$A_{33} = \not{p}_1\gamma_\mu\not{p}_1 + \not{p}_2\gamma_\mu\not{p}_2 - \not{p}_1\gamma_\mu\not{p}_2 - \not{p}_2\gamma_\mu\not{p}_1\,,$$

$$\Delta^2 = (1-y)C + yB - y(1-y)A\,, \tag{B.12}$$

$$A = M_{\xi^{--}}^2\left[-rx^2 - x(s_\mu - r - s_e) + s_\mu\right]\,,\quad B = M_{\xi^{--}}^2\left[-rx^2 + rx + s_k\right]\,,$$
$$C = M_{\xi^{--}}^2\,,\quad s_{e,\mu} = \frac{m_{e,\mu}^2}{M_{\xi^{--}}^2}\,,\quad s_k = \frac{m_k^2}{M_{\xi^{--}}^2}\,,\quad r = -\frac{q^2}{M_{\xi^{--}}^2}\,. \tag{B.13}$$

Performing the integration with respect to the phase space, one obtains the following equalities:

$$\int \frac{d^dk}{(2\pi)^d}\frac{1}{(k^2-\Delta^2)^3} = -\frac{i}{32\pi^2\Delta^2}\,, \tag{B.14}$$

$$\frac{2(d-2)}{d}\mu^\varepsilon \int \frac{d^dk}{(2\pi)^d}\frac{k^2}{(k^2-\Delta^2)^3} = \frac{i}{16\pi^2}\left(C_{UV} - 1 - \log\Delta^2\right)\,. \tag{B.15}$$

where, the ultraviolet divergence C_{UV} is

$$C_{UV} = \frac{2}{\varepsilon} + \log 4\pi\mu^2 \,, \tag{B.16}$$

and $\gamma = 0.5772$ is Euler-Mascheroni constant.

Substituting eqs. (B.14) and (B.15) into (B.10), after simplifying the result obtained, the formula becomes:

$$\begin{aligned}\Lambda_\mu^{(a)} &= -\frac{A_0\ (y_N^*)_{ek}(y_N)_{\mu k}P_L}{16\pi^2}(C_{UV}-1) + \frac{A_0\ (y_N^*)_{ek}(y_N)_{\mu k}P_L}{8\pi^2}\int_0^1 dx\int_0^1 dy\ y\ \log\Delta^2 \\ &+ \frac{(y_N^*)_{ek}(y_N)_{\mu k}P_R}{16\pi^2}\int_0^1 dx\int_0^1 dy\,\big[A_1 y - y^2(A_{21}+xA_{22}) \\ &+ y^3(A_{31}+xA_{32}+x^2A_{33})\big]\,. \end{aligned}\tag{B.17}$$

To carry out the integration with respect to x and y variables in the above formula, one has to expand the function Δ in term of leading and subdominant contributions. For $\Delta^2 = C(1-y) + By - Ay(1-y)$ with $C \gg A, B$, we have approximations:

$$\int_0^1 dy\ y\log\Delta^2 = \frac{1}{2}\log C - \frac{3}{4} - \frac{1}{3}\frac{A}{C} - \frac{1}{2}\frac{B}{C} - \frac{B}{C}\log\frac{B}{C}\,, \tag{B.18}$$

$$\int_0^1 dy\ \frac{y}{\Delta^2} = -\frac{1}{C}\left[1 + \log\frac{B}{C} + \frac{B}{C} + \frac{2B}{C}\log\frac{B}{C} + \frac{5}{2}\frac{A}{C} + \frac{A}{C}\log\frac{B}{C}\right]\,, \tag{B.19}$$

$$\int_0^1 dy\ \frac{y^2}{\Delta^2} = -\frac{1}{C}\left[\frac{3}{2} + \log\frac{B}{C} + \frac{5B}{2C} + \frac{3B}{C}\log\frac{B}{C} + \frac{17}{6}\frac{A}{C} + \frac{A}{C}\log\frac{B}{C}\right]\,, \tag{B.20}$$

$$\int_0^1 dy\ \frac{y^3}{\Delta^2} = -\frac{1}{C}\left[\frac{11}{6} + \log\frac{B}{C} + \frac{13B}{3C} + \frac{4B}{C}\log\frac{B}{C} + \frac{37}{12}\frac{A}{C} + \frac{A}{C}\log\frac{B}{C}\right]\,. \tag{B.21}$$

Applying the above equalities, while keeping in mind new notations

$$B' = \frac{B}{M^2_{\xi^{--}}}\,, \quad A' = \frac{A}{M^2_{\xi^{--}}}\,, \tag{B.22}$$

then the eq. (B.17) can be rewritten as:

$$\Lambda_\mu^{(a)} = -\frac{A_0\ (y_N^*)_{ek}(y_N)_{\mu k}P_L}{16\pi^2}\,(C_{UV}-1) + \mathrm{I}_1 + \mathrm{I}_2 + \mathrm{I}_3 + \mathrm{I}_4\,, \tag{B.23}$$

$$
\begin{aligned}
\mathrm{I}_1 &= -\frac{A_1\ (y_N^*)_{ek}(y_N)_{\mu k}P_L}{16\pi^2 M^2_{\xi^{--}}}\int_0^1 dx\left[\left(1+B'+\frac{5}{2}A'\right)+(1+2s_k+s_\mu)\log B'\right.\\
&+ \left.(3r-s_\mu)x\log B'-3rx^2\log B'\right]\,, \qquad \text{(B.24)}\\
\mathrm{I}_2 &= \frac{(y_N^*)_{ek}(y_N)_{\mu k}P_R}{16\pi^2 M^2_{\xi^{--}}}\int_0^1 dx\left[(A_{21}+A_{22}x)\left(\frac{3}{2}+\frac{5}{2}B'+\frac{17}{6}A'\right)\right.\\
&+ A_{21}(1+3s_k+s_\mu)\log B'+\{A_{21}(4r-s_\mu)+A_{22}(1+3s_k+s_\mu)\}\,x\log B'\\
&+ \left.\{-A_{21}(4r-s_e)+A_{22}(4r-s_\mu)\}\,x^2\log B'-A_{22}(4r-s_e)x^3\log B'\right]\,, \qquad \text{(B.25)}\\
\mathrm{I}_3 &= -\frac{(y_N^*)_{ek}(y_N)_{\mu k}P_R}{16\pi^2 M^2_{\xi^{--}}}\int_0^1 dx\left[(A_{31}+A_{32}x+A_{33}x^2)\left(\frac{11}{6}+\frac{13}{3}B'+\frac{37}{12}A'\right)\right.\\
&+ A_{31}(1+4s_k+s_\mu)\log B'+\{A_{31}(5r-s_\mu)+A_{32}(1+4s_k+s_\mu)\}\,x\log B'\\
&+ \{A_{33}(1+4s_k+s_\mu)-A_{31}(5r-s_e)+A_{32}(5r-s_\mu)\}\,x^2\log B'\\
&- \left.\{A_{32}(5r-s_e)-A_{33}(5r-s_\mu)\}\,x^3\log B'-A_{33}(5r-s_e)x^4\log B'\right]\,, \qquad \text{(B.26)}\\
\mathrm{I}_4 &= \frac{A_0\ (y_N^*)_{ek}(y_N)_{\mu k}P_L}{8\pi^2}\int_0^1 dx\left[\left(\frac{1}{2}\log C-\frac{3}{4}-\frac{1}{3}A'-\frac{1}{2}B'\right)-s_k\log B'\right.\\
&- \left.rx\log B'+rx^2\log B'\right]\,. \qquad \text{(B.27)}
\end{aligned}
$$

Taking the integration with respect to x, then keeping only the leading terms, after rearranging the result, one gets:

$$
\begin{aligned}
\Lambda_\mu^{(a)} &= \frac{(y_N^*)_{ek}(y_N)_{\mu k}\gamma_\mu P_L}{32\pi^2}\,C_{UV}+\frac{(y_N^*)_{ek}(y_N)_{\mu k}\gamma_\mu P_L}{16\pi^2}\left(\frac{1}{4}-\frac{5r}{36}-\frac{s_k}{2}+\frac{s_e+s_\mu}{6}\right.\\
&- \left.\frac{1}{2}\log M^2+\frac{r}{6}\,f(r,s_k)\right)+\frac{(y_N^*)_{ek}(y_N)_{\mu k}P_L}{16\pi^2 M^2_{\xi^{--}}}\left(-\frac{5}{36}+\frac{f(r,s_k)}{6}\right)\\
&\times (\not{p}_1\gamma_\mu\not{p}_1+\not{p}_2\gamma_\mu\not{p}_2)-\frac{(y_N^*)_{ek}(y_N)_{\mu k}P_L}{16\pi^2 M^2_{\xi^{--}}}\left(\frac{1}{36}+\frac{f(r,s_k)}{6}\right)\not{p}_1\gamma_\mu\not{p}_2\\
&+ \frac{(y_N^*)_{ek}(y_N)_{\mu k}P_L}{16\pi^2 M^2_{\xi^{--}}}\left(\frac{17}{36}-\frac{f(r,s_k)}{6}\right)\not{p}_2\gamma_\mu\not{p}_1\,. \qquad \text{(B.28)}
\end{aligned}
$$

Here, the well-known function $f(r,s_k)$ is

$$
f(r,s_k)=\frac{4s_k}{r}+\log(s_k)+\left(1-\frac{2s_k}{r}\right)\sqrt{1+\frac{4s_k}{r}}\,\log\frac{\sqrt{r+4s_k}+\sqrt{r}}{\sqrt{r+4s_k}-\sqrt{r}}\,. \qquad \text{(B.29)}
$$

Similarly, we also have the contribution of the diagrams (b) (see Fig. B.3) to the form factor

$$
\Lambda_\mu^{(b)}=-2i(y_N^*)_{ek}(y_N)_{\mu k}\mu^\varepsilon\int\frac{d^dk}{(2\pi)^d}\frac{P_R(\not{k}+m_k)P_L(p_1+p_2-2k)_\mu}{(k^2-m_k^2)\left[(p_2-k)^2-M^2_{\xi^{--}}\right]\left[(p_1-k)^2-M^2_{\xi^{--}}\right]}\,. \qquad \text{(B.30)}
$$

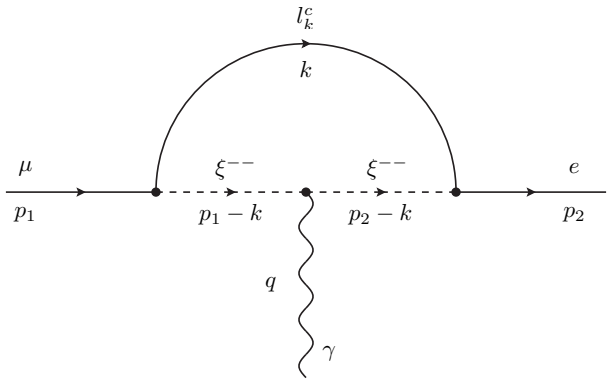

FIGURE B.3: Diagram (b)

After using the Feynman parametrization, eq. B.30 becomes

$$\Lambda_\mu^{(b)} = -2i(y_N^*)_{ek}(y_N)_{\mu k}\ \mu^\varepsilon \int_0^1 dx \int_0^1 2y\ dy \int \frac{d^dk'}{(2\pi)^d} \frac{P_R\ NM}{(k'^2 - \Delta^2)^3}\,, \tag{B.31}$$

$$k' = k - [p_1(1-x) + p_2 x]\, y\,, \tag{B.32}$$

$$\Delta^2 = [p_1(1-x) + p_2 x]^2\, y^2 + M_{\xi^{--}}^2 y + m_k^2(1-y) - \left[p_1^2(1-x) + p_2^2 x\right] y\,. \tag{B.33}$$

For $M_{\xi^{--}} \gg m_\alpha$, in order to expand Δ^2 in leading and subdominant terms, one has to change $y \to 1-y$. After changing the variable, we have

$$\Lambda_\mu^{(b)} = -2i(y_N^*)_{ek}(y_N)_{\mu k}\ \mu^\varepsilon \int_0^1 dx \int_0^1 2(1-y)\ dy \int \frac{d^dk''}{(2\pi)^d} \frac{P_R\ NM}{(k''^2 - \Delta^2)^3}\,, \tag{B.34}$$

$$k'' = k - [p_1(1-x) + p_2 x]\,(1-y)\,, \tag{B.35}$$

$$\Delta^2 = (1-y)C + yB + C_1 y^2 + C_2 y + C_3\,, \quad C = M_{\xi^{--}}^2\,, \tag{B.36}$$

$$B = M_{\xi^{--}}^2(-rx^2 + rx + s_k)\,, \quad C_1 = M_{\xi^{--}}^2\left[-rx^2 + x(s_e + r - s_\mu) + s_\mu\right]\,, \tag{B.37}$$

$$C_2 = M_{\xi^{--}}^2\left[3rx^2 + x(s_\mu - 3r - s_e) - s_\mu\right]\,, \quad C_3 = M_{\xi^{--}}^2 rx(1-x)\,, \tag{B.38}$$

$$NM = \frac{2B_0}{d}k^2 + (1-y)B_1 + (1-y)^2 B_2\,, \quad B_0 = -\gamma_\mu\,, \tag{B.39}$$

$$B_1 = (1-x)(\not{p}_1 p_{1\mu} + \not{p}_1 p_{2\mu}) + x(\not{p}_2 p_{1\mu} + \not{p}_2 p_{2\mu})\,, \tag{B.40}$$

$$B_2 = -2\left[(1-x)^2 \not{p}_1 p_{1\mu} + x(1-x)\not{p}_1 p_{2\mu} + x(1-x)\not{p}_2 p_{1\mu} + x^2 \not{p}_2 p_{2\mu}\right]\,. \tag{B.41}$$

Using eq. (B.14) and

$$\frac{2}{d}\ \mu^\varepsilon \int \frac{d^dk}{(2\pi)^d} \frac{k^2}{(k^2 - \Delta^2)^3} = \frac{i}{32\pi^2}\left(C_{UV} - \log\Delta^2\right)\,, \tag{B.42}$$

$\Lambda_\mu^{(b)}$ is arrived at:

$$\Lambda_\mu^{(b)} = -\frac{(y_N^*)_{ek}(y_N)_{\mu k}P_R}{8\pi^2}\int_0^1 dx\int_0^1 dy\left[\frac{(1-y)^2}{\Delta^2}B_1+\frac{(1-y)^3}{\Delta^2}B_2 + (1-y)B_0\log\Delta^2\right]+\frac{(y_N^*)_{ek}(y_N)_{\mu k}P_R}{16\pi^2}\,B_0\,C_{UV}\,. \tag{B.43}$$

The final expression for $\Lambda_\mu^{(b)}$ is obtained after performing the integration with respect to the Feynman variables x and y:

$$\Lambda_\mu^{(b)} = -\frac{(y_N^*)_{ek}(y_N)_{\mu k}\gamma_\mu P_L}{16\pi^2}\,C_{UV}-\frac{(y_N^*)_{ek}(y_N)_{\mu k}\gamma_\mu P_L}{8\pi^2}\left(\frac{1}{4}-\frac{r}{18}-\frac{s_k}{2}+\frac{s_e+s_\mu}{12} - \frac{1}{2}\log M^2\right)-\frac{(y_N^*)_{ek}(y_N)_{\mu k}P_R}{8\pi^2}\left(\frac{\not p_1 p_{1\mu}}{36}+\frac{5\not p_1 p_{2\mu}}{36}+\frac{5\not p_2 p_{1\mu}}{36}+\frac{\not p_2 p_{2\mu}}{36}\right). \tag{B.44}$$

Here, one has used the approximations:

$$\int_0^1 dy(1-y)\log\Delta^2 = -\frac{1}{4}+\frac{B}{2C}+\frac{C_1}{3C}+\frac{C_2}{2C}+\frac{C_3}{C}+\frac{1}{2}\log C\,, \tag{B.45}$$

$$\int_0^1 dy\frac{(1-y)^2}{\Delta^2} = \frac{1}{C}\left[\frac{1}{2}-\frac{B}{2C}-\frac{C_1}{3C}-\frac{C_2}{2C}-\frac{C_3}{C}\right], \tag{B.46}$$

$$\int_0^1 dy\frac{(1-y)^3}{\Delta^2} = \frac{1}{C}\left[\frac{1}{3}-\frac{B}{6C}-\frac{C_1}{12C}-\frac{C_2}{6C}-\frac{C_3}{2C}\right]. \tag{B.47}$$

Let us continue by calculating the diagram (c). From the Fig. B.4, applying the Feynman rules quoted above, it is not difficult to have

$$\Lambda_\mu^{(c)} = i\frac{(y_N^*)_{ek}(y_N)_{\mu k}}{m_\mu^2-m_e^2}\mu^\varepsilon\int\frac{d^dk}{(2\pi)^d}\frac{P_R\,\not k(\not p_2+m_\mu)\gamma_\mu}{\left(k^2-m_k^2\right)\left[(p_2-k)^2-M_{\xi^{--}}^2\right]}\,. \tag{B.48}$$

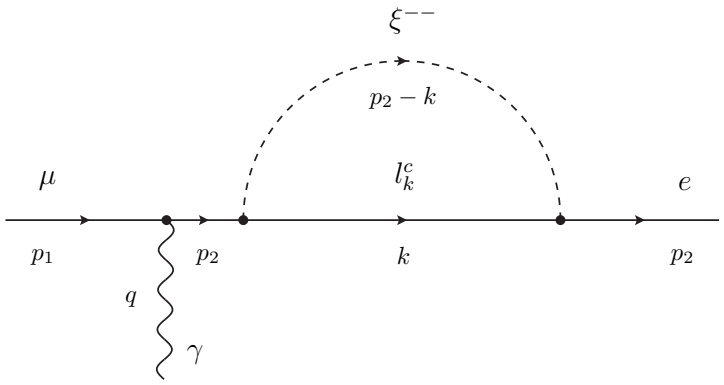

FIGURE B.4: Diagram (c)

After few steps of modifying, eq. (B.48) becomes

$$\Lambda_\mu^{(c)} = i\frac{(y_N^*)_{ek}(y_N)_{\mu k}}{m_\mu^2 - m_e^2}\mu^\varepsilon \int \frac{d^dk'}{(2\pi)^d}\frac{(1-x)(m_e^2 P_R + m_\mu m_e P_L)\gamma_\mu}{(k'^2 - \Delta_e^2)^2}\,, \tag{B.49}$$

$$k' = k + (1-x)p_2, \quad \Delta_e^2 = M_{\xi^{--}}^2(1-x) + m_k^2 x - m_e^2 x(1-x)\,. \tag{B.50}$$

To arrive at eq. (B.49) expression, we have used the Feynman parametrization

$$\frac{1}{a\;b} = \int_0^1 \frac{dx}{[a(1-x)+bx]^2}\,, \tag{B.51}$$

for $a = (p_2 - k)^2 - M_{\xi^{--}}^2$ and $b = k^2 - m_k^2$.

Performing the integration in D dimensional phase space, the result reads

$$\mu^\varepsilon \int \frac{d^dk}{(2\pi)^d}\frac{1}{(k^2-\Delta^2)^2} = \frac{i}{16\pi^2}\left(C_{UV} - \log\Delta^2\right)\,. \tag{B.52}$$

Substituting eq. (B.52) into eq. (B.49), it is easy to get

$$\Lambda_\mu^{(c)} = -\frac{(y_N^*)_{ek}(y_N)_{\mu k}}{32\pi^2}\frac{(m_e^2 P_R + m_\mu m_e P_L)\gamma_\mu}{m_\mu^2 - m_e^2}\left[C_{UV} - 2\int_0^1 dx(1-x)\log\Delta_e^2\right]\,. \tag{B.53}$$

The contribution of the (d) diagram to the form factor can be obtained directly from eq. (B.53) by exchanging m_e and m_μ. The result is straightforward

$$\Lambda_\mu^{(d)} = \frac{(y_N^*)_{ek}(y_N)_{\mu k}}{32\pi^2}\frac{(m_\mu^2 P_R + m_\mu m_e P_L)\gamma_\mu}{m_\mu^2 - m_e^2}\left[C_{UV} - 2\int_0^1 dx(1-x)\log\Delta_\mu^2\right]\,, \tag{B.54}$$

$$\tag{B.55}$$

where

$$\Delta_\mu^2 = M_{\xi^{--}}^2(1-x) + m_k^2 x - m_\mu^2 x(1-x)\,. \tag{B.56}$$

After expanding $\Delta_{e,\mu}$ in a series of leading and subdominant terms, the integrations with respect to x in eqs. (B.53) and (B.54) are easy to be carried out, the results read:

$$\int_0^1 dx(1-x)\log\Delta_e^2 = \frac{1}{2}\log M_{\xi^{--}}^2 - \frac{1}{4} - \frac{1}{6}s_e + \frac{1}{2}s_k\,, \tag{B.57}$$

$$\int_0^1 dx(1-x)\log\Delta_\mu^2 = \frac{1}{2}\log M_{\xi^{--}}^2 - \frac{1}{4} - \frac{1}{6}s_\mu + \frac{1}{2}s_k\,. \tag{B.58}$$

Using above equations, while keeping in mind equality $\gamma_\mu m_e m_\mu P_R = P_R \not{p}_2 \gamma_\mu \not{p}_1$, the sum of the diagrams (c) and (d) becomes

$$\begin{aligned}\Lambda_\mu^{(c)} + \Lambda_\mu^{(d)} &= \frac{(y_N^*)_{ek}(y_N)_{\mu k}\gamma_\mu P_L}{32\pi^2}\, C_{UV} + \frac{(y_N^*)_{ek}(y_N)_{\mu k}\gamma_\mu P_L}{16\pi^2}\left(-\frac{1}{2}\log M^2_{\xi^{--}} + \frac{1}{4}\right. \\ &+ \left.\frac{s_e + s_\mu}{6} - \frac{1}{2}s_k\right) + \frac{(y_N^*)_{ek}(y_N)_{\mu k}}{16\pi^2}\frac{P_R\, \not{p}_2\gamma_\mu \not{p}_1}{6}\,. \end{aligned} \tag{B.59}$$

The effective coupling, which is contributed by the doubly-charged scalar is now straightforward to be obtained by summing up the results of the first four diagrams

$$\Lambda_\mu^{(\xi^{--})} = \sum_{i=a}^{d}\Lambda_\mu^{(i)} \;=\; {}^1\Lambda_\mu^{(\xi^{--})} + \;{}^2\Lambda_\mu^{(\xi^{--})}\,, \tag{B.60}$$

$${}^1\Lambda_\mu^{(\xi^{--})} = \frac{(y_N^*)_{ek}(y_N)_{\mu k}}{16\pi^2}\frac{f(r,s_k)}{6M^2_{\xi^{--}}}\left(\not{p}_1\gamma_\mu\not{p}_1 - \not{p}_1\gamma_\mu\not{p}_2 - \not{p}_2\gamma_\mu\not{p}_1 + \not{p}_2\gamma_\mu\not{p}_2 - \gamma_\mu q^2\right)P_L\,, \tag{B.61}$$

$$\begin{aligned}{}^2\Lambda_\mu^{(\xi^{--})} &= \frac{(y_N^*)_{ek}(y_N)_{\mu k}\gamma_\mu P_L}{16\pi^2}\left(-\frac{r}{36} + \frac{s_e+s_\mu}{6}\right) + \frac{(y_N^*)_{ek}(y_N)_{\mu k}}{16\pi^2}\frac{P_L}{36M^2_{\xi^{--}}}\left(-5\not{p}_1\gamma_\mu\not{p}_1\right. \\ &- \left.\not{p}_1\gamma_\mu\not{p}_2 + 23\not{p}_2\gamma_\mu\not{p}_1 - 5\not{p}_2\gamma_\mu\not{p}_2 - 2\not{p}_1 p_{1\mu} - 10\not{p}_1 p_{2\mu} - 10\not{p}_2 p_{1\mu} - 2\not{p}_2 p_{2\mu}\right)\,. \end{aligned} \tag{B.62}$$

As a property of the form factors with photon exchange, it is possible to write eqs. (B.61) and (B.62) in the gauge covariant forms. For ${}^1\Lambda_\mu^{(\xi^{--})}$, after using

$$\not{q}\gamma_\mu\not{q} = -q^2\gamma_\mu + 2q_\mu q_\nu\gamma^\nu\,, \tag{B.63}$$

the formula is arrived at

$${}^1\Lambda_\mu^{(\xi^{--})} = -\frac{(y_N^*)_{ek}(y_N)_{\mu k}}{48\pi^2 M^2_{\xi^{--}}}\, f(r,s_k)\left(q^2\gamma_\mu - q_\mu q_\nu\gamma^\nu\right)P_L\,, \tag{B.64}$$

which is gauge covariant as being expected.

For the case of ${}^2\Lambda_\mu^{(\xi^{--})}$, one has

$$\begin{aligned}{}^2\Lambda_\mu^{(\xi^{--})} &\sim \gamma_\mu\left(-q^2 - 6m_e^2 - 6m_\mu^2\right) + 5\not{p}_1\gamma_\mu\not{p}_1 + \not{p}_1\gamma_\mu\not{p}_2 - 23\not{p}_2\gamma_\mu\not{p}_1 + 5\not{p}_2\gamma_\mu\not{p}_2 + 2\not{p}_1 p_{1\mu} \\ &+ 10\not{p}_1 p_{2\mu} + 10\not{p}_2 p_{1\mu} + 2\not{p}_2 p_{2\mu} \\ &= \gamma_\mu\left[-7m_e^2 - 7m_\mu^2 + 2(p_1p_2)\right] + 12\not{p}_1(p_1+p_2)_\mu + 12\not{p}_2(p_1+p_2)_\mu - 10\not{p}_1 p_{1\mu} \\ &- 10\not{p}_2 p_{2\mu} - 2\not{p}_1 p_{2\mu} - 2\not{p}_2 p_{1\mu} + 5\not{p}_1\gamma_\mu\not{p}_1 + 5\not{p}_2\gamma_\mu\not{p}_2 + \not{p}_1\gamma_\mu\not{p}_2 - 23\not{p}_2\gamma_\mu\not{p}_1\,, \end{aligned} \tag{B.65}$$

$$ {}^{2}\Lambda_{\mu}^{(\xi^{--})} = -\frac{(y_N^*)_{ek}(y_N)_{\mu k}}{48\pi^2 M^2_{\xi^{--}}}\left[(\not{p}_1+\not{p}_2)(p_1+p_2)_\mu - (m_e^2+m_\mu^2)\gamma_\mu - 2\not{p}_2\gamma_\mu\not{p}_1\right] P_L \ . \quad \text{(B.66)} $$

Here, to obtain eq. (B.66) from eq. (B.65), one has used:

$$ \not{p}q_\mu = \frac{1}{2}(\not{p}\gamma_\mu\not{q} + \not{p}\not{q}\gamma_\mu) = \frac{1}{2}(\not{q}\gamma_\mu\not{p} + \gamma_\mu\not{q}\not{p}) = \frac{1}{4}(\not{p}\gamma_\mu\not{q} + \not{q}\gamma_\mu\not{p} + \not{p}\not{q}\gamma_\mu + \gamma_\mu\not{q}\not{p}) \ , \quad \text{(B.67)} $$

$$ \frac{1}{2}\gamma_\mu(\not{p}_1\not{p}_2 + \not{p}_2\not{p}_1) + \frac{1}{2}(\not{p}_1\not{p}_2 + \not{p}_2\not{p}_1)\gamma_\mu = 2(p_1p_2)\gamma_\mu \ . \quad \text{(B.68)} $$

From eq. (B.66), it is straightforward to have (see eqs. (A.29) and (A.30))

$$ \overline{u}(p_2)\ {}^{2}\Lambda_{\mu}^{(\xi^{--})}\ u(p_1) = -\frac{(y_N^*)_{ek}(y_N)_{\mu k}}{48\pi^2 M^2_{\xi^{--}}}\ \overline{u}(p_2)\left[m_e P_L i\sigma_{\mu\nu}q^\nu + m_\mu P_R i\sigma_{\mu\nu}q^\nu\right] u(p_1) \ , \quad \text{(B.69)} $$

or

$$ {}^{2}\Lambda_{\mu}^{(\xi^{--})} = -\frac{(y_N^*)_{ek}(y_N)_{\mu k}}{48\pi^2 M^2_{\xi^{--}}}\ \left[m_e P_L i\sigma_{\mu\nu}q^\nu + m_\mu P_R i\sigma_{\mu\nu}q^\nu\right] \ . \quad \text{(B.70)} $$

In the same way, it is not difficult to calculate the diagrams (e), (f) and (h) with the participation of singly charged scalar, the result reads:

$$ \Lambda_{\mu}^{(\xi^{-})} = \sum_{i=f}^{h}\Lambda_{\mu}^{(i)} = {}^{1}\Lambda_{\mu}^{(\xi^{-})} + {}^{2}\Lambda_{\mu}^{(\xi^{-})} \ , \quad \text{(B.71)} $$

$$ {}^{1}\Lambda_{\mu}^{(\xi^{-})} = -\frac{(y_N^*)_{ek}(y_N)_{\mu k}}{12\times 48\pi^2 M^2_{\xi^{-}}}\left(q^2\gamma_\mu - q_\mu q_\nu\gamma^\nu\right) P_L \ , \quad \text{(B.72)} $$

$$ {}^{2}\Lambda_{\mu}^{(\xi^{-})} = -\frac{(y_N^*)_{ek}(y_N)_{\mu k}}{8\times 48\pi^2 M^2_{\xi^{-}}}\ \left[m_e P_L i\sigma_{\mu\nu}q^\nu + m_\mu P_R i\sigma_{\mu\nu}q^\nu\right] \ , \quad \text{(B.73)} $$

Finally, gathering the results of the calculation, we have the one-loop form factor for type II see-saw model (HTM) with the participation of both singly and doubly charged scalars:

$$ {}^{1}\Lambda_{\mu} = -\frac{(y_N^*)_{ek}(y_N)_{\mu k}}{48\pi^2}\left(\frac{1}{12M^2_{\xi^{-}}} + \frac{f(r,s_k)}{M^2_{\xi^{--}}}\right)\left(q^2\gamma_\mu - q_\mu q_\nu\gamma^\nu\right) P_L \ , \quad \text{(B.74)} $$

$$ {}^{2}\Lambda_{\mu} = -\frac{(y_N^*)_{ek}(y_N)_{\mu k}}{48\pi^2 M^2_{\xi^{-}}}\left(\frac{1}{8M^2_{\xi^{-}}} + \frac{1}{M^2_{\xi^{--}}}\right)\ \left[m_e P_L i\sigma_{\mu\nu}q^\nu + m_\mu P_R i\sigma_{\mu\nu}q^\nu\right] \ . \quad \text{(B.75)} $$

Bibliography

[1] K. Nakamura and S. T. Petcov, *"Neutrino Masses, Mixing and Oscillations"*, in J. Beringer *et al.* (Particle Data Group), Phys. Rev. D **86** (2012) 010001.

[2] B. Pontecorvo, *"Inverse beta processes and nonconservation of lepton charge"*, Sov. Phys. JETP **7** (1958) 172 [Zh. Eksp. Teor. Fiz. **34** (1957) 247].

[3] B. Pontecorvo, *"Neutrino experiments and the question of leptonic-charge conservation"*, Zh. Eksp. Teor. Fiz. **53** (1967) 1717.

[4] Z. Maki, M. Nakagawa and S. Sakata, *"Remarks on the unified model of elementary particles"*, Prog. Theor. Phys. **28** (1962) 870.

[5] S. M. Bilenky, J. Hosek and S. T. Petcov, *"On Oscillations of Neutrinos with Dirac and Majorana Masses"*, Phys. Lett. B **94** (1980) 495.

[6] E. Molinaro and S. T. Petcov, *"The Interplay Between the 'Low' and 'High' Energy CP-Violation in Leptogenesis"*, Eur. Phys. J. C **61** (2009) 93 [arXiv:0803.4120 [hep-ph]].

[7] L. Wolfenstein, *"CP Properties of Majorana Neutrinos and Double beta Decay"*, Phys. Lett. B **107** (1981) 77.

[8] S. M. Bilenky, N. P. Nedelcheva and S. T. Petcov, *"Some Implications Of The Cp Invariance For Mixing Of Majorana Neutrinos"*, Nucl. Phys. B **247** (1984) 61.

[9] B. Kayser, *"CPT, CP, and c Phases and their Effects in Majorana Particle Processes"*, Phys. Rev. D **30** (1984) 1023.

[10] Y. Fukuda *et al.* [Super-Kamiokande Collaboration], *"Evidence for oscillation of atmospheric neutrinos"*, Phys. Rev. Lett. **81** (1998) 1562 [hep-ex/9807003].

[11] Q. R. Ahmad *et al.* [SNO Collaboration], *"Measurement of the rate of $\nu_e + d \to p + p + e^-$ interactions produced by B-8 solar neutrinos at the Sudbury Neutrino Observatory"*, Phys. Rev. Lett. **87** (2001) 071301 [nucl-ex/0106015].

[12] S. Fukuda *et al.* [Super-Kamiokande Collaboration], *"Solar B-8 and hep neutrino measurements from 1258 days of Super-Kamiokande data"*, Phys. Rev. Lett. **86** (2001) 5651 [hep-ex/0103032].

[13] K. Eguchi *et al.* [KamLAND Collaboration], *"First results from KamLAND: Evidence for reactor anti-neutrino disappearance"*, Phys. Rev. Lett. **90** (2003) 021802 [arXiv:hep-ex/0212021].

[14] T. Nakaya [for the T2K Collaboration], talk at Neutrino 2012; see also: K. Abe *et al.* [T2K Collaboration], *"Indication of Electron Neutrino Appearance from an Accelerator-produced Off-axis Muon Neutrino Beam"*, Phys. Rev. Lett. **107** (2011) 041801 [arXiv:1106.2822 [hep-ex]].

[15] P. Adamson *et al.* [MINOS Collaboration], *"Improved search for muon-neutrino to electron-neutrino oscillations in MINOS"*, Phys. Rev. Lett. **107** (2011) 181802 [arXiv:1108.0015 [hep-ex]].

[16] Y. Abe *et al.* [DOUBLE-CHOOZ Collaboration], *"Indication for the disappearance of reactor electron antineutrinos in the Double Chooz experiment"*, Phys. Rev. Lett. **108** (2012) 131801 [arXiv:1112.6353 [hep-ex]].

[17] G. L. Fogli, E. Lisi, A. Marrone, A. Palazzo and A. M. Rotunno, *"Evidence of $\theta_{13} > 0$ from global neutrino data analysis"*, Phys. Rev. D **84** (2011) 053007 [arXiv:1106.6028 [hep-ph]].

[18] T. Schwetz, M. Tortola and J. W. F. Valle, *"Where we are on θ_{13}: addendum to 'Global neutrino data and recent reactor fluxes: status of three-flavour oscillation parameters"'*, New J. Phys. **13** (2011) 109401 [arXiv:1108.1376 [hep-ph]].

[19] F. P. An *et al.* [DAYA-BAY Collaboration], *"Observation of electron-antineutrino disappearance at Daya Bay"*, Phys. Rev. Lett. **108** (2012) 171803 [arXiv:1203.1669 [hep-ex]].

[20] J. K. Ahn *et al.* [RENO Collaboration], *"Observation of Reactor Electron Antineutrino Disappearance in the RENO Experiment"*, Phys. Rev. Lett. **108** (2012) 191802 [arXiv:1204.0626 [hep-ex]].

[21] G. L. Fogli, E. Lisi, A. Marrone, D. Montanino, A. Palazzo and A. M. Rotunno, *"Global analysis of neutrino masses, mixings and phases: entering the era of leptonic CP violation searches"*, Phys. Rev. D **86** (2012) 013012 [arXiv:1205.5254 [hep-ph]].

[22] M. C. Gonzalez-Garcia, M. Maltoni, J. Salvado and T. Schwetz, *"Global fit to three neutrino mixing: critical look at present precision"*, JHEP **1212** (2012) 123 [arXiv:1209.3023 [hep-ph]].

[23] A. Osipowicz *et al.* [KATRIN Collaboration], *"KATRIN: A Next generation tritium beta decay experiment with sub-eV sensitivity for the electron neutrino mass. Letter of intent"*, hep-ex/0109033.

[24] T. .M. Nieuwenhuizen, *"Do non-relativistic neutrinos constitute the dark matter?"*, Europhys. Lett. **86** (2009) 59001 [arXiv:0812.4552 [astro-ph]].

[25] P. A. R. Ade *et al.* [Planck Collaboration], *"Planck 2013 results. XVI. Cosmological parameters"*, arXiv:1303.5076 [astro-ph.CO].

[26] R. B. Patterson [NOvA Collaboration], *"The NOvA Experiment: Status and Outlook"*, Nucl. Phys. Proc. Suppl. **235-236** (2013) 151 [arXiv:1209.0716 [hep-ex]].

[27] M. Aoki, K. Hagiwara, Y. Hayato, T. Kobayashi, T. Nakaya, K. Nishikawa and N. Okamura, *"Prospects of very long baseline neutrino oscillation experiments with the KEK / JAERI high intensity proton accelerator"*, Phys. Rev. D **67** (2003) 093004 [hep-ph/0112338].

[28] S. M. Bilenky and S. T. Petcov, *"Massive Neutrinos and Neutrino Oscillations"*, Rev. Mod. Phys. **59** (1987) 671.

[29] W. Rodejohann, *"Neutrino-less Double Beta Decay and Particle Physics"*, Int. J. Mod. Phys. E **20** (2011) 1833 [arXiv:1106.1334 [hep-ph]].

[30] F. Alessandria, E. Andreotti, R. Ardito, C. Arnaboldi, F. T. Avignone, III, M. Balata, I. Bandac and T. I. Banks *et al.*, *"Sensitivity of CUORE to Neutrinoless Double-Beta Decay"*, arXiv:1109.0494 [nucl-ex].

[31] I. Abt, M. F. Altmann, A. Bakalyarov, I. Barabanov, C. Bauer, E. Bellotti, S. T. Belyaev and L. B. Bezrukov *et al.*, *"A New Ge-76 double beta decay experiment at LNGS: Letter of intent"*, hep-ex/0404039.

[32] M. Agostini *et al.* [GERDA Collaboration], *"Results on neutrinoless double beta decay of 76Ge from GERDA Phase I"*, arXiv:1307.4720 [nucl-ex].

[33] C. E. Aalseth *et al.* [Majorana Collaboration], *"The Majorana neutrinoless double beta decay experiment"*, Phys. Atom. Nucl. **67** (2004) 2002 [Yad. Fiz. **67** (2004) 2025] [hep-ex/0405008].

[34] M. Auger *et al.* [EXO Collaboration], *"Search for Neutrinoless Double-Beta Decay in ^{136}Xe with EXO-200"*, Phys. Rev. Lett. **109** (2012) 032505 [arXiv:1205.5608 [hep-ex]].

[35] M. C. Chen [SNO+ Collaboration], *"The SNO+ Experiment"*, arXiv:0810.3694 [hep-ex].

[36] A. Gando *et al.* [KamLAND-Zen Collaboration], *"Measurement of the double-β decay half-life of ^{136}Xe with the KamLAND-Zen experiment"*, Phys. Rev. C **85** (2012) 045504 [arXiv:1201.4664 [hep-ex]].

[37] J. Adam *et al.* [MEG Collaboration], *"New constraint on the existence of the $\mu^+ \to e^+ + \gamma$ decay"*, arXiv:1303.0754 [hep-ex].

[38] U. Bellgardt *et al.* [SINDRUM Collaboration], *"Search for the Decay $\mu^+ \to e^+ + e^+ + e^-$"*, Nucl. Phys. B **299** (1988) 1.

[39] C. Dohmen *et al.* [SINDRUM II Collaboration.], *"Test of lepton flavor conservation in $\mu \to e$ conversion on titanium"*, Phys. Lett. B **317** (1993) 631.

[40] B. Aubert *et al.* [BABAR Collaboration], *"Searches for Lepton Flavor Violation in the Decays $\tau^\pm \to e^\pm + \gamma$ and $\tau^\pm \to \mu^\pm + \gamma$"*, Phys. Rev. Lett. **104** (2010) 021802 [arXiv:0908.2381 [hep-ex]].

[41] See, e.g., http://comet.phys.sci.osaka-u.ac.jp:8080/comet .

[42] See, e.g., http://mu2e.fnal.gov/.

[43] Y. Mori *et al.* [The PRIME Working Group], "An Experimental Search for $\mu^- \to e^-$ Conversion Process at an Ultimate Sensitivity of the Order of 10^{-18} with PRISM", LOI-25.

[44] See, e.g., http://projectx.fnal.gov/.

[45] This is part of the program of research planned to be realised with the MuSIC facility at Osaka University, Japan (private communication by Y. Kuno); see also N. Berger, *"A Novel experiment searching for the lepton flavour violating decay $\mu \to eee$"*, J. Phys. Conf. Ser. **408** (2013) 012070 [J. Phys. Conf. Ser. **408** (2013) 012070] [arXiv:1110.1504 [hep-ex]].

[46] A. G. Akeroyd *et al.* [SuperKEKB Physics Working Group Collaboration], *"Physics at super B factory"*, hep-ex/0406071.

[47] J. Bernabeu, S. Palomares Ruiz and S. T. Petcov, *"Atmospheric neutrino oscillations, theta(13) and neutrino mass hierarchy"*, Nucl. Phys. B **669** (2003) 255 [hep-ph/0305152].

[48] S. Palomares-Ruiz and S. T. Petcov, *"Three-neutrino oscillations of atmospheric neutrinos, θ_{13}, neutrino mass hierarchy and iron magnetized detectors"*, Nucl. Phys. B **712** (2005) 392 [hep-ph/0406096].

[49] S. T. Petcov and T. Schwetz, *"Determining the neutrino mass hierarchy with atmospheric neutrinos"*, Nucl. Phys. B **740** (2006) 1 [hep-ph/0511277].

[50] R. Gandhi *et al.*, *"Mass Hierarchy Determination via future Atmospheric Neutrino Detectors"*, Phys. Rev. D **76** (2007) 073012 [arXiv:0707.1723 [hep-ph]].

[51] S. T. Petcov and M. Piai, *"The LMA MSW solution of the solar neutrino problem, inverted neutrino mass hierarchy and reactor neutrino experiments"*, Phys. Lett. B **533** (2002) 94 [hep-ph/0112074].

[52] S. Choubey, S. T. Petcov and M. Piai, *"Precision neutrino oscillation physics with an intermediate baseline reactor neutrino experiment"*, Phys. Rev. D **68** (2003) 113006 [hep-ph/0306017].

[53] P. Ghoshal and S. T. Petcov, *"Neutrino Mass Hierarchy Determination Using Reactor Antineutrinos"*, JHEP **1103** (2011) 058 [arXiv:1011.1646 [hep-ph]].

[54] S. Pascoli and S. T. Petcov, *"Majorana Neutrinos, Neutrino Mass Spectrum and the $| < m > | \sim 10^{-3}$ eV Frontier in Neutrinoless Double Beta Decay"*, Phys. Rev. D **77** (2008) 113003 [arXiv:0711.4993 [hep-ph]].

[55] S. Pascoli, S. T. Petcov and A. Riotto, *"Connecting low energy leptonic CP-violation to leptogenesis"*, Phys. Rev. D **75** (2007) 083511 [hep-ph/0609125].

[56] S. Pascoli, S. T. Petcov and A. Riotto, *"Leptogenesis and Low Energy CP Violation in Neutrino Physics"*, Nucl. Phys. B **774** (2007) 1 [hep-ph/0611338].

[57] E. Molinaro and S. T. Petcov, *"A Case of Subdominant/Suppressed 'High Energy' Contribution to the Baryon Asymmetry of the Universe in Flavoured Leptogenesis"*, Phys. Lett. B **671** (2009) 60 [arXiv:0808.3534 [hep-ph]].

[58] S. T. Petcov, *"The Processes Mu → E Gamma, Mu → E E Anti-E, Neutrino' → Neutrino Gamma In The Weinberg-Salam Model With Neutrino Mixing"*, Sov. J. Nucl. Phys. **25** (1977) 340 [Yad. Fiz. **25** (1977) 641].

[59] S. M. Bilenky, S. T. Petcov and B. Pontecorvo, *"Lepton mixing, $\mu \to e + \gamma$ decay and neutrino oscillations"*, Phys. Lett. B **67** (1977) 309.

[60] M. Shaposhnikov, *"A Possible symmetry of the nuMSM"*, Nucl. Phys. B **763** (2007) 49 [hep-ph/0605047].

[61] M. B. Gavela, T. Hambye, D. Hernandez and P. Hernandez, *"Minimal Flavour Seesaw Models"*, JHEP **0909** (2009) 038 [arXiv:0906.1461 [hep-ph]].

[62] A. Ibarra, E. Molinaro and S. T. Petcov, *"Low Energy Signatures of the TeV Scale See-Saw Mechanism"*, Phys. Rev. D **84** (2011) 013005 [arXiv:1103.6217 [hep-ph]].

[63] M. Raidal, A. Strumia and K. Turzynski, *"Low-scale standard supersymmetric leptogenesis"*, Phys. Lett. B **609** (2005) 351 [Erratum-ibid. B **632** (2006) 752] [hep-ph/0408015].

[64] M. Yoshimura, *"Neutrino Pair Emission from Excited Atoms"*, Phys. Rev. D **75** (2007) 113007 [hep-ph/0611362].

[65] M. Yoshimura, *"Solitons and Precision Neutrino Mass Spectroscopy"*, Phys. Lett. B **699** (2011) 123 [arXiv:1101.2749 [hep-ph]].

[66] M. Yoshimura, A. Fukumi, N. Sasao and T. Yamaguchi, *"Parity violating observables in radiative neutrino pair emission from metastable atoms"*, Prog. Theor. Phys. **123** (2010) 523 [arXiv:0907.0519 [hep-ph]].

[67] P. Minkowski, *"$\mu \to e\gamma$ at a Rate of One Out of 1-Billion Muon Decays?"*, Phys. Lett. B **67** (1977) 421.

[68] M. Gell-Mann, P. Ramond and R. Slansky, *Proceedings of the Supergravity Stony Brook Workshop*, New York 1979, eds. P. Van Nieuwenhuizen and D. Freedman.

[69] T. Yanagida, *Proceedinds of the Workshop on Unified Theories and Baryon Number in the Universe*, Tsukuba, Japan 1979, eds. A. Sawada and A. Sugamoto.

[70] R. N. Mohapatra and G. Senjanovic, *"Neutrino Mass and Spontaneous Parity Violation"*, Phys. Rev. Lett. **44** (1980) 912.

[71] A. Ibarra, E. Molinaro and S. T. Petcov, *"TeV Scale See-Saw Mechanisms of Neutrino Mass Generation, the Majorana Nature of the Heavy Singlet Neutrinos and $(\beta\beta)_{0\nu}$-Decay"*, JHEP **1009** (2010) 108 [arXiv:1007.2378 [hep-ph]].

[72] A. Kleppe, *"Extending The Standard Model With Two Right-Handed Neutrinos", in *Lohusalu 1995, Neutrino physics*, 118-125.*

[73] E. Ma, D. P. Roy and U. Sarkar, *"A Seesaw model for atmospheric and solar neutrino oscillations"*, Phys. Lett. B **444** (1998) 391 [hep-ph/9810309].

[74] P. H. Frampton, S. L. Glashow and T. Yanagida, *"Cosmological sign of neutrino CP violation"*, Phys. Lett. B **548** (2002) 119 [arXiv:hep-ph/0208157].

[75] M. Raidal and A. Strumia, *"Predictions of the most minimal see-saw model"*, Phys. Lett. B **553**, 72 (2003) [arXiv:hep-ph/0210021].

[76] V. Barger, D. A. Dicus, H. J. He and T. j. Li, *"Structure of cosmological CP violation via neutrino seesaw"*, Phys. Lett. B **583** (2004) 173 [arXiv:hep-ph/0310278].

[77] T. Endoh, S. Kaneko, S. K. Kang, T. Morozumi and M. Tanimoto, *"CP violation in neutrino oscillation and leptogenesis"*, Phys. Rev. Lett. **89** (2002) 231601 [arXiv:hep-ph/0209020].

[78] A. Ibarra and G. G. Ross, *"Neutrino phenomenology: The case of two right handed neutrinos"*, Phys. Lett. B **591** (2004) 285 [arXiv:hep-ph/0312138].

[79] A. Ibarra and G. G. Ross, *"Neutrino properties from Yukawa structure"*, Phys. Lett. B **575** (2003) 279 [arXiv:hep-ph/0307051].

[80] S. T. Petcov, W. Rodejohann, T. Shindou and Y. Takanishi, *"The See-Saw Mechanism, Neutrino Yukawa Couplings, LFV Decays $\ell_i \to \ell_j + \gamma$ and Leptogenesis"*, Nucl. Phys. B **739** (2006) 208 [arXiv:hep-ph/0510404].

[81] S. Antusch, J. P. Baumann and E. Fernandez-Martinez, *"Non-Standard Neutrino Interactions with Matter from Physics Beyond the Standard Model"*, Nucl. Phys. B **810** (2009) 369 [arXiv:0807.1003 [hep-ph]].

[82] S. Antusch *et al.*, *"Unitarity of the Leptonic Mixing Matrix"*, JHEP **0610** (2006) 084 [arXiv:hep-ph/0607020].

[83] E. Akhmedov, A. Kartavtsev, M. Lindner, L. Michaels and J. Smirnov, *"Improving Electro-Weak Fits with TeV-scale Sterile Neutrinos"*, JHEP **1305** (2013) 081 [arXiv:1302.1872 [hep-ph]].

[84] T. -P. Cheng and L. -F. Li, *"Muon Number Nonconservation Effects in a Gauge Theory with V A Currents and Heavy Neutral Leptons"*, Phys. Rev. D **16** (1977) 1425.

[85] T. P. Cheng and L. F. Li, *"Mu $\to$ E Gamma In Theories With Dirac And Majorana Neutrino Mass Terms"*, Phys. Rev. Lett. **45** (1980) 1908.

[86] A. Ilakovac and A. Pilaftsis, *"Flavor violating charged lepton decays in seesaw-type models"*, Nucl. Phys. B **437** (1995) 491 [hep-ph/9403398].

[87] R. Kitano, M. Koike and Y. Okada, *"Detailed calculation of lepton flavor violating muon electron conversion rate for various nuclei"*, Phys. Rev. D **66** (2002) 096002 [Erratum-ibid. D **76** (2007) 059902] [arXiv:hep-ph/0203110].

[88] M. Magg and C. Wetterich, *"Neutrino Mass Problem And Gauge Hierarchy"*, Phys. Lett. B **94** (1980) 61.

[89] J. Schechter and J. W. F. Valle, *"Neutrino Masses in SU(2) x U(1) Theories"*, Phys. Rev. D **22** (1980) 2227.

[90] R. N. Mohapatra and G. Senjanovic, *"Neutrino Masses and Mixings in Gauge Models with Spontaneous Parity Violation"*, Phys. Rev. D **23** (1981) 165.

[91] M. Kakizaki, Y. Ogura and F. Shima, *"Lepton flavor violation in the triplet Higgs model"*, Phys. Lett. B **566** (2003) 210 [hep-ph/0304254].

[92] A. G. Akeroyd, M. Aoki and H. Sugiyama, *"Lepton Flavour Violating Decays $\tau^- \to l^+ l^- l^-$ and $\mu \to e\gamma$ in the Higgs Triplet Model"*, Phys. Rev. D **79** (2009) 113010 [arXiv:0904.3640 [hep-ph]].

[93] T. Han, B. Zhang, *"Signatures for Majorana neutrinos at hadron colliders"*, Phys. Rev. Lett. **97** (2006) 171804 [hep-ph/0604064].

[94] F. del Aguila, J. A. Aguilar-Saavedra, R. Pittau, *"Heavy neutrino signals at large hadron colliders"*, JHEP **0710** (2007) 047 [hep-ph/0703261].

[95] A. Atre, T. Han, S. Pascoli and B. Zhang, *"The Search for Heavy Majorana Neutrinos"*, JHEP **0905** (2009) 030 [arXiv:0901.3589 [hep-ph]].

[96] F. del Aguila, J. A. Aguilar-Saavedra, *"Distinguishing seesaw models at LHC with multi-lepton signals"*, Nucl. Phys. **B813** (2009) 22-90 [arXiv:0808.2468 [hep-ph]].

[97] A. G. Akeroyd, S. Moretti and H. Sugiyama, *"Five-lepton and six-lepton signatures from production of neutral triplet scalars in the Higgs Triplet Model"*, Phys. Rev. D **85**, 055026 (2012) [arXiv:1201.5047 [hep-ph]].

[98] E. J. Chun, K. Y. Lee and S. C. Park, *"Testing Higgs triplet model and neutrino mass patterns"*, Phys. Lett. B **566**, 142 (2003) [arXiv:hep-ph/0304069].

[99] M. C. Chen, *"Generation of small neutrino Majorana masses in a Randall-Sundrum model"*, Phys. Rev. D **71**, 113010 (2005) [arXiv:hep-ph/0504158].

[100] E. Ma, M. Raidal and U. Sarkar, *"Verifiable model of neutrino masses from large extra dimensions"*, Phys. Rev. Lett. **85** (2000) 3769 [hep-ph/0006046].

[101] A. G. Akeroyd and C. -W. Chiang, *"Phenomenology of Large Mixing for the CP-even Neutral Scalars of the Higgs Triplet Model"*, Phys. Rev. D **81** (2010) 115007 [arXiv:1003.3724 [hep-ph]].

[102] E. Ma, M. Raidal and U. Sarkar, *"Phenomenology of the neutrino mass giving Higgs triplet and the low-energy seesaw violation of lepton number"*, Nucl. Phys. B **615** (2001) 313 [hep-ph/0012101].

[103] M. Raidal and A. Santamaria, *"mu e conversion in nuclei versus $\mu \to e\gamma$: An effective field theory point of view"*, Phys. Lett. B **421** (1998) 250 [arXiv:hep-ph/9710389].

[104] J. Bernabeu, A. Pich and A. Santamaria, *"Cp Phases In The Charged Current And Higgs Sectors For Majorana Neutrinos"*, Z. Phys. C **30** (1986) 213.

[105] G. K. Leontaris, K. Tamvakis and J. D. Vergados, *"Lepton And Family Number Violation From Exotic Scalars"*, Phys. Lett. B **162** (1985) 153.

[106] S. T. Petcov, *"Remarks on the Zee Model of Neutrino Mixing (mu $\to$ e gamma, Heavy Neutrino $\to$ Light Neutrino gamma, etc.)"*, Phys. Lett. B **115** (1982) 401.

[107] D. N. Dinh, A. Ibarra, E. Molinaro and S. T. Petcov, *"The $\mu - e$ Conversion in Nuclei, $\mu \to e\gamma$, $\mu \to 3e$ Decays and TeV Scale See-Saw Scenarios of Neutrino Mass Generation"*, JHEP **1208** (2012) 125, Erratum-ibid. 1309 (2013) 023 [arXiv:1205.4671v4].

[108] R. Foot, H. Lew, X. G. He and G. C. Joshi, *"See-saw neutrino masses induced by a triplet of leptons"*, Z. Phys. C **44** (1989) 441.

[109] E. Ma, *"Pathways to naturally small neutrino masses"*, Phys. Rev. Lett. **81** (1998) 1171 [hep-ph/9805219].

[110] A. Abada, C. Biggio, F. Bonnet, M. B. Gavela and T. Hambye, *"Low energy effects of neutrino masses"*, JHEP **0712** (2007) 061 [arXiv:0707.4058 [hep-ph]].

[111] A. Abada, C. Biggio, F. Bonnet, M. B. Gavela, T. Hambye, *"$\mu \to e\gamma$ and $\tau \to l\gamma$ decays in the fermion triplet seesaw model"*, Phys. Rev. **D78** (2008) 033007. [arXiv:0803.0481 [hep-ph]].

[112] K. Schreckenbach, G. Colvin, W. Gelletly and F. Von Feilitzsch, *"Determination Of The Anti-neutrino Spectrum From U-235 Thermal Neutron Fission Products Up To 9.5-mev"*, Phys. Lett. B **160** (1985) 325.

[113] G. Mention, M. Fechner, T. .Lasserre, T. .A. Mueller, D. Lhuillier, M. Cribier and A. Letourneau, *"The Reactor Antineutrino Anomaly"*, Phys. Rev. D **83** (2011) 073006 [arXiv:1101.2755 [hep-ex]].

[114] M. L. Brooks *et al.* [MEGA Collaboration], *"New Limit for the Family-Number Non-conserving Decay $\mu^+ \to e^+ + \gamma$ "*, Phys. Rev. Lett. **83** (1999) 1521 [arXiv:hep-ex/9905013].

[115] J. Adam *et al.* [MEG Collaboration], *"New limit on the lepton-flavour violating decay $\mu^+ \to e^+\gamma$"*, Phys. Rev. Lett. **107** (2011) 171801 [arXiv:1107.5547 [hep-ex]].

[116] J. Hisano, T. Moroi, K. Tobe and M. Yamaguchi, *"Lepton flavor violation via right-handed neutrino Yukawa couplings in supersymmetric standard model"*, Phys. Rev. D **53** (1996) 2442 [hep-ph/9510309].

[117] A. J. Buras, B. Duling, T. Feldmann, T. Heidsieck and C. Promberger, "Lepton Flavour Violation in the Presence of a Fourth Generation of Quarks and Leptons", JHEP **1009** (2010) 104 [arXiv:1006.5356 [hep-ph]].

[118] R. Alonso, M. Dhen, M. B. Gavela and T. Hambye, *"Muon conversion to electron in nuclei in type-I seesaw models"*, JHEP **1301**, 118 (2013) [arXiv:1209.2679 [hep-ph]].

[119] J. Hisano and K. Tobe, *"Neutrino masses, muon g-2, and lepton flavor violation in the supersymmetric seesaw model"*, Phys. Lett. B **510** (2001) 197.

[120] J. Chakrabortty, P. Ghosh and W. Rodejohann, *"Lower Limits on $\mu \to e\gamma$ from New Measurements on U_{e3}"*, Phys. Rev. D **86** (2012) 075020 [arXiv:1204.1000 [hep-ph]].

[121] S. M. Bilenky, S. Pascoli and S. T. Petcov, *"Majorana neutrinos, neutrino mass spectrum, CP violation and neutrinoless double beta decay. 1. The Three neutrino mixing case"*, Phys. Rev. D **64** (2001) 053010 [hep-ph/0102265].

[122] S. T. Petcov, *"Theoretical prospects of neutrinoless double beta decay"*, Phys. Scripta T **121** (2005) 94 [hep-ph/0504166].

[123] S. T. Petcov, *"Neutrino mixing, leptonic CP violation, the seesaw mechanism and beyond"*, Int. J. Mod. Phys. A **25** (2010) 4325.

[124] S. T. Petcov, H. Sugiyama and Y. Takanishi, *"Neutrinoless Double Beta Decay and $H^{\pm\pm} \to l'^{\pm} l^{\pm}$ Decays in the Higgs Triplet Model"*, Phys. Rev. D **80** (2009) 015005 [arXiv:0904.0759 [hep-ph]].

[125] H. V. Klapdor-Kleingrothaus, I. V. Krivosheina, A. Dietz and O. Chkvorets, *"Search for neutrinoless double beta decay with enriched Ge-76 in Gran Sasso 1990-2003"*, Phys. Lett. B **586** (2004) 198 [hep-ph/0404088].

[126] H. V. Klapdor-Kleingrothaus, A. Dietz, H. L. Harney and I. V. Krivosheina, *"Evidence for neutrinoless double beta decay"*, Mod. Phys. Lett. A **16** (2001) 2409 [hep-ph/0201231].

[127] S. Pascoli and S. T. Petcov, *"The SNO solar neutrino data, neutrinoless double beta decay and neutrino mass spectrum"*, Phys. Lett. B **544** (2002) 239; *ibid.* **580** (2004) 280 [hep-ph/0205022].

[128] J. Bernabeu, E. Nardi, D. Tommasini, *"μ - e conversion in nuclei and Z' physics"*, Nucl. Phys. **B409** (1993) 69-86. [hep-ph/9306251].

[129] M. Yoshimura, C. Ohae, A. Fukumi, K. Nakajima, I. Nakano, H. Nanjo, and N. Sasao, *"Macro-coherent two photon and radiative neutrino pair emission"*, arXiv:0805.1970[hep-ph] (2008); M. Yoshimura, *"Neutrino Spectroscopy using Atoms (SPAN)"*, in Proceedings of 4th NO-VE International Workshop, edited by M. Baldo Ceolin (2008).

[130] M. Yoshimura, N. Sasao and M. Tanaka, *"Dynamics of paired superradiance"*, Phys. Rev. A **86** (2012) 013812 [arXiv:1203.5394 [quant-ph]].

[131] S. T. Petcov, *"Cp Violation Effect In Neutralino Pair Production In e^+e^- Annihilation And The Electric Dipole Moment Of The Electron"*, Phys. Lett. B **178** (1986) 57.

[132] NIST (National Institute of Standards and Technology) Atomic Spectra Database: http://www.nist.gov/pml/data/asd.cfm

[133] For example, B.H. Bransden and C.J. Joachain, *"Physics of Atoms and Molecules"*, second edition, Prentice Hall (2003).

[134] A. Fukumi, S. Kuma, Y. Miyamoto, K. Nakajima, I. Nakano, H. Nanjo, C. Ohae and N. Sasao *et al.*, *"Neutrino Spectroscopy with Atoms and Molecules"*, PTEP **2012** (2012) 04D002 [arXiv:1211.4904 [hep-ph]].

[135] S. Pascoli, S. T. Petcov and W. Rodejohann, *"On the CP violation associated with Majorana neutrinos and neutrinoless double beta decay"*, Phys. Lett. B **549** (2002) 177 [hep-ph/0209059].

[136] S. Pascoli, S. T. Petcov and T. Schwetz, *"The Absolute neutrino mass scale, neutrino mass spectrum, majorana CP-violation and neutrinoless double-beta decay"*, Nucl. Phys. B **734** (2006) 24 [hep-ph/0505226], and references quoted therein.

[137] V. Barger, S. L. Glashow, P. Langacker and D. Marfatia, *"No go for detecting CP violation via neutrinoless double beta decay"*, Phys. Lett. B **540** (2002) 247 [hep-ph/0205290].

[138] K. I. Aoki, Z. Hioki, M. Konuma, R. Kawabe and T. Muta, *"Electroweak Theory. Framework of On-Shell Renormalization and Study of Higher Order Effects"*, Prog. Theor. Phys. Suppl. **73** (1982) 1.